

On the build-up of storm water solids in gully pots

Rietveld, M.W.J.

DOI

[10.4233/uuid:cfa75a61-32e8-40df-946e-5f022940cdd0](https://doi.org/10.4233/uuid:cfa75a61-32e8-40df-946e-5f022940cdd0)

Publication date

2021

Document Version

Final published version

Citation (APA)

Rietveld, M. W. J. (2021). *On the build-up of storm water solids in gully pots*. [Dissertation (TU Delft), Delft University of Technology]. <https://doi.org/10.4233/uuid:cfa75a61-32e8-40df-946e-5f022940cdd0>

Important note

To cite this publication, please use the final published version (if applicable).
Please check the document version above.

Copyright

Other than for strictly personal use, it is not permitted to download, forward or distribute the text or part of it, without the consent of the author(s) and/or copyright holder(s), unless the work is under an open content license such as Creative Commons.

Takedown policy

Please contact us and provide details if you believe this document breaches copyrights.
We will remove access to the work immediately and investigate your claim.

**ON THE BUILD-UP OF STORM WATER
SOLIDS IN GULLY POTS**

ON THE BUILD-UP OF STORM WATER SOLIDS IN GULLY POTS

Proefschrift

ter verkrijging van de graad van doctor

aan de Technische Universiteit Delft,

op gezag van de Rector Magnificus Prof.dr.ir. T.H.J.J. van der Hagen,

voorzitter van het College voor Promoties

in het openbaar te verdedigen op

dinsdag 1 juni 2021 om 10.00 uur

door

Matthijs Willem Jan RIETVELD

Natuurkundig Ingenieur, Technische Universiteit Delft, Nederland

Geboren te Papendrecht, Nederland

Dit proefschrift is goedgekeurd door de promotoren.

Samenstelling promotiecommissie bestaat uit:

Rector magnificus	voorzitter
Prof.dr.ir. F.H.L.R. Clemens	Technische Universiteit Delft, Nederland, promotor
Dr.ir. J.G. Langeveld	Technische Universiteit Delft, Nederland, promotor

Onafhankelijke leden:

Prof.dr. J.L. Bertrand-Krajewski	Institut National des Sciences Appliquées de Lyon, Frankrijk
Prof.dr.-ing. U. Dittmer	Technische Universität Kaiserslautern, Duitsland
Prof.dr.-ing. M. Uhl	Fachhochschule Münster, Duitsland
Prof.dr.ir. W.S.J. Uijttewaai	Technische Universiteit Delft, Nederland
Dr. J. Rieckermann	Eawag, Zwitserland
Prof.dr. Z. Kapelan	Technische Universiteit Delft, Nederland, reservelid

Dit proefschrift is tot stand gekomen met ondersteuning van het Kennisprogramma Urban Drainage. De betrokken partijen zijn: ARCADIS, Deltares, Evides, Gemeente Almere, Gemeente Arnhem, Gemeente Breda, Gemeente Den Haag, Gemeentewerken Rotterdam, Gemeente Utrecht, GMB Rioleringsstechniek, KWR Watercycle Research Institute, Royal HaskoningDHV, Stichting RIONED, STOWA, Sweco, Tauw, vandervalk+degroot, Waterschap De Dommel, Waternet and Witteveen+Bos.

© 2021 by M.W.J. Rietveld

ISBN: 978-94-6419-220-9

Printed by: Gildeprint, Enschede

An electronic version of this document is available free of charge in the Delft University Repository at repository.tudelft.nl.

Faith is taking the first step even when you don't see the whole staircase

Martin Luther King Jr.

ACKNOWLEDGEMENTS

It must have been during an open day of TU Delft in 2008 that I visited a lecture in the faculty of Civil Engineering on Sanitary Engineering. Despite the great enthusiasm of the lecturer and the interesting lecture, I decided not to study Civil Engineering, considering it to be too specific, and started my studies in Applied Physics in 2010. During my BSc I realised that I would like to leave university after my graduation and would not apply for a PhD. However, about a decade later I finished my PhD in Civil Engineering, which illustrates that personal perspectives can change, in particular due to new insights developed in relation with others. Therefore, I would like to thank all who contributed to this PhD journey, of which I would like to name a few explicitly.

Francois and Jeroen, I would like to thank you for all technical discussions and personal support. I enjoyed the intense discussions on the experiments and on the interpretation of the results. You made clear that chaotic results do not necessarily reflect the quality of the work of a researcher, but can also reflect the beauty of nature. Thank you both for your willingness to discuss any issues whenever I dropped by.

The nice looking figures of the flow velocity fields in a gully pot would not have been there without the help of Gosse, Wout, and Paul, who introduced me into the world of PIV, LDA, and stereo photography. Wout, I remember the joyful moment that we agreed that the LDA measurements showed large similarity with the PIV measurements. Moreover, the experimental setup itself would not have been there without the help of Frans, Wim, Jos, and Goof. I am still amazed by the creativity and experience you were willing to share with me. Thank you all for your practical help and technical advises.

I would also like to thank my colleagues Adithya, Antonio, Kostas, Job, Bram, Eva, Danai, and Guan for sharing a somewhat noisy office with me, and Alex for our eyebrow-raising discussions in ‘the cave’ of Deltares. And of course Petra, Elena, Mathieu, Matthieu, Didrik, Dirk, and Marco for our shared lunch and coffee breaks. These informal discussions helped me

to improve my research and to develop as a person. Mariska and Riëlle, thanks for ordering all required materials, arranging meeting rooms, being available for a chat, and of course the candy.

A large number of students have blessed me with their contributions to the research projects as part of their study curriculum. Anna, Carlos, Anne, Cédric, Nadia, Panagioti, André, Fabrice, Mauricio, Yang, and Demi thank you all for trusting me as your supervisor. I wish you all the best in your future career/studies and personal lives.

I would like to thank all parties participating in the ‘Kennisprogramma Urban Drainage’, without whom this PhD journey would not have been possible. A special note of thanks goes to Erik Laurentzen, Marcel Tirion, John Hilberding, Kees Bos, Annemarij de Groot, Marcel Wolf, and Willem Blom. Without your support, I would not have been able to perform two extensive field experiments.

Being thankful for what I have been given and have achieved is something I learnt early on from my parents by them emphasising ‘we komen niets te kort dan dankbaarheid’. Thank you for what you have learnt me and for all your support. I would like to thank family and friends for their interest and for all their stories about underperforming drainage systems, but also for the moments we discussed metaphysics.

Niels and Gert-Jan, you have a very special role in the success of this thesis by being my paranymphs. Niels, thanks for your example as an highly motivated academic researcher. It was an honour to be your paranymph once, and it’s an honour to have you as my paranymph now. Gert-Jan, this adds another story to our friendship, which already included some interesting chapters. With your help, I suppose the thesis defense will be ‘goed te doen’, as you are used to say.

Jozanne, you encouraged me take this step with me without seeing the whole staircase. Thanks for your love, support, and interest. You celebrated positive outcomes with me and brightened the difficult moments. I thank you for being my wife and supporter. A next step is coming up and similarly to the previous one, I would neither want take this one without the everlasting love of God, the One overseeing all staircases in life.

CONTENTS

ACKNOWLEDGEMENTS.....	VII
CONTENTS.....	IX
1 INTRODUCTION	1
1.1 URBAN RUNOFF AND SOLIDS.....	1
1.2 GULLY POTS	1
1.3 TRANSPORT OF SOLIDS TO GULLY POTS	3
1.3.1 <i>Field measurements</i>	3
1.3.2 <i>Modelling</i>	5
1.4 SOLIDS ACCUMULATION IN GULLY POTS.....	6
1.5 GULLY POT REMOVAL EFFICIENCY	8
1.6 THESIS OBJECTIVE.....	10
1.7 THESIS OUTLINE.....	11
PART I: TRANSPORT OF SOLIDS TO GULLY POTS	14
2 THE SOLIDS LOADING TO GULLY POTS	15
2.1 INTRODUCTION	15
2.2 METHODS	15
2.2.1 <i>Experimental setup</i>	15
2.2.2 <i>Monitoring area</i>	16
2.2.3 <i>Data collection and analysis</i>	17
2.3 RESULTS AND DISCUSSION.....	24
2.3.1 <i>Solids loading</i>	24
2.3.2 <i>Solids' characteristics</i>	30
2.4 CONCLUSIONS.....	35
3 MODELLING THE SOLIDS LOADING TO GULLY POTS	37
3.1 INTRODUCTION	37
3.2 METHODS	39

3.2.1 Solids loading data	39
3.2.2 Parameters related to the solids loading	40
3.2.3 Modelling	42
3.3 RESULTS.....	44
3.3.1 Data exploration	44
3.3.2 Regression tree	44
3.3.3 BUWO	47
3.4 DISCUSSION.....	50
3.5 CONCLUSION	52
PART II: ACCUMULATION OF SOLIDS IN GULLY POTS	54
4 THE SOLIDS ACCUMULATION RATE IN GULLY POTS.....	55
4.1 INTRODUCTION	55
4.2 METHODS	55
4.2.1 Monitoring area	56
4.2.2 Solids accumulation rate	57
4.2.3 Parameters	59
4.2.4 Statistical modelling	64
4.2.5 Linear mixed model	65
4.2.6 Sensitivity analysis	66
4.3 RESULTS AND DISCUSSION.....	66
4.3.1 Explorative analysis	66
4.3.2 Parameters related to the solids accumulation rate	69
4.3.3 Sensitivity analysis	72
4.4 DISCUSSION.....	74
4.5 CONCLUSIONS.....	77
PART III: GULLY POT HYDRAULICS	80
5 THE REMOVAL EFFICIENCY OF GULLY POTS.....	81
5.1 INTRODUCTION	81
5.2 METHODS	82
5.2.1 Experimental setup	82
5.2.2 Instrumentation	84
5.2.3 Test conditions	86
5.2.4 Post-processing	88
5.3 RESULTS AND DISCUSSION.....	88

5.3.1 Preliminary visual observations	88
5.3.2 Discharge	90
5.3.3 Gully pot depth	95
5.3.4 Sediment size	96
5.3.5 Outlet position	98
5.3.6 Position impinging jets	100
5.4 CONCLUSIONS.....	101
6 THE FLOW FIELD IN GULLY POTS.....	103
6.1 INTRODUCTION	103
6.2 METHODS	104
6.2.1 Experimental setup	104
6.2.2 Instrumentation	105
6.2.3 PIV	105
6.2.4 LDA	108
6.2.5 Test conditions	111
6.2.6 Stereo photography	113
6.3 RESULTS AND DISCUSSION.....	115
6.3.1 Preliminary observations in PIV and LDA measurements	115
6.3.2 The effect of the sediment bed	119
6.3.3 The effect of the discharge	122
6.3.4 The effect of the gully pot depth	126
6.3.5 The effect of the outlet position	127
6.4 CONCLUSIONS.....	129
7 SYNTHESIS AND DISCUSSION.....	131
7.1 PARAMETERS CORRELATED WITH WASH-OFF.....	131
7.1.1 Gully pot catchment	132
7.1.2 Rain intensity, rain volume, water volume, discharge	132
7.1.3 Antecedent dry period	133
7.1.4 Temperature	133
7.1.5 Street sweeping	133
7.1.6 Vegetation density, tree phase	134
7.1.7 Pavement type	134
7.2 CHAOS IN WASH-OFF	134
7.3 REMOVAL EFFICIENCY MODEL	135

7.4 EXPECTED REMOVAL EFFICIENCY IN PRACTICE.....	136
7.5 GULLY POT CLEANING.....	137
7.6 GULLY POT DESIGN	137
8 GENERAL CONCLUSIONS AND RECOMMENDATIONS	139
8.1 CONCLUSIONS.....	139
8.1.1 Solids accumulation in gully pots	139
8.1.2 Transport of solids to gully pots	139
8.1.3 Gully pot hydraulics	140
8.2 RECOMMENDATIONS	140
8.2.1 Research	140
8.2.2 Applications	142
BIBLIOGRAPHY.....	143
APPENDIX A MONITORING AREAS CHAPTER 4	156
APPENDIX B VALIDATION STATISTICAL MODELS CHAPTER 4	159
APPENDIX C ASSESSED VARIABLES CHAPTER 4	163
APPENDIX D TREE PHASES CHAPTER 3	165
APPENDIX E ASSESSED VARIABLES CHAPTER 3	171
APPENDIX F TESTS OVERVIEW CHAPTER 5	172
SUMMARY	175
SAMENVATTING	179
LIST OF PUBLICATIONS.....	183
ABOUT THE AUTHOR	184

1 INTRODUCTION

1.1 Urban runoff and solids

A substantial part of urban surfaces is to some extent impermeable. Rainfall on these areas turns into runoff, which mobilises solids present on these surfaces. The solids carry associated pollutants (Sartor and Boyd 1972; Fulcher 1994; Ashley and Hvitved-Jacobsen 2002; Herngren 2005; Deletic and Orr 2005) and originate from a broad range of sources, such as traffic, construction activities, and vegetation.

Runoff can be dealt with by different types of urban drainage systems, such as sewer systems and sustainable urban drainage systems (SUDS, see Fletcher et al. 2015). The solids loading to these systems should be managed to avoid hydraulic losses in for example sewer pipes or infiltration facilities due to sedimentation (Crabtree 1989; Ashley et al. 1992; Van Bijnen et al. 2018), and to reduce negative environmental impact (e.g. Sartor and Boyd 1972; Novotny et al. 1985) when infiltrated into the soil or discharged into receiving water bodies through storm sewer overflows (SSO's) or combined sewer overflows (CSO's).

1.2 Gully pots

Gully pots, also known as catch basins in North America (Ellis et al. 2004), convey runoff from urban impervious surfaces to urban drainage systems. The term gully pot refers to the presence of a sand trap, which is the volume below the outlet pipe (see **Figure 1.1b**). The sand trap can be thought of as an interceptor acting as a small settling tank, in which the solids accumulate to reduce the solids loading to the downstream drainage system. The objective of a gully pot is

therefore twofold, namely 1) to convey runoff to the drainage system with minimal hydraulic losses, while 2) removing the entrained solids.



(a)

(b)

Figure 1.1. (a) Photo of a gully pot; (b) Schematic drawing of a corresponding gully pot.

However, due to the accumulation of the removed solids in the sand trap, the hydraulic capacity reduces (Silvagni and Volpi 2002; Bolognesi et al. 2008), which could induce flooding and consequently substantial damage (Spekkers et al. 2013) and public health risks through flooding itself and spreading of pollutants (De Man et al. 2014).

Emptying these sand traps, which is usually done once a year in residential areas and two to four times a year at vulnerable places like markets in The Netherlands (Ten Veldhuis and Clemens 2011), is a vital and cost-effective (Ashley et al. 2000) sewer asset management measure to protect a liveable environment in urban areas. The fact that gully pots blockages are a dominant cause of urban flooding (Caradot et al. 2011; Ten Veldhuis and Clemens 2011) calls for the optimisation of maintenance strategies, since the choice for the cleaning interval is based on available budget, the vulnerability of the drained area, or expert judgement, rather than quantitative data (Post et al. 2017). The cyclic cleaning costs amount to 26 million euros per year in the Netherlands (Post et al. 2017), equivalent to 1.5 euro/inhabitant.

Moreover, gully pots also do not hold back all suspended solids from runoff (Lager et al. 1977; Butler and Karunaratne 1995). The removal efficiency seems to decrease due to the accumulation of removed solids (Post et al. 2016), which implies that the solids loading to the downstream drainage system increases over time. Therefore, effective maintenance of gully pots should not only prevent gully pot blockages, but also prevent the loss of removal efficiency,

which is expected to reduce the costs of solids' removal from drainage pipes, support the efficiency of Waste Water Treatment Plants (WWTP's), and help safeguard the quality of receiving water bodies.

The blockage process of gully pots is largely unknown (Ten Veldhuis et al. 2009) and so is the reduction in the removal efficiency. Therefore, even an approximate quantification of the timescale of these processes would support the choice for the cleaning interval of the sand trap. This requires the quantification of the transport of solids to gully pots and the removal efficiency of solids by gully pots.

1.3 Transport of solids to gully pots

1.3.1 Field measurements

The composition of solids present in urban areas depends on the characteristics and conditions of the area (Xanthopoulos and Augustin 1992). The solids originate from various sources, such as: local traffic (Barrett et al. 1998; Brunner 1975; Kerri et al. 1985; Wada et al. 1996; Deletic et al. 2000; Simperler et al. 2019), atmosphere (Galloway et al. 1982; Sabin et al. 2006), construction activities (Ashley and Crabtree 1992; Broeker 1984), weathering of buildings (Jartun et al. 2008), animal wastes (Brinkmann 1985), trash (Brinkmann 1985), de-icing grit (Simperler et al. 2019), and vegetation (Welker et al. 2019; James and Shivalingaiah 1985). Many of these sources have a seasonal pattern, in particular the effects of vegetation (Pratt and Adams 1984; Ellis and Harrop 1984) and de-icing (Simperler et al. 2019).

Street sweeping is applied in most urban areas for aesthetic and hygienic purposes, but is also regarded as a sink for solids present on streets and consequently for the solids loading to gully pots (Sartor and Boyd 1972; Sutherland and Jelen 1997; Amato et al. 2010; Hixon and Dymond 2018). However, the significance of this effect for the solids loading to drainage systems is under debate in literature.

Street sweeping is more effective for gross solids than small solids (e.g. Walker and Wong 1999; Pitt et al. 2005; Amato et al. 2010). Sartor and Boyd (1972) found that street sweeping can remove up to 80% of particles >2 mm under test conditions (i.e. by sweeping more frequently than the occurrence of rainfall events and effective use of parking restrictions). Bender and Terstriep (1984) found that the average street load reduced by 50% by increasing the sweeping frequency from 0 to 3 times a week, while Pitt (1979) concluded that typical street cleaning programs (once or twice a month) removed <5% of the total solids.

Bender and Terstriep (1984) concluded that the street cleaning operations tested would decrease the concentration of solids in runoff by a maximum of 10%. The statistical analysis also showed that frequent rain events were probably more effective than street sweeping in keeping the streets clean. Walker and Wong (1999) concluded that the benefits of increasing the frequency of street sweeping, beyond what is required to meet aesthetic criteria, are expected to be small in relation to the solids loading. Grottke (1987) even concluded that in some cases the reservoir of free solids on streets increased due to street sweeping. The brushes released part of the fixed load which is not entirely removed by the vacuum cleaner of the street sweeper vehicles. Street sweeping is likely to be effective in removing gross pollutants, while it has an adverse impact on finer materials by loosening them from the surface and making them available for wash-off during a next storm event (Vaze and Chiew 2002).

Vaze and Chiew (2002) concluded that the spatial variation of the solids load within a street is high, since the correlation between the solids load on areas of 0.5 m², which they vacuum cleaned and manually brushed, was low. Large areas need to be monitored to identify the typical solids load and composition on a street. This solids load can be described by the mass and the composition of the solids. Philippe and Ranchet (1987) reported solids deposition rates between 1.4 and 4.5 kg·day⁻¹·ha⁻¹ for residential areas in France.

The composition of the solids load can be described in terms of the solids' sizes, density, and organic content. Bertrand-Krajewski et al. (1993) found in their literature review 300< D_{50} <400 µm, Lau and Stenstrom (2005) 200< D_{50} <350 µm, Droppo et al. (2006) 120< D_{50} <660 µm, Zafra et al. (2008) 100< D_{50} <360 µm, and Gelhardt et al. (2017) 200< D_{50} <550 µm. Butler et al. (1992) reported densities between 2100< ρ <2510 kg/m³. Welker et al. (2019) found organic fractions of 0.18-0.34 for particles between 0-2000 µm and 0.45 – 0.64 for particles between 2000 – 8000 µm for areas with high vegetation (distinguished by the tree canopy coverage), and Gromaire-Mertz et al. (1999) reported fractions of 0.40 to 0.70 in street runoff.

The transport of the solids by runoff results in grading (e.g. Walker and Wong 1999; Vaze and Chiew 2002), which implies that the composition of solids entering the drainage system is not equal to the composition of solids present on streets. Pratt and Adams (1984) concluded that the magnitude of the solids loading to the drainage system depends on factors related to the transport, rather than on factors related to the availability of solids on the street. Shivalingaiah and James (1984) concluded that the maximum rain intensity is the parameter which is correlated strongest to the mass of the solids loading on the scale of a single rainfall event. The rain volume or event duration are also correlated to the solids loading and are sometimes

included in models representing the solids loading on the scale of an entire storm or several consecutive storms (e.g. Ellis and Harrop 1984; Pratt and Adams 1984).

Monitoring data on the solids loading to drainage systems, in particular covering all seasons and a number of sites/a large surface area, are scarce. Pratt and Adams (1984) monitored 5 drainage inlets for 9-12 months, Ellis and Harrop (1984) monitored 2 drainage inlets during spring and summer, Sansalone et al. (1998) monitored 13 rain events spread over 2 years at 1 drainage inlet, and Hong et al. (2016) monitored 1 drainage inlet for 6 months.

Pratt et al. (1987) provided some insight into the variability of the solids loading, based on the results of Pratt and Adams (1984). The spatial variation could not be attributed to any physical parameter, while the temporal variation could be partially explained by rainfall and seasonal variations. The maximum loadings were observed in June, “when soil surfaces dried and water- or wind-mobilised material was readily available, because of gardening and other human and animal activities.” The minimum loadings were observed after June and until February “as outdoor activities decreased; soils became wetter, binding particles to surfaces; and available plant matter was limited.” In November and December, leaf abscission increased the solids loading to some gully pots. “Around February-March snow and freezing conditions resulted in an increase in supply, either as a result of road gritting, or during the thaw when frost-loosened material was transported to gullies.” Ellis and Harrop (1984) found the maximum solids loadings during summer and reported peak values of $1.1 \text{ kg}\cdot\text{day}^{-1}\cdot\text{ha}^{-1}$. The minimum loadings ($0.032 < L < 0.67 \text{ kg}\cdot\text{day}^{-1}\cdot\text{ha}^{-1}$) were observed in spring.

1.3.2 Modelling

The solids loading to drainage systems is usually modelled with Build-Up and Wash-Off (BUWO) models (e.g. Sartor and Boyd 1972; Pitt 1979; Egodawatta et al. 2007; Muthusamy et al. 2018). These describe the solids build-up on urban surfaces and the wash-off to drainage systems by rain. Some of these models are implemented in urban hydrodynamic models (such as SWMM, Infoworks ICM, and MIKE URBAN) and are applied both to large catchments (e.g. Bonhomme and Petrucci 2017) and small scale lab setups (e.g. Naves et al. 2020). Therefore, from a technical perspective, these models could also be used to model the solids loading to individual gully pot catchments (order of magnitude 100 m^2).

BUWO models contain physical parameters such as the rainfall intensity and the antecedent dry weather period, and some calibration parameters that are not unambiguously linked to physical quantities or processes (grey-box models). A classical BUWO model (labelled as such by

Bonhomme and Petrucci 2017) involves four calibration parameters, and assumes that the wash-off is a source limited process and is non-linearly dependent on the runoff. It also assumes that the build-up occurs during the dry weather period, which grows exponentially to a maximum (which was observed by Chow et al. 2015). The model is represented by the following equations:

$$\frac{dM}{dt} = k_B(B_{max} - M_0) \cdot e^{k_B t_{ADWP}}, \text{ if } R_i(t) = 0 \quad (1)$$

$$\frac{dM}{dt} = k_W \cdot Q(t)^{N_W} M(t), \text{ if } R_i(t) \neq 0 \quad (2)$$

In which M (in kg/m^2) is the solid load on the street, k_B (in day^{-1}) the growth parameter of the build-up, B_{max} (in kg/m^2) the parameter representing the maximum possible load on the street, M_0 (in kg/m^2) the residual mass after the last rain event, t_{ADWP} the time (in days) of the antecedent dry weather period, R_i (in mm/hour) the rain intensity, k_W the wash-off rate parameter, Q (in mm/hour) the runoff, N_W the wash-off exponent. If the delay of runoff due to overland flow is set to zero (which is acceptable for relatively small gully pot catchments):

$$Q(t) = R_i(t) \quad (3)$$

Although BUWO models are widely applied, the outcome of model validation is often unsatisfactory (e.g. Gaume et al. 1998; Bonhomme and Petrucci 2017). Detailed monitoring data on the solids loading to drainage systems/gully pots could support the analysis of the problems with BUWO models.

1.4 Solids accumulation in gully pots

Naves et al. (2019) demonstrated that wash-off and transport in a drainage system cause grading in the sizes of the solids. To replicate these processes a lab experiment with an artificial street including two identical gully pots (at different locations) and a small pipe system was performed. An initial load of sand was placed on the street surface and consecutively artificial rainfall events were created (of several intensities) for 5 minutes. **Figure 1.2** shows the effect of several rain storm intensities on the particle size distribution (PSD) in different parts of the drainage system. The solids at the outlet are smaller than the solids on the road surface and the solids settled in the gully pots are generally larger than the solids on the road surface.

Table 1.1 presents an overview of reported D_{50} values in literature of solids at different sampling locations.

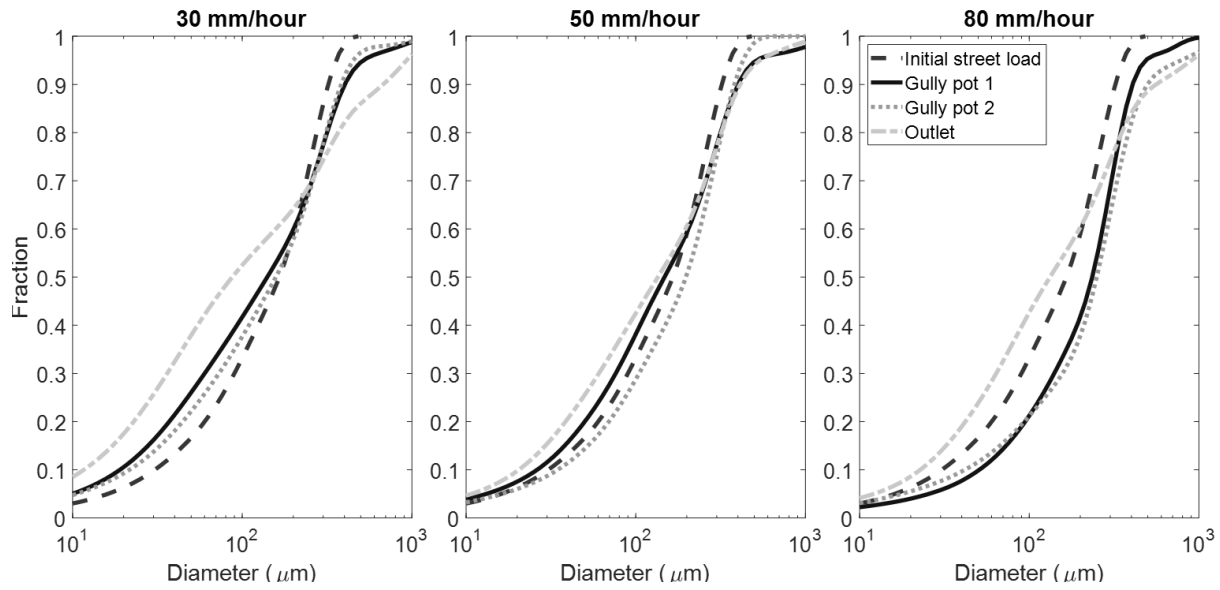


Figure 1.2. The particle size distribution after a rainfall event depends not only on the initial street load, but also on the rainfall characteristics and the sampling location. The finest particles can be found at the outlet of the system, and larger particles can usually be found in the sand traps of the two gully pots. Source: Naves et al. (2019).

The results of Grottker (1990) show that the organic content of the solids in gully pots is 6 to 10% larger in autumn than in spring. Chen et al. (2017) revealed through maintenance records of gully pots that >50% of citizens' complaints on gully pot blockages were made in autumn, indicating that leaf abscission influences the chance on gully pot blockages.

Post et al. (2016) monitored the bed level of the accumulated solids in 300 gully pots over a period of 15 months. Roughly 5% of the gully pots got progressively filled with solids and eventually got blocked. The sediment bed levels in the remaining 95% asymptotically grew to an equilibrium, indicating that the removal efficiency tends to zero due to an increasing sediment bed level. Consequently, the transport of solids to the drainage system increases over time, which is confirmed by Langeveld et al. (2016), who showed that the mass of removed solids increased by a factor 3 by cleaning out gully pots six times per year instead of once a year.

Table 1.1. Reported D_{50} values of solids at different sampling locations.

Location	D_{50} (μm)	Measurement method	Reference
Street	200 – 550	Combination of dry and wet sieving	Gelhardt et al. (2017)
Street	100 – 360	Combination of dry and wet sieving	Zafra et al. (2008)
Street	200 - 350	Dry sieving	Lau and Stenstrom (2005)
Street	300 - 400	Various	Bertrand-Krajewski et al. (1993)
Gully pot inflow	680	Wet sieving	Pratt and Adams (1984)
Gully pot inflow	350 – 800	Dry sieving	Sansalone et al. (1998)
Gully pot inflow	600 – 1000	Wet sieving	Ellis and Harrop (1984)
Gully pot settled	1500	Not reported	Pratt and Adams (1984)
Gully pot settled	400	Wet sieving	Grottker (1990)

1.5 Gully pot removal efficiency

The accumulation rate of solids in gully pots depends on the solids loading to the gully pot and the removal efficiency of the solids by the sand trap. This removal efficiency has been studied by several researchers. Lager et al. (1977) found in their lab studies that the efficiency is proportional to the diameter of the particles, and inversely proportional to the discharge. Grottker (1990) observed similar relations in field and lab experiments and proposed the following empirical relation:

$$\varepsilon = a \cdot Q^b \quad (4)$$

In which ε is the removal efficiency, a and b are empirically determined parameters depending on the sediment size, and Q is the discharge.

Sartor and Boyd (1972) simulated the erosion process due to rain in gully pots with a substantial sediment bed level. It was found that even in the case of a heavy rain event lasting 1 hour, only about 1% of the mass of the sediment bed was eroded and subsequently removed. Butler and Karunaratne (1995) studied the effect of an increasing sediment bed level by lab experiments on a gully pot with a sand trap depth of 40 cm and a false bottom to simulate the increasing bed level. The false bottom was covered with sand and placed at heights of 20, 30, and 40 cm (implicitly assuming a flat sediment bed development). The bed level hardly affected the removal efficiency and continuous resuspension was only observed for the tests with the smallest particles, highest flow rate, and thickest sediment bed (D_{50} of 68 μm , a bed height of 40 cm, and a discharge of 1.5 L/s or a surface loading of 35 m/h).

Since in both studies the sediment bed level hardly affected the removal efficiency, this process was not incorporated in the removal efficiency model proposed by Butler and Karunaratne (1995). They regarded the removal of solids as a trade-off between surface loading and settling velocity, implicitly assuming complete mixing in the gully pot. The settling velocity was quantified by application of Stokes' law:

$$\varepsilon = \frac{\alpha w_s}{\alpha w_s + \frac{Q}{A}} \quad (5)$$

$$w_s = \frac{g d^2 \left(\frac{\rho_s - \rho_w}{\rho_w} \right)}{18\nu} \quad (6)$$

In which w_s is the settling velocity, A the free water surface area of the gully pot, d the particle diameter, ρ_w is the density of water, ρ_s is the density of the particle, and ν is the kinematic viscosity. The factor α (set at 0.6 to obtain an acceptable agreement with the experimental results of Butler and Karunaratne 1995) accounts for the effect of turbulence, since Stokes' law is applicable for $Re < 0.1$.

Butler and Memon (1998) proposed a model which includes resuspension of the sediment bed at the start of a rain event, but does not include the effect of a growing sediment bed in later stages. The gully pot is assumed to function as a completely mixed reactor in which sedimentation and resuspension occur as described by:

$$\frac{dc_{rs}}{dt} = \frac{Q}{V} (f_{rs} c_{in} - c_{rs}) - \frac{w_{srs} A c_{rs}}{V} \quad (7)$$

$$\frac{dc_{ss}}{dt} = \frac{Q}{V} (f_{ss} c_{in} - c_{ss}) - \frac{w_{ss} A c_{ss}}{V} + \frac{R}{V} \quad (8)$$

In which c is the concentration, the subscripts rs and ss refer to readily settleable solids and slowly settleable solids, respectively, the subscript in refers to inflow, f is the fraction, V is the water volume (which reduces when the bed level increases), and R is the resuspension. The description of this resuspension was taken from Fletcher and Pratt (1981), who studied the resuspension of gully pot solids obtained from a gully emptying tanker.

$$R = 0.278 \cdot Q + 2.59 \cdot 10^{-5} \text{ for } t < \frac{M_r}{R} \quad (9)$$

In which M_r is the mass of suitable material for release, which is assumed to be known.

Instead of physically assessing the gully pot hydraulics, Yang et al. (2018) simulated the flow and removal of solids in a gully pot by means of Computational Fluid Dynamics (CFD). The removal efficiency was validated by some physical tests performed by Tang et al. (2016) (since only a few grams of sediment were used in these tests, the reduction of the removal efficiency due to an increasing sediment bed level, was not studied), which showed that the CFD model provided acceptable results for particles $\geq 250 \mu\text{m}$, while it overestimated the efficiency for smaller particles. The flow pattern of their CFD model was validated by the flow velocity measurements of Howard et al. (2012). However, the latter modelled a sump with a horizontal inlet, which results should not have been extrapolated to gully pots with a vertical impinging jet. Faram and Harwood (2003) also modelled the removal efficiency of gully pots and validated the results with a few physical tests of the removal efficiency, no validation of the velocity fields was reported.

1.6 Thesis objective

Gully pots have two main purposes, namely 1) removing runoff from urban built areas with minimal hydraulic losses and 2) maximal reduction of the solids loading to the downstream system. However, both the hydraulic capacity and the removal efficiency reduce over time due to an increasing sediment bed level. Insight into these processes is required to quantify the timescale of these processes, which would support the choice for a maintenance strategy (Swanson 2001).

This is a relevant issue, since it involves a significant part of the maintenance budget of municipalities. Ten Veldhuis et al. (2009) reported for example that in two Dutch cities (Breda and Haarlem) 15% of the total maintenance budget is spent on preventive cleaning and 5% on reactive cleaning of gully pots.

Despite the relevance, most of the studies related to this topic are performed in the 80s and 90s and include limited observations and timespans, and outdated statistical methods and/or measurement techniques. Therefore, the generalisability of the conclusions from these studies is limited.

The objective of this study is to quantify the processes that influence the accumulation rate of solids in gully pots, which will be based on large datasets, and new measurement and statistical techniques. Four research questions have been formulated to meet the study objective:

1. What is the solids loading to gully pots in terms of mass and composition?
2. Does street sweeping reduce the solids loading to gully pots?
3. What is the removal efficiency of solids of a gully pot?
4. How do the in-gully-pot hydraulics influence the removal efficiency?

1.7 Thesis outline

The work in this thesis is divided into three parts and eight chapters (see **Figure 1.3**), which can be read separately. The first part describes the transport of solids to gully pots and consists of a monitoring campaign on the solids loading to gully pots (chapter 2) and evaluates methods to model this loading (chapter 3). The second part presents a monitoring campaign and statistical models on the accumulation of solids in gully pots (chapter 4). The third part is dedicated to the gully pot hydraulics and consists of a study of the removal efficiency (chapter 5) and a study of the flow field in a gully pot (chapter 6). Chapter 7 presents the synthesis and discussion of the combined results of all studies, while chapter 8 summarises the general conclusions and recommendations.

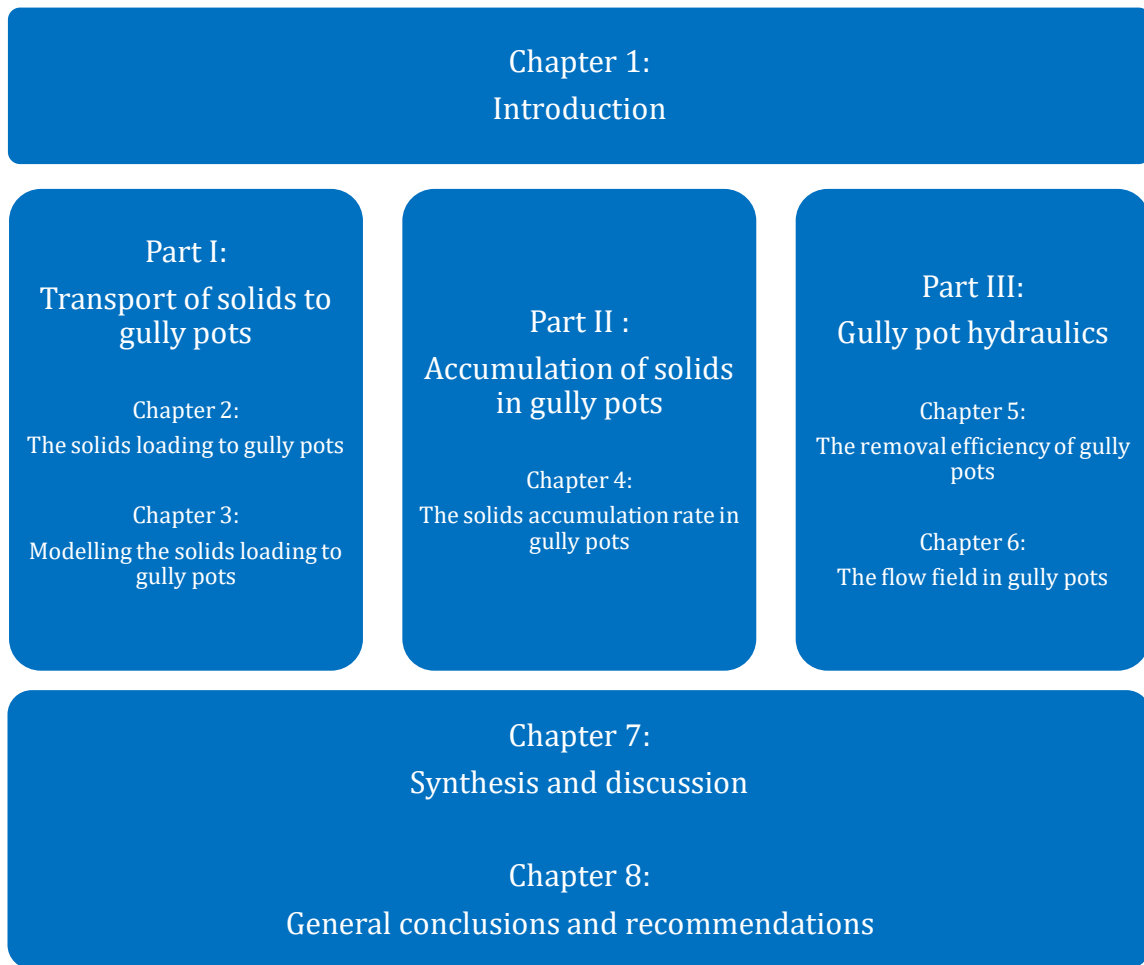


Figure 1.3. Thesis outline.

PART I: TRANSPORT OF SOLIDS TO GULLY POTS

2 THE SOLIDS LOADING TO GULLY POTS

2.1 Introduction

The solids that are transported to gully pots originate from urban surfaces. Vaze and Chiew (2002) concluded that the spatial variation of the solids load on these surfaces is high, since the correlation between the solids load on areas of 0.5 m², which they vacuum cleaned and manually brushed, was low. Consequently, the solids loading to gully pots is highly variable, both spatially and temporally (Pratt et al. 1987). Large areas/a number of sites need to be monitored to identify the typical composition and mass flux of the solids loading to gully pots.

This chapter aims to provide insight into the drivers and the dynamics of the solids loading, both in mass and composition, to gully pots over time, by means of a monitoring campaign with a newly designed measurement device, which has been applied to 104 gully pots for a period of 2 years. The results provide information on the variability and predictability of build-up and wash-off related processes. While this chapter focusses on the dynamics of the solids loading to a set of gully pots or from a catchment, chapter 3 also analyses the difference between the individual gully pots by modelling the solids loading to them.

2.2 Methods

2.2.1 Experimental setup

Pratt and Adams (1984) and Ellis and Harrop (1984) developed a method consisting of a stack of 5 sieves in gully pots to filter the solids out of the runoff, which does not hinder the upstream

runoff and applied it to 5 and 2 gully pots, respectively. A similar, but even less labour intensive system consisting of only one filter per gully pot was applied in this study, since a substantial number of sampling locations and a long monitoring period is required to be able to reliably represent an urban catchment and include seasonal and meteorological variations.

The pore size of 50 μm of the filter applied is a trade-off between two conflicting interests, namely a minimum pore size to keep the hydraulic capacity of the gully pot sufficient, and a maximum pore size to remove most solids from the runoff. The scarce literature on the size distribution of solids flowing into gully pots suggests that most solids are filtered out with this pore size: Sansalone et al. (1998) found that solids $<50\ \mu\text{m}$ contributed in all samples less than 8 mass%, Pratt and Adams (1984) (who collected solids $>90\ \mu\text{m}$) concluded that 8 mass% of the solids was $<400\ \mu\text{m}$, and Ellis and Harrop (1984) (who collected solids $>60\ \mu\text{m}$) concluded that 10 mass% of the solids was $<400\ \mu\text{m}$. Therefore, the collected mass should be regarded as a lower limit, but close to the real value of the solids loading to a drainage system.

The hydraulic capacities of both a nylon and a stainless steel filter were evaluated during an initial test period of approximately 3 months at the monitoring area. The nylon filter bags were selected for the study, since the steel filters proved to be very susceptible to rapid clogging (likely to be contributed to the cohesive nature of the sediment/metal interface) which induced local flooding. These tests proved that filter characteristics change over time due to the filtered material which acted as a secondary filter. This effect was significantly smaller for the nylon filters than for the steel filter, but its magnitude remained unknown.

The filters (with a diameter of 18 cm and a length of 50 cm) were attached to metal plates that were installed in the gully pots **Figure 2.1b**). These plates were sealed off around the gully pot wall to prevent solids bypassing the filters. 104 gully pots were monitored being a trade-off between a feasible maximum number for data collection and a minimum number for a reliable representation of the solids loading to the drainage system in an urban catchment.

2.2.2 Monitoring area

The monitoring area was located in a relatively new residential area (the construction started in 2000), named Nesseland, in the Northeast of the city of Rotterdam. Rotterdam is the second-largest city in The Netherlands (in terms of population), has a maritime climate with cool summers and moderate winters, and a rainfall of 870 mm/year during the monitoring campaign. The monitored impervious area is 1.1 ha, consists of bricks, and has no significant cardinal slope (as can be seen in **Figure 2.1c**), therefore the flow is driven by local gradients.

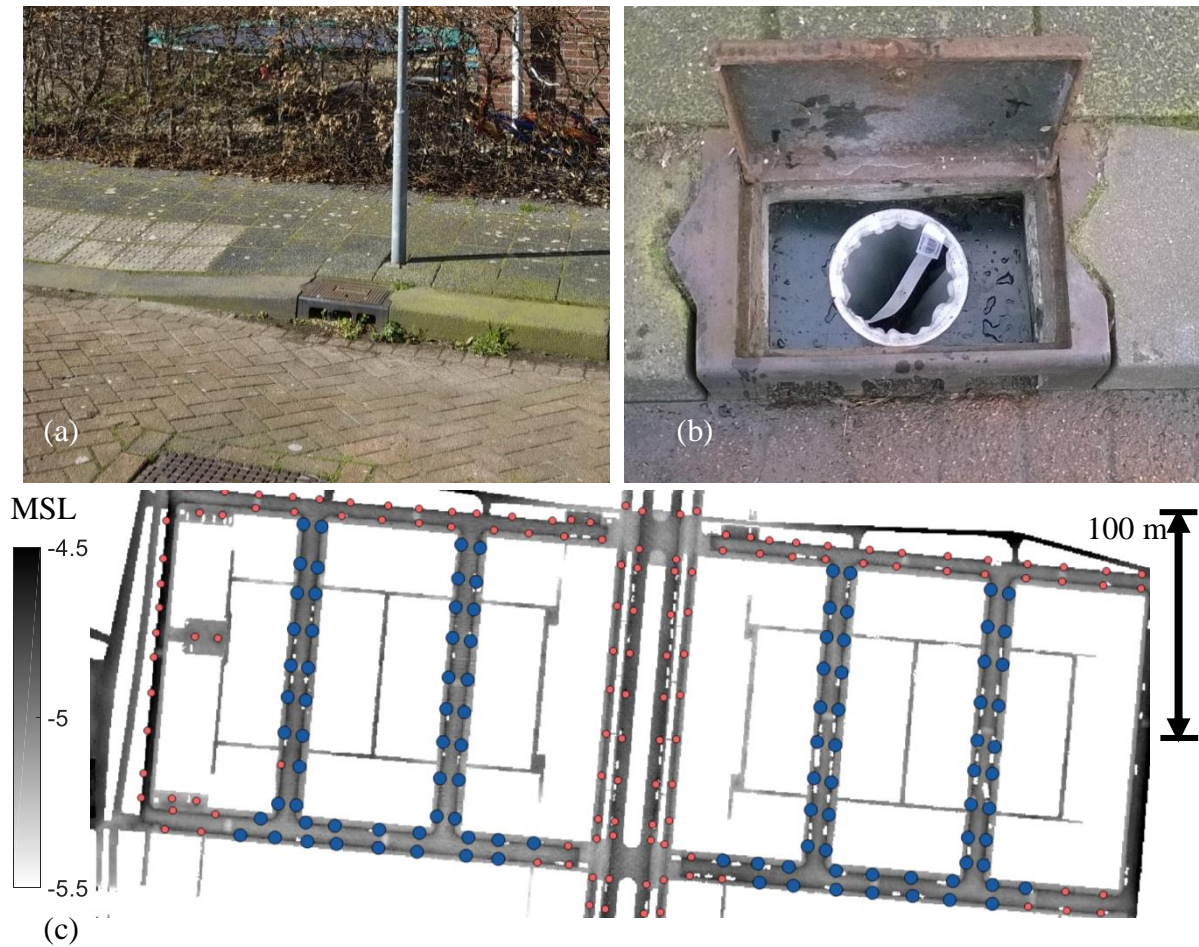


Figure 2.1. (a) Gully pot in the monitored streets; (b) Experimental setup in the gully pot; (c) Altitude street map of the monitoring area in which the blue dots indicate the selected gully pots and the red ones not selected gully pots.

This particular neighbourhood was selected since most gully pots in this area have a similar geometry (which made a uniform design of the experimental setup possible) and the land use is homogeneous (which made comparisons between the eastern and western side of the monitoring area possible). The locations of the gully pots are shown in **Figure 2.1c**.

2.2.3 Data collection and analysis

After an initial period of approximately 3 months of testing the methods, materials, and protocols, measurements were performed from April 2018 till April 2020. The filters were emptied every ~3-4 weeks, both to prevent clogging of the filters and to identify the time dependency of the solids loading. An overview of the analyses during each monitoring period is provided in **Figure 2.2**.

Since the presence of a seasonal periodicity is suspected because of the solids' reservoir on urban surfaces, in particular by inducing leaf abscission from deciduous trees, photos were made during the monitoring period (see Appendix D) to determine the actual status of the vegetation. Following Halverson et al. (1985), four tree phases are distinguished, namely 'leaf growth', 'full capacity', 'leaf abscission', and 'no leaves'.

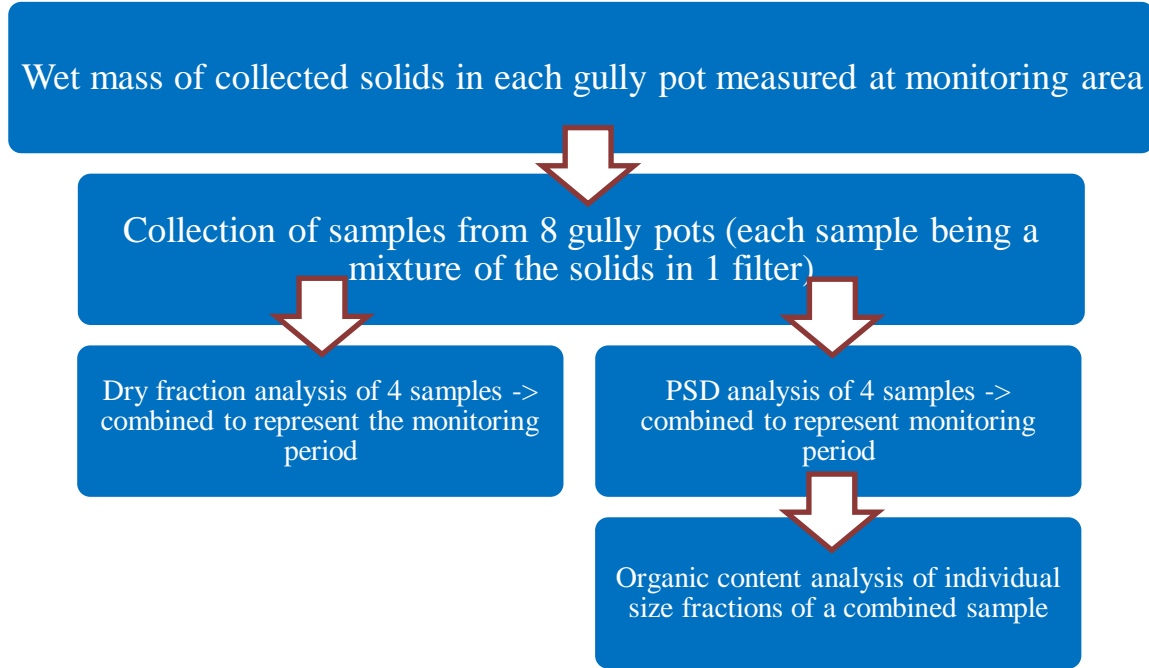


Figure 2.2. Experimental procedure during each of the 31 monitoring periods.

2.2.3.1 Solids loading

The wet masses of the collected solids are registered at the monitoring area. The dry masses were estimated by multiplying the average dry fraction with the wet mass for each gully pot. The average dry fraction for each monitoring period was determined by drying 4 samples in an oven at 105 °C. This drying protocol and estimation of the dry mass are identical to the procedure followed by Butler et al. (1992). The solids loading ($\text{kg} \cdot \text{day}^{-1} \cdot \text{ha}^{-1}$) is defined as:

$$L = \frac{f_d \cdot \sum_i m_w(i)}{\Delta t \cdot \sum_i A(i)} \quad (1)$$

In which f_d is the dry fraction, $m_w(i)$ the wet mass of filter i , Δt the length of the corresponding monitoring period, and $A(i)$ the (paved) catchment area of gully pot i . The uncertainty is defined as (the covariance between the parameters and the uncertainty in the measurement interval are taken to be negligible):

$$u(L) = \sqrt{\left(\frac{\Sigma_i m_w(i)}{\Delta t \cdot \Sigma_i A(i)} u(f_d)\right)^2 + \left(\frac{f_d}{\Delta t \cdot \Sigma_i A(i)} u(\Sigma_i m_w(i))\right)^2 + \left(\frac{f_d \cdot \Sigma_i m_w(i)}{\Delta t \cdot \Sigma_i A(i)^2} u(\Sigma A(i))\right)^2} \quad (2)$$

In which the uncertainty (95% confidence interval) in f_d is estimated at $\pm 30\%$, which is estimated based on the observed variability of this parameter for different gully pots during the same measurement day. The uncertainty (95% confidence interval) in $\Sigma_i m_w(i)$ is determined by 2 times the standard error in the solids loading to the individual gully pots. The impervious catchment area for individual gully pots is determined by application of the eight-direction flow approach (Jenson and Domingue 1988) on a Digital Elevation Model (DEM) provided by the municipality of Rotterdam. This DEM is obtained by laser altimetry measurements in 2016 and has a spatial resolution of 0.5 x 0.5 m. Errors in this dataset caused by cars on the street have been filtered out by kriging. The summed catchment areas of all gully pots, which is part of the equation, is equal to the impervious area of the catchment.

This impervious area is registered in the Basisregistratie Grootschalige Topografie [Register of Large-Scale Topography] of the Dutch government, which states that the uncertainty in the position of the objects in this register is ± 0.2 m. Considering streets with a width of ~ 10 m, some impervious areas in front gardens (which is not part of the register) that could contribute to the runoff, and some permeable areas in front gardens that could handle some runoff from the streets, the uncertainty in the summed catchment area is estimated at $\pm 10\%$ (95% confidence interval).

2.2.3.2 Particle size distribution

Butler et al. (1992) subjected samples from streets and gully pots to a dry sieving procedure to obtain the Particle Size Distribution (PSD). However, this method proved to be unsuitable in this study, since it changed the PSD, mainly due to the agglomeration of particles during the drying process. Instead of dry sieving, wet sieving was applied to determine the PSD.

In the work presented here, sieves with mesh sizes 53, 300, 1180, 1800, 4750, 14000, and 50000 μm were used. With this number and type of sieves, a relatively smooth PSD curve could be obtained of the samples. The 300 and 1180 μm sieves were added after almost one year to improve the PSD curve, since a large mass fraction proved to be < 1800 μm . After sieving the subsamples were dried at 105 °C and the PSD was obtained based on the dry mass.

For each monitoring period, the PSD is obtained for 4 different samples. These 4 PSDs are combined into 1 PSD to represent the typical PSD for the corresponding monitoring period. Therefore, the samples need to be representative for all gully pots. Since the variance in the 4

PSDs proved to be relatively large, the uncertainty in the combined PSD needs to represent the possible variability of all gully pots rather than the uncertainty in the individual PSD. Based on the observed variability, the relative uncertainty (95% confidence interval) in the fraction collected at each of the 7 sieves is estimated at ± 0.2 of the total mass in the combined PSD.

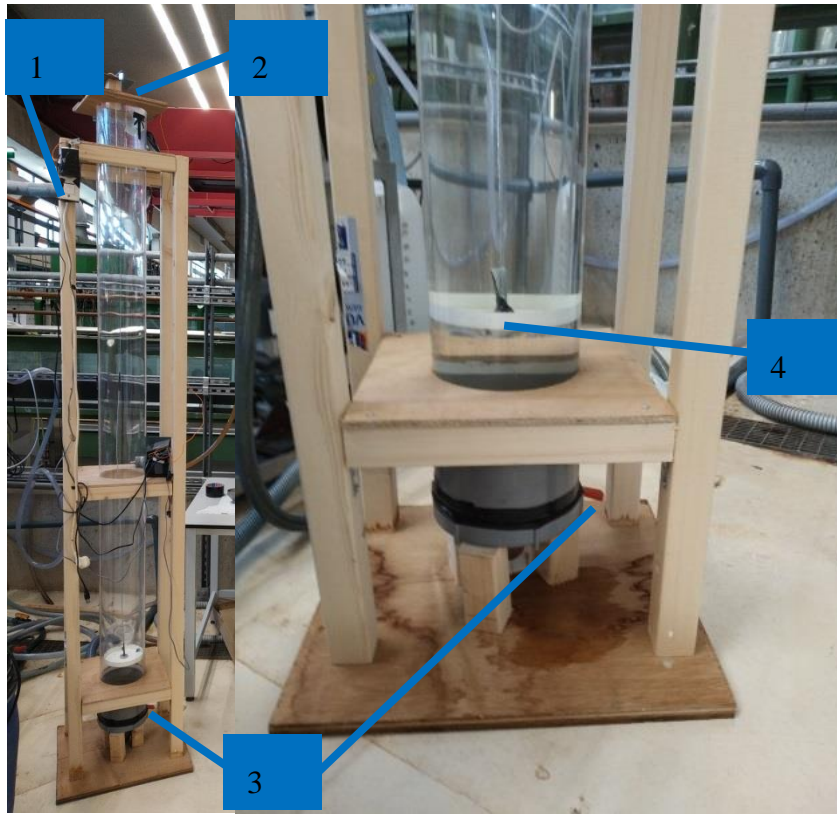
2.2.3.3 Organic content

The 7 remaining subsamples from each of the 4 samples used in the PSD analysis, were combined into 7 samples of different size fractions to analyse the organic content per size fraction. The organic content was assumed to be equal to the mass loss during a burning process in an oven at 600 °C, following the protocol by Melanen (1981). The relative uncertainty (95% confidence interval) of this burning procedure for each size fraction is estimated at ± 0.1 of the total mass.

2.2.3.4 Settling velocity

Solids transported to gully pots have a wide variety of sizes, shapes, and densities and consequently a wide variety of settling velocities. This is of importance for the accumulation rate of particles in gully pots, drainage pipes, etc. The settling velocity is determined for solids $< 1800 \mu\text{m}$, since larger solids would disturb the measurement (and a sieve of $1800 \mu\text{m}$ was used to determine the PSD).

The expected settling velocity of some of these particles is relatively high. For example, the settling velocity of sand particles with a diameter of $1000 \mu\text{m}$, quantified using the universal drag coefficient for spheres (e.g. Terfous et al. 2013), is $\sim 0.16 \text{ m/s}$. The particles with these relatively high settling velocities make it an unpractical task to obtain a reliable velocity distribution curve with common measurement devices, including the relatively small VICAS setup or conventional settling columns with taps at the side. Therefore, a new device was developed, which is shown in **Figure 2.3**. This device measured the settled mass on a disk close to the bottom of a transparent settling column.



(a)

(b)

Figure 2.3. (a) Settling column; (b) Close-up of the bottom part of the settling column. 1. Switch to start measurement. 2. Weighing scale. 3. Emptying tap. 4. Dish connected to the weighing scale.

Before the measurement started the column was filled from the top with water. A wet sample was carefully dropped from a cup into the column and the measurement was started simultaneously with a switch (at ‘1’ in **Figure 2.3**). The settling column (of 2 m in height) contained a dish close to the bottom of the column (at ‘4’ in **Figure 2.3**) which was connected with a force meter (at ‘2’ in **Figure 2.3**), which continuously measures the settled mass (minus the buoyancy). The force meter was a Saintbond Mini 046 with a range of 0.250 kg. The uncertainty of the weighing construction was estimated at ± 0.5 g (95% confidence interval).

Since the weighing scale measured the mass of the settled particles minus the buoyancy, the variation in density should not be too large, to avoid underestimation of the mass of low-density solids compared to high-density solids. The mass is converted into a relative mass as following:

$$m_{rel}(t) = \frac{m(t) - m(t_0)}{m(t_{end}) - m(t_0)} \quad (3)$$

In which m is the mass measured by the weighing scale, t_0 is the start time, and t_{end} is the end time of the experiment. The relative mass over time (which is smoothened with a moving median and moving average filter with a length of 1 second) is transformed into a velocity distribution curve by the following two transformations:

$$F = (1 - m_{rel}) \quad (4)$$

$$v = \frac{H}{t} \quad (5)$$

In which F is the cumulative velocity distribution curve and v the corresponding settling velocity. The validation of the settling column was performed by comparing the PSD obtained by dry sieving and by the settling column of 3 different size fractions of spherical glass beads, with a density of 2500 kg/m^3 and an uncertainty of $\pm 4\%$ (95% confidence interval as provided by the manufacturer) in the density. The settling velocity curves of these glass beads fractions were obtained 13 times in total and resulted in graphs as shown in **Figure 2.4**.

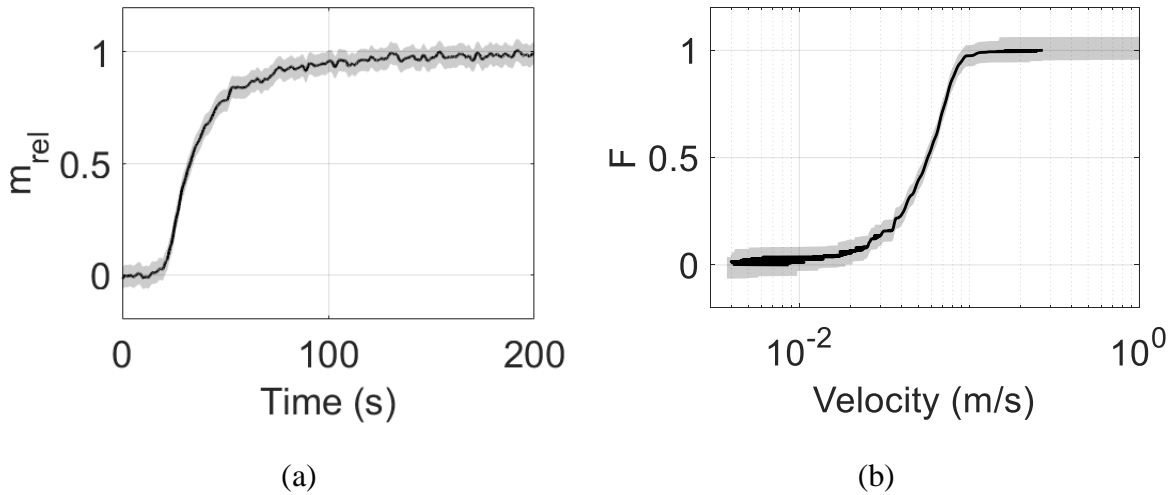


Figure 2.4. (a) Relative mass over time measured by the settling column; (b) Settling velocity curve and its confidence interval. The confidence intervals originate from the uncertainty of the force meter.

The velocity distribution curves were transformed into size distribution curves for the validation by balancing the buoyancy force by the drag:

$$D = \frac{v^2 \rho_w}{g(\rho_s - \rho_w)} \cdot \frac{24}{32} \cdot C_d \quad (6)$$

In which D is the particle diameter, ρ the density, g the gravitational constant, and C_d the drag coefficient. The drag coefficient was obtained using the empirical relation of Terfous et al.

(2013), which represents the drag coefficient on a spherical particle with an uncertainty of $\pm 3\%$ (95% confidence interval):

$$C_d = A_1 + \frac{A_2}{Re} + \frac{A_3}{Re^2} + \frac{A_4}{Re^{0.1}} + \frac{A_5}{Re^{0.2}} \quad (7)$$

$$A_1 = 2.689, A_2 = 21.683, A_3 = 0.131, A_4 = -10.616, A_5 = 12.216 \quad (8)$$

In which A_i is an empirical coefficient and Re the Reynolds number. Re depends on the dynamic viscosity which is calculated via the empirical relation of Viswanath and Natarajan (1989):

$$\mu = 2.94 \cdot 10^{-5} \cdot e^{\left(\frac{508}{T-149.3}\right)} \quad (9)$$

In which T is temperature, and μ the dynamic viscosity. The temperature of the water was measured with an Extech TM20 with an uncertainty of ± 1 °C (95% confidence interval). The PSDs of the glass beads fractions were also obtained by dry sieving with an uncertainty of $\pm 10\%$ (95% confidence interval) in the sieve size. The comparison between the two methods is shown in **Figure 2.5**.

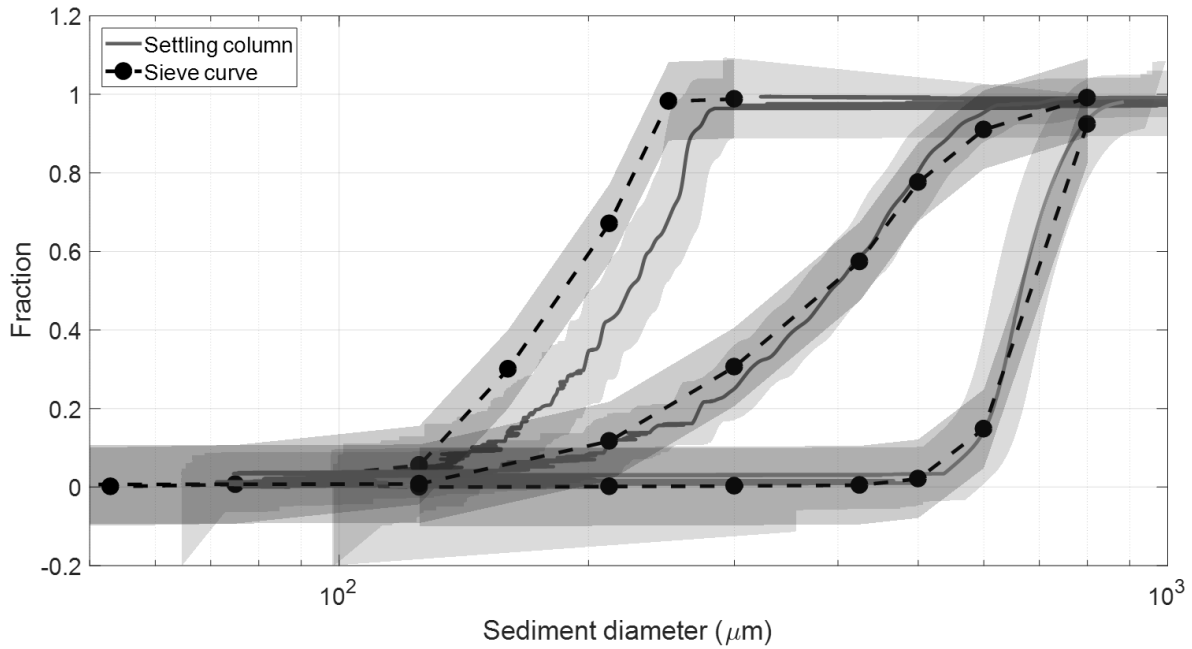


Figure 2.5. The settling velocity curves (as shown in **Figure 2.4**) are transformed into size distribution curves and compared with the 3 directly obtained sieve curves of the glass beads. The confidence intervals are based on the numerical propagation of the uncertainty in the settling velocity curve, the drag coefficient (depending on the uncertainty of the temperature and the uncertainty in the value itself), and the density.

The settling column provided similar results as the sieve analysis for the two larger size fractions, but overestimated the size (i.e. the settling velocity) of the smaller particles. Whether this overestimation originated from non-perfectly spherical particles, a systematic overestimation of the drag coefficient or the viscosity (i.e. the temperature), or non-ideal settling conditions was not determined.

2.2.3.5 Rainfall

Runoff transports solids from streets to the gully pot. Therefore, regressions are made between the solids loading and the rainfall. The rainfall data used in this article originate from the meteorological radar dataset of the Royal Dutch Meteorological Institute (KNMI). This dataset contains rain volume measurements on a grid with a spatial resolution of 1 km² and a temporal resolution of 5 minutes, which is the shortest time interval available. This short time interval is selected, since a gully pot catchment is relatively small, implying a short response time (typically in the order of minutes). As the monitoring area is relatively small, rainfall is considered to be spatially homogeneous within the monitoring area.

Information on the uncertainty in the data is not provided by KNMI and is therefore estimated by the author. The uncertainty in the rain volume (95% confidence interval) is estimated at $\pm 10\%$ in each time interval of 5 minutes (which is used to represent the rainfall intensity). The uncertainty in the cumulative rainfall volume for an entire monitoring period is estimated at $\pm 3\%$ (95% confidence interval).

2.2.3.6 Temperature

The air temperature measured (at a temporal resolution of 5 minutes) by a nearby weather station (at a distance of 4 km) is used to represent the approximate average daily temperature of the environment.

2.3 Results and discussion

2.3.1 Solids loading

2.3.1.1 Season and weather

The influence of season and weather on the solids loading is assessed for the western side of the monitoring area, since the eastern side was subjected to another street sweeping regime for 5 months, which effect is analysed in section 2.3.1.2. The western side contained 52 gully pots and the paved area connected to these gully pots was 5.300 m². During the monitoring

campaign, spanning 737 days, a total amount of 313 kg dry material was collected, resulting in a time-averaged solids loading of $0.80 \text{ kg} \cdot \text{day}^{-1} \cdot \text{ha}^{-1}$. This number is lower than the solids deposition on the street surface, which was reported by Philippe and Ranchet (1987) to vary between 1.4 and $4.5 \text{ kg} \cdot \text{day}^{-1} \cdot \text{ha}^{-1}$ in residential areas in France. Possible explanations for this difference could be, the removal of solids from the street by e.g. street sweeping or wind.

On some occasions, the filters contained divergent and/or illegally dumped material, e.g. concrete, wall plaster, and paint, which was registered. In some cases this could not visually be noticed, but the extraordinary high mass (which lower limit was set at three times the mean value of the corresponding monitoring period, which was chosen based upon the measurements) indicated illegally dumped material. These outliers were removed during the post-processing of the data to obtain the solids loading as shown in **Figure 2.6** and **Figure 2.7**, since these graphs link the solids loading to the rainfall and the materials found were most likely not transported by rain. This removal of outliers reduced the dataset from 1538 to 1478 observations.

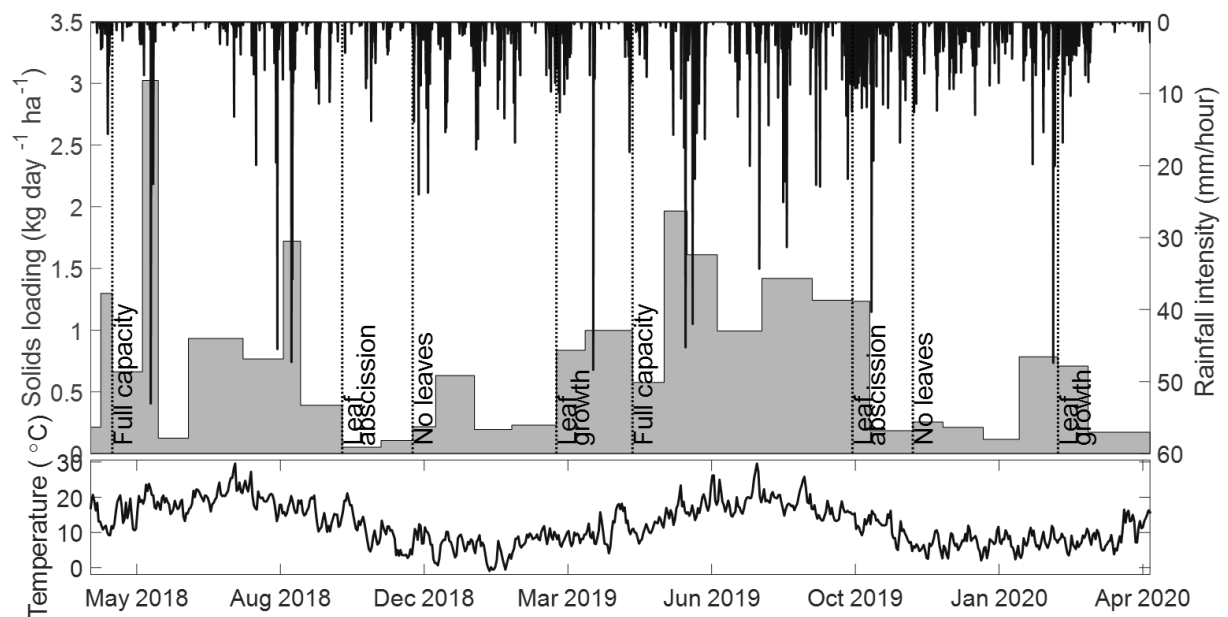


Figure 2.6. Solids loading, rainfall intensity (5-minute interval), tree phase, and day average temperature over time in the 52 gully pots in the western side of the catchment.

Figure 2.6 shows that the solids loading varies two orders of magnitude over the year. Most high values are observed in conjunction with the tree phases ‘leaf growth’ and ‘full capacity’ (roughly corresponding with spring and summer) in which $0.22 < L < 3.0 \text{ kg} \cdot \text{day}^{-1} \cdot \text{ha}^{-1}$ (except from the low solids loadings found in June 2018 and April 2020, which are likely due to a lack

of rainfall in those periods). Most low values can be found during the tree phases ‘leaf abscission’ and ‘no leaves’ in which $0.051 < L < 1.2 \text{ kg} \cdot \text{day}^{-1} \cdot \text{ha}^{-1}$. Initially, it was expected that the solids loading would show a peak during the ‘leaf abscission’ phase due to extra organic material available for transport, and there is increased transport of organic as will be discussed in section 2.3.2.2, but these materials may have such a low mass density that other processes dominate the solids loading expressed in terms of mass.

The difference between these two regimes, namely i) during the ‘leaf growth’ and ‘full capacity’ phase and ii) during the ‘leaf abscission’ and ‘no leaves phase’, might be explained by the temperature. **Figure 2.6** shows that the average daily temperature is highest during the ‘leaf growth’ and ‘full capacity’ phase. The temperature might influence the dryness of the soil and since dry soil is more prone to erosion than wet soil, the parameter ‘temperature’ might represent the erodibility of solids. The relation of the solids loading with the erodibility of solids was also suggested by Pratt et al. (1987) by analysing the results of Pratt and Adams (1984). It was concluded that the maximum loading occurred in June, “when soil surfaces dried and water- or wind-mobilised material was readily available, because of gardening and other human and animal activities.” They also stated that the solids loading between June and February decreased, due to decreased outdoor activities, wetter soils that bind particles to the surface, and limited available plant matter. While leaf abscission between November and December increased the solids loading in some catchments. “Around February-March snow and freezing conditions resulted in an increase in supply, either as a result of road gritting”.

Ellis and Harrop (1984), who monitored the solids loading to gully pots in area of 533 m^2 at a frequency of once in two weeks during spring and summer, found the maximum solids loadings during summer and reported peak values of $1.1 \text{ kg} \cdot \text{day}^{-1} \cdot \text{ha}^{-1}$, and somewhat lower loadings ($0.032 < L < 0.67 \text{ kg} \cdot \text{day}^{-1} \cdot \text{ha}^{-1}$) during spring. Those values are in the same order of magnitude as the ones found in the current study.

Wash-off models (such as Sartor and Boyd 1972; Pitt 1979; Egodawatta et al. 2007; Muthusamy et al. 2018) usually include the antecedent dry period and the rain intensity to estimate the solids loading. Since the observed parameter ‘solids loading’ is the integral of the build-up and wash-off processes over a couple of weeks, the rainfall volume could be considered as a parameter influencing the solids loading. In the current study, the solids loading proved to be correlated strongest to the rainfall intensity.

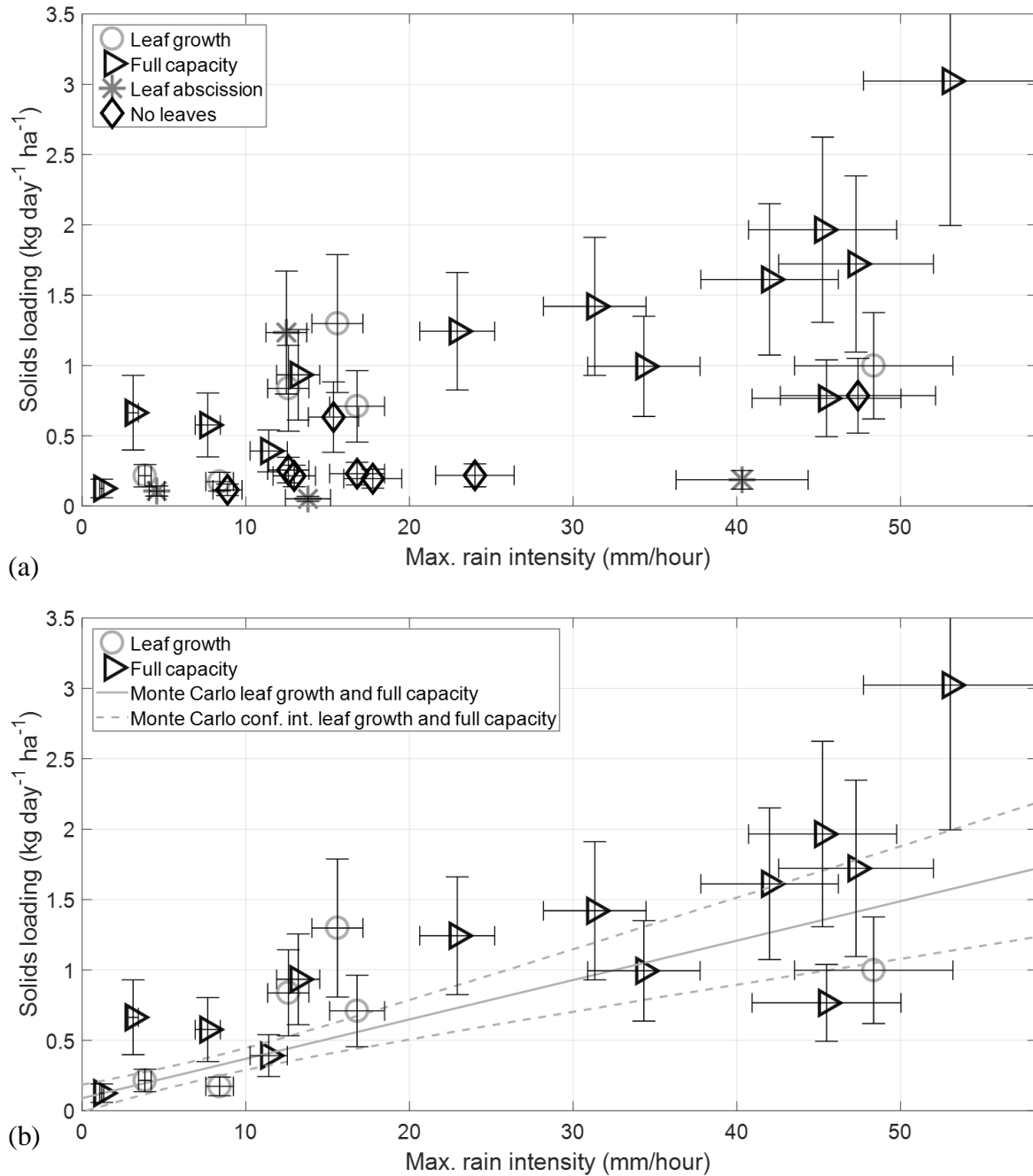


Figure 2.7. The maximum rain intensity versus the solids loading including the 95% confidence interval of the measurements. **(a)** Measurements obtained in all four tree phases; **(b)** The solids loading during the ‘leaf growth’ and ‘full capacity’ phase is correlated with the maximum rain intensity as indicated by the linear regression and its 95% confidence interval, which are based on a Monte Carlo simulation.

Figure 2.7a shows the solids loading versus the maximum rain intensity in the corresponding period and the markers indicate the tree phases. As previously discussed, two regimes seem to be present regarding the solids loading. **Figure 2.7a** suggests that the solids loading during the

regime ‘leaf growth’ and ‘full capacity’ phase is correlated with the rain intensity, which is assessed in **Figure 2.7b** by a Monte Carlo simulation of a linear regression (minimizing χ^2) including the uncertainty in the data. The confidence interval of the regression shows that a significant, positive correlation (with $R^2=0.45$) exists between the solids loading and the maximum rain intensity (while a significant correlation is not present during the other regime).

2.3.1.2 Street sweeping

Street sweeping is expected to have a long-term effect, since sweeping reduces the solids load on streets (e.g. Sartor and Boyd 1972; Bender and Terstriep 1984; Sutherland and Jelen 1997; Amato et al. 2010), which makes less solids available for the next storm events.

Therefore, the effect of street sweeping was analysed by adjusting the street sweeping frequency over two periods of 5 months. While in section 2.3.1.1 the temporal dynamics of the solids loading in the western side of the catchment was analysed, in this section the mean loading in the eastern and western side (both containing 52 gully pots) are compared. In the first 5-month period the sweeping frequency was approximately similar in both catchments, while in the second 5-month period the frequency differed substantially.

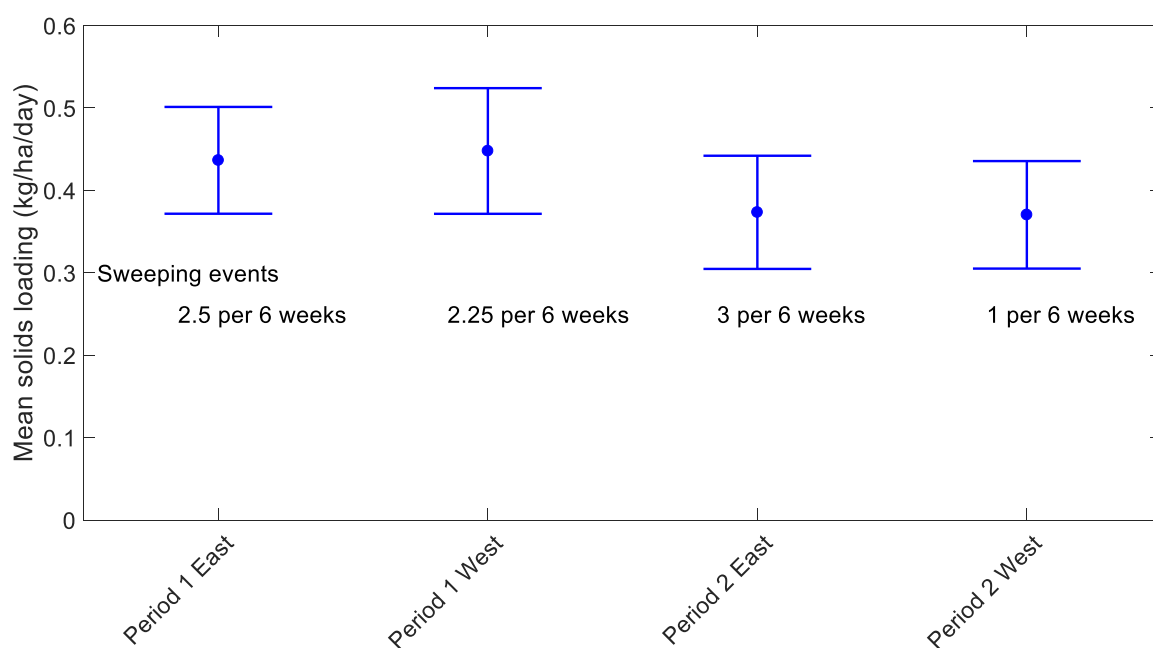


Figure 2.8. Street sweeping frequency and the mean solids loading in the two monitoring periods and two catchments. The difference in street sweeping frequency does not significantly affect the solids loading. There is also no significant difference between monitoring period 1 and 2.

Figure 2.8 shows that the solids loadings in the two catchments do not significantly differ during period 1. Therefore, this period can be used as the reference period. The solids loading in the two catchments neither significantly differ in period 2. Therefore, in accordance with the findings of Walker and Wong (1999), it is concluded that increasing the sweeping frequency (in these catchments and at the evaluated frequencies) results in a negligible effect on the solids loading to gully pots.

Bender and Terstriep (1984) concluded that the frequent rain events in their study were probably also more effective in keeping the streets clean than street sweeping. Therefore, a significant reduction of the solids loading can only be expected when the time between street sweeping events is shorter than the time between rain events. **Figure 2.9** shows the relation between the inter-sweeping-event time and the relative fraction of inter-sweeping-event periods without rainfall. The markers in the figure indicate the two applied street sweeping frequencies. The fraction of dry periods at these two points differ approximately 10%, which was apparently not enough to substantially influence the solids loading.

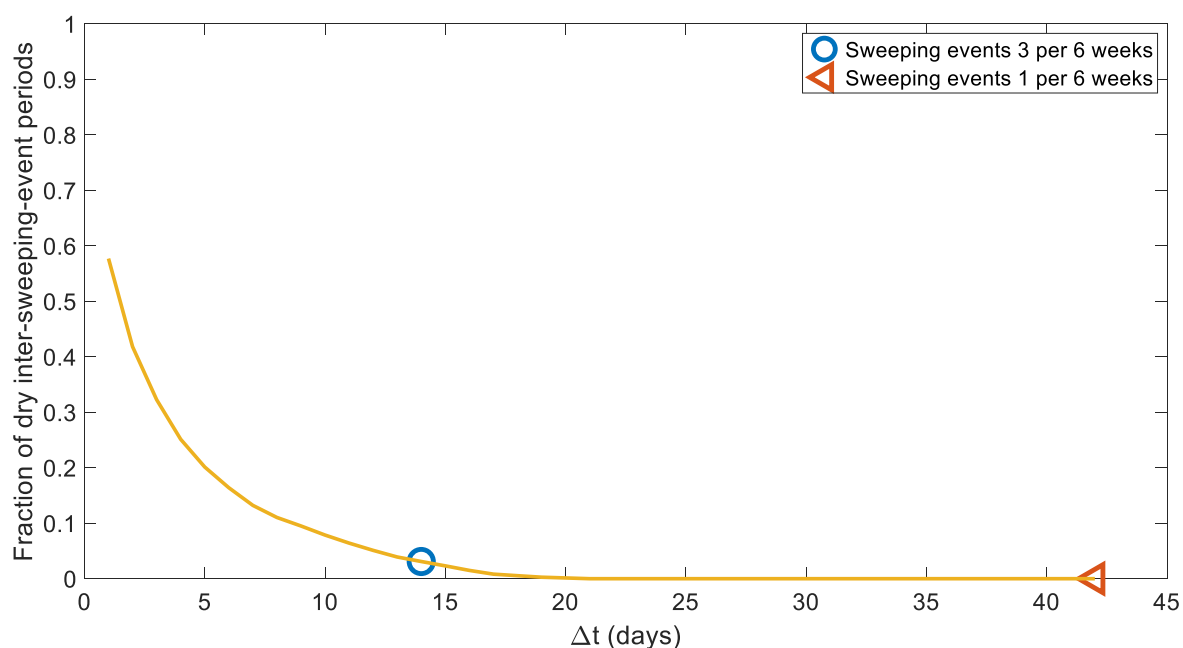


Figure 2.9. The relation between the inter-sweeping-event time and the relative fraction of dry periods of these timeslots, based upon the rainfall data shown in **Figure 2.6**.

2.3.2 Solids' characteristics

2.3.2.1 Particle size distribution

An obvious manner to characterise the collected solids is their grain size range. Solids with a size range between 53 and 1800 μm were mainly sand particles. Larger solids were mainly fibres and leaves. The PSDs (of which two examples are shown **Figure 2.10**) and therefore the D_{50} values vary strongly over the year as shown in **Figure 2.11**. D_{50} is calculated by logarithmic interpolation and varies between 420 (September 2018) and 24000 μm (November 2018). Sansalone et al. (1998) measured (with dry sieving) $350 < D_{50} < 800 \mu\text{m}$, Pratt and Adams (1984) 680 μm and Ellis and Harrop (1984) $600 < D_{50} < 1000 \mu\text{m}$ (both with wet sieving).

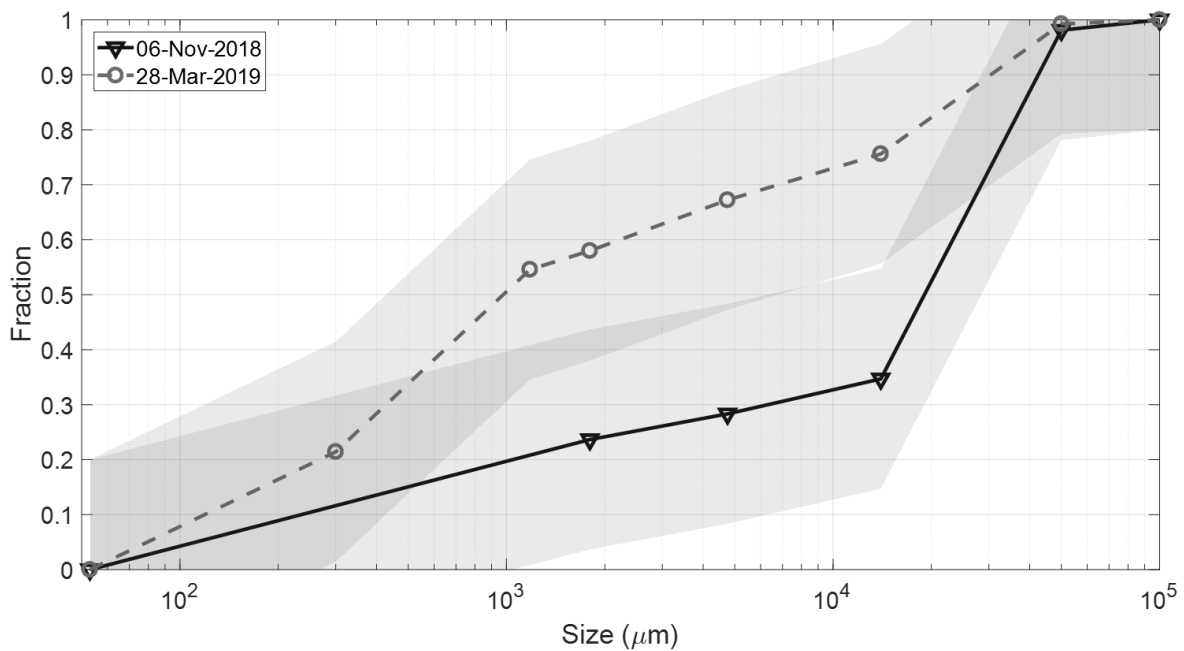


Figure 2.10. Two examples of PSDs obtained by wet sieving.

Figure 2.11 shows that the D_{50} is large during the ‘leaf abscission’ phases, the summer of 2018, and in April 2020. This is caused by the dominance of leaves in the samples during these periods, which was to be expected for the ‘leaf abscission’ phase. The summer of 2018 and April 2020 were extraordinarily dry, reducing the transport capacity of fine solids, while leaves could still be transported by wind. The drought even caused deciduous trees to drop their leaves in the summer of 2018, which has been recorded in the photographs taken during sampling.

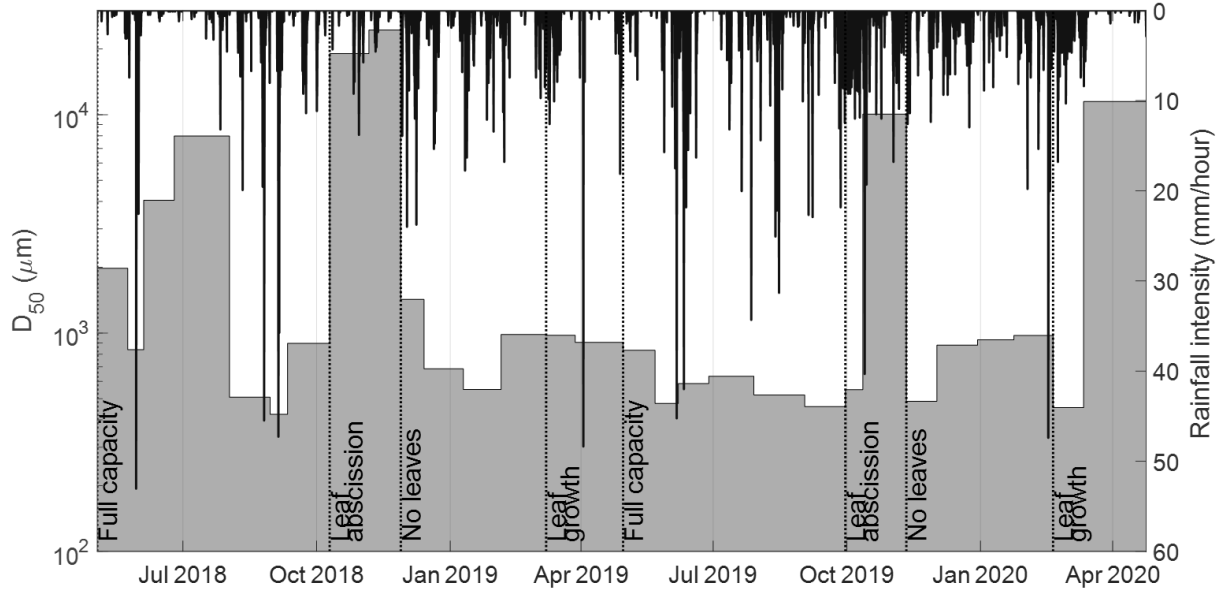


Figure 2.11. D_{50} , rainfall intensity (5-minute interval), and tree phase over time

In section 4.3.2 is concluded that the accumulation rate (in volume) of solids in gully pots shows a maximum during the ‘leaf abscission’ phase, but **Figure 2.6** shows that the ‘leaf abscission’ phase corresponds with the lowest solids loading. Therefore, the volume captured in the gully pot is not directly proportional to the mass inflow and the characteristics of the solids have to be taken into account, when the mass inflow is transformed into the volume captured in the gully pot.

2.3.2.2 Organic content

Figure 2.12 shows the distributions of the organic fraction per size fraction. Similarly to Welker et al. (2019) a positive correlation between the size and the organic fraction is observed. Welker et al. (2019) found organic fractions of 0.18-0.34 for particles between 0-2000 μm and 0.45 – 0.64 for particles between 2000 – 8000 for areas with high vegetation (distinguished by the tree canopy coverage). These values are comparable with the two smallest size fractions in **Figure 2.12**.

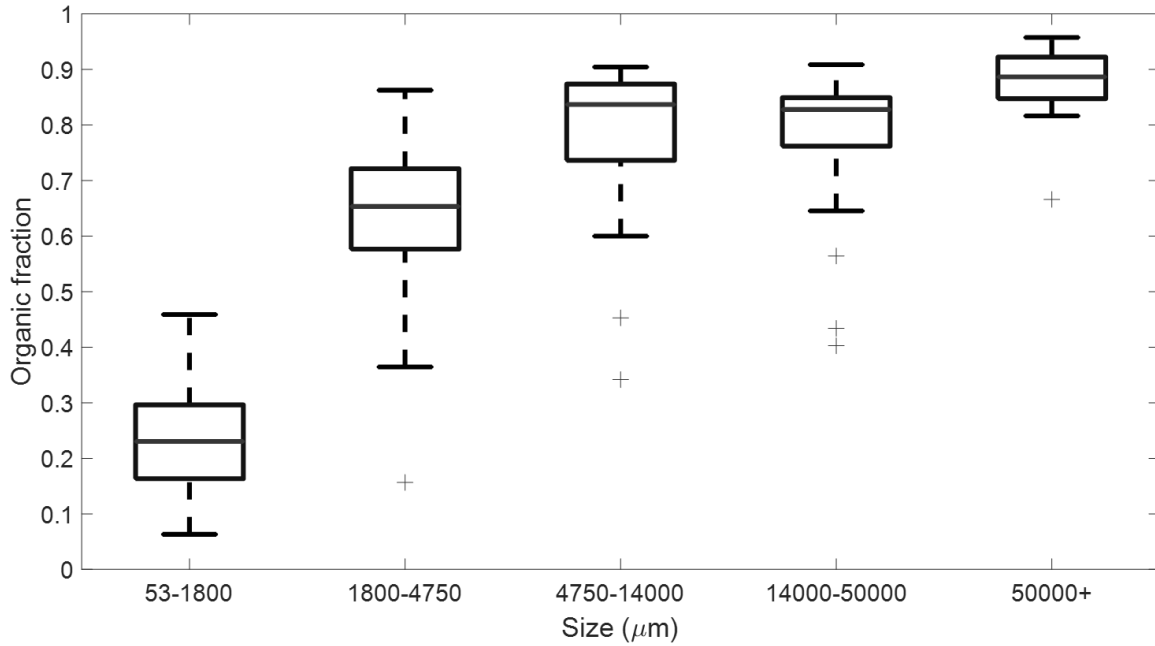


Figure 2.12. Boxplot of the organic fraction by size fraction, which indicates that the larger size fractions contain more organic material.

The organic content fraction of the entire sample, which varies between 0.17 and 0.78 over the year, is shown in **Figure 2.13**. This broad range is comparable with the organic fraction of 0.40 to 0.70 found in street runoff in Paris (Gromaire-Mertz et al. 1999). **Figure 2.13** shows that relatively large organic fractions are present during the ‘leaf abscission’ phase, the dry summer of 2018, and in April 2020. Generally, the processes influencing the D_{50} coincide with those influencing the organic fraction, which is due to the relation between the size of the solids and the organic fraction as indicated in **Figure 2.12**. Additionally, a relatively large rain volume often corresponds with an increased fraction of fine solids while fine solids hold most inorganic material. The rain volume in the ‘leaf abscission’ phase of 2019 is relatively large, which might explain why the peak in the organic fraction in the ‘leaf abscission’ phase of 2018 is substantially larger.

Pratt and Adams (1984) found an increased organic content between October and December due to leaf abscission and between May and September due to the summer shedding of flower petals and grass cutting debris. The first finding can also be recognised in **Figure 2.13**, while the second is virtually absent (only for a short period in the summer of 2018 for reasons discussed earlier). This may be due to the absence of lawns and parks in the study area.

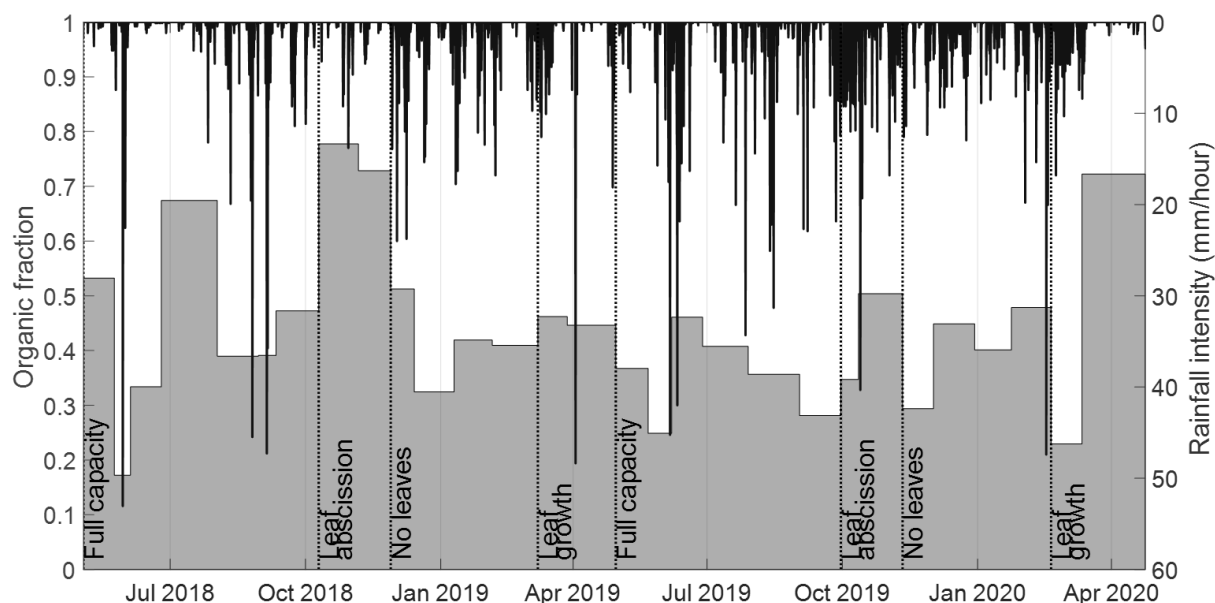


Figure 2.13. Organic fraction, rainfall intensity (5-minute interval), and tree phase over time.

2.3.2.3 Settling velocity

The settling velocity of samples consisting of particles $<1800 \mu\text{m}$ have been assessed with the newly designed settling column (**Figure 2.3**). **Figure 2.14a-c** shows the PSD, the organic fraction, and the velocity distribution of one such sample. The v_{50} of this sample is approximately 0.04 m/s , which is comparable with the settling velocity of sand particle with a diameter of approximately $300 \mu\text{m}$ (by applying the universal using the universal drag coefficient for spheres, e.g. Terfous et al. 2013).

The removal efficiency of sand particles by a gully pot is assessed in chapter 5 in an artificial gully pot with a cross-section of $0.35 \times 0.35 \text{ m}$ and an outlet at the opposite side of the inlet. The removal efficiency at discharges $\leq 1.8 \text{ L/s}$ for sand particles with a diameter of approximately $400 \mu\text{m}$ was $>75\%$ and for particles with a diameter of approximately $180 \mu\text{m}$ was $>45\%$. These removal rates decrease when the sediment bed level was close to the outlet pipe. A discharge of 1.8 L/s corresponds with a rain intensity of 61 mm/hour , by dividing the flow rate by a virtual drained area of 106 m^2 (which is the mean of catchments in the monitoring area). This rain intensity occurs approximately once a year for 10 minutes in The Netherlands (Beersma and Versteeg 2019), so for most rainfall events higher removal efficiencies can be expected, if the sediment bed is below the outlet pipe.

The v_{50} of the analysed samples varies relatively strongly, which cannot be explained by the slight variation in the PSD. **Figure 2.14d** shows that this variation can be explained by the

strong variation in the organic fraction of the samples (with $R^2=0.73$). The organic fraction influences both the density and the shape of the particles.

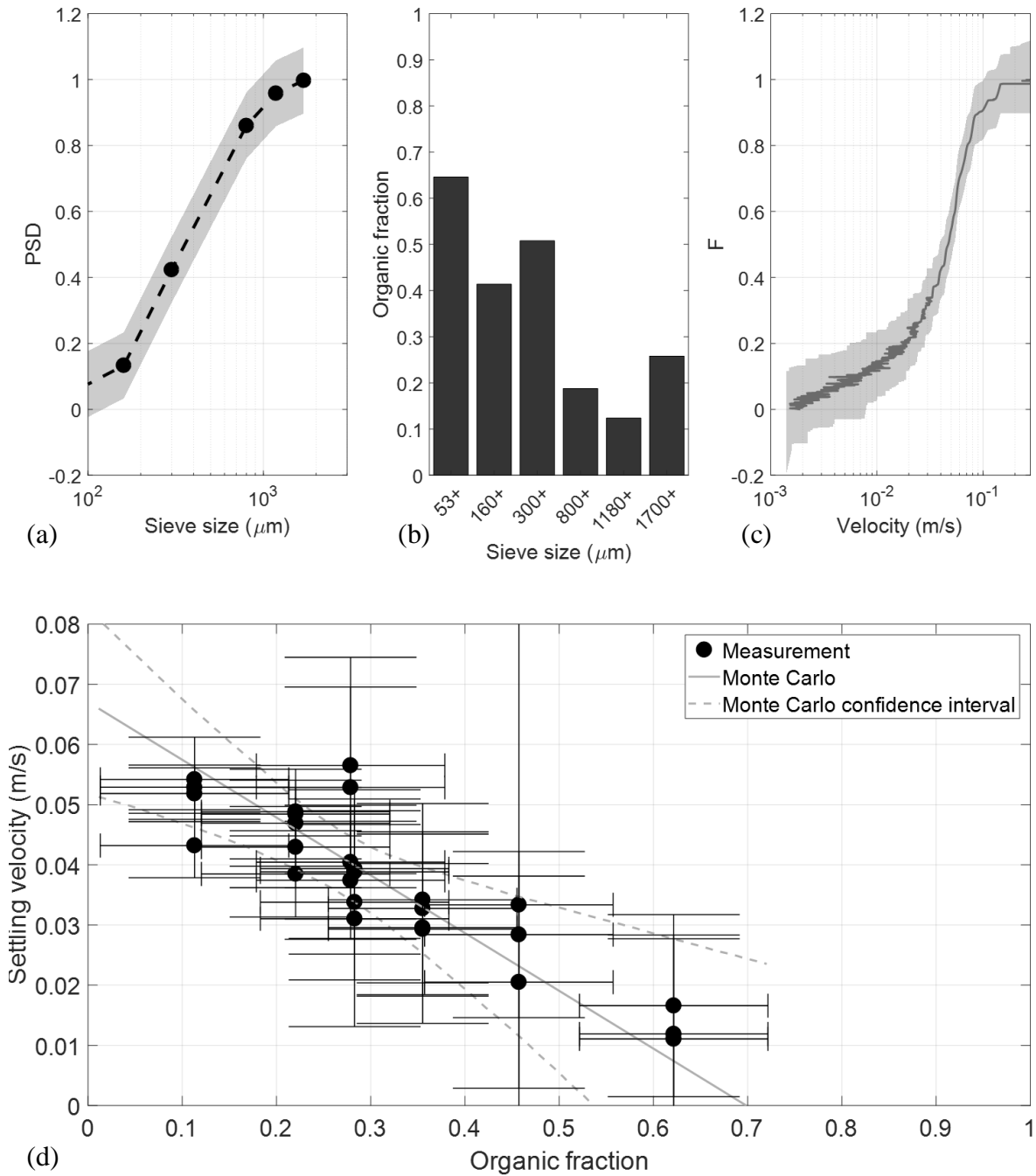


Figure 2.14. (a)-(c) The PSD, organic fraction, and velocity distribution of one sample of solids from a gully pot filter; (d) The v_{50} of the analysed samples is correlated with the overall organic fraction as indicated by the linear regression and its 95% confidence interval, which are based on a Monte Carlo simulation. All displayed confidence intervals originate from the uncertainty in the measurements and their propagation.

2.4 Conclusions

This chapter on the solids loading to drainage systems is based on an extensive monitoring campaign compared to literature in terms of the number of gully pots sampled as well as in terms of the duration. The solids build-up is highly variable even within a street (Vaze and Chiew 2002), resulting in a strong variation in terms of mass and composition to individual gully pots. Therefore, a large number of sampling locations is required to determine the typical loading to gully pots. Moreover, the solids loading strongly varies over time and can substantially differ between the same season in consecutive years. Therefore, a monitoring campaign of at least 2 years is required to capture the seasonal fluctuations.

The solids loading in the monitoring area reached a maximum during the ‘leaf growth’ and ‘full capacity’ phase (which are related to spring and summer). The highest average daily temperatures, which can be found during the same phases, seems to influence the solids loading too. The temperature might represent the erodibility of the available solids, since dry soil is more prone to erosion than wet soil. The parameter ‘rain intensity’ is correlated with the solids loading during the ‘leaf growth’ and ‘full capacity’ phase and might represent the transport capacity.

Street sweeping cannot be regarded as a measure to decrease the solids loading to gully pots unless unrealistically high sweeping frequencies are applied. Therefore, the choice for a street sweeping frequency should rather be based on aesthetic/hygienic criteria than water quality criteria in the studied environment.

The D_{50} and the organic fraction are correlated, since the coarse sediment fraction consists mainly of organic material. Both show a maximum during the ‘leaf abscission’ phase, the summer of 2018, and in April 2020. This is mainly due to leaves dropped by deciduous trees and the lack of rain which is the main transport driver of fine, inorganic material. The settling velocity of particles $<1800 \mu\text{m}$ ranges between 0.01 and 0.06 m/s and is strongly correlated with their organic fraction.

3 MODELLING THE SOLIDS LOADING TO GULLY POTS

3.1 Introduction

Chapter 2 presented the results of a monitoring campaign on the solids loading both in terms of mass and composition to a set of gully pots. This chapter addresses the questions i) what parameters influence the solids loading to individual gully pots in terms of mass and, ii) whether this can be effectively modelled by Build-Up and Wash-Off (BUWO) models.

BUWO modelling is the usual approach to determine the solids loading to drainage systems. These models are applied both to large catchments (e.g. Bonhomme and Petrucci 2017) and to small scale lab setups (e.g. Naves et al. 2020). They contain physical parameters such as the rainfall intensity and the antecedent dry weather period, and some calibration parameters that are not unambiguously linked to physical quantities or processes and can therefore be seen as grey-box models. In this chapter BUWO models are compared with field measurement on the intermediate scale of gully pot catchments.

A classical BUWO model (which was already introduced in chapter 1) contains four calibration parameters and models the wash-off as a source-limited process which is non-linearly dependent on the runoff. The build-up occurs during the dry weather period and grows exponentially to a maximum:

$$\frac{dM}{dt} = k_B(B_{max} - M_0) \cdot e^{k_B t_{ADWP}}, \text{ if } R_i(t) = 0 \quad (1)$$

$$\frac{dM}{dt} = k_W \cdot Q(t)^{N_W} M(t), \text{ if } R_i(t) \neq 0 \quad (2)$$

In which M (in kg/m^2) is the solid load on the street, k_B (in day^{-1}) the growth parameter of the build-up, B_{max} (in kg/m^2) the parameter representing the maximum possible load on the street, M_0 (in kg/m^2) the residual mass after the last rain event, t_{ADWP} the time (in days) of the antecedent dry weather period, R_i (in mm/hour) the rain intensity, k_W the wash-off rate parameter, Q (in mm/hour) the runoff, and N_W the wash-off exponent. If the delay of runoff due to overland flow is set to zero (which is acceptable for the small gully pot catchments):

$$Q(t) = R_i(t) \quad (3)$$

Several studies question the benefit of relatively complex models over simpler formulations (Charbeneau and Barrett 1998; Freni et al. 2009; Shaw et al. 2010). To identify whether this is also true for a large dataset of detailed field measurements, a second model is evaluated in this study with only two calibration parameters, that models the build-up as a linear process (similarly to e.g. Barbé et al. 1996; Morgan et al. 2017) and the wash-off as an exponential process. In this study, it will be referred to as the “simple model” to distinguish it from the “classical model”.

$$\frac{dM}{dt} = k_B - k_W \cdot R_i(t) \cdot M(t) \quad (4)$$

Although BUWO models are widely applied, the outcome of model validation is often unsatisfactory. Bonhomme and Petrucci (2017) reported several reasons, which can be found in literature, that could explain these unsatisfactory results:

- The BUWO process is not well described: studying the process at small scale should be performed to improve the models (e.g. Wijesiri et al. 2015).
- The calibration data: calibrating the models on data measured at the outlet of an urban catchment (which is common practice) is impossible (e.g. Gaume et al. 1998), due to lack of variability or large uncertainty in the data.
- Scaling issues: the models are derived at small scale (order m^2) and applied at catchment scale (order ha) which is not comparable due to for example heterogeneous land-use at the catchment scale. The same holds for the time scale. Calibrating a model for a single rainfall event is possible, but a series of events is challenging, since each rainfall event requires its own calibration parameters (e.g. Naves et al. 2020).

Bonhomme and Petrucci (2017) measured the solids concentration at the outfall over a period of 11 months and calibrated the model represented by equation 1 and 2. The calibration

parameters were highly variable with time, which led to the conclusion that parameters “can hardly represent some physical characteristics of the catchment, and even if this was the case, these characteristics would be so variable that they would have a little practical interest for modelling.” This suggests that the model, although physically based at a small spatial scale, is performing as a grey- or black-box model at catchment-scale.

In this study, the solids loading to drainage systems is measured in the gully pot. This could help to study some of the problems listed:

- The data are additionally studied by a Regression Tree (RT), which includes the effect of some parameters that are not represented in the BUWO models, such as the season and the temperature, but are likely to contribute significantly (chapter 2).
- Measuring the solids loading in gully pots instead of at the outfall of a drainage system excludes all the processes (e.g. sedimentation, erosion) within the gully pots and in the downstream drainage pipes.

3.2 Methods

The monitoring data on the solids loading is described in section 3.2.1, while the data collection of the parameters influencing the solids loading is described in section 3.2.2. Section 3.2.3 contains the modelling procedure.

3.2.1 Solids loading data

The solids loading is measured in 104 gully pots with a frequency of once every ~3-4 weeks between April 2018 and April 2020 (the reader is referred to section 2.2 for more information on the monitoring area and the experimental method). Filters in these gully pots collected the inflowing solids, of which the wet mass was registered for each gully pot at the monitoring location. Each measurement day 4 samples were collected to determine the average wet content in the lab. This average dry fraction was multiplied by the wet mass to estimate the solids’ dry mass of each gully pot. The solids loading to a gully pot ($\text{kg}\cdot\text{day}^{-1}$) is defined as:

$$L(i) = \frac{f_d \cdot m_w(i)}{\Delta t} \quad (5)$$

In which f_d is the average dry fraction, $m_w(i)$ the wet mass of the solids in filter i , and Δt the time measurement interval.

3.2.2 Parameters related to the solids loading

The solids loading to gully pots is influenced by i) the availability of solids on the street and ii) the transport capacity of runoff. A Regression Tree (RT) is used to determine what factors related to these two processes contribute significantly to the solids loading. The BUWO models only use the factors ‘gully pot catchment area’ and ‘rain intensity’ and lump all other factors in calibration parameters. An overview of the evaluated parameters and their origin is provided in **Table 3.1** and **Table 3.2**, the range and units of the variables are provided in Appendix E.

3.2.2.1 Build-up parameters

The availability of solids per gully pot depends on the size of the gully pot catchment area, which is determined by the application of the eight-direction flow approach (Jenson and Domingue 1988) on a Digital Elevation Model (DEM) provided by the municipality of Rotterdam. This DEM is obtained by laser altimetry measurements in 2016 and has a spatial resolution of 0.5 x 0.5 m. Errors in this dataset caused by cars on the street have been filtered out by kriging.

The season influences the availability of solids on the streets by leaf abscission from deciduous trees. Similar to Halverson et al. (1985), four seasons/tree phases are distinguished, namely leaf growth, full capacity, leaf abscission, and no leaves. The start and end dates of the tree phases depend highly on climate and weather and are based upon images of the streets and trees made during the measurements.

In chapter 2 it was suggested that the temperature might influence the erodibility of solids, since dry soil is more prone to erosion than wet soil. Therefore, the mean temperature during a monitoring period is used as a parameter and is assumed to be homogeneous in this relatively small monitoring area.

Street sweeping with sweeping vehicles was applied in the monitored area by the municipality, which also registered when it was applied. The solids load on streets increases over time if they are not removed by e.g. rain or street sweeping. Therefore, the length of the antecedent dry period is usually assumed to contribute positively to the solids loading to drainage systems (Sartor and Boyd 1972; Irish et al. 1995; Vaze and Chiew 2002; Chow et al. 2015; Morgan et al. 2017). In this study, a day is defined dry if the rainfall volume is less than 1 mm.

Table 3.1. Solids build-up parameters evaluated by the RT.

Parameter	Calculation	Data source
Gully pot catchment area	The eight-direction flow approach (Jenson & Domingue 1988) to determine the size of the paved area connected to a gully pot	Digital elevation model based on laser altimetry measurement from 2016 owned by the municipality of Rotterdam
Tree phase	Classification	Visual observation and photos
Temperature	Mean air temperature during the measurement period.	Temperature measurement (at a temporal resolution of 5 minutes) by weather station Ommoord (at a distance of 4 km).
Street sweeping	Events per week during the measurement period.	Timesheets of the municipality
Antecedent dry period	The number of dry days before the measurement period, while a day is considered dry when the rainfall volume is less than 1 mm.	Rain radar KNMI

3.2.2.2 Wash-off parameters

The rainfall data used originate from the meteorological radar dataset of the Koninklijk Nederlands Meteorologisch Instituut (KNMI), which contains 5-minute interval rain volume measurements on a 1 km² grid. This relatively short time-interval is used, since a gully pot's catchment area is small, which results in a short response time.

The 5-minute interval data is used in the BUWO models, while only the maximum rainfall intensity during a monitoring period is used in the RT, since a RT can only handle a single value. The maximum intensity was chosen, since it is the most important parameter for the wash-off during a rainfall event (Shivalingaiah and James 1984). The solids loading is studied on a timescale of a few weeks, so the wash-off rate is integrated over the time between two measurement days. Therefore, the wash-off in that period depends on the integral of the rainfall intensity as well, which is the rainfall volume.

The rainfall intensity affects the transport capacity and the erosion capacity by raindrop impact and the rainfall volume affects the total transport over an event. The street surface of the gully pot catchment might also be more effectively cleaned when the volume and discharge of water flowing over the area (which equal the multiplication of the catchment area with the rainfall volume and the rainfall intensity respectively) is larger.

Table 3.2. Solids wash-off parameters evaluated by the RT.

Parameter	Calculation	Data source
Rainfall volume	Mean rainfall per day during the monitoring period.	Rain radar KNMI
Rainfall intensity	Maximum rainfall intensity in 5-minute interval during the measurement period.	Rain radar KNMI
Discharge	Maximum rain intensity multiplied by the connected area.	Rain radar KNMI and digital elevation data.
Water volume	Rain volume multiplied by the connected area.	Rain radar KNMI and digital elevation data.

3.2.3 Modelling

3.2.3.1 Regression tree analysis

RTs (Breiman et al. 1984) are commonly used in data mining to explore the structure of datasets. It shows the structure of the data (in this study on the solids loading) by rules, which appear at each node and split the dataset into two subsets. In this study, the criterion for the best

split is defined as the split predictor that minimizes the p -value of χ^2 tests of independence between each (pair of) explanatory variable(s) and the response variable. If all tests yield p -values larger than 0.05, or the subset is smaller than 60, splitting is stopped.

The procedure to obtain a single tree is based upon the procedure of De'ath and Fabricius (2000) and consists of 6 steps:

- i. Divide the data into n (usually a number between 5 and 10, in this study $n=5$) random subsets of approximately equal size.
- ii. Cross-validate by dropping each subset in turn (test data) and build a tree using data from the remaining subsets (training data).
- iii. Predict the responses for the omitted subset, calculate the mean squared error for each subset and sum over all subsets.
- iv. Repeat steps (ii)-(iii) for a series of tree sizes.
- v. Take the smallest tree (the pruned tree), such that the error is within one standard deviation of the minimum error of the cross-validation trees.
- vi. Repeat m times (in this study $m=50$ resulted in a clear distribution) steps (i)-(v) and select the most frequently occurring tree size from the distribution of selected tree sizes and subsequently a common tree.

3.2.3.2 BUWO models

The solids loading obtained from the monitoring data as defined in equation 5 is used to calibrate the BUWO models as represented in equations 1-4. The solids loading from the models is calculated as following:

$$L_{model}(i) = \frac{A(i)}{\Delta t} \int_{t_{start}}^{t_{end}} \frac{dM_{wash-off}}{dt} dt \quad (6)$$

In which L_{model} is the modelled solids loading, $A(i)$ the paved surface area connected to gully pot i , and $M_{wash-off}$ the wash-off as represented by equation 2 or the second term of equation 4. The calibration parameters of the models are obtained by minimising the mean squared error.

3.3 Results

3.3.1 Data exploration

On some occasions, the filters contained divergent and/or illegally dumped material, e.g. concrete, wall plaster, and paint, which was registered. In some cases this could not visually be noticed, but the extraordinary high mass (which lower limit was set at three times the mean value of the corresponding monitoring period, which was chosen based upon the measurements) indicated illegally dumped material. These outliers were removed during the post-processing of the data to avoid wrong associations in the statistical analyses, since these materials are most likely manually dumped into the gully pots, instead of transported by the runoff process. This removal of outliers reduced the dataset from 3046 to 2919 observations.

3.3.2 Regression tree

Table 3.3 contains the type of relation between the parameters and the solids loading to gully pots in the Regression Tree (RT). Parameters that correlate positively are indicated with a plus sign, whereas negative correlations with a minus sign. The RT with 15 terminal nodes is shown in **Figure 3.1**.

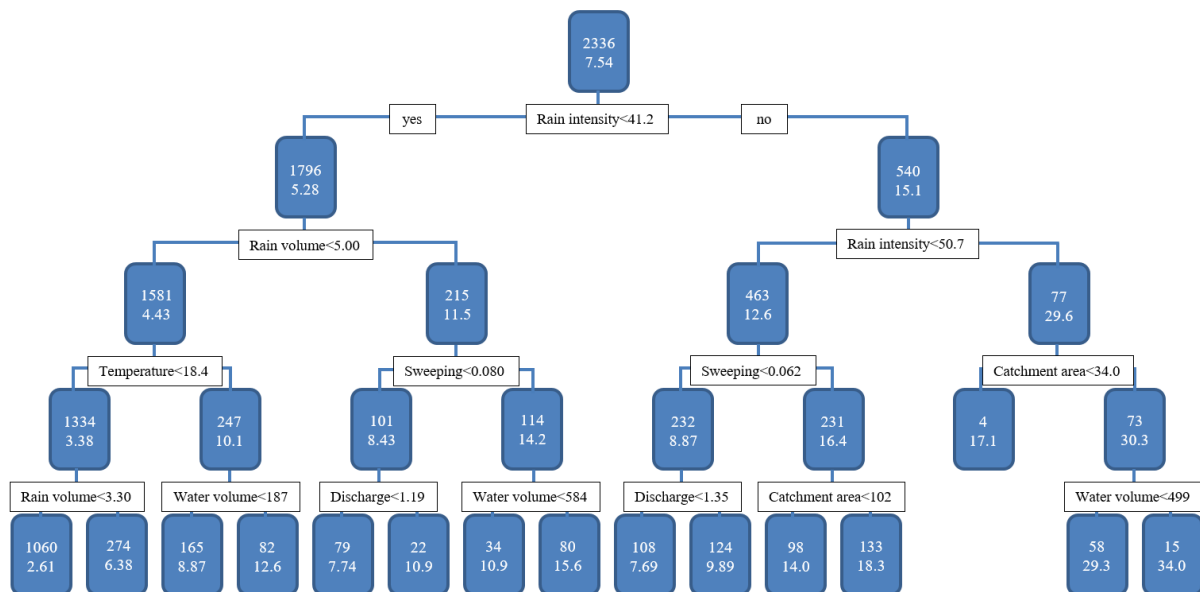


Figure 3.1. The RT for the solids loading to gully pots. A step to the left is taken if the criterion is met and to the right if it is not met. The values at the nodes are the number of observations in the group and the mean solids loading of the group.

The rainfall intensity is the most influential parameter in the RT. It represents the transport capacity and the erosion capacity by raindrop impact and is positively correlated with the solids

loading. Shivalingaiah and James (1984) concluded that this parameter correlated strongest to the wash-off on the timescale of a single rainfall event, which is apparently also the case for a period of ~3-4 weeks with several rainfall events. The rainfall volume is also related to the transport capacity of solids. It is the second most important parameter in the RT and is positively correlated with the solids loading.

Table 3.3. Type of relations between the parameters and the solids loading to gully pots and their relative importance (based on the reduction of the mean squared error). Positive correlations are indicated with a plus sign and negative correlations with a minus sign.

Parameter	Relation with solids loading	Relative importance	Importance rank
Catchment area	+	0.018	5
Leaf abscission	No relation	0	-
Leafless	No relation	0	-
Leaf growth	No relation	0	-
Full capacity	No relation	0	-
Temperature	+	0.102	3
Street sweeping	+	0.091	4
Antecedent dry period	No relation	0	-
Rainfall volume	+	0.135	2
Rainfall intensity	+	0.633	1
Discharge	+	0.005	7
Water volume	+	0.017	6

As suggested in chapter 2, the temperature correlates positively with the solids loading. There are several possible explanations for this relation. The temperature is related to the season and subsequently to the tree phase. However, in this case the tree phase is evaluated separately (and found not to be correlated to the solids loading), so the temperature is not likely to be a proxy of the tree phase.

Temperature (differences) is also related to the wind speed. In autumn and winter the mean wind speed is larger than in spring and summer in The Netherlands. A larger wind speed could increase the transport capacity of solids. However, the data shows that the solids loading to gully pots increases during spring and summer.

The air temperature (and road temperature) might also influence the wetness of solids on the streets by evaporation. Since, dry solids are more prone to erosion than wet soil, the temperature will be positively correlated to the erodibility of solids and therefore with the solids loading to gully pots.

Street sweeping contributes positively to the solids loading, which could be due to loosening of solids stuck to the road surface and making them available for transport. The parameters rain volume and rain intensity are represented in the BUWO models as described in section 3.1. However, the temperature and street sweeping, which are the third and fourth most influential parameters, are not.

The parameters catchment area, discharge, and water volume all contribute positively to the solids loading, but less strong than the parameters previously discussed. The contribution of the catchment area is small, but also contributes via the parameters discharge and water volume, since these are multiplications of the catchment area with respectively the rain intensity and the rain volume.

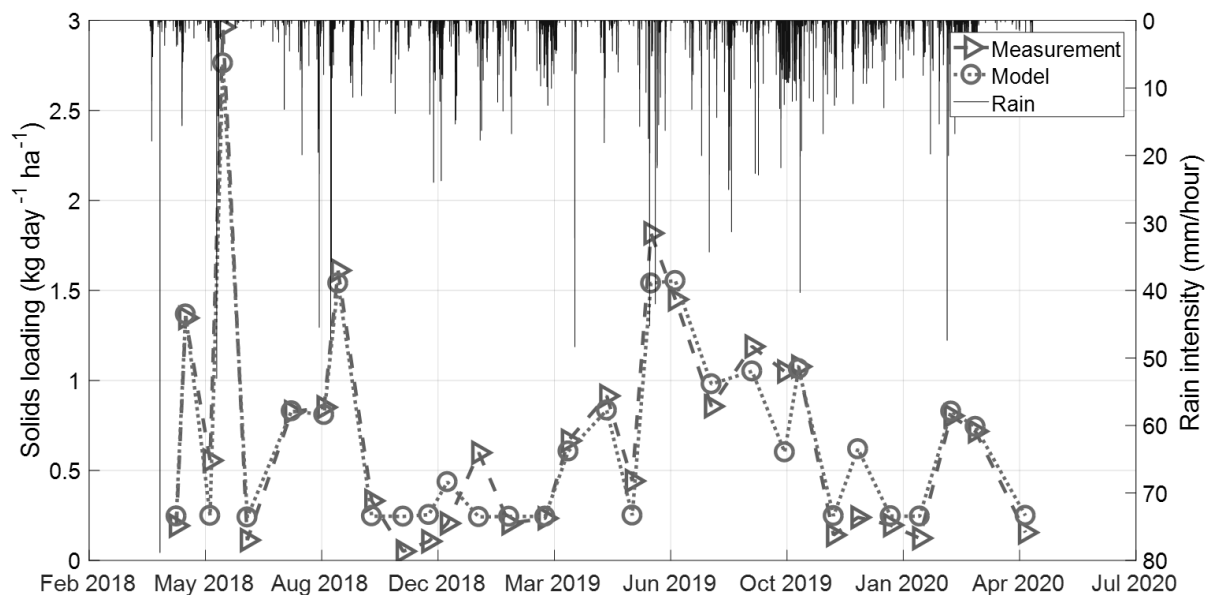


Figure 3.2 Comparison between the total measured and modelled (by the RT) solids loading to all monitored gully pots over time.

The performance of this RT could be represented by the R^2 value which equals 0.57 for the randomly selected (as described in section 3.2.3.1) training set and 0.60 for the test set (usually the training set shows a higher R^2 value). These values are moderate, and it is concluded that the prediction of the solids loading to individual gully pot should not be made using this model. However, **Figure 3.2** shows that the dynamics of the total loading to all gully pots are well captured by this RT and the R^2 value of this total loading equals 0.92.

3.3.3 BUWO

In equation 1-4 the “classical” and “simple” BUWO models are introduced. The models are calibrated using the observations of each individual gully pot. Both the simple and classical model have very low R^2 values of respectively -0.053 and -0.0013, which indicates that the mean value represents the solids loading to individual gully pots equally well as the models. The performance of the models for the total solids loading (the summation of the individual gully pots), as shown in **Figure 3.3**, is slightly better than for individual gully pots, with a R^2 of 0.030 for the simple and 0.30 for the classical model.

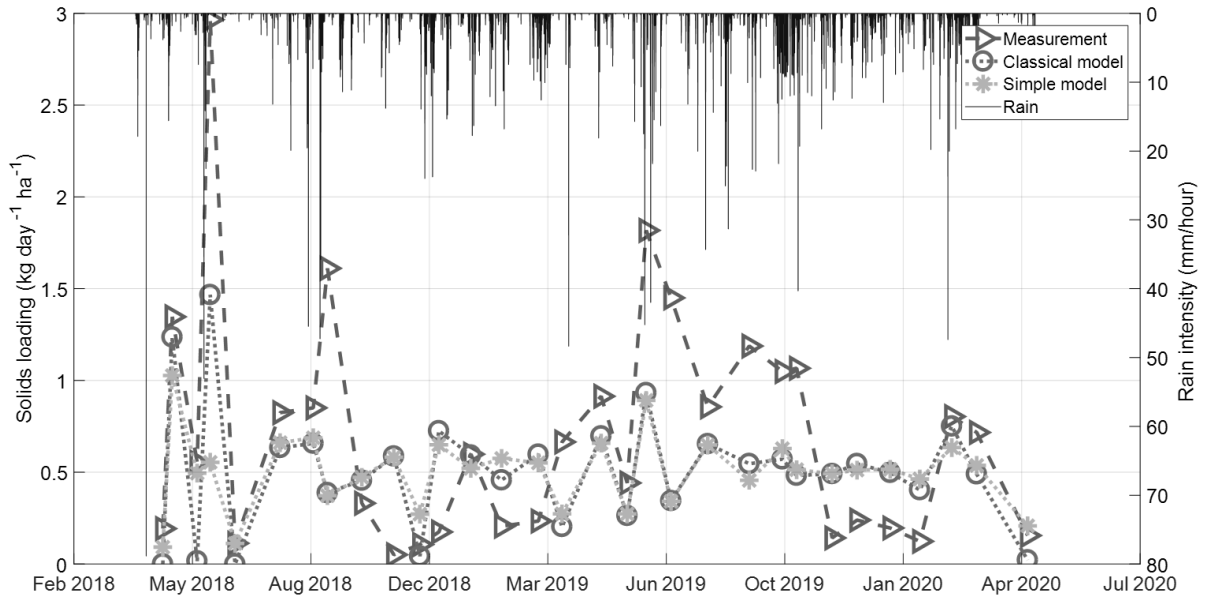


Figure 3.3. Comparison between the calibrated BUWO models and the measurements. Calibration parameters simple BUWO model: $k_B=5.27 \cdot 10^{-2} \text{ g} \cdot \text{m}^{-2} \cdot \text{day}^{-1}$ and $k_W=7.01 \text{ hour} \cdot \text{day}^{-1} \cdot \text{mm}^{-1}$. Calibration parameters classical BUWO model: $B_{max}=4.45 \text{ g} \cdot \text{m}^{-2}$, $k_B=1.38 \cdot 10^{-2} \text{ day}^{-1}$, $k_W=9.03 \cdot 10^{-5}$, and $N_W=6.14$.

In **Table 3.4** a comparison is made between the values of the calibration parameters of the classical model found in this study and found in literature. The build-up parameters are comparable to values in literature, but the wash-off parameters are not. In some studies, N_w is a priori fixed to 1. If this is applied, the value for k_w becomes more comparable with the values reported in literature (but the R^2 value becomes even lower with -0.12 for individual gully pots and 0.19 for the total solids loading).

Table 3.4. Calibration parameters reported in literature.

Reference	B_{max}	k_B	k_w	N_w
Gaume et al. (1998)	7.3	0.52	0.014	1.65
Liu et al. (2012)	1.26-3.52	0.01-0.05		
Liu et al. (2012)	37.2	0.085		
Liu et al. (2012)	0.95-1.74	0.03-0.19		
Liu et al. (2012)	1.94-4.25	0.16-0.95		
Wicke et al. (2012)	0.276	0.2	0.24	1
Wicke et al. (2012)	0.134	0.23	0.27	1
Shorshani et al. (2014)			0.1	1.5
Bonhomme and Petrucci (2017)	0.2-30	0.03-20	0.01	0.2-3
Classical model in this study	4.45	0.0138	$9.03 \cdot 10^{-5}$	6.14
Classical model in this study with fixed N_w	4.68	0.0165	0.0161	1

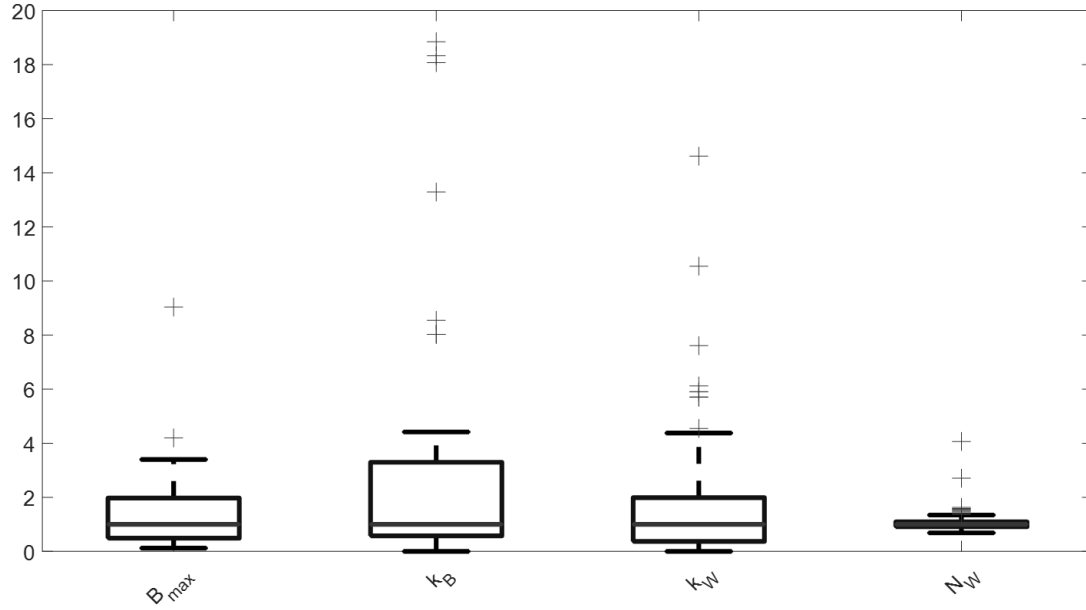


Figure 3.4. The spread in the calibration parameters is displayed in this boxplot by dividing them by their median values, which are: $B_{max}=5.29 \text{ g}\cdot\text{m}^{-2}$, $k_B=1.45\cdot 10^{-1} \text{ day}^{-1}$, $k_W=0.577$, and $N_W=2.36$.

Instead of one model representing all gully pots, each gully pot could also be modelled with a separate model. This approach is followed to evaluate the sensitivity of the calibration parameters. **Figure 3.4** shows the spread of the calibration parameters in this set of models. This spread is substantial, in particular in k_B and k_W . Therefore, it is questionable whether the dominant processes are captured in this model. This notion is supported by Bonhomme and Petrucci (2017) who found in their study that the calibration parameters showed very limited portability, which led them to the conclusion that the parameters “can hardly represent some physical characteristics of the catchment, and even if this was the case, these characteristics would be so variable that they would have little practical interest for modelling.”

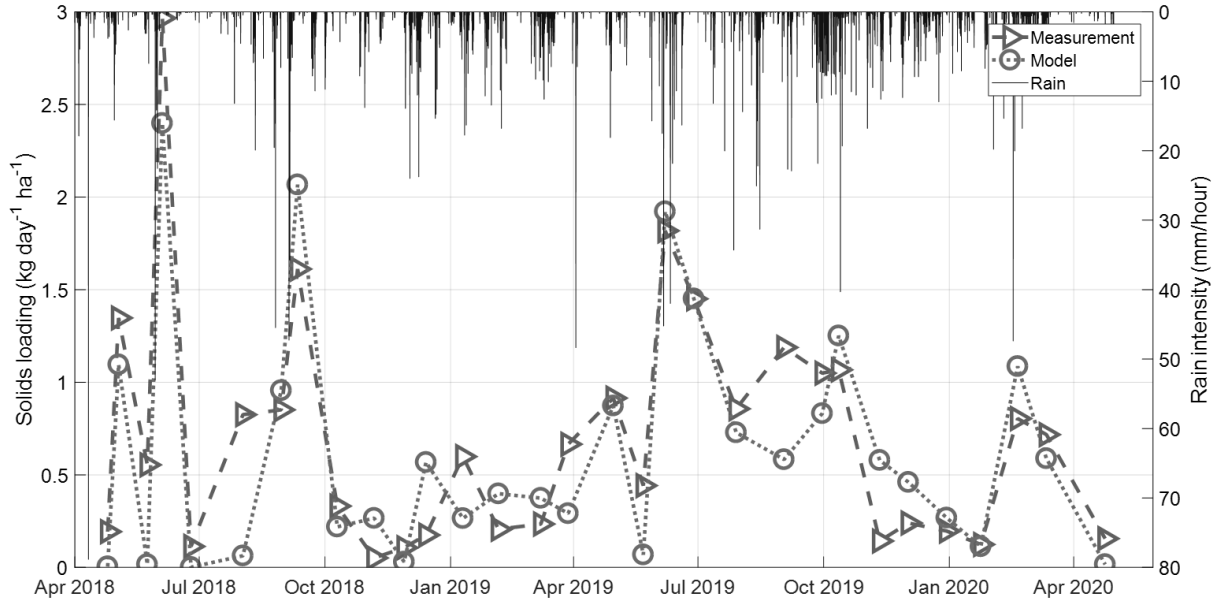


Figure 3.5. Comparison between overall solids loading measured and modelled solids loading.

The performance of this set of classical models is obviously better than the application of a single classical model as in **Figure 3.3**. The R^2 value is 0.36 for the individual gully pots and 0.76 for the total solids loading to all gully pots, as shown in **Figure 3.5**.

3.4 Discussion

The R^2 values of the two BUWO models evaluated in this study are approximately zero, indicating that the mean value of the observations explains the variation in the observations equally well as the models. The R^2 value slightly increases when the performance is evaluated for the summation of all gully pots, but it is still relatively small. When a model is developed for each gully pot, the dynamics of the summed solids loading is pretty well described, as shown in **Figure 3.5**.

These results confirm the findings of Naves et al. (2020), who modelled the solids wash-off of predefined solids from an artificial street, based on the experiments of Naves et al. (2019). Despite the accurate definition of the (initial) conditions (such as the solids load on the street and the rainfall), for each tested situation, a wide range for the values of the calibration parameters was suitable when calibrating their physically-based BUWO model. Individual tests could be represented relatively well with the model, however the portability of the values to other tests was virtually absent. It is concluded, supporting to Bonhomme and Petrucci (2017),

that the calibration parameters in the BUWO models can hardly be regarded as representing some physical characteristics of the catchment.

The performance of the RT is better than the BUWO models as indicated by the R^2 value of approximately 0.60 for the loading to individual gully pots and 0.95 for the summed loading to all gully pots. This suggests that a data-driven model produces better results than the semi-physical BUWO models. The evaluated data-driven model includes some parameters that are not included in the BUWO models, of which the temperature is found to be the most influential. The effect of this parameter on processes influencing the solids loading to gully pots should be studied in future research. It may have been overlooked in literature, as many studies do not span several years.

Nevertheless, it is questionable whether the addition of parameters is the only reason the RT performs better than the BUWO models. RTs allow local relations within subgroups of the data, which clarifies the effects of (a combined set of) parameters on the outcome variable. This property results in a very flexible type of modelling, resulting in a site-specific model. Moreover, these types of models describe the dynamics, but lack the fundamental understanding of the processes. BUWO models, which are usually continuous and seem to contain a more physical description of the processes, have neither proved to be portable, since either each gully pot catchment has to be modelled separately with a large range of calibration parameters, or the application of one model results in poor performance.

Despite decades of research into wash-off and related processes (theoretical and experimental research) reported in literature (e.g. Sartor and Boyd 1972; Pitt 1979; Pratt and Adams 1984; Ellis and Harrop 1984; Pitt et al. 2005; Bonhomme and Petrucci 2017), hardly any generic conclusions can be drawn and at best site-specific statistical relations have been identified with an unknown validity beyond the monitoring period. This implies that model calibration is required for each catchment, and on top of that the portability of calibrated parameters for one location to another rain event proves to be troublesome as well (Naves et al. 2020), indicating that the calibrated models are likely to be only able to “now- and here cast”.

An option worth considering for further research is to find out if the processes influencing the solids loading to gully pots contain non-linear feedbacks, which can initiate inherent unpredictable dynamic behaviour, also known as chaos (see e.g. Genesio and Tesi 1991). The suspicion of chaotic characteristics has been uttered for some of these or related processes.

The wash-off process starts with rainfall, which is known to show chaotic behaviour in space and time (Rodriguez-Iturbe et al. 1989; Sivakumar 2000). The impact of the raindrops erodes solids from the surface, depending on the erodibility of the solids. This erodibility is influenced by the characteristics of the individual particle, the moisture content of the particles (as discussed in section 3.3.2), the way they are deposited on the surface, the cohesiveness of surrounding particles, the street surface, etc.

The transition of rain into runoff might also be a chaotic process (Sivakumar et al. 2001). The eroded solids can get transported by runoff over the (street) surface. This flow is strongly intermittent depending on the rainfall intensity, which influences the settling (which is chaotic in some conditions, Verjus et al. 2016) and erosion processes in this flow. These settling and erosion processes are to some extent comparable to coastal morphology, which might exhibit chaotic behaviour (Baas 2002).

These individual processes have to be studied in more detail and in relation to each other to conclude whether wash-off is a chaotic process and if so, under what conditions. A first step could be to describe the individual processes in simple 1D mathematical models and search for non-linear feedbacks. If these are found, the impact of the individual processes on the overall wash-off can be evaluated. If the overall perspective proves to be inherently chaotic, it would imply that for all practical purposes a data-driven approach for a specific catchment is a better alternative when compared to using a BUWO model with parameters taken from literature.

3.5 Conclusion

The statistical analysis of the large monitoring data set, both in terms of sampling locations and duration, reveals several parameters that significantly influence the solids loading to gully pots. The Regression Tree (RT), shows that the rain intensity, rain volume, and temperature are the most influential parameters. The rain intensity and rain volume are related to the erosion of solids from the street and the transport of solids over the street. The temperature might influence the erodibility of solids from the street.

The Build-Up and Wash-Off (BUWO) models generally show poor performance, in particular when compared with the performance of the RT. Therefore, it is not recommended to use a single BUWO model, calibrated for a set of gully pots or catchments, to predict the solids loading to individual gully pots or catchments. If each gully pot or catchment is separately modelled by a BUWO model, the performance increases strongly. However, since this results in a large variation in the calibration parameters, it is questionable whether this set of models

is a better description of the physical processes or whether the additional calibration parameters only act as fitting parameters. The latter would mean that the model acts as a black-box model and cannot be used in other catchments without calibration which requires a large amount of data of the new catchment.

PART II: ACCUMULATION OF SOLIDS IN GULLY POTS

4 THE SOLIDS ACCUMULATION RATE IN GULLY POTS

4.1 Introduction

To reduce the solids loading to the drainage system, gully pots contain a sand trap to remove suspended solids from runoff. The accumulation of these solids is not only influenced by the loading of solids to the gully pots as studied in chapter 2 and 3, but also by the hydraulic conditions in the gully pot which also undergo temporal and spatial variation.

The objective of this chapter is to obtain more insight into the dynamics of the accumulation of solids in gully pots over time. Therefore, instead of studying the sediment bed level itself, the accumulation rate of solids is studied to determine what parameters significantly influence the accumulation of solids. Physical parameters linked to three relevant processes, namely the build-up of solids in a catchment, the wash-off of these solids from the catchment, and the retention of solids in the gully pot, are assessed.

The determination of the dominant processes might eventually be used in the planning of the operation and maintenance cycle of gully pots to reduce the solids loading to the downstream part of the drainage system.

4.2 Methods

The solids accumulation rate in 407 gully pots is monitored over time and modelled by statistical models to determine what physical parameters significantly influence this process.

Section 4.2.1 describes the monitoring area, section 4.2.2 the measurement technique and the calculation of the accumulation rate, section 4.2.3 what parameters are considered in the statistical models, and section 4.2.4 the modelling procedure.

4.2.1 Monitoring area

Figure 4.1 shows the locations of the 7 monitored streets in Rotterdam and The Hague, which are two of the largest cities in The Netherlands and have a maritime climate with cool summers and moderate winters. The annual rainfall was ~840 mm/year at these locations during the monitoring period which lasted from November 2017 until December 2018. During this period ~60% of the days were dry (which was defined as a day with a maximal rain intensity <1 mm/hour).

Table 4.1. Characteristics of the monitored streets .

Street	City	Number of gully pots	Road material(s)	Monitored surface area (ha)
De Lugt	Rotterdam	60	Bricks	0.69
Ludolf de Jonghstraat	Rotterdam	57	Bricks	0.86
Kanaalweg	Den Haag	49	Asphalt / Bricks	0.61
Keukenhoflaan	Den Haag	71	Bricks	0.67
Leuvensestraat	Den Haag	62	Asphalt / Bricks	1.32
Paul Krugerlaan	Den Haag	55	Asphalt	0.87
Van Stolkweg	Den Haag	51	Bricks	0.81

The monitored streets vary strongly in terms of vegetation, pavement type, and traffic intensity (as shown in more detail in Appendix A), which allows relating the results to other areas. A common characteristic of these areas is the absence of (high) gradients, which is very common in (the western part of) The Netherlands. In total 407 gully pots were monitored (as shown in

Table 4.1); a trade-off between a feasible maximum number for data collection and a minimum number for a reliable statistical model.

Other researchers, for example Pratt and Adams (1984) and Ellis and Harrop (1984), reported detailed measurements in a few gully pots only. With the current approach, conclusions are drawn on a larger scale and the effect of environmental characteristics can be assessed.



Figure 4.1. Locations of the monitored streets.

4.2.2 Solids accumulation rate

The sediment bed thickness in the gully pots was measured approximately once per 3 to 4 weeks using the device shown in **Figure 4.2a**. This device is similar to the one used by Post et al. (2016). It consists of a punctured disk (diameter 210 mm and 20 mm holes) with a vertical hollow cylinder (inner diameter 10 mm) and a movable rod (diameter 8 mm) inside this cylinder. The disk was used to compress the sediment bed to remove the air captured in the bed and to reduce the effect of consolidation on the measurement. The movable rod was pushed through the bed to the bottom of the gully pot as shown in **Figure 4.2c**. The sediment bed thickness was determined with measuring tape (2 mm intervals) on the rod indicating the distance between the end of the rod and the disk. Since the measurement is performed manually, the force on the disk differs each measurement, which affects the reproducibility of the

measurement. Despite this drawback of the measurement techniques, a discussion of alternative measurement techniques (in section 4.4) shows that those have substantial drawbacks too.

The volume of solids present is calculated by multiplying the bed thickness by the cross-section of the gully pot. The solids accumulation rate is defined by the division of the change in solids volume by the number of days between consecutive measurements (in L/day):

$$S_{i,g} = \frac{A \cdot (d_{i+1,g} - d_{i,g})}{(t_{i+1,g} - t_{i,g})} \quad (1)$$

In which S is the solids accumulation rate, A the horizontal cross-section of the gully pot, $d_{i,g}$ the i^{th} measured depth in gully pot g , and t the measurement day. Post et al. (2016) showed that the sediment bed in most gully pots stabilised after a few months, which implies that $S=0$. The current study is meant to determine the factors influencing the solids accumulation rate prior to the occurrence of gully pot blockages or the accumulation rate approaches zero. Therefore, in case of substantial sediment bed levels, all gully pots in a street were cleaned by the municipality on the author's request and a new measurement series was started, in this manner three measurement series for most streets were obtained during the monitoring period.

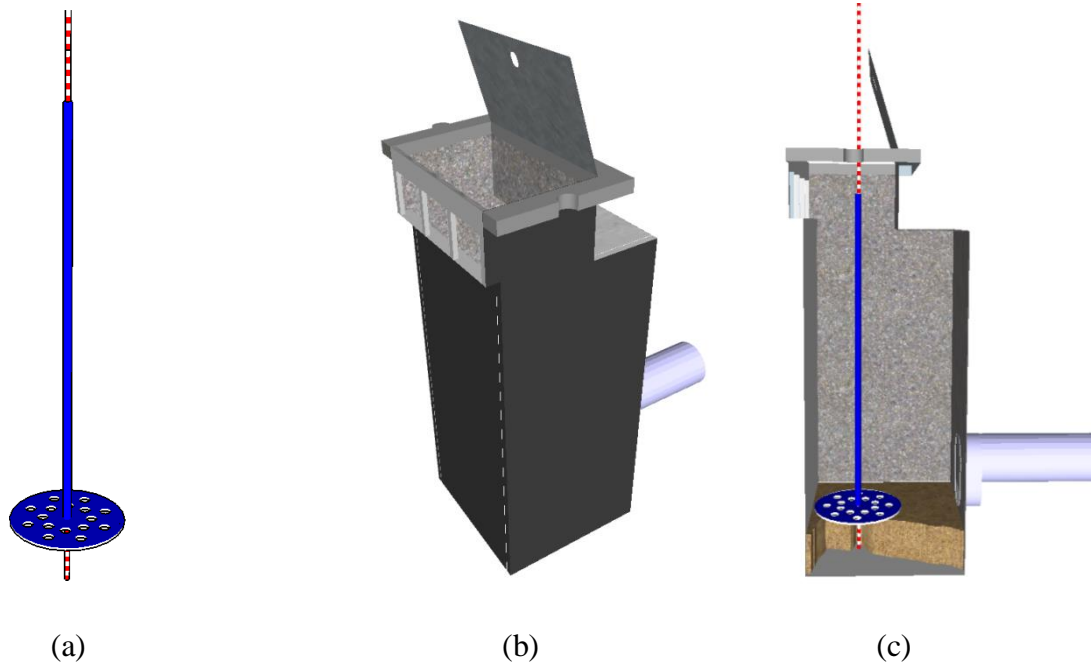


Figure 4.2. (a) Measurement device for the sediment bed level; (b) Gully pot; (c) Side view of sediment bed level measurement in gully pot.

4.2.3 Parameters

Post et al. (2016) identified several parameters that are correlated with the bed level in a gully pot, namely the connected area, road use, rainfall volume, and sand trap depth. In this study, parameters related to the build-up of solids on surfaces, the wash-off of these solids, and the removal of solids by the gully pot are added to the parameters mentioned above, to model the accumulation rate. These parameters are described in the next sections. The data used originate from readily available datasets from governmental organisations.

4.2.3.1 Parameters related to build-up

Table 4.2 provides an overview of the parameters included in the model to schematise the build-up of solids on streets.

Vegetation influences the solids load on streets (e.g. Welker et al. 2019; James and Shivalingaiah 1985), which subsequently influences the accumulation rate of solids in gully pots. Instead of monitoring the material loss of vegetation, a proxy is proposed to estimate the organic material potential. Both municipalities gave access to a dataset containing the tree types, locations, and heights. It is assumed that trees are dominant in the material loss by vegetation. Therefore, a vegetation factor is proposed and is defined per street, because leaves (and other organics) can easily spread over the street surface and end up in several gully pot catchments; and the trees were spread over the length of monitored streets.

The loss of material by a tree is assumed to be proportional to the size/volume of the tree. The size is estimated by the cube of the tree height, which is known. This results in the following definition of the vegetation factor (in m²):

$$V = \frac{1}{L} \sum_{j=1}^n H_j^3 \quad (2)$$

In which V is the vegetation factor, L is the length of the street, H_j is the height of tree j , and n is the total number of trees in the street. The vegetation factor is meant to represent the organic material potential. This potential varies over the year in reality (Welker et al. 2019). Halverson et al. (1985) distinguished four different phases for trees regarding the presence and absence of leaves, namely leaf abscission, leafless, leaf growth, and full capacity. These phases are combined in one categorical variable named tree phase. The start and end dates of the tree phases depend highly on climate and weather, and are based upon photos of the streets and trees made during the measurements. Only a few blossoming trees were present, which effect is therefore not separately analysed.

Table 4.2. Parameters related to the build-up of solids.

Parameter	Calculation	Data source
Connected area	The eight-direction flow approach (Jenson & Domingue 1988) to determine the size of the paved area connected to a gully pot	Digital elevation data of The Hague (from 2014) from AHN3 (Van der Zon 2013) and a similar dataset owned by the municipality for Rotterdam (from 2016).
Vegetation factor	$V = \frac{1}{L} \sum_{j=1}^n H_j^3$	Datasets from the municipalities of The Hague and Rotterdam containing tree locations and heights.
Tree phase	Classification	Visual observation
Traffic intensity	Numbers copied from the model and for streets not included in the model, estimation based upon surrounding streets with similar traffic conditions.	Traffic model (Het Samenwerkingsorgaan Holland Rijnland 2015).
Pavement type	Classification	Visual observation
Commercial land use	Classification	Visual observation
Street sweeping frequency	Estimation based upon data of ~1 year.	Tracking data of street sweepers from The Hague and timesheets from Rotterdam.

Traffic increases the solids load on streets, due to vehicles losing material (e.g. Barrett et al. 1998; Kerri et al. 1985; Deletic et al. 2000; Post et al. 2016; Simperler et al. 2019). The pavement material and the pavement condition influence the availability and transportability of solids over the street surface. This material also affects the infiltration capacity and, as a result, the discharge into a gully pot.

The solids deposition in commercial areas is generally more than in residential areas (Sartor and Boyd 1972). This can be masked by street sweeping, which is often more frequently applied in commercial areas and reduces the solids load (Sutherland and Jelen 1997). Visual observations (not quantified) during the monitoring period made clear that the street surface close to shops were more densely littered with gross solids, which could be transported to gully pots, when compared to residential areas.

4.2.3.2 Parameters related to wash-off

Build-up and wash-off models (see e.g. Sartor and Boyd 1972; Shaheen 1975; Pitt 1979; Egodawatta et al. 2007; Muthusamy et al. 2018) include usually two or three processes to model the solids transport. Firstly, the accumulation of solids on the street, secondly the wash-off rate by rain, and sometimes the removal of solids by street sweeping. The second process is schematised in this section by the wash-off related parameters presented in **Table 4.3**.

Table 4.3. Parameters related to the wash-off of solids

Parameter	Calculation	Data source
Rainfall intensity	Maximum rainfall intensity in 5-minute interval during the measurement period.	Rain radar KNMI
Rainfall volume	Mean rainfall per day during the measurement period.	Rain radar KNMI
Antecedent dry period	The number of dry days prior to the measurement period, while a day is considered dry when the rainfall intensity stays lower than 1 mm/hour in each 5-minute time slot.	Rain radar KNMI

The rainfall data used originate from the meteorological radar dataset of the Koninklijk Nederlands Meteorologisch Instituut (KNMI) or Royal Dutch Meteorological Institute. This dataset contains 5-minute interval measurements on a 1 km² grid. The 5-minute interval is used, because of the relatively small size of a gully pot catchment, which implies a short response time.

To represent the rainfall intensity the maximum rainfall intensity is taken as a parameter since it is the most important parameter for the wash-off in a rain event (Shivalingaiah and James

1984). The accumulation process is studied on a timescale of a few weeks (observation interval is 3-4 weeks), so it is integrated over the time between two measurement days. This approach to a large extent filters out processes on a smaller timescale like the variation in rain intensity. Therefore, the wash-off in that period depends on the integral of the rainfall intensity as well, which is the rainfall volume (this dependency is also observed by Shaw et al. 2010).

The solids load on streets is usually assumed to increase during dry periods (Sartor and Boyd 1972; Irish et al. 1995; Vaze and Chiew 2002; Chow et al. 2015; Morgan et al. 2017). Therefore, the initial load and subsequently the transport of solids to the gully pot in a measurement interval depend on the length of the antecedent dry period.

4.2.3.3 Parameters related to removal

An overview of the parameters included in the model to schematise the removal of solids by gully pots is provided in **Table 4.4**.

Table 4.4. Parameters related to the retention of solids.

Parameter	Calculation	Data source
Discharge	Maximum rain intensity multiplied by the connected area (Tables 3.2 and 3.3).	Rain radar KNMI and digital elevation data.
Cross-sectional area	-	Measured with measuring tape
Inlet type	Classification	Visual observation
Sand trap depth	-	Measured with measurement device
Sediment bed depth	-	Measured with measurement device
Filling degree	Sediment bed depth divided by the sand trap depth.	Measured with measurement device

Butler and Karunaratne (1995) studied the removal efficiency of gully pots in lab experiments and proposed an efficiency relation. Chapter 5 shows that this equation is in most cases a valid (engineering) estimation of the initial efficiency.

$$\eta = \frac{\alpha w}{\alpha w + \frac{Q}{A}} \quad (3)$$

In which η is the efficiency, w is the settling velocity, Q is the discharge and A is the horizontal cross-sectional area of the gully pot. The factor α (set at 0.6 by Butler and Karunaratne 1995 to obtain an acceptable agreement with their experimental results) accounts for the reducing effect of turbulence on the settling velocity, which was calculated by the application of Stokes' law, which is applicable for $Re < 0.1$.

Equation 3 contains two important concepts, namely the settling velocity and the surface loading. The settling velocity of a particle represents the gravitational force, while the surface loading represents the inertial force on a particle. The latter is defined as the discharge divided by the horizontal cross-sectional area. While the maximum rain intensity is assumed to be the main driver of solids wash-off, the maximum discharge is assumed to be the main driver of the gully pot hydraulics.

The settling velocity is not solely addressed in this study. This would involve a study of the variation in the solids' characteristics at the monitored areas and over time. These processes are already represented by parameters related to the build-up (section 4.2.3.1). Studies as e.g. Bertrand-Krawjewski et al. (1993); Zafra et al. (2008); Droppo et al. (2006); Gelhardt et al. (2017) addressed the solids' characteristics.

Post et al. (2016) showed that the sand trap depth is related to the accumulation of solids. Avila et al. (2008) and Avila et al. (2011) observed that if the water depth above the sediment bed in the gully pot is sufficiently deep, the bed did not erode. In chapter 5 it is concluded that the accumulation rate differed significantly from equation 3 when the sediment bed level increased, and eventually reduced to practically zero in conjunction with an equilibrium bed depth and bed morphology. Butler and Clark (1995) found that the equilibrium bed depth is close to the invert of the outlet pipe. Therefore, the filling degree might be the parameter that influences the removal efficiency, rather than the bed depth itself.

The type of inlet influences the hydraulic conditions in the gully pot and could reduce the inflow of solids. The dataset contains gully pots with side inlets, top inlets, and combination inlets (**Figure 4.3**). However, considering combination inlets as a separate group could lead to wrong

associations, since they are located in 1 street and their number in the dataset is limited (~4%). Since this kind of inlets is similar to side inlets from a hydraulic perspective, combination inlets are labelled as side inlets in the analysis. They have also been combined with the top inlets in the statistical analyses which did not significantly affect the results.

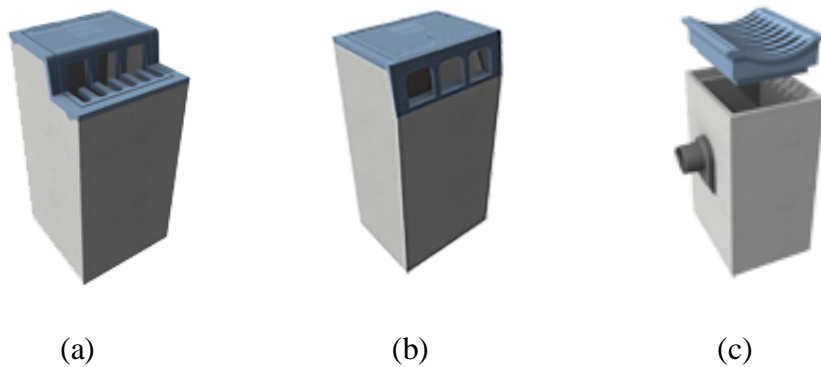


Figure 4.3. (a) Combination inlet; (b) side inlet; (c) top inlet. Source: Struyk Verwo Aqua.

4.2.4 Statistical modelling

A descriptive statistical model is required to identify the parameters which influence the accumulation rate of solids in gully pots. A Regression Tree (RT) and a Linear Mixed Model (LMM) are used to identify these parameters. Using two techniques could assist in understanding the data structure and prevent method bias.

4.2.4.1 Regression tree

RTs are commonly used in data mining to explore the structure of datasets. They contain a rule at each node, which splits the dataset into two subsets. In this research, the criterion for the best split is defined as the split predictor that minimizes the p -value of chi-square tests of independence between each (pair of) explanatory variable(s) and the response variable. If all tests yield p -values >0.05 , splitting is stopped.

The procedure to obtain a single tree for the description of the data is based upon the procedure of De'ath and Fabricius (2000) and consists of 6 steps (and is also applied in chapter 3):

- i. Divide the data into n (in this study $n=5$) random subsets of approximately equal size.
- ii. Cross-validate by dropping each subset in turn (test data) and build a tree using data from the remaining subsets (training data).
- iii. Predict the responses for the omitted subset, calculate the mean squared error for each subset and sum over all subsets.

- iv. Repeat steps (ii)-(iii) for a series of tree sizes.
- v. Take the smallest tree (the pruned tree), such that the error is within one standard deviation of the minimum error of the cross-validation trees.
- vi. Repeat m times (in this study $m=50$) steps (i)-(v) and select the most frequently occurring tree size from the distribution of selected tree sizes and subsequently a common tree.

4.2.5 Linear mixed model

LMMs are suited for repeated measurements in different groups, which are in this case the individual gully pots. The model is described as:

$$S_{i,m,g} = \beta_0 + \beta_1 X_{i,m,g,1} + \dots + \beta_p X_{i,m,g,p} + b_g + \varepsilon_{i,m,g} \quad (4)$$

In which $S_{i,m,g}$ is the i^{th} observation of the solids accumulation rate in the m^{th} measurement period in the g^{th} gully pot, $X_{i,m,g,p}$ the corresponding observation of explanatory variable p , b_g is the random effect of gully pot g , and $\varepsilon_{i,m,g}$ is the observation error. The random effect and observation error are described as:

$$\varepsilon_{i,m,g} = N(0, \sigma^2) \quad (5)$$

$$b_g = N(0, \sigma_g^2) \quad (6)$$

The residuals of the accumulation rate in an individual gully pot could be related due to, for example, inaccurate values of the independent variables. The random effect compensates for these accumulation rate differences between gully pots. The observation error accounts for errors in all observations.

The model validation (shown in Appendix B) consists of 6 steps:

- i. Take the training set, which was used for the RT (as described in section 4.2.4.1) and build a LMM.
- ii. Remove observations with a Cook's Distance larger than the 3 times the mean Cook's Distance to avoid wrong associations due to influential outliers (whenever possible the cause of the outliers was identified using the logbooks or other circumstantial evidence that exceptional situations occurred).
- iii. Evaluate the homogeneity of the residuals.

- iv. Evaluate the independence of observations by analysing the correlation of residuals in time and space.
- v. Remove step by step explanatory variables with p -values larger than 0.05.
- vi. Validate the LMM with the test set.

4.2.6 Sensitivity analysis

The accumulation rates found, as defined in equation 1, are highly scattered due to two reasons. Firstly, the depth differences between two consecutive measurements (at a small measurement interval) are relatively small compared to the measurement uncertainty, which was found to be ~5 mm by repeated (field) measurements. Since the accumulation rate is the time derivative of the solid depth, the uncertainty in the accumulation rate is substantial. Secondly, processes with both short and long timescales, both on the street and in the gully pot determine the accumulation rate. These two reasons might influence the parameter identification by the models, which are based upon non-continuous measurements of the accumulation rate. Therefore, a sensitivity analysis is performed with a dataset with a different measurement interval.

The second dataset is composed of the same measurements, but every even measurement is leapfrogged, which effectively increases the measurement interval. This reduces the relative uncertainty in the accumulation rate, but reduces the size of the dataset and smoothens the processes influencing the accumulation rate. The latter can become a disadvantage, since time-dependent parameters (such as the rainfall volume and the tree phase) lose their meaning if the time interval becomes too large. The reduced dataset is labelled as dataset 2. An overview of the range of the parameters in the two datasets is provided in Appendix C.

4.3 Results and discussion

4.3.1 Explorative analysis

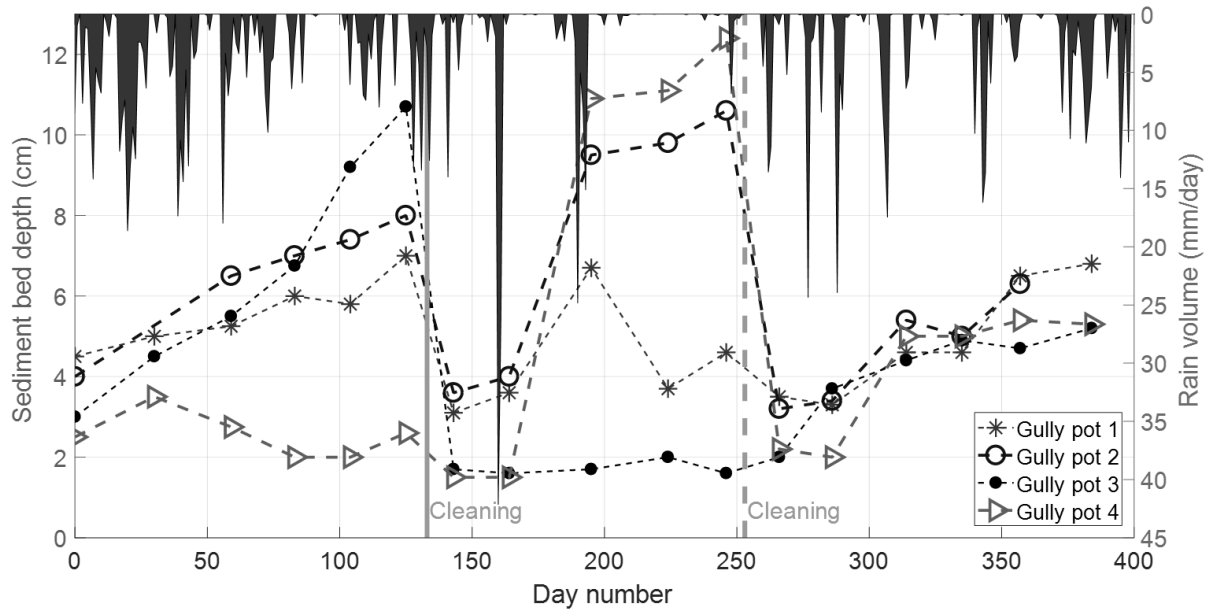


Figure 4.4. Sediment bed depth development over time in 4 gully pots, which restarts after cleaning.

Figure 4.4 shows the measured sediment bed depth development in several gully pots. The depth generally increases over time, but sometimes decreases. Such a decrease can for example be seen around day 200 for gully pot 1, which represents resuspension from the bed and might be explained by the (local) hydraulic conditions. It should also be noted that the pattern is not similar for all gully pots, due to the local (hydraulic) conditions. Gully pot 4 for example has a slower build-up rate in the beginning than the other 3 gully pots, which might have to do with hindered inflow in that period (which was not noticed during the measurements). The build-up process restarts after cleaning, which is indicated by the vertical lines in the figure.

Equation 1 is used to calculate the accumulation rate from these measurements, which results in a dataset of 4173 data points with an average accumulation rate of +18 mL/day. In section 4.3.2 and 4.3.3 statistical models are used to evaluate to what extend a range of physical parameters can explain the differences in the accumulation rate, as appearing in **Figure 4.4**.

Table 4.5. VIF values of the explanatory variables.

Variable	VIF step 1	VIF step 2
Connected area	2.87	2.86
Vegetation factor	1.55	1.53
Leafless/leaf abscission	1.66	1.65
Leaf growth/leaf abscission	1.31	1.31
Full capacity/leaf abscission	2.11	2.11
Traffic intensity	2.21	2.03
Pavement type	3.61	3.56
Commercial land use	2.81	2.68
Street sweeping	4.33	4.20
Rainfall volume	1.34	1.34
Rainfall intensity	3.95	3.93
Antecedent dry period	1.13	1.13
Discharge	5.18	5.18
Cross-sectional area	1.72	1.67
Top inlet	1.64	1.60
Sand trap depth	2.41	-
Solid layer thickness	8.68	-
Filling degree	10.1	1.09

The Variance Inflation Factor (VIF) is used to assess the collinearity in the explanatory variables. Variables with a VIF larger than 10 are removed to avoid multicollinearity (as recommended by Montgomery et al. 2012). Initially, the VIF value associated with the filling degree exceeds 10 (shown in **Table 4.5**). The filling degree is closely related to the sand trap depth and the solid layer thickness. The physical process that is expected to be influenced by these parameters is the resuspension induced by the impinging jet of the inflowing water or the reduced settling due to increased local velocities and turbulence (section 6.3.2). The closer the

sediment bed gets to the outlet pipe, the stronger these processes. To avoid overfitting and schematise this physical process, only the filling degree is selected as an explanatory variable, which makes all VIF values lower than 10.

4.3.2 Parameters related to the solids accumulation rate

The type of relation between the parameters and the accumulation rate of solids in gully pots (for dataset 1) is shown in **Table 4.6**. Parameters that correlate positively are denoted with a plus sign, whereas negative correlations with a minus sign. The β -values, standard errors, and p -values of the parameters used in the LMM are not provided here, but in Appendix B. The RT with 9 terminal nodes is shown in **Figure 4.5**.

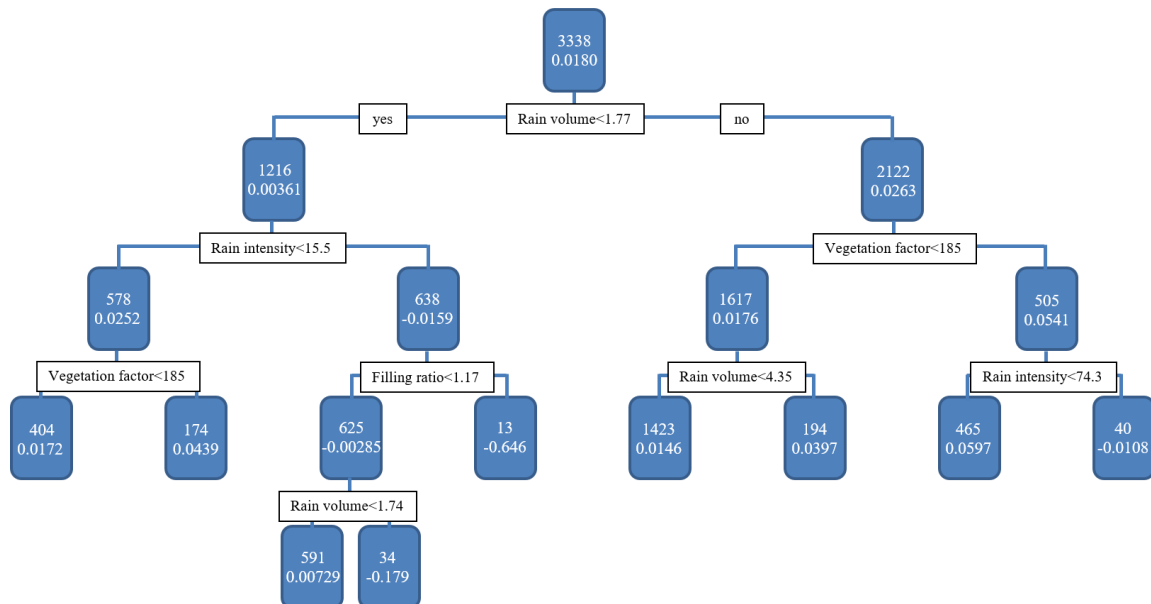


Figure 4.5. RT for dataset 1. The values at the nodes are the number of observations in the group and the mean accumulation rate of the group.

The RT contains less parameters than the LMM. The parameters used in the RT are also used in the LMM, except for the rainfall intensity which is negatively correlated with the accumulation rate in the RT. The LMM uses the discharge instead of the rainfall intensity (which is directly related) and shows a negative correlation with the accumulation rate.

Butler and Karunaratne (1995) tested discharges between 0.5 L/s and 1.5 L/s and found an inversely proportional relation between the discharge and the removal efficiency. The same physical relation was expected in particular since the range of discharges in this study is even larger (between ~0.0029 and 16 L/s).

Table 4.6. Type of relations between the parameters and the accumulation rate in gully pots. Positive correlations are denoted with a plus sign and negative correlations with a minus sign.

Parameter	Dataset 1		Dataset 2	
	RT	LMM	RT	LMM
Connected area	No relation	+	+	+
Vegetation factor	+	+	+	+
Leaf abscission	No relation	+	+	+
Leafless	No relation	-	-	-
Leaf growth	No relation	-	+	-
Full capacity	No relation	-	-	-
Traffic intensity	No relation	No relation	No relation	No relation
Pavement type (asphalt)	No relation	No relation	No relation	+
Commercial land use	No relation	No relation	No relation	No relation
Street sweeping	No relation	No relation	+	No relation
Rainfall volume	+/-	+	+/-	+
Rainfall intensity	-	No relation	-	No relation
Antecedent dry period	No relation	-	+	+
Discharge	No relation	-	+	-
Cross-sectional area	No relation	No relation	+	No relation
Top inlet	No relation	+	No relation	+
Filling degree	-	-	+/-	-

RT analysis allows investigating local relations within subgroups of the data. This reveals an interesting relation between the rainfall volume and the accumulation rate. The rainfall volume usually contributes positively, as this parameter represents the transport capacity of solids towards gully pots. However, it contributes negatively when it is combined with a high rainfall intensity. The rainfall intensity is related to the discharge to the gully pot, as stated above. An increased discharge results not only in less settling, but also in more resuspension from the

sediment bed. This resuspension increases when the high rainfall intensity is combined with a large rainfall volume.

The removal efficiency, as described by equation 2, contains not only the discharge, but also the cross-sectional area of the gully pot. However, this parameter is neither part of the LMM nor the RT. The range of cross-sectional areas (between ~ 0.045 and 0.16 m^2) might be too small to detect significant differences and the hydraulic conditions could be described sufficiently by the water inflow (discharge or rainfall intensity) which have a wider spread.

The parameters traffic intensity, pavement type, commercial land use, and street sweeping don't contribute significantly. While these parameters might have influence on the composition of the solids (on streets), the volume of these solids accumulating in gully pots does not contribute significantly to the overall solids accumulation. Traffic intensity might for example have a strong influence on the presence of heavy metals and rubber particles, but its total (volume) contribution to the accumulation rate is negligible. Moreover, the range of this parameter might be too small to detect significant differences, since only residential areas have been monitored and no highways with high traffic intensities.

The antecedent dry period is negatively correlated with the accumulation rate in the LMM, which contradicts the results of Vaze and Chiew (2002), who found that the solids load on streets increases during dry days. However, other researchers (e.g. Ellis and Harrop 1984; Charbeneau and Barrett 1998; Kerri et al. 1985; Shaw et al. 2010) concluded that the length of the dry period prior to the storm event has only a weak relationship with the solids load. Chow et al. (2015) found that the maximum solids load on a street was reached in five dry days. Considering the fact that the measurement frequency was once in 3 to 4 weeks and that $\sim 60\%$ of the days during the monitoring were dry days, several dry and wet periods could occur in between two measurements. Therefore, the antecedent dry period is less relevant in this study.

The antecedent dry period also has the largest p -value of the parameters used in the LMM. This shows at least that a proper schematisation of the effect of dry periods on the solids load in a statistical model based on non-continuous measurements of the accumulation rate in gully pots is demanding. Therefore, a sensitivity analysis (which is provided in the next section) is important for this parameter.

The vegetation factor is positively correlated with the accumulation rate in the LMM. Welker et al. (2019) found a relation between the presence of vegetation and the presence of solids on streets. These solids can be directed to gully pots via rain and wind. This process increases

during the leaf abscission phase, which is therefore positively correlated with the accumulation rate. This confirms the conclusions of Chen et al. (2017) who found that >50% of the gully pot blockages reported by citizens were registered in autumn.

The other parameters relating to the tree phases are negatively correlated with the accumulation rate when compared with the leaf abscission phase. The phases can also be mutually compared by their β -values. However, they do not differ significantly, considering the standard uncertainties.

The connected area is, similarly to the results of Post et al. (2016), positively correlated with the accumulation rate in the LMM, since it is related to the amount of solids available for transport from the street. The LMM indicates that the geometry of the gully pot is important as well; gully pots with a top inlet show a higher accumulation rate than ones with a side inlet. From visual inspection, it appeared that grids of side inlets block more solids, which reduces the accumulation rate in those gully pots.

Finally, both models signify that the accumulation rate decreases as the sand trap gets filled, which is also observed in chapter 5. This can be caused by two subsequent processes, namely the reduction of settling due to increased flow velocities and resuspension of solids from the sediment bed followed by transport to the drainage pipes.

4.3.3 Sensitivity analysis

A sensitivity analysis was performed to assess whether the selection of parameters (and their type of relation) is influenced by the uncertainty in the measurements (as discussed in section 4.2.6). Therefore, a second dataset is composed of accumulation rates over an increased time interval, by leapfrogging every even sediment depth measurement, resulting in a dataset of 3195 data points.

In general, the models (both the LMM and the RT) based upon dataset 2 identify the same type of relations as the models based upon dataset 1 (**Table 4.6**), confirming these findings. The main difference is the addition of extra parameters. **Figure 4.6** shows the RT for the dataset with an increased time interval. The tree consists of 17 terminal nodes, while the one based upon the original dataset consists of 9 terminal nodes, this implies that the data patterns are more discernible due to the reduced uncertainty.

Moreover, the performance (although still poor) of the models based upon dataset 2 improves significantly compared with the ones based upon dataset 1 (**Table 4.7**). The R^2 values indicate

that the RTs fit the measurements better than the LMMs. The RT for dataset 2 explains 29% of the variance in the training data and 17% in the test data.

Table 4.7. R^2 values of the RTs and LMMs.

Dataset	RT		LMM	
	R^2 training set	R^2 test set	R^2 training set	R^2 test set
1	0.201	0.119	0.0603	0.0315
2	0.285	0.174	0.258	0.0695

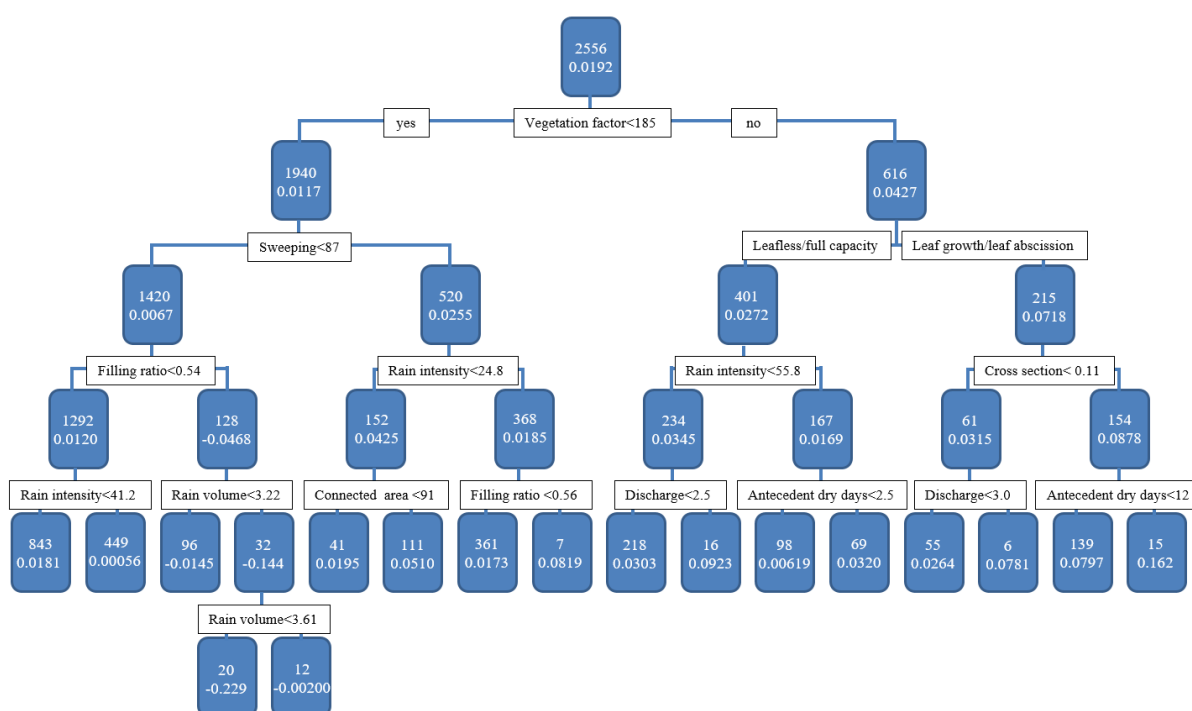


Figure 4.6. RT for dataset 2. The values at nodes are the number of observations in the group and the mean accumulation rate of the group.

The LMMs based upon dataset 1 and 2 contain the same parameters, except for the pavement type. This parameter has a p -value close to 0.05 and its impact is, therefore, less clear than other parameters. The only remaining difference is the type of relation of the antecedent dry period. This parameter is negatively correlated with the accumulation rate in dataset 1, while it is positively correlated in dataset 2. A positive correlation is expected, since the solids load on streets increases during dry days (Vaze and Chiew 2002). The RT based upon dataset 2 contains this positive relation as well.

The impact of street sweeping on the accumulation rate is discussed in literature and is generally found to be more effective for large debris than small particles (e.g. Pitt et al. 2005; Walker and Wong 1999; Amato et al. 2010). Sutherland and Jelen (1997) concluded that outdated street sweeping technologies could not pick up the finer solids and increased solids loadings to gully pots by loosening immobile solids. It was concluded that sweeping technology improved meanwhile and became efficient in reducing solids loadings. However, Walker and Wong (1999) concluded that the benefits of increasing the frequency of street sweeping, beyond what is required to meet street aesthetic criterion, is expected to be small in relation to water quality improvements. In this study, the sweeping frequency is found to correlate positively with the accumulation in dataset 2. **Figure 4.6** shows that sweeping is the second decision parameter. It splits observations from 5 streets, in subgroups representing 2 and 3 streets. Research in more streets is needed to verify that this is not coincidental and actually represents a missing parameter. Another verification method is to change the street sweeping frequency in a street that is monitored over time.

The importance of the connected area and the parameters relating to the tree phases is emphasised by the fact that they are part of both LMMs and for the RT based on dataset 2. The split in the categorical parameter tree phase in the RT is made between at one side the leaf abscission and leaf growth phase and at the other side the leafless and the full capacity phase. The LMMs show that the leaf abscission phase is the main contributor to the accumulation rate.

Although the LMMs show a negative relation between the discharge and the accumulation rate, the RT in **Figure 4.6** shows a positive relation. The significance of this relation is judged to be low, however: the parameter only appears in the lowest ranks of the tree, and, moreover, the split is defined such that only a few observations end up in one of the subgroups.

4.4 Discussion

The parameters selected by the LLMs and the RTs as being the most important in terms of describing the experimental data provide hints to identify the dominant processes in the solids accumulation rate in a batch of gully pots. However, since the model results show small R^2 values, the measured solids accumulation rate in a single gully pot cannot be successfully reproduced by these models.

A common characteristic of reported projects looking into the build-up and wash-off of solids from urban surfaces is the fact that over the past decades (Sartor and Boyd 1972; Pitt 1979; Pratt and Adams 1984; Ellis and Harrop 1984; Pitt et al. 2005) hardly any generic conclusions

have been drawn on the quantifiability of the solids loading from runoff, and only site-specific statistical relations between the solids loading and, for instance, rainfall parameters, presence of trees etc. It is a well-known fact that non-linear systems having feedback processes may initiate unpredictable dynamic behaviour, also referred to as chaotic behaviour (Genesio and Tesi 1991). In literature, some indications for such behaviour for wash-off related processes are found.

Post et al. (2016) monitored the sediment bed development of ~300 gully pots and found that ~5% got clogged due to a growing bed after ~15 months, while the sediment bed of the remaining 95% reached an equilibrium in a few months. A clear difference between these two groups of gully pots causing this difference could not be determined.

Naves et al. (2020) performed lab experiments on the wash-off from an artificial street surface and modelled this with a physically-based model. They found that despite the accurate definition of the (initial) conditions (such as the solids load on the street and the rainfall), a wide range of model (calibration) parameters was possible.

Vaze and Chiew (2002) measured the solids load in three zones of a 300 m long street over a period of 36 days on an almost daily basis. The results showed that the correlations in the solids load (collected from surfaces of 0.5 m²) between the three zones over the 36 days period are relatively low, which indicated that the spatial variability of the load is quite high. Liu et al. (2012) found that the variability of some build-up parameters within the same land use is higher than the variability between land uses.

Since the statistical models in the current study are applied to monitoring data from strongly varying spatial and temporal environments, a small R^2 value on the level of an individual gully pot could be expected. Nevertheless, patterns in the accumulation rate of solids in gully pots can and are recognised by monitoring a batch of gully pots. The limited predictability in this study and related problems in other studies may be due to inherent randomness in the processes (e.g. rain-induced uncertainty), or even non-linear feedbacks in these processes causing inherent unpredictability (chaos). Further research may assess whether the latter is the case, and if so what would be the prediction horizon. This would require more frequent and more precise observations of the sediment bed development, which proved to be impossible with the method used in this study, since the observation uncertainty relative to the bed growth is too large.

If the solids accumulation rate is not chaotic or is predictable for a substantial period, such a study could be used to assess whether the reduction in uncertainty in both the bed depth

measurements and the explanatory variables could improve the accuracy of the models significantly, as the model parameters are not fully independent, represent short- and long-term processes, and describe processes on the street and in the gully pot, reducing the predictability of statistical models based upon non-continuous measurements.

To reduce the uncertainty in the accumulation rate, a non-invasive measurement technique is required which measures at high precision (a discussion on sewer inspection techniques can be found in Tscheikner-Gratl et al. 2019). Optical techniques are not likely to be effective due to the different material phases and the dirty environment. Lepot et al. (2017) showed that sonar (which is a non-invasive technique) provides relatively small uncertainties in locating the surface of sediment layers in a sewer pipe.

The biggest advantage could be gained if sonar would be installed in the gully pot for continuous measurements to analyse the impact of individual storm events. This is substantially more expensive than the current approach (and requires some engineering for installation), especially since a considerable number of gully pots (and therefore sonars) is required for reliable analyses.

Another measurement technique to determine the sediment level, could be transferring radio waves (Moghadas et al. 2019) or current from one side to the other of the height of the gully pot. However, these techniques have not been applied in drainage systems yet, to the author's knowledge.

The vegetation factor, rainfall volume, rainfall intensity, and filling degree are the most important parameters in the RTs. The LMMs add the connected area, tree phase, discharge, and inlet type to these parameters. The most important uncertainties are found in the rainfall intensity (and consequently the discharge) and the vegetation factor. These uncertainties could be reduced by using other measurement techniques.

The discharge could be measured with discharge meters in the gully pot outlet pipes, which requires a large investment in discharge meters. These measurements can also be used to correct the connected area by comparing the discharge in adjacent gully pots.

The vegetation factor is a proxy for the amount of organic material from trees, but does not include the type of trees, other types of vegetation in the public area, or vegetation in nearby private areas. Including these parameters would make the vegetation factor more representative, but the introduction of more parameters requires also a larger dataset.

Another approach is to define a parameter that directly represents the organic material from trees present on streets. Cameras could be installed and some recognition software has to be developed. This would make the parameters that represent the tree phase redundant. Nevertheless, both approaches require a major effort.

4.5 Conclusions

The objective of this chapter was to assess to what extent the accumulation rate is influenced by physical parameters linked to the build-up of solids in a catchment, the wash-off of these solids from this catchment, and the retention of solids in the gully pot. Several parameters are identified with Linear Mixed Models (LMMs) and Regression Trees (RTs). The performance of RTs in this study is better than the LMMs, most likely due to their capability to describe different relationships between explanatory and response variables in different parts of the measurement space, which is necessary to identify the impact of parameters which are related to the accumulation rate in both a positive and negative way, such as the rainfall volume. This parameter usually contributes positively, since it increases the transport capacity, but combined with a high rainfall intensity it contributes negatively, due to increased erosion of the sediment bed.

The parameters vegetation factor, rainfall volume, and filling degree appeared in all models. Therefore, it is concluded that these are the main drivers of the accumulation rate of solids in gully pots. This implies that none of the three processes (build-up of solids in a catchment, the wash-off of these solids from this catchment, and the retention of solids in the gully pot) dominates the accumulation rate.

The sensitivity analysis shows that the parameter identification by the RT is more sensitive than the LMM for the relatively high uncertainties in dataset 1 compared to dataset 2. The sensitivity analysis indicates that the accumulation rate is also dependent on other factors (i.e. connected area, tree phase, rainfall intensity, discharge, and inlet type).

The R^2 values of these models are moderate, indicating that the solids accumulation rate in a single gully pot cannot be predicted by the models, which raises questions to what extent the models are generalisable to other spatial and temporal environments, and even (combined with literature) whether the solids accumulation would be inherently chaotic. These questions may be addressed in further research, since it affects the required research methodology. Firstly, a thorough analysis should be made of the dynamics of the individual processes influencing the accumulation rate, such as rainfall, build-up, erosion, settling etc. Secondly, it should be

analysed how the potential chaotic behaviour of these processes influence the dynamics of the solids accumulation.

If the solids accumulation process is not chaotic, it could be studied whether the reduction in uncertainty in both the bed depth measurements and the explanatory variables could improve the accuracy of the models significantly. Such a study could involve more frequent or even (semi-)continuous monitoring of the sediment bed depth and more precise measurements of the explanatory variables. The parameters 'vegetation factor' and the 'discharge' (or rainfall intensity) are the most important parameters in this respect.

PART III: GULLY POT HYDRAULICS

5 THE REMOVAL EFFICIENCY OF GULLY POTS

5.1 Introduction

The accumulation rate of solids in a gully pot depends on the solids loading to the gully pot, which was studied in chapter 2 and 3, and the removal efficiency of these solids by the gully pot. The removal efficiency of a gully pot is studied in this chapter. Butler and Karunaratne (1995) proposed an equation (related to the work of Camp 1936 and Camp 1946) to estimate this removal efficiency and regarded the removal of solids as a trade-off between surface loading and settling velocity (the latter is quantified by application of Stokes' law):

$$\varepsilon = \frac{\alpha w_s}{\alpha w_s + \frac{Q}{A}} \quad (1)$$

$$w_s = \frac{g d^2 \left(\frac{\rho_s - \rho_w}{\rho_w} \right)}{18 \nu} \quad (2)$$

In which ε is the removal efficiency, Q the discharge, w_s is the settling velocity, A the free water surface area of the gully pot, d the particle diameter, ρ_w is the density of water, ρ_s is the density of the particle, and ν is the kinematic viscosity. The factor α (set at 0.6 to obtain an acceptable agreement with the experimental results of Butler and Karunaratne 1995) accounts for the effect of turbulence, since Stokes' law is applicable for $Re < 0.1$.

The model describes a steady-state situation in which the gully pot acts as a non-return valve: i.e. it is implicitly assumed that the (growing) sediment bed does not influence the removal efficiency. Moreover, the gully pot is assumed to function as a completely mixed reactor

meaning that the concentration of solids is homogeneous and therefore the flow pattern (for example affected by the gully pot geometry) does not influence the removal efficiency. However, it has been observed that an increasing sediment bed level reduces the removal efficiency (Post et al. 2016; Langeveld et al. 2016) and the gully pot geometry does too (Post et al. 2016).

Therefore, the work presented here aims to determine, by means of scale 1:1 lab experiments, whether the sediment bed level and the gully pot geometry significantly affect the removal efficiency. Additionally, the validity of the equation provided by Butler and Karunaratne (1995) for the incorporated parameters, such as the solids' characteristics and discharge are assessed.

5.2 Methods

The experimental setup and procedure are described in section 5.2.1, the details of the measurement devices are provided in section 5.2.2, the test conditions are described in section 5.2.3, and in section 5.2.4 the post-processing of the measurements is described.

5.2.1 Experimental setup

Figure 5.1 shows the main components of the setup which was used to replicate the sedimentation and erosion processes in a gully pot. The sediment feeder (indicated with the encircled '1' in **Figure 5.1**) consists of a tank filled with the sediment selected for the experiment (described in section 5.2.3.1) and a screw conveyor which is located at the bottom of the tank to regulate the sediment flow. The motor is operated at a constant, controlled speed so as to assure a known supply rate of sediment.

The sediment gets suspended in water and is transported through an aluminium canal (with a slope of approximately 1%) to the gully pot (at '2' in **Figure 5.1**). The gully pot has a side inlet, in line with the predominant type applied in The Netherlands. The inlet (at '5' in **Figure 5.1**) splits the water in three jets which impinge on the water in the gully pot. This inlet is convertible to ensure accessibility of the setup (for e.g. cleaning or making geometrical changes).

In real conditions storm water also runs from the side to the gully pot. However, the tested conditions correspond to relatively intense rain events, in which cases a layer of water is formed in front of the gully pot inlet on the relatively flat street surfaces in The Netherlands. In those conditions the inflow direction is of less importance for the jets, except that this construction enforces a uniform depth in front of the inlet and distribution of the water over the width of the gully pot inlet (which enlarges the reproducibility of a test).

The gully pot is made out of transparent material (PMMA, also known as acrylic) to ensure optical access and its dimensions (at scale 1:1 except from the roughness) are shown in **Figure 5.1b**. It is mounted with a height-adjustable bottom as different sand trap depths are applied in practice. The outlet (at '6' in **Figure 5.1**) contains a siphon, which in practice acts as a water lock to prevent hindrance due to odours. A butterfly valve is mounted in the outlet pipe of the gully pot, which opening is adjustable to control the water level in the gully pot independent from the discharge. The water level was set at the top of the outlet pipe.

The gully pot is placed on top of a weighing scale, which is used to determine the mass of accumulated solids over time. The sediment that does not settle in the gully pot is transported to two separation tanks (at '3' in **Figure 5.1**) and settles there. These two tanks are connected with hoses to a third tank, which contains a pump. This pump recirculates the sediment-free water via another hose (at '4' in **Figure 5.1**) to the gully. In this hose, a ball valve and a flow meter (with a straight up- and downstream pipe larger than 10 and 5 times the diameter respectively) are mounted, which are used to regulate the discharge through the system.

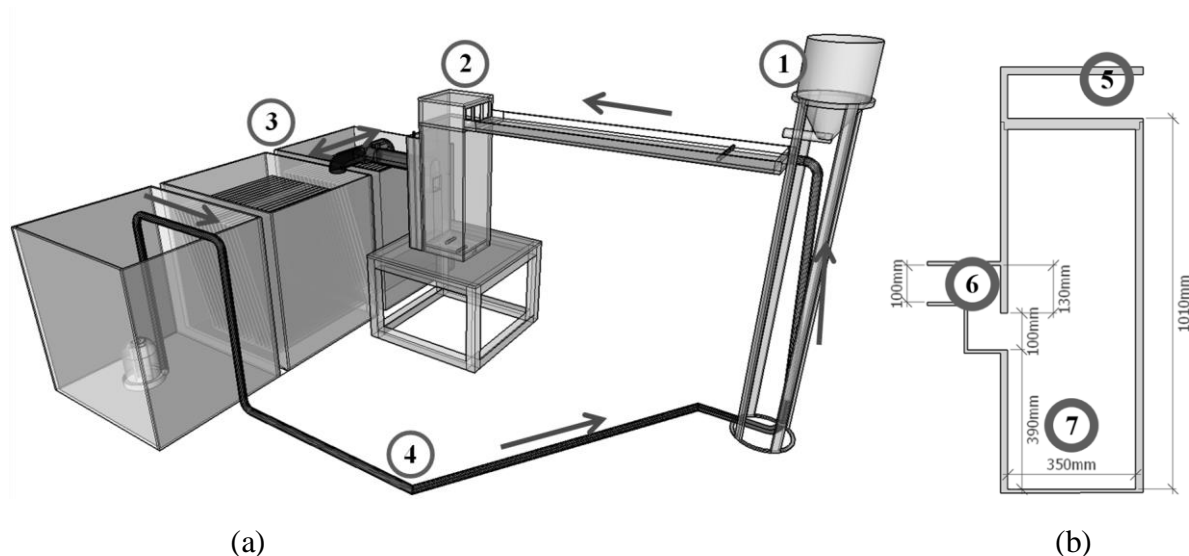


Figure 5.1. (a) Experimental setup with arrows indicating the flow direction; (b) Side view of the gully pot including its dimensions. 1. Sediment feeder 2. Gully pot 3. Separation tanks 4. Hose with control valve. 5. Convertible inlet 6. Outlet and siphon 7. Sand trap.

The tests performed were continued until the gully pot's removal efficiency of solids became $<10\%$. To decrease the duration of the tests, the concentration in the inflow was set relatively high, typically 3-4 g/L (the concentration was reduced for discharges ≤ 1.0 L/s, since sedimentation would otherwise occur in the aluminium inflow canal), compared with concentrations in the field. This resulted in test durations ranging from 3.5 up to 38 hours.

These high concentrations were assumed to have little effect on the conclusions of the phenomena influencing the removal efficiency of gully pots. Butler and Karunaratne (1995) assumed that the removal efficiency of the gully pot is independent from the inflow concentration. Moreover, the selected concentrations were lower than the generally assumed lower limit of 5 g/L for hindered settling (see for example Dankers 2006). This limit is not exceeded, except from the region close to the bed, where a transition region exists between the solid/slurry bed phase and the fluid phase. This region would also exist at lower concentrations, but its size might be larger at higher concentrations.

5.2.2 Instrumentation

5.2.2.1 Flow meter

The flowmeter is a Fischer and Porter magnetic flowmeter, model D10d, with a measurement range of 0 to 3.5 L/s. The uncertainty (95% confidence interval) of the device is estimated at $\pm 1\%$ of the full scale.

5.2.2.2 Thermometer

The temperature of the water was measured with a PT100rs thermometer in the tank which contained the pump. The device has an uncertainty $< \pm 0.05^\circ \text{C}$, but since the water's temperature in the system wasn't entirely homogeneous, the uncertainty (95% confidence interval) is estimated at $\pm 1^\circ \text{C}$. The relation between the temperature and the dynamic viscosity is described by Viswanath and Natarajan (1989):

$$\mu = 2.94 \cdot 10^{-5} \exp\left(\frac{508}{T-149.3}\right) \quad (3)$$

In which μ is the dynamic viscosity and T the temperature. The temperature in all experiments ranged $286 < T < 297 \text{ K}$, and the (kinematic) viscosity ranged $0.915 \cdot 10^{-6} < \mu < 1.21 \cdot 10^{-6} \text{ kg} \cdot \text{m}^{-1} \cdot \text{s}^{-1}$. The effect of the uncertainty in equation 3 is assumed to be negligible compared with the effect of the uncertainty in the temperature when applying equation 1.

5.2.2.3 Weighing scale

The mass of the accumulated sediment is determined with a submergible weighing scale, which is shown in **Figure 5.2**. This weighing scale was constructed by means of a platform and two Sauter CP 50-3P9 force meters with a range of 500 Newton. The uncertainty (95% confidence interval) specified by the manufacturer is $\pm 0.13 \text{ N}$, which was validated with calibrated test weights and found to be correct.

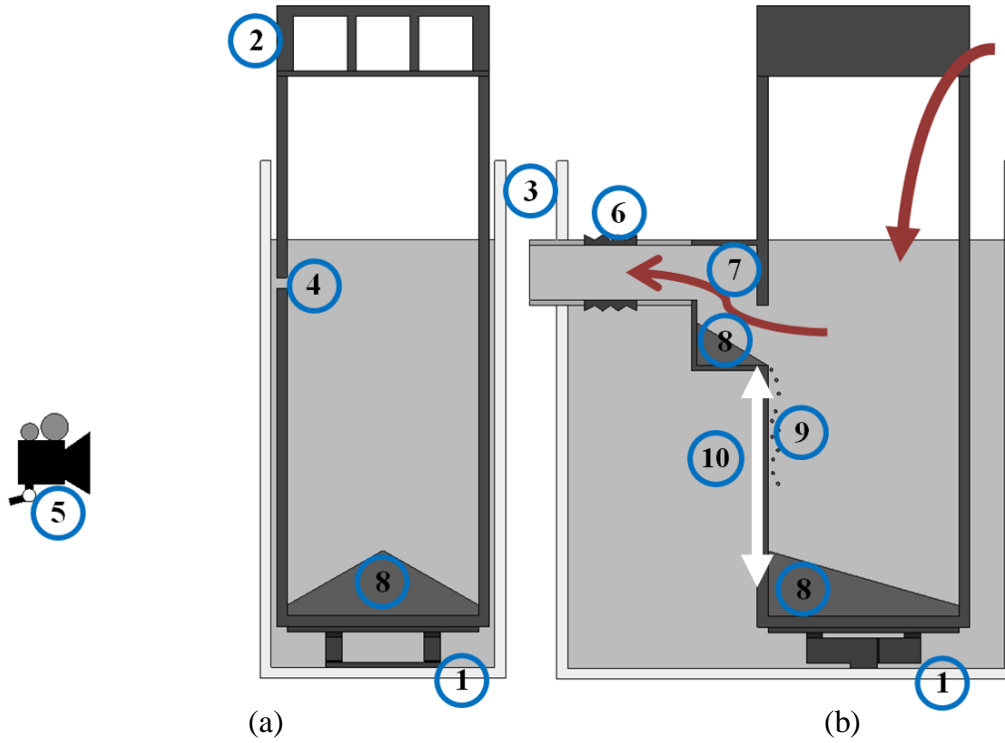


Figure 5.2. Schematic drawing of the experimental setup with red arrows indicating the flow direction; **(a)** Front view; **(b)** Side view 1. Weighing scale 2. Gully pot inlet. 3. Surrounding box. 4. Hydraulic connection between gully pot and surrounding box. 5. Camera. 6. Flexible joint. 7. Siphon. 8. Sediment accumulation. 9. Particles sliding out of the siphon into the sand trap. 10. Arrow indicating the mean free depth.

The weighing device (indicated with the encircled ‘1’ in **Figure 5.2**) was located underneath the gully pot. The gully pot itself was placed inside a PMMA box (at ‘3’ in **Figure 5.2**), which was slightly larger than the gully pot itself. To cancel out the hydrostatic pressure in the measurements, the water in the box was hydraulically connected with the water inside the gully pot via small holes in the gully pot wall (at ‘4’ in **Figure 5.2**). Small holes are applied to cancel out the effects of (slight) water level variations during the experiments. The observed increase in weight during the experiments represents the weight of the sediment itself minus the buoyancy, allowing to apply force meters with a small range and high precision. The outlet of the gully pot was connected with a flexible joint (at ‘6’ in **Figure 5.2**) to the outlet pipe and the gully pot inlet (at ‘2’ in **Figure 5.2**) was mounted a few mm above the gully pot, so as to avoid the force on the weighing scale to be affected by disturbances in the inlet or outlet. The removal efficiency of the gully pot is determined using these measurements and is defined as:

$$\epsilon = \frac{M_{accumulated}}{M_{supplied}} = \frac{\frac{F_{ws} \cdot \rho_s}{g \cdot (\rho_s - \rho_w)}}{M_{supplied}} \quad (4)$$

In which $M_{accumulated}$ is the mass of the sediment accumulated in the gully pot measured by the weighing scale, $M_{supplied}$ the mass supplied by the sediment feeder, F_{ws} is the force measured by weighing scale, and g is the gravitational acceleration. The supply rate of the sediment feeder is determined by capturing the sediment for a couple of minutes (before the experiment starts) and divide its weight by the time. The uncertainty in the mass supply rate (95% confidence interval) is estimated at $\pm 3\%$ by repeated, independent tests.

The accumulated mass (as measured by the weighing scale) can also be transformed into the depth of the sand trap not occupied by solids, which can be used to compare the results with gully pots with other cross-sectional areas. The free depth (at '10' in) is defined as:

$$D_{free} = D - \frac{M_{retained}}{\rho_s \cdot (1-pr) \cdot A} \quad (5)$$

In which D is the sand trap depth and pr the porosity. The porosity of sand depends on the compaction. Das (2008) reports $0.26 < pr < 0.43$ for coarse sand, but a more precise estimation is made in this study, by comparing the accumulated mass and volume by means of stereo photography of a sediment bed in the gully pot, resulting in a porosity of 0.33 with an estimated uncertainty (95% confidence interval) of ± 0.05 .

5.2.3 Test conditions

5.2.3.1 Solids

In literature several reports can be found on size distributions of the solids flowing into gully pots. Sansalone et al. (1998) reported $350 < D_{50} < 800 \mu m$, Pratt and Adams (1984) a D_{50} of approximately $680 \mu m$, and Ellis and Harrop (1984) $600 < D_{50} < 1000 \mu m$. Gelhardt et al. (2017) reported ρ of approximately 2500 kg/m^3 and Naves et al. (2020) of approximately 2600 kg/m^3 for street solids. To avoid health hazards and for practical reasons, it was decided to use clean sand (ρ approximately 2650 kg/m^3) to mimic real street solids in the experiments. The D_{50} 's used in the experiment were 125, 176, 389, and $1080 \mu m$ and the uncertainty (95% confidence interval) in these D_{50} 's is estimated at $\pm 10\%$ of their nominal value. The size distributions are provided in **Figure 5.3**.

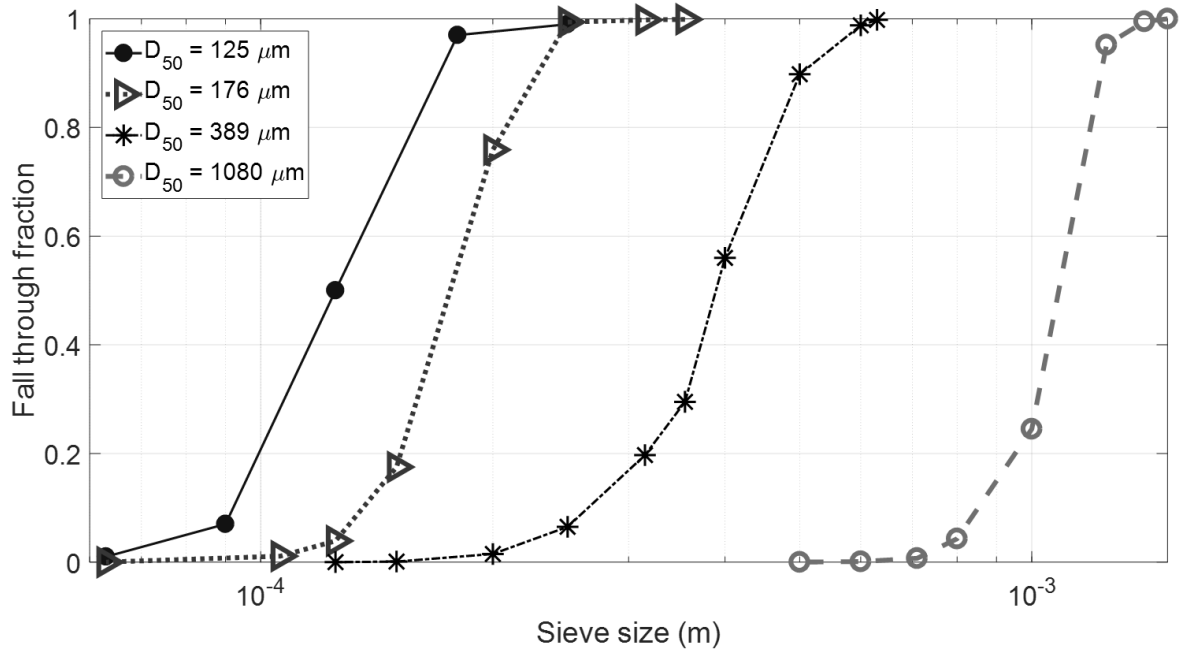


Figure 5.3. The four sieve curves of the applied solids.

5.2.3.2 Flow

Tests were performed at constant flow rates ranging between 0.35 and 2.0 L/s. This range represents a rainfall inflow intensity between 8.4 and 48 mm/hour (which is comparable to the range tested by Ciccarello et al. 2012), by dividing the flow rate by a virtual drained area of 150 m² (which is a common value in The Netherlands).

5.2.3.3 Depth

In practice, gully pots with a range of sand trap depths are applied. The influence of this parameter on the accumulation of solids was tested by adding a (transparent) false bottom. Three different depths were tested namely 0.39, 0.30, and 0.21 m.

5.2.3.4 Outlet side

Post et al. (2016) found that the orientation of the gully pot outlet (relative to the inlet) influences the solids build-up in a gully pot. This was assessed in this study by turning the gully pot relative to the inlet by respectively 90 and 180 degrees. **Figure 5.4** shows a graphical representation of the different positions.

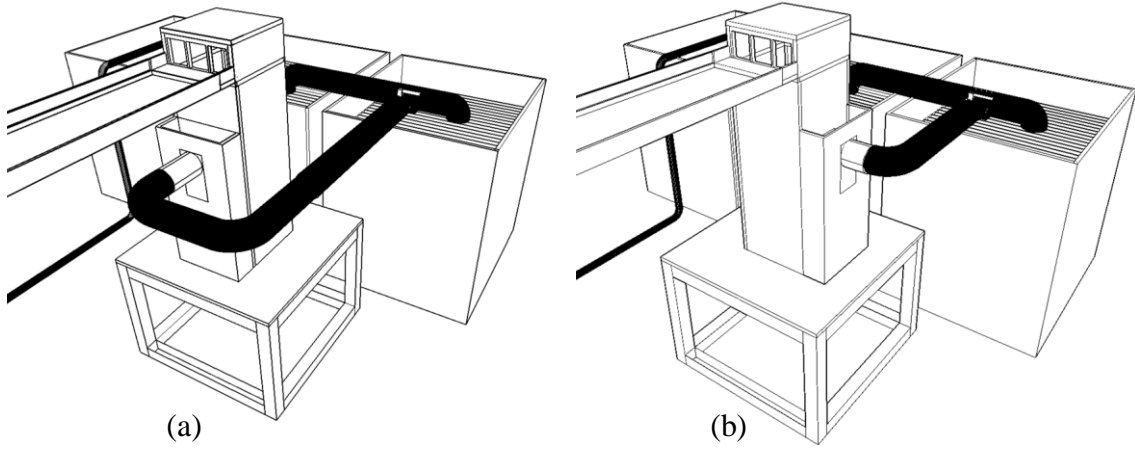


Figure 5.4. Experimental setup. (a) Front outlet; (b) Side outlet.

5.2.4 Post-processing

The observed sedimentation and erosion phenomena are quantified by means of weight measurements at a frequency of 10 Hz. These measurements show high-frequency noise, which is most likely caused by vibrations of the setup and water level fluctuations due to the impinging jets. A moving average and moving median filter were applied consecutively to identify the accumulation process in this data. The chosen time window for both filters was chosen such that 0.5 kg of solids was supplied in the time window:

$$t_w = \frac{0.5}{\left(\frac{dM_{supply}}{dt}\right)} \quad (6)$$

Filtering can be applied, since the time window of the filter is substantially shorter than the characteristic time of the accumulation process, which is estimated by an exponential fit of the accumulated mass over time. This characteristic time is for each test at least 70 times larger than the filter time window. The weight measurements over time are also converted into efficiencies over time by equation 4, which are calculated over a time window which is comparable to a supplied mass of 1 kg.

5.3 Results and discussion

For brevity, this chapter does not present all the tests. Appendix F provides an overview of the performed tests.

5.3.1 Preliminary visual observations

A webcam was installed next to the gully pot (perpendicular to the inlet, see **Figure 5.2**) to monitor the sediment bed development. **Figure 5.5** shows some characteristic images for a test

with a discharge of 1.0 L/s, gully pot depth 0.21 m, sediment size of 389 μm , and the outlet at the back.

Figure 5.5 shows that the sediment bed level was not uniform over the gully pot's cross-section. The shape of the bed depends on the position of the impinging jets, the particle's characteristics, and the gully pot geometry. In the first few hours, no resuspension was observed. Particles moved over the sediment as bed load, but already settled particles were not resuspended in the water. Some of the particles that didn't settle in the gully pot, settled in the siphon behind the gully pot (the weight of these particles is included in the weight measurement). These particles reduce the flow area, thus increasing the flow velocity. After some time, resuspension started to occur in the siphon and this bed reached an equilibrium. Sediment was continuously added, transported to the outlet to eventually slide downhill back into the gully pot itself. The latter created an extra hill on the sediment bed below the siphon as indicated in **Figure 5.2**.

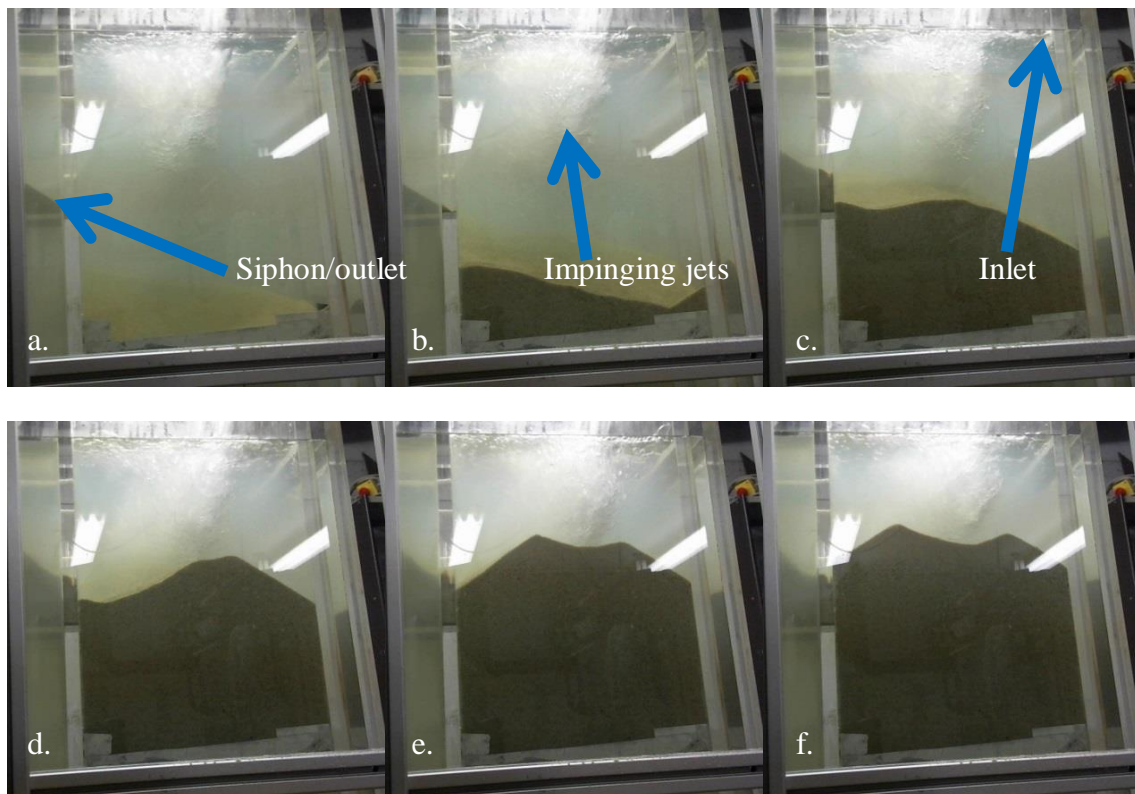


Figure 5.5. Progressive accumulation of solids over time observed from the side as indicated in **Figure 5.2**. (a) 1 hour; (b) 2.5 hours; (c) 4 hours; (d) 5.5 hours; (e) 7 hours; (f) 8.5 hours.

The three impinging jets originating from the gully pot cause air entrainment (as shown in **Figure 5.5**). The sediment bed keeps growing until it gets close to these jets, which cause increased local flow velocities. At this bed level, the effect of the sediment bed on the flow becomes apparent and the accumulation process becomes highly dynamic, particles can be

directly transported out of the gully pot, settle in the gully pot, or resuspend from the sediment bed. The sediment bed keeps growing, particularly at locations where it is still relatively thin, resulting in morphological changes (as can be seen in **Figure 5.5d-f**), until a balance between settling and resuspension is reached.

In the field measurements, presented in section 4.3.1, negative accumulation rates were reported sometimes. These negative accumulation rates are caused by the intermittent character of the inflow in field conditions, causing increased turbulence and changing balance levels. In the lab experiments only constant flows are evaluated.

5.3.2 Discharge

The effect of the growing sediment bed and the discharge is quantified by means of weight measurements. The solid line in **Figure 5.6** shows the accumulated mass in the gully pot, while the dashed line shows the supplied mass (the measurement methodologies for these masses are described in section 5.2.2.3). The lines overlap until t is approximately 4.5 hours, implying that nearly all inflowing solids settle in the gully pot. Then, the accumulated mass shows an asymptotic pattern, which means that the efficiency tends to zero. This asymptotic pattern is caused by the interaction of the growing sediment bed and the flow. The space not occupied by the sediment bed influences the start of this interaction, which is represented with the parameter free depth, as defined in equation 5 (since the sediment bed level is not uniform over the cross-section, as shown in **Figure 5.5**, it actually represents the mean free depth). **Figure 5.7** shows the removal efficiency for tests at several discharges versus the free depth.

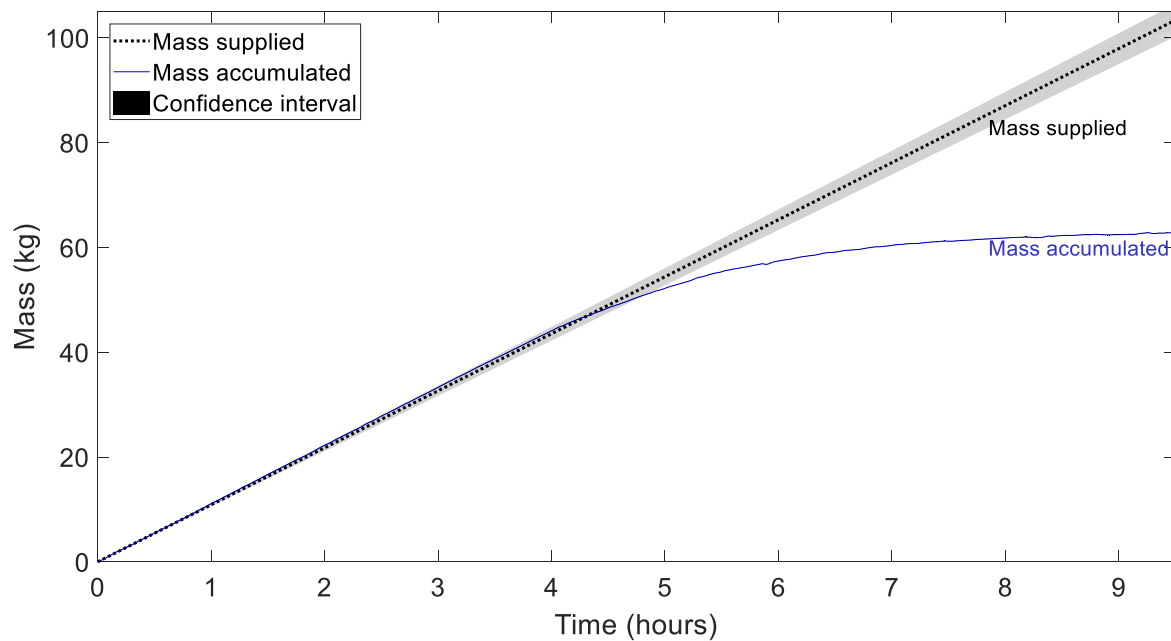


Figure 5.6. Supplied and accumulated mass over time for test with discharge 1.0 L/s, sand trap depth 0.21 m, sediment size 389 μm , and outlet at the back. Note 1: the confidence interval in the accumulated mass is small and therefore hardly visible.

Initially, the removal efficiency of the tests, shown in **Figure 5.7**, is relatively constant over the free depth. The fluctuations around these constant values can be caused by imperfections in the construction of the flexible joint (**Figure 5.2**), which could cause time lags in the weight measurements due to mechanical shocks caused by sudden lateral movement of the joint, which explains also why the efficiency can temporarily be (significantly) higher than 100% (for the test at 1.0 L/s). At a certain free depth, for example at approximately 0 m for the test at 1.0 L/s, the efficiency decreases almost linearly towards 0%. As described in section 5.3.1, this is caused by the interaction of the flow with the sediment bed.

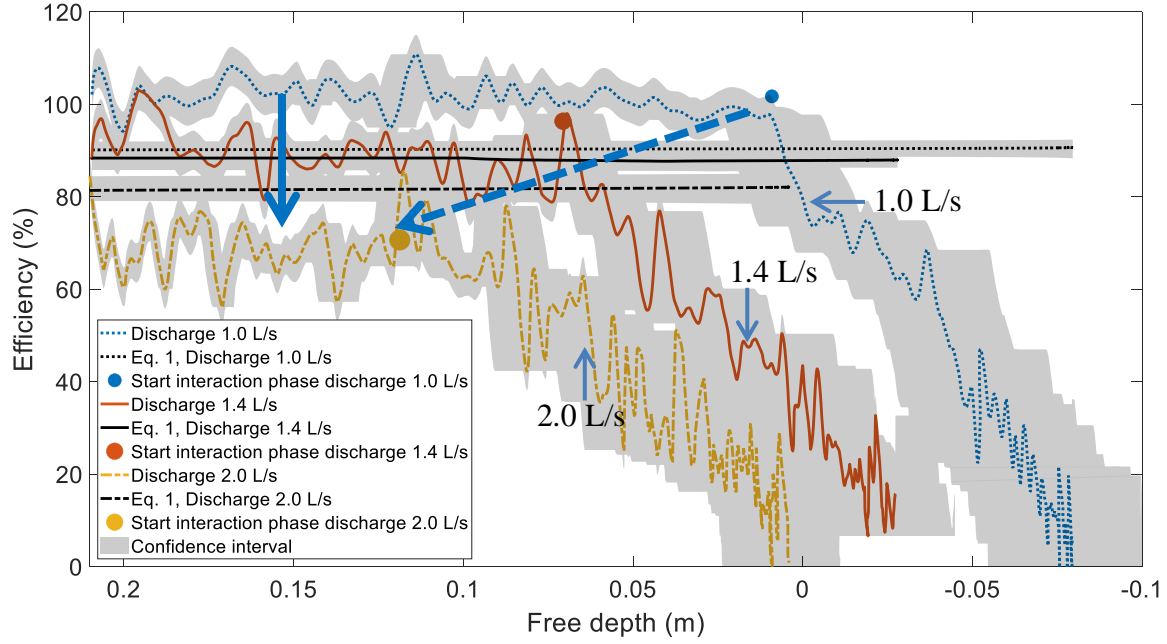


Figure 5.7. Measured and theoretical (Butler and Karunaratne 1995) efficiency and $\overline{\epsilon_1(t_x)}$ versus the free depth (a negative depth refers to a bed level higher than the invert of the siphon) for tests at several discharges. The arrows indicate the effect of an increased discharge. The solid arrow indicates a decreased initial efficiency and the dashed arrow indicates a decreased free depth at which the removal efficiency collapses.

Butler and Karunaratne (1995) hardly observed an effect of the bed on the removal efficiency in their setup with an artificially made flat sediment bed at a free depths ≥ 0 m. In the tests with discharges ≤ 1.0 L/s, the removal efficiency started to decrease at a free depth less than 0 m (and locally an even smaller free depths since the bed was not flat). This might explain why this process was negligible in the tests of Butler and Karunaratne (1995), but not in the experimental results presented here. Free depths less than 0 m (which means that the sediment bed level is higher than the invert level of the outlet) occur in practice (Post et al. 2016), since gully pot maintenance is most often aimed at preventing blockages rather than at reducing the solids loading to the downstream sewer system (Memon and Butler 2002).

Figure 5.7 shows that the discharge is inversely proportional to the removal efficiency (even when the sand trap is empty), since increasing the discharge implies increasing the inertia relative to the gravitational force. Moreover, the interaction with the bed starts at lower bed levels at increased discharges, since the shear stress increases with the flow velocity (i.e. discharge). This effect is illustrated in **Figure 5.7**, as the collapse of the efficiency tends to

occur at decreasing values of the free depth with increasing discharge. The increased local flow velocities also reduce the total mass that can accumulate in the gully pot (the retention capacity).

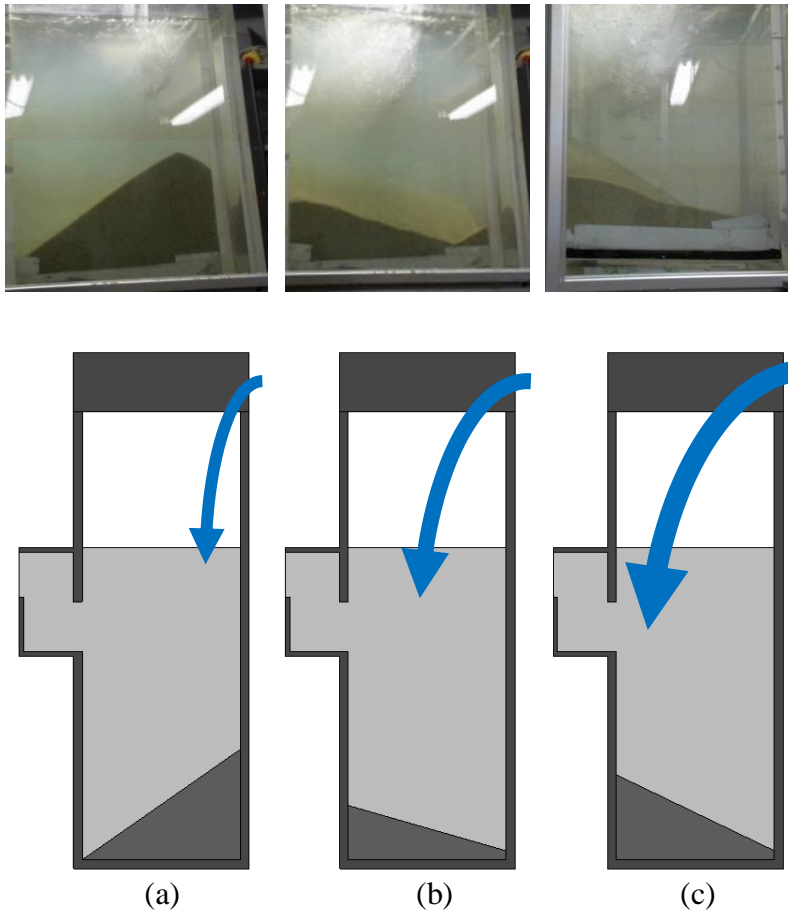


Figure 5.8. Images and schematic drawings of the sediment bed at different discharges. **(a)** Discharge 0.55 L/s; **(b)** Discharge 1.0 L/s; **(c)** Discharge 1.8 L/s.

The discharge does not only affect the magnitude of the velocity field but the position where the jets impinge on the water in the gully pot (see **Figure 5.8**) as well. At the smallest discharge, the jets stay close to the inlet, while they move closer to the outlet at increased discharges. This affects the morphological evolution of the sediment bed, since it starts building up directly below the inlet at low discharges, and below the outlet at an increased discharge. Furthermore, the intrusion depth of the impinging jet increases with increasing discharge (see **Figure 5.8**), which also influences the free depth (**Figure 5.7**) at which the sediment bed starts to influence the removal efficiency.

As discussed, two phases in the accumulation process can be distinguished, which are labelled as non-interaction and interaction phase. The distinction is based on the physical processes, but can be directly linked to the removal efficiency. Almost all tests performed in this research show a constant efficiency during the non-interaction phase and an almost linear decrease of

the efficiency during the interaction phase. The starting point of the interaction phase was identified (the black points in **Figure 5.7**) in such a manner that the combined squared error of two linear models, that fit the data at the left and right of this point, was minimised (equation 7-8).

$$\overline{\epsilon_1(t)} = \beta_{1,1}t + \beta_{1,0}, \quad t \in [0, t_x] \quad (7)$$

$$\overline{\epsilon_2(t)} = \beta_{2,1}t + \beta_{2,0}, \quad t \in [t_x + 1, t_{end}] \quad (8)$$

$$\min(SE) = \min_{t_x \in [0, t_{end}]} \left(\sum_{t=0}^{t_x} (\epsilon(t) - \overline{\epsilon_1(t)})^2 + \sum_{t=t_x+1}^{t_{end}} (\epsilon(t) - \overline{\epsilon_2(t)})^2 \right) \quad (9)$$

In which β_i is a coefficient of the linear model and t_x the time at which interaction starts. The identification of the start of the interaction phase by this set of equations should be regarded as an empirical estimation, and not a physical description of the phenomena.

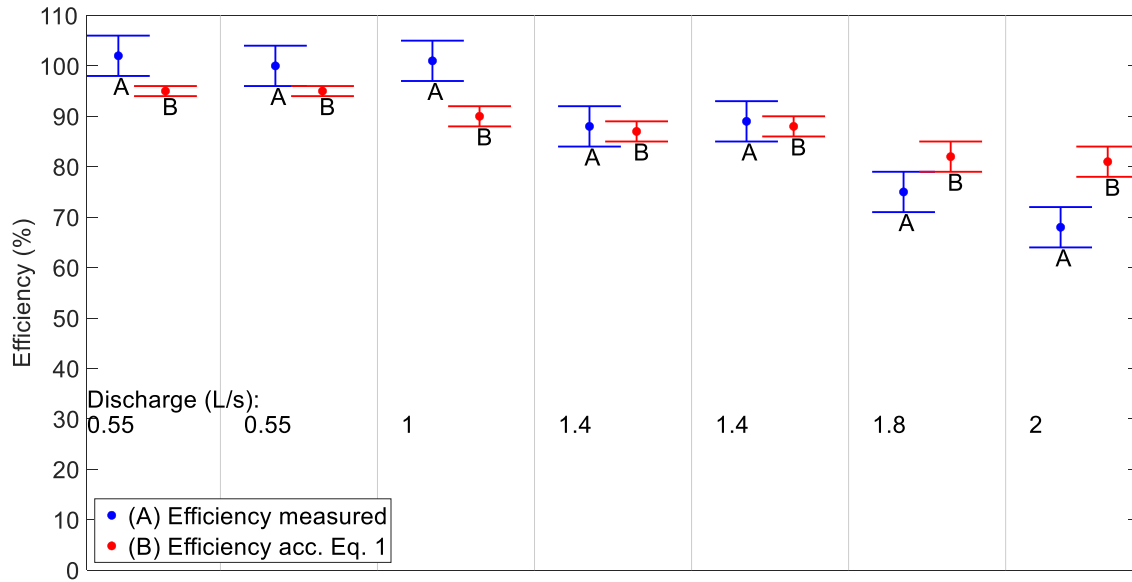


Figure 5.9. Measured and theoretical (Butler and Karunaratne 1995) efficiency during the non-interaction phase for tests with sand trap depth 0.21 m, sediment size 389 μm , and outlet at the back (the discharge is defined per column). The whiskers indicate the uncertainty induced by the uncertainty in the weight measurement and mass supply rate for the measured efficiency, and induced by the discharge, temperature/viscosity, and particle size for the theoretical efficiency.

As discussed before, the theoretical efficiency of equation 1 does not include the effect of a growing sediment bed on the removal efficiency, therefore, this theoretical efficiency is compared with the efficiency measured during the non-interaction phase in **Figure 5.9** (and in

similar figures in the next sections). The measured efficiency is significantly larger at discharges ≤ 1.0 L/s, and significantly smaller at discharges ≥ 1.8 L/s than the efficiency obtained when applying equation 1, which was proposed by Butler and Karunaratne.

Memon and Butler (2002) assessed the impact of more frequent gully pot cleanings, without considering the effect of an increasing sediment bed level on the removal efficiency. This means that a substantial reduction of the efficiency or even a stabilisation of the sediment bed was not taken into account and one might arrive at the conclusion that more frequent gully pot cleaning hardly affects the suspended solids concentration in storm water. However, Langeveld et al. (2016) showed that by cleaning out gully pots six times per year instead of once a year, the amount of removed solids increased by a factor 3. This suggests that gully pots operate in the interaction phase in practice. More frequent cleaning would keep them operating in the non-interaction phase, which reduces the solids loading to downstream parts of the drainage system.

5.3.3 Gully pot depth

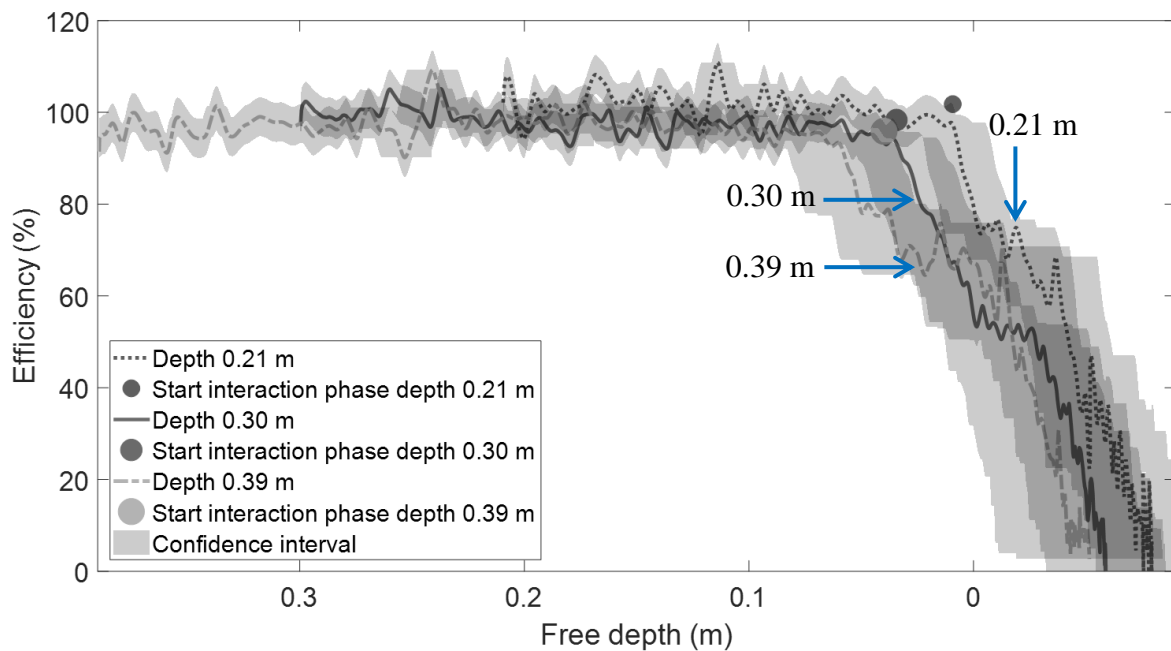


Figure 5.10. Measured efficiency and $\overline{\epsilon_1(t_x)}$ versus the free depth for tests with sediment size $389 \mu\text{m}$, discharge 1.0 L/s , and outlet at the back.

The gully pot depth is not included as a parameter in the Butler and Karunaratne (1995) model describing the removal efficiency. Post et al. (2016) showed that deeper gully pots retain more solids. Both findings are confirmed by **Figure 5.10**, which shows tests with different sand trap depths, using the same discharge and sediment size. The graphs start at different free depths due to the different sand trap depths, but do not show significant differences in the removal

efficiency. Visual observation also made clear that the development of the shape of the sediment is similar for different gully pot depths. In **Figure 5.11** an overview of the initial efficiencies is provided, which makes clear that the discharge significantly affects the efficiency, but the gully pot depth does not.

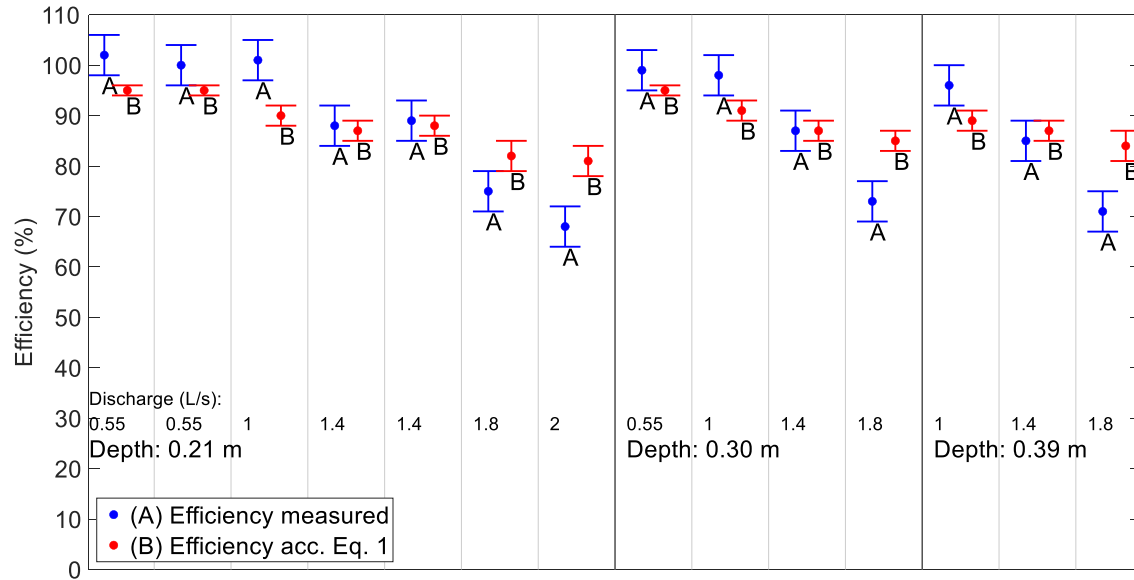


Figure 5.11. Measured and theoretical (Butler and Karunaratne 1995) efficiency during the non-interaction phase for tests with sediment size 389 μm and outlet at the back.

5.3.4 Sediment size

The settling velocity, which follows from the application of Stokes' law (shown in equation 2), depends quadratically on the sediment size. Therefore, the removal efficiency is strongly dependent on the sediment size, as shown in **Figure 5.12** for four different grain size fractions at a discharge of 1.0 L/s. For each fraction, the effect of the discharge is similar: it is inversely proportional to the efficiency during the non-interaction phase (as shown in **Figure 5.13**) and inversely proportional to the retention capacity of the gully pot.

There are no significant differences between the measured initial efficiencies and the theoretical efficiency for tests with a sediment size of 1080 μm , while significant differences exist for all other sediment sizes, which indicates that the applicability depends on the sediment size, as shown in **Figure 5.13**. Generally, the impact of the discharge is somewhat stronger than captured in the model. The efficiency is underestimated at low discharges and in some cases overestimated at high discharges.

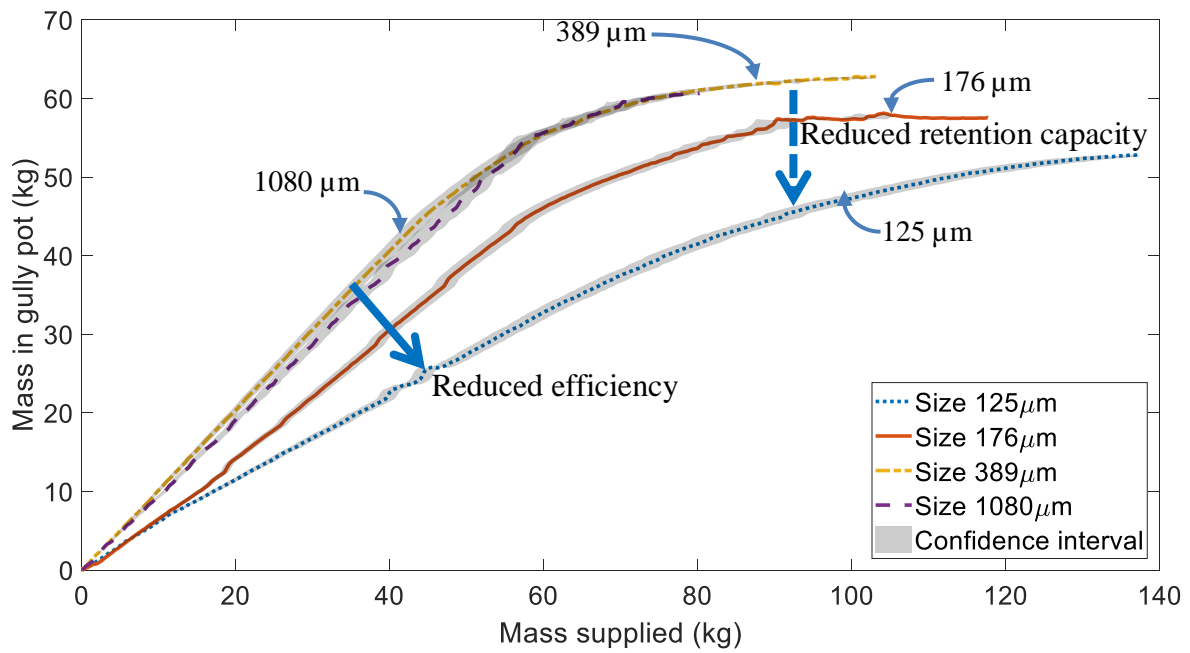


Figure 5.12. Accumulated mass versus supplied mass for tests with discharge 1.0 L/s, sand trap depth 0.21 m, and outlet at the back. The solid arrow indicates a reduced initial efficiency and the dashed arrow a reduced retention capacity due to the decreased solids size.

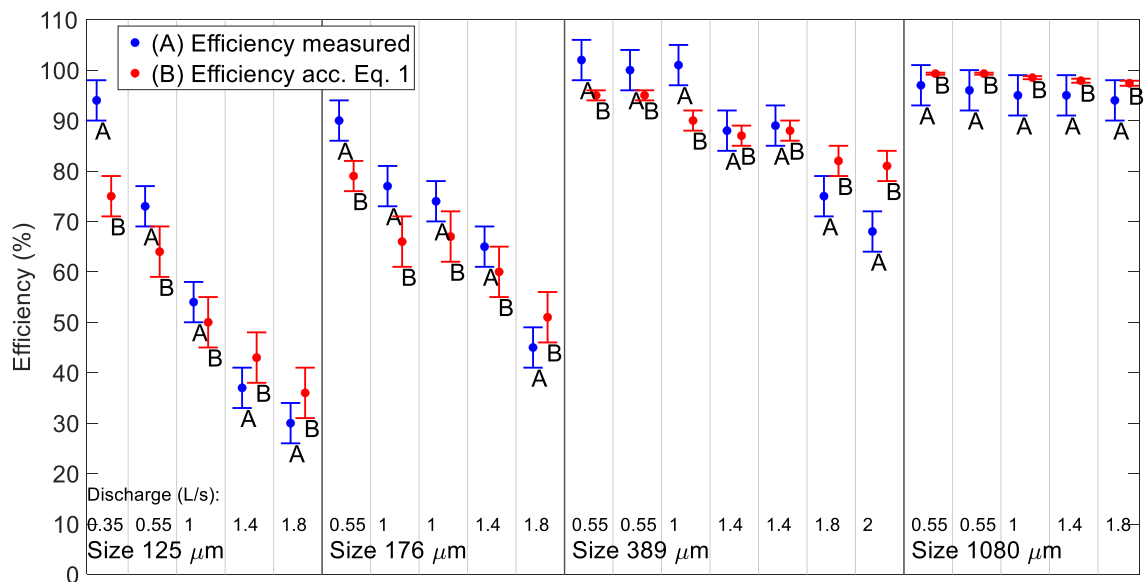


Figure 5.13. Measured and theoretical (Butler and Karunaratne 1995) efficiency during the non-interaction phase for tests with sand trap depth 0.21 m and outlet at the back.

5.3.5 Outlet position

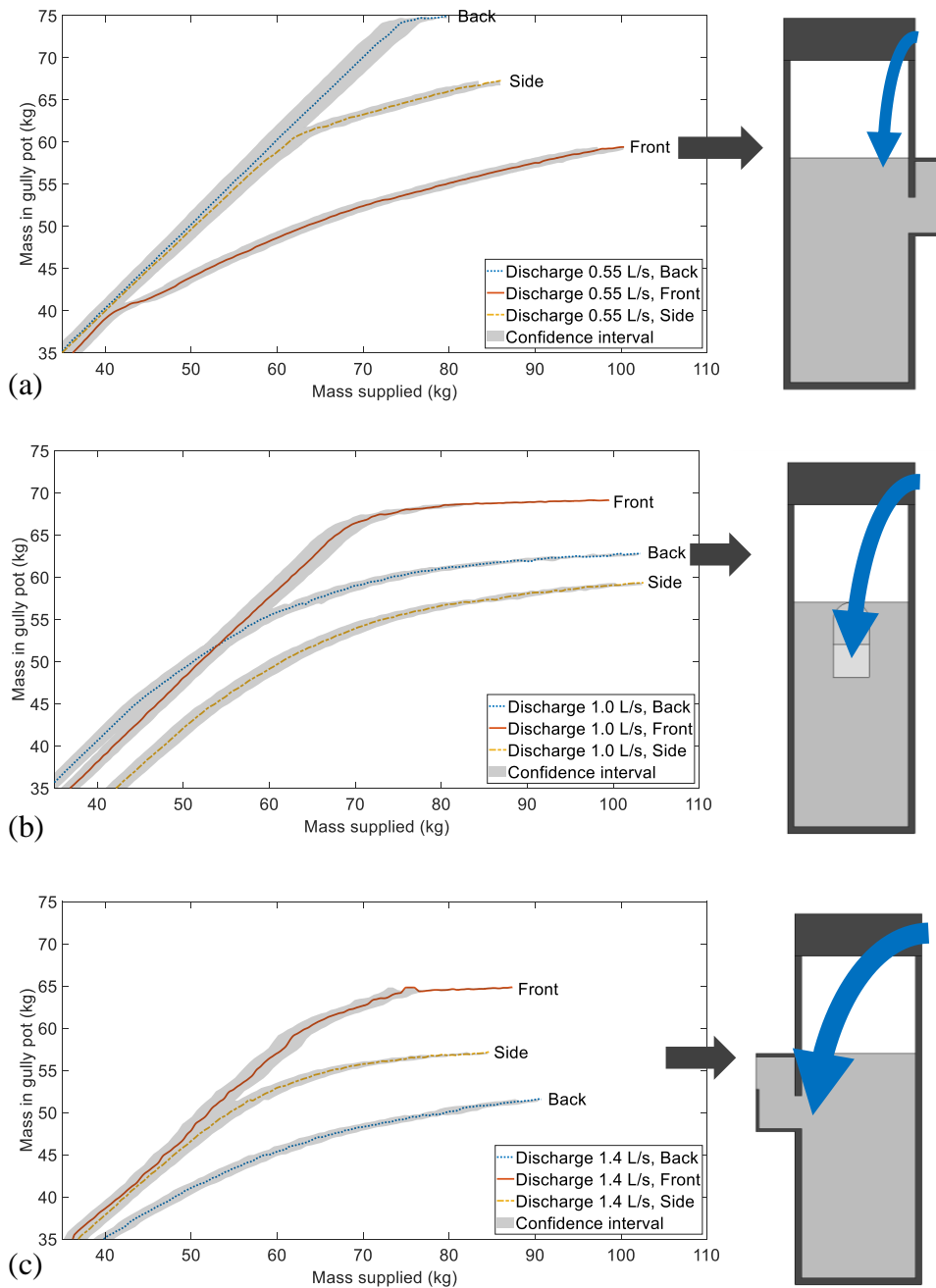


Figure 5.14. Accumulated mass versus supplied mass for tests with different outlet positions and sediment size $389\ \mu\text{m}$. **(a)** discharge 0.55 L/s; **(b)** discharge 1.0 L/s; **(c)** discharge 1.4 L/s. The drawings at the right indicate for each discharge the outlet position with the lowest removal efficiency.

The outlet position of the gully pot influences the flow pattern in the gully pot, which consecutively influences the magnitude and direction of the drag force on the particles. Since the gully pot is schematised as a completely mixed reactor in equation 1, the effects of geometrical changes on the efficiency are not considered as the hydraulic conditions are solely

represented by the surface loading. In the previous sections, the outlet of the setup was located adjacent to the inlet, at the back of the gully pot. Tests are also performed with the outlet at the front and at the side. In the latter configuration, the flow pattern is likely to be most complex, because there is no plane of symmetry.

The accumulation process is significantly influenced by the combination of the position the jets impinge on the water and the gully pot's outlet position. The closer these are together, the lower the removal efficiency, this likely to be caused by the reduction of residence time which largely depends on the distance between jet and outlet. **Figure 5.14a** shows the situation for a discharge of 0.55 L/s. At this discharge, the build-up of the sediment bed starts at the front. If the outlet is also located at the front, the crown of the bed is directly in front of the siphon. The bed partially blocks the outlet, which results in an increased flow velocity and eventually in interaction of the bed with the flow. The distance to the outlet is longest if the outlet is located at the back, which results in the latest start of the interaction phase.

At a discharge of 1.0 L/s, the jets impinge on the water in the middle of the gully pot, which is directly in front of the outlet, if it is located at the side (see **Figure 5.14b**). This induces immediate transport of suspended solids towards the outlet pipe, resulting in a reduced removal efficiency and retention capacity. At a discharge of 1.4 L/s, the jets are close to the back of the gully pot. Therefore, the removal efficiency and capacity are lowest if the outlet is located at the back, and highest if the outlet is located at the front.

The retention capacity of the gully pot with the outlet at the side was the same at all discharges (except from the lowest discharge). It might be that the local velocities above the sediment bed, and therefore the flow-bed interaction, is dominated by the layout of the gully pot and not by the discharge.

Figure 5.15 shows that the outlet position induces significant differences in the removal efficiencies. While the efficiency for a gully pot with the outlet at the back is inversely proportional to the discharge (similar to equation 1), there is no significant relation if the outlet is located at the front, and the relation for an outlet at the side is even more complex. This means that the effect of the distance between the position the jets impinge on the water and the outlet is stronger than the effect of the discharge on the removal efficiency.

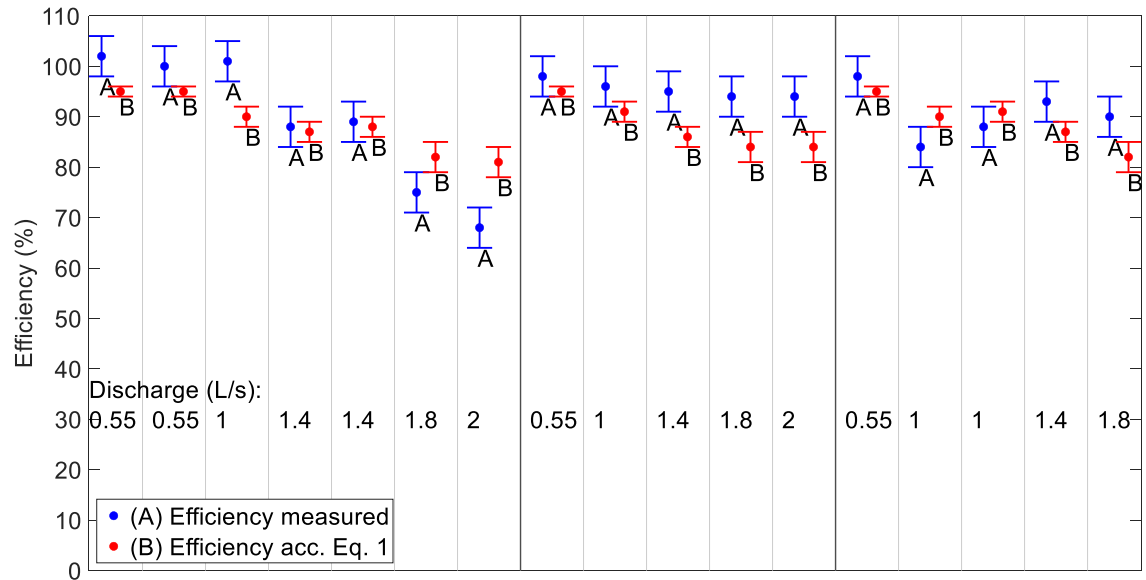


Figure 5.15. Measured and theoretical (Butler and Karunaratne 1995) efficiency during the non-interaction phase for tests with sand trap depth 0.21 m and sediment size 389 μm .

5.3.6 Position impinging jets

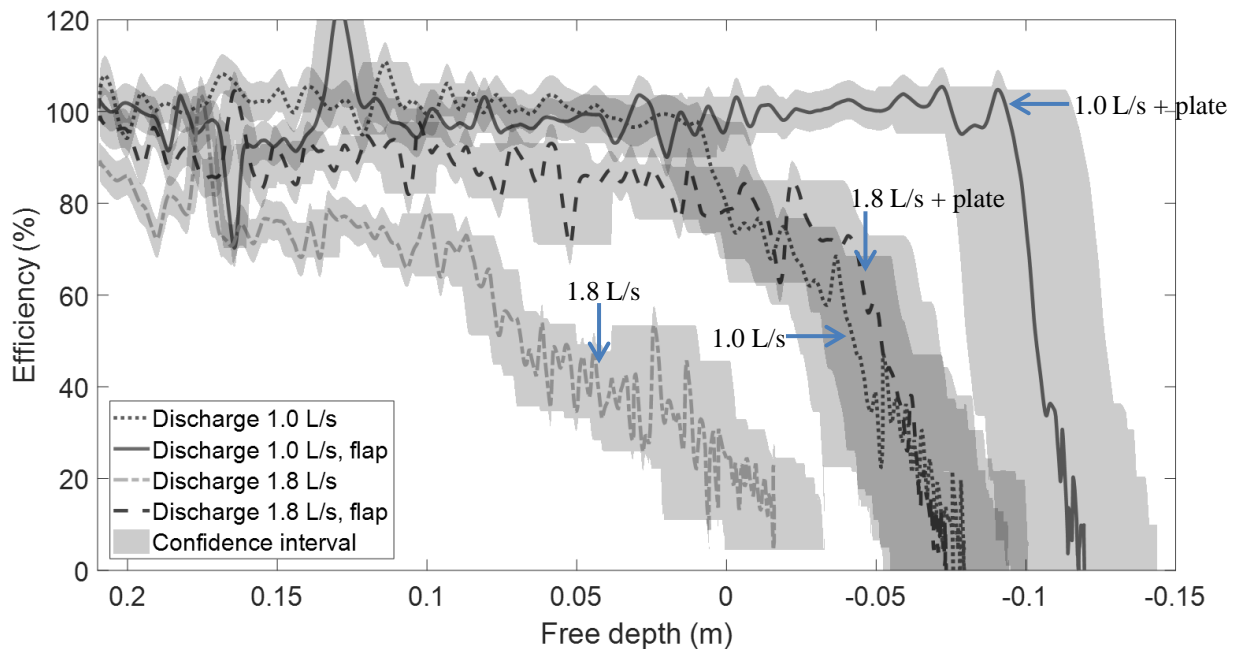


Figure 5.16. Measured efficiency versus the free depth for tests with sediment size 389 μm , discharge 1.0 L/s, outlet at the back, and with or without the plate.

In section 5.3.2 and section 5.3.5 it was concluded that not only the discharge itself, but also its effect on the position the jets impinge on the water affect the removal efficiency. To distinguish

the influence of the two phenomena, a steel plate was placed at 3 cm behind the water inlet to force the jets to impinge at a similar position (namely at the front of the gully pot, while the outlet was located at the back in these tests) regardless of the discharge. **Figure 5.16** shows that the addition of the plate increases the initial efficiency at a discharge of 1.8 L/s. The initial efficiency at a discharge of 1.0 L/s does not increase, since even without the plate it is roughly 100%.

Due to the relocation of the impinging jets, the bed morphology changes. **Figure 5.8b** and **c** show that without the plate the crown of the sediment bed is formed beneath the siphon at a discharge of 1 L/s and 1.8 L/s. **Figure 5.17a** and **b** show that with the plate the crown is formed below the inlet. The transportation length of particles resuspended at the crown of the sediment bed to the outlet is therefore strongly increased. Therefore, the reduction of the removal efficiency starts at a smaller free depth for both discharges, and the retention capacities increase.

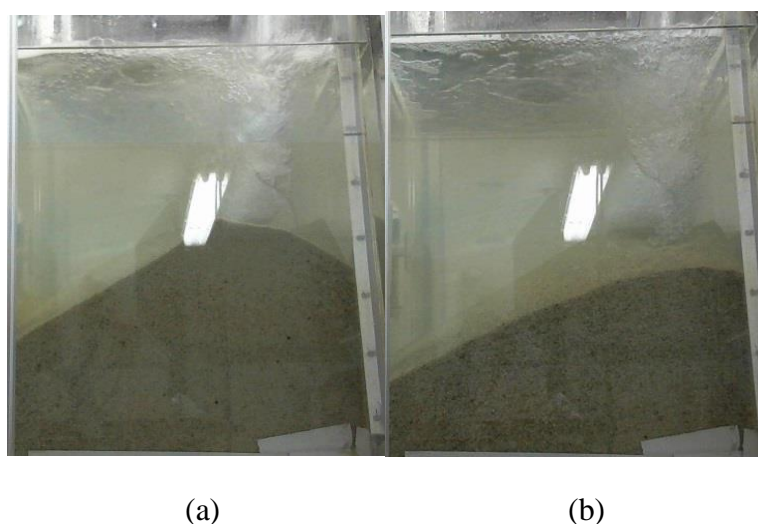


Figure 5.17. Images and schematic drawings of the sediment bed at different discharges. **(a)** Discharge 1.0 L/s; **(b)** Discharge 1.8 L/s.

5.4 Conclusions

The sediment bed development in gully pots is initially dominated by settling in the gully pot. This sediment bed develops non-uniformly in depth over the gully pot cross-section. The shape of the bed depends on the position of the impinging jet, the particle's characteristics, and the flow pattern. In the course of time, the evolution of the bed morphology starts to influence the flow field and hence the removal efficiency. Due to increased local velocities and turbulence,

settling of solids is reduced and solids in the bed can resuspend, eventually the removal efficiency tends to 0%.

Apart from the sediment bed level relative to the invert level of the outlet, the removal efficiency depends on the discharge, sediment size, and geometry. An increased discharge reduces the efficiency and the retention capacity (if the outlet is located at the back), since it increases the inertia relative to the gravitational force on the solids. The particle size has the opposite effect; larger particles result in an increased removal efficiency and retention capacity. The accumulation process is strongly affected by the flow pattern which is influenced by the combination of the position the jets impinge on the water and the outlet position (**Figure 5.14**). The tests with the plate and changed outlet positions show that this effect is, in several cases, stronger than the effect of the discharge on the accumulation process. This effect should be taken into account in the design of new gully pots.

The Butler and Karunaratne (1995) equation can be used as a first estimation of the removal efficiency before interaction with the bed starts, but generally underestimated the efficiency at low discharges (<1 L/s) and sometimes overestimated at high discharges (>1.8 L/s). Moreover, the calculated efficiencies correspond better to the experimental data for larger particles (1080 μm) than for smaller particles (125 μm).

The experimental results presented in this study show that the accumulation of solids in a gully pot is a highly dynamic process. The flow pattern and its interaction with the sediment bed are dynamic processes, influencing the solids' accumulation. A quantitative description of these processes is required to improve the efficiency models, such as the Butler and Karunaratne (1995) model.

The gully pot depth determines when the interaction of the bed with the flow starts. A deeper gully pot shows the same removal efficiency, but it takes much longer before the bed reaches the level where interaction with the flow starts. Deeper gully pots could be selected when an urban area is (re)designed, to avoid the necessity of frequent cleanings and thus high cleaning costs, while keeping a high removal efficiency.

6 THE FLOW FIELD IN GULLY POTS

6.1 Introduction

In chapter 5 the removal efficiency of solids by gully pots is discussed. This efficiency was compared with the efficiency model proposed by Butler and Karunaratne (1995) in which the gully pot is approximated as a completely mixed reactor:

$$\epsilon = \frac{\alpha w_s}{\alpha w_s + \frac{Q}{A}} \quad (1)$$

In which w_s is the settling velocity, Q the discharge, A the free water surface of the gully pot, and α a factor to include the reduction of the settling velocity by turbulence. The validity of this equation is limited to the initial removal efficiency of gully pots with an outlet at the opposite side from the inlet only, as shown in chapter 5. As soon as the sand trap gets filled, the removal efficiency drops rapidly. Since this decrease is not described by the Butler and Karunaratne equation, the model does not perform well for (partially) filled sand traps.

In addition, equation 1 models the gully pot hydraulics solely by the surface loading, implicitly assuming complete mixing. Post et al. (2016) and section 5.3 show that this is not the only process parameter, thereby suggesting that the assumption of complete mixing is not valid. Therefore, information on the flow pattern and its interaction with the sediment bed is required to understand the settling and erosion processes and to improve the efficiency models eventually.

Yang et al. (2018) simulated the flow and removal of solids in a gully pot using Computational Fluid Dynamics (CFD). The removal efficiency was validated by some physical tests performed by Tang et al. (2016) (since only a few grams of sediment were used in these tests, the reduction of the removal efficiency due to an increasing sediment bed level, was not studied), which showed that the CFD model provided acceptable results for particles $\geq 250 \mu\text{m}$, while it overestimated the efficiency for smaller particles. The flow pattern of their CFD model was validated by the flow velocity measurements of Howard et al. (2012). However, since the latter modelled a sump with a horizontal submerged inlet, the results should not have been extrapolated to gully pots with a vertical impinging jet. Faram and Harwood (2003) also modelled the removal efficiency of gully pots and validated the results with a few physical tests of the removal efficiency, no validation of the velocity fields was reported.

A quantification of the relation between parameters such as the gully pot geometry, discharge, sand trap depth, and the flow pattern is required, to understand their effect on the settling and erosion processes in a gully pot. This study presents the results from (Stereo) Particle Image Velocimetry (Westerweel et al. 2013) and Laser Doppler Anemometry measurements (Drain 1980) on the flow patterns in a gully pot. These results may be used to validate CFD simulations of the hydraulics and the water-solids interaction a gully pot.

6.2 Methods

6.2.1 Experimental setup

Figure 6.1 shows the experimental setup, which was used to mimic the flow pattern in a gully pot. The 1:1 scale gully pot, which is part of this setup, is also used in chapter 5 and is constructed using transparent material (PMMA, also known as acrylate) to ensure optical access.

The water in the setup is discharged into an aluminium canal (with a bottom slope of $\sim 1\%$) and flows towards the gully pot. This gully pot has a side inlet, in line with the predominant type applied in The Netherlands, and is mounted with a height-adjustable bottom to mimic a range of sand trap depths as applied in practice. The top of the gully pot is convertible to ensure accessibility and for changing the relative position of inlet and outlet (see **Figure 6.1b**). A butterfly valve is mounted in the outlet pipe of the gully pot, which opening is adjustable to control the water level in the gully pot independent from the discharge. The water level was set at the top of the outlet pipe. The water ends up in the reservoir and is recirculated by a pump

via a hose to the canal. The hose contains a ball valve and a flow meter, which are used to regulate the discharge through the system.

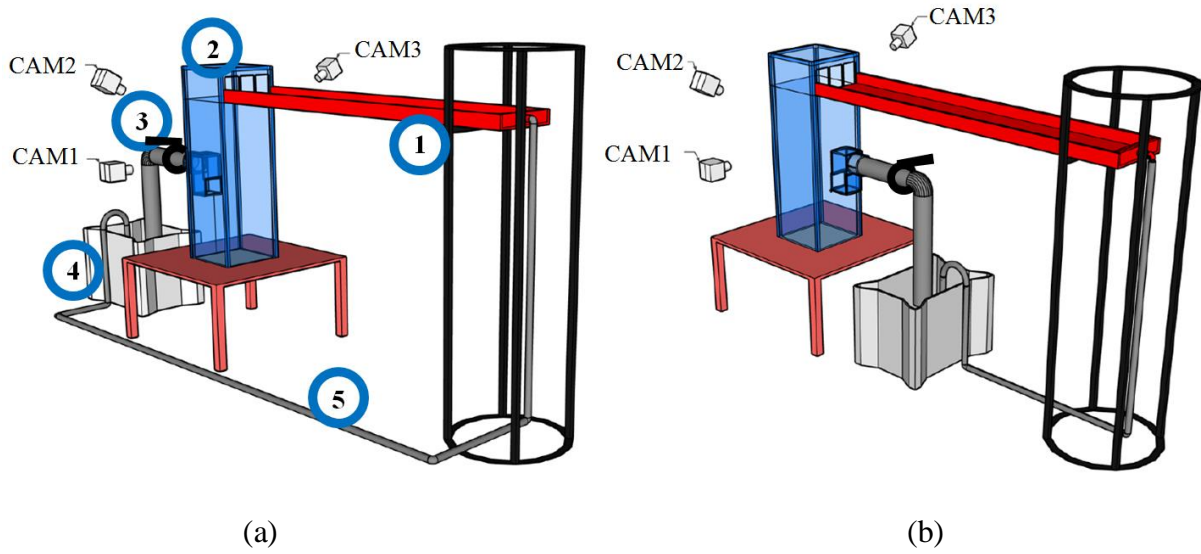


Figure 6.1. Experimental setup and camera positions 1. Aluminium canal 2. Gully pot 3. Control valve. 4. Water reservoir with pump 5. Hose with valve and flow meter. **(a)** Setup with the outlet at the back; **(b)** Setup with the outlet at the front.

6.2.2 Instrumentation

6.2.2.1 Flowmeter

The flowmeter is a Fischer and Porter magnetic flowmeter, model D10d. The measurement range is 0 to 3.5 L/s. The uncertainty (95% confidence interval) of the device is estimated at $\pm 1\%$ of the full scale.

6.2.2.2 Thermometer

The water temperature changed during the experiments due to the friction in the recirculation system, influencing the viscosity of the water. The temperature of the water in the reservoir was measured during each experiment with a PT100rs thermometer. Since the temperature in the system wasn't entirely homogeneous, the uncertainty (95% confidence interval) is estimated at $\pm 1^\circ \text{C}$.

6.2.3 PIV

The PIV equipment consists of tracer particles, laser (optics), and camera(s). The laser illuminates the tracer particles in a plane in the gully pot. The camera captures images of the tracer particles and the flow velocity is obtained by dividing the displacement of the tracer

particles in two consecutive images by the time interval between these two images. The post-processing is performed with the software package DaVis 8.4.

6.2.3.1 Tracer particles

The polyethylene tracer particles used had a density similar to water (0.99 – 1.01 kg/L) and a diameter of 90-106 μm , such that the particles followed the local stream lines (Stokes number <1). The water originating from the gully pot inlet impinges on the water surface in the gully pot, causing air entrainment. The resulting bubbles reflect the laser light and could be interpreted as tracer particles. Therefore, fluorescent (orange) tracer particles and a camera with a colour filter were applied. The filter removed the scattered light originating from the air bubbles and allowed the camera to capture the light from the illuminated fluorescent particles.

6.2.3.2 Laser

A pulsed Nd:YAG laser (Litron Nano) at 532 nm and a maximum output of 400 mJ is used to generate a laser bundle. The laser bundle is converted into a laser sheet with the use of lenses to illuminate the plane of interest.

6.2.3.3 Imaging

PIV estimates the displacement of tracer particles within a window (interrogation area) of two consecutive images taken with a known time interval. The velocity within the interrogation area (in this research an interrogation area of 32 x 32 pixels for 2D flow fields and 48 x 48 pixels for 3D flow field with 50% overlap was used) was estimated by the displacement of the particles divided by the time interval between the two images. Universal outlier detection was used for vector validation (Westerweel and Scarano 2005). The images were obtained by LaVision Imager MX cameras (sensor size of 2040 x 2048 pixels) with a Nikon Nikkor 28 mm f/2.8 lens (diaphragms used: f/4 and f/5.6).

Images were made with one camera for normal PIV to obtain a 2D flow field and with two cameras for Stereo PIV (SPIV) to obtain a semi 3D flow field (a 2D flow field and its out of plane velocity component). 2D flow fields were obtained in vertical planes, while 3D flow fields were obtained in horizontal planes (**Figure 6.4**). Camera position 1 in **Figure 6.1** was used for the PIV flow fields and positions 2 and 3 for the SPIV flow fields. For the latter, the cameras were equipped with Scheimpflug adapters at the angle such that the horizontal Plane Of Interest (POI) was in focus. The cameras were positioned at opposite sides of the gully pot at an angle of ~ 45 degrees. Acrylate water-filled prisms were mounted on the gully pot (**Figure 6.2**) to

improve the imaging by reducing the refraction effects. For each measurement 1000 double images at a sampling rate of 3 Hz were acquired to calculate the average velocity field.

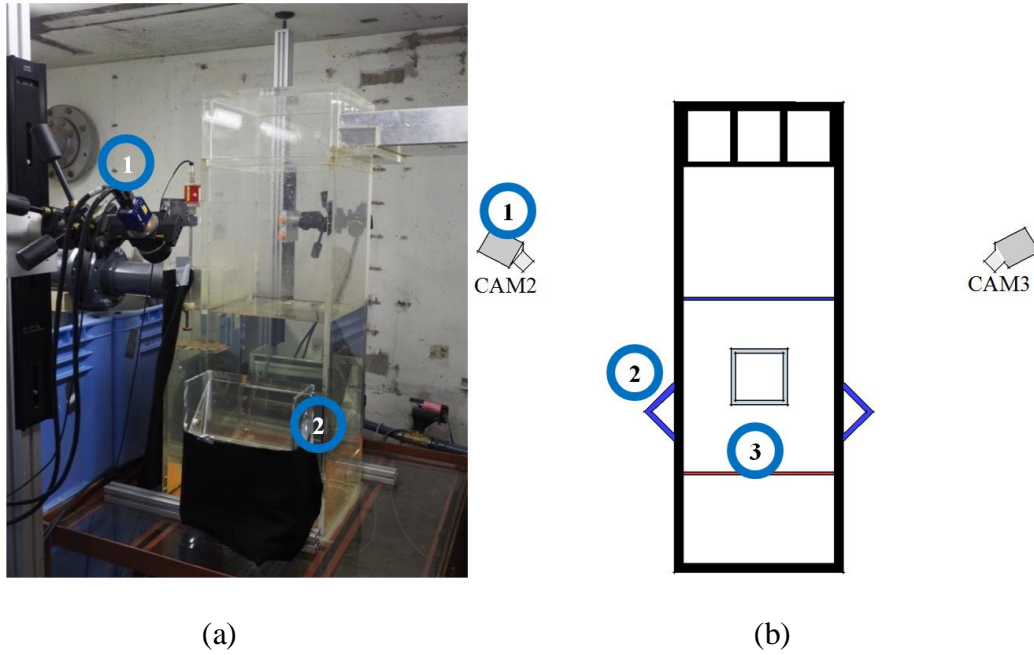


Figure 6.2. Camera setup for SPIV. 1. Camera equipped with Scheimpflug adapter 2. Acrylate prism 3. POI (a) Photo of the setup; (b) Schematic drawing of the setup.

6.2.3.4 Camera calibration

The camera calibration for each plane is performed with a calibration plate. The laser sheet was aimed at and aligned with the calibration plate. The known dimensions of the plate are used to calculate the reprojection parameters (i.e. the extrinsic and intrinsic camera parameters) and are eventually used to map the displacement of tracer particles in the camera images to real-world coordinates.

This type of calibration includes the refraction at the air/acrylate and acrylate/water interfaces, which improves the accuracy, but limits (reliable) measurements to the calibrated area. For PIV a specially designed calibration plate of 700 x 349 mm (just fitting in the gully pot) with circular markers every 10 mm was used and for the SPIV measurements a dual-level calibration plate with circular markers (LaVision, type 21) was used. The latter calibration plate is required to calculate the out of plane component of the velocity. The calibration for these SPIV measurements was further improved by self-calibration correction.

6.2.4 LDA

6.2.4.1 LDA equipment

Laser Doppler Anemometry (LDA) measurements are performed to acquire information on the turbulent fluctuations, which might influence the resuspension. The LDA system (**Figure 6.3**) consists of four main components, namely a laser unit, two optical receivers, and an electronic signal processing unit. The He-Ne laser generates a continuous 5 mW beam, which is split into three beams: one main beam and two reference beams. The beams interfere at the focal point (~40 cm in this study). Reflections of the main beam on particles in this focal point interfere with the reference beams, and contain a frequency shift due to the Doppler effect. The two modulated beams are captured by the optical receivers and processed by the electronic signal processing unit. The latter converts the frequency of the modulated signal into a two-directional flow velocity. The third component can be obtained by rotating the system 90 degrees and focus at the same measurement location.

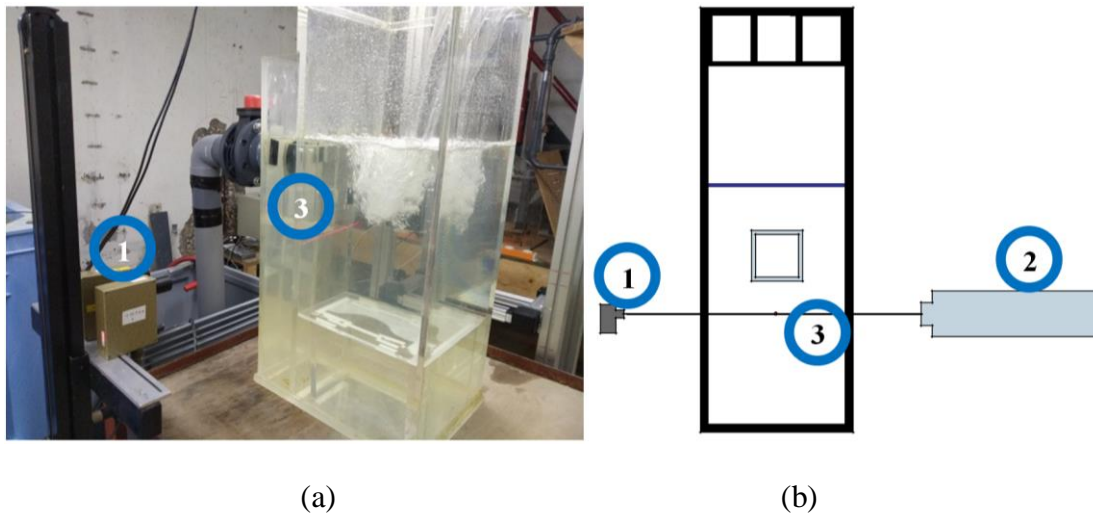


Figure 6.3. LDA setup. 1. Optical receiver 2. Laser 3. Laser beam (a) Photo of the setup; (b) Schematic drawing of the setup.

Both the laser unit and the optical receivers were placed on a traverse system. These traverse systems were used to change the measurement location. The measurement location was verified with a calibration plate (similar to the one used for the PIV system) of 600 x 349 mm (just fitting in the gully pot) with circular markers.

6.2.4.2 LDA post-processing

The LDA measurements are used to study the turbulent fluctuations, which are defined as:

$$u'_j(t) = u_j(t) - \bar{u}_j \quad (2)$$

In which u' is the turbulent fluctuation, \bar{u} the mean velocity, and u the instantaneous velocity. This decomposition of the instantaneous velocity is commonly referred to as Reynolds decomposition. The mean velocity and variance are defined as:

$$\bar{u}_j = \frac{1}{N} \sum_{i=1}^N u_j(t) \quad (3)$$

$$\overline{u_j'^2} = \frac{1}{N-1} \sum_{i=1}^N (u_j(t_i) - \bar{u}_j)^2 \quad (4)$$

The turbulent kinetic energy (TKE) is a measure of the amount of energy in the turbulent fluctuations and the turbulent intensity (TI) is a measure of the amount of energy in the turbulent fluctuations relative to the energy in the mean flow. These parameters are defined by Nieuwstadt et al. (2016):

$$TKE = \frac{1}{2} \sum_{j=1}^3 \overline{u_j'^2} \quad (5)$$

$$TI = \frac{\sum_{j=1}^3 \overline{u_j'^2}}{\sum_{j=1}^3 \overline{u_j'^2}} = \frac{TKE}{\frac{1}{2} \bar{u}^2} \quad (6)$$

The kinetic energy is distributed over eddies of various length-scales. Energy is fed from the mean flow to the large eddies and cascades down to the smallest eddies which are damped out by viscosity and eventually dissipate into molecular movement (heat). This can be displayed by the energy spectrum, which is defined as the Fourier transform of the autocorrelation of the velocity fluctuations:

$$S(\omega) = \frac{1}{2\pi} \int_{-\infty}^{\infty} e^{-i\omega\tau} R(\tau) d\tau \quad (7)$$

$$R(\tau) = \overline{u'(t)u'(t+\tau)} = \overline{u'^2} \rho(\tau) \quad (8)$$

In which ω is the angular frequency, and ρ the normalised autocorrelation function. The time-scale of the large turbulent structures, the integral time-scale, is defined as:

$$T_0 = \int_0^{t_{end}} \rho(\tau) d\tau \quad (9)$$

In which t_{end} is specified as the time at which the correlation function is zero. In addition to the integral time-scale, a turbulent flow is characterised by the integral velocity-scale (u_0) and the integral length-scale (l_0), which are defined as:

$$u_0 = \sqrt{\overline{u'^2}} \quad (10)$$

$$l_0 = T_0 \cdot u_0 \quad (11)$$

The dissipation of the kinetic energy (ϵ) at the smallest scale (Kolmogorov scale) is proportional to:

$$\epsilon \propto \frac{u_0^3}{l_0} \quad (12)$$

And in terms of these smallest scales:

$$\epsilon \propto \nu \frac{u_\eta^2}{\eta^2} \quad (13)$$

In which ν is the kinematic viscosity, and u_η and η the Kolmogorov velocity- and length-scale, which are defined as:

$$\eta = \left(\frac{\nu^3}{\epsilon} \right)^{1/4} \quad (14)$$

$$u_\eta = (\nu \epsilon)^{1/4} \quad (15)$$

The Taylor microscale can be found in between the integral and Kolmogorov scale. At this scale, the dissipation is estimated by:

$$\epsilon \propto \nu \frac{u_0^2}{\lambda^2} \quad (16)$$

In which λ is the Taylor length-scale and is defined as:

$$\lambda = l_o Re_0^{-1/2} \quad (17)$$

In case of anisotropic turbulence, equations 7-15 are defined for each direction separately, while in most cases isotropic turbulence is assumed and one value can be used. The kinetic energy is distributed over the three length-scales, which is usually displayed by the graphical representation of the energy spectrum versus the wavenumber. In case of a large mean flow compared to the turbulent fluctuations, the transformation from the angular frequency (in equation 7) to the wavenumber can easily be made via Taylor's hypothesis. In the case of a highly turbulent flow, this is not possible and the energy spectrum is expressed as energy contribution as a function of the (angular) frequency of the fluctuations (Wilczek and Narita 2012). The spectrum can mathematically be described by:

$$E(\omega) = C_\omega \epsilon^{2/3} \omega^{-5/3} \quad (18)$$

The presence of the power -5/3 can be used to validate whether real turbulence is measured.

6.2.5 Test conditions

6.2.5.1 Planes of Interest

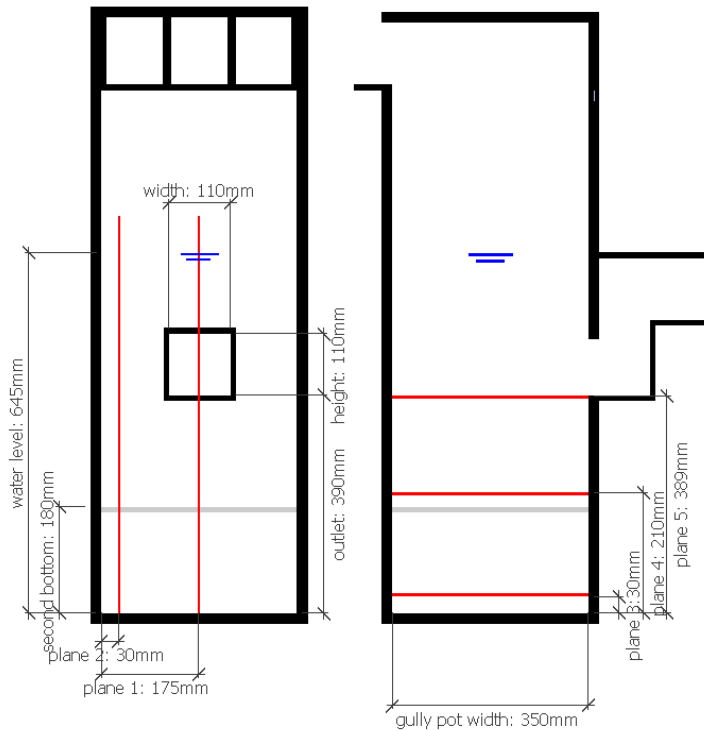


Figure 6.4. Side and front view of the planes of interest (in red) in the gully pot. The double blue lines indicate the water level, the grey line the second bottom.

Five planes of interest (POI's) were selected for (S)PIV measurements, two vertical and three horizontal planes, which are shown in **Figure 6.4**. LDA measurements are only performed in plane 1, which is the plane of symmetry in the gully pot. The flow in plane 2 includes the effect of the gully pot wall. The flow in these planes (in particular plane 1) should be mainly within rather than through the plane. Therefore, PIV measurements are performed for these planes (with the camera located at position 1 in **Figure 6.1**).

Plane 3 and 4 contain information on the flow field close to the gully pot's (second) bottom. Plane 5 contains the contraction region of the flow due to the outlet. The flow directions in plane 3, 4, and 5 are both within and through the plane. Therefore, SPIV measurements are performed for these planes, which requires two cameras (camera positions 2 and 3 in **Figure 6.1**). These measurements involved a more extensive and precise positioning and calibration of the cameras (as described in section 6.2.3.4).

6.2.5.2 Discharge

The water discharged into the gully pot represents runoff from rainfall events. The range of discharges tested in this study is 0.55 to 1.8 L/s, assuming a drained area of 150 m² (which is a common value in The Netherlands), it represents a rainfall intensity between 13.2 and 43.2 mm/hour. Rainfall events causing the latter rain intensity over at least 10 minutes occur ~2 times a year in The Netherlands (Beersma and Versteeg 2019).

Section 5.3.4 shows that for particles with a density of 2650 kg/m³ and a diameter $\geq 125 \mu\text{m}$ the initial removal efficiency is $\geq 73\%$ at a discharge of 0.55 L/s. Lower discharges will result in even higher removal efficiencies and the evaluation of the removal efficiency at these discharges will provide limited additional data for model validation. Therefore, only the velocity fields at discharges $\geq 0.55 \text{ L/s}$ is studied.

6.2.5.3 Sand trap depth

Gully pots come with a range of sand trap depths in practice, therefore a (transparent) double bottom was added to evaluate its effect on the flow pattern. Two different depths were tested namely 0.21 and 0.39 m, equal to the depths tested in chapter 5 for their effect on the removal efficiency.

6.2.5.4 Outlet position

The position of the gully pot outlet relative to the inlet influences the solids accumulation (Post et al. 2016; section 5.3.5). **Figure 6.1** shows the two outlet positions which are evaluated in this study, namely with the outlet at the back (opposite to the inlet) and at the front (adjacent to the inlet).

6.2.5.5 The presence of a sediment bed

The flow pattern and its interaction with the sediment bed are the predominant dynamic processes influencing the accumulation of solids (chapter 5). The visualisation and quantification of the flow pattern in the gully pot for a range of sediment beds provide insight into the time dependency of the efficiency. However, (S)PIV and LDA cannot be used in combination with regular loose sand because of the interference of the sand particles with the tracer particles. Therefore, artificial sediment beds were made, which represent the sand bed at various stages in the accumulation process. The development of these artificial sediment beds is described in section 6.2.6.

By using an artificial sediment bed and clean water, the influence of suspended particles on the flow pattern is excluded. This implies that, at locations with a high suspended solids

concentration (i.e. close to the sediment bed), the measured turbulent fluctuations in the sediment-free situation represent the upper limit of its intensity compared with the normal situation.

6.2.6 Stereo photography

Stereo photography, a method of combining two 2D images into a 3D object, was used to create a 3D model of the sediment bed at various stages. **Figure 6.5a** shows the setup for these measurements, which consisted of two PointGrey Blackfly cameras (sensor size of 2448 x 2048 pixels) with Fujinon HF12.5SA-1 12.5 mm f/1.4 lenses and an extra light source to improve the contrast in the images.

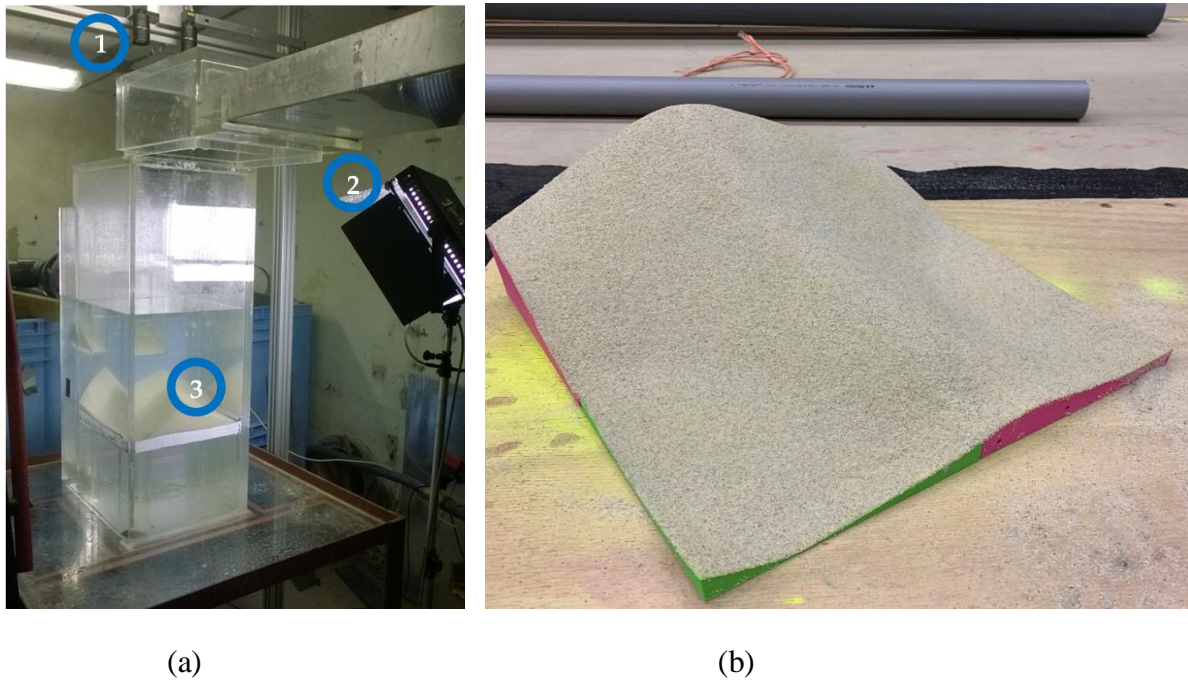


Figure 6.5. (a) The build-up of the sediment bed was carefully stopped, while the water level was kept constant and consecutively stereo photos of the bed were made with the shown setup. 1. Cameras 2. Light source 3. Sediment bed; (b) The printed sediment bed which is covered with a glued layer of sand.

The stereo camera system was calibrated (Heikkila and Olli 1997; Zhang 2000) with a calibration plate with a checkerboard pattern of 340 x 330 mm (squares of size 10 x 10 mm), which was submerged in the water in the gully pot (**Figure 6.5a**). This plate was placed in 15 different positions, varying in height and inclination to calibrate the cameras over the range of the sediment bed.

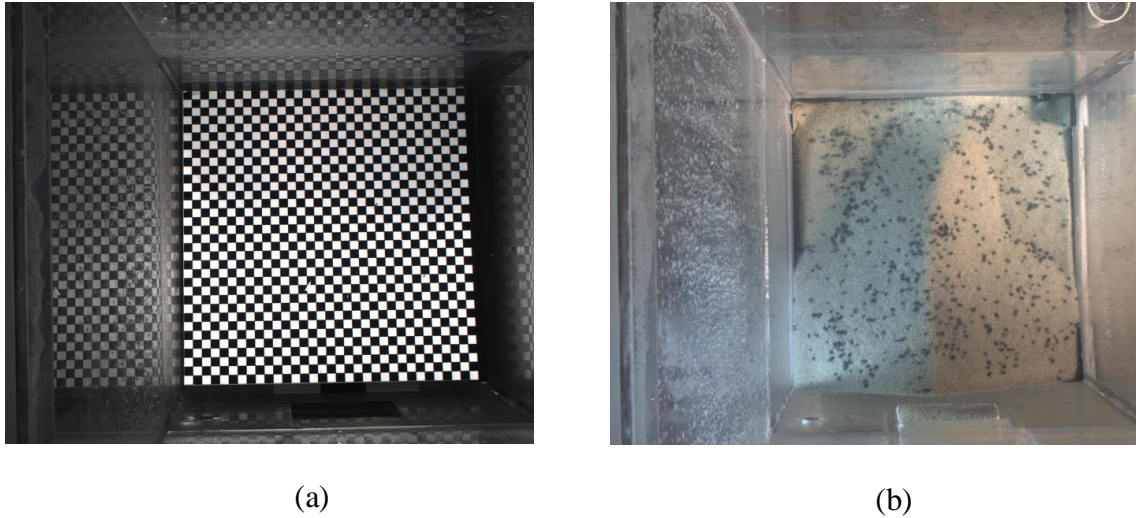


Figure 6.6. (a) Image used to calibrate the stereo photography setup; (b) Image of the sediment bed used to create the artificial sediment bed shown in **Figure 6.5b**.

Since the cameras were located above the water surface, the water level height slightly influenced the reprojection parameters, due to the light diffraction at the water/air interface. Therefore, the water level during the calibration phase (**Figure 6.6a**) was adjusted to the same height as during the measurement phase (**Figure 6.5b**). The reprojection parameters were obtained with the Stereo Camera Calibrator App in MATLAB (version 2019a). The calibration resulted in a reproduction mean error of ~ 0.33 pixels.

The recorded beds originated from a test at a discharge of 1.0 L/s, with the outlet at the back, a gully pot depth of 0.21 m, and sand with a D_{50} of 400 μm . The sediment accumulation occurred non-uniformly over the gully pot's cross-section. The shape of the bed depends on the position of the impinging jets, the particle's characteristics, and the gully pot geometry. In this test, all inflowing particles settle in the gully pot or in the siphon behind the gully pot initially, as indicated by the efficiency of $\sim 100\%$ in **Figure 6.7**. The efficiency curve shown in this figure originates from a removal efficiency test (as performed in chapter 5) at the same conditions. The mass supply rate and the elapsed time of the current test were known, which made it possible to estimate the corresponding points in the graph at which the test was stopped to obtain the stereo photos; these points are indicated in the figure.

The first recording of the sediment bed was performed in this first phase. When the sediment bed gets close to the impinging jets, originating from the gully pot inlet, the interaction between the sediment bed and the flow becomes apparent; particles can resuspend from the sediment bed and be transported out of the gully pot. The second recording was performed before and the third recording after this effect became apparent.

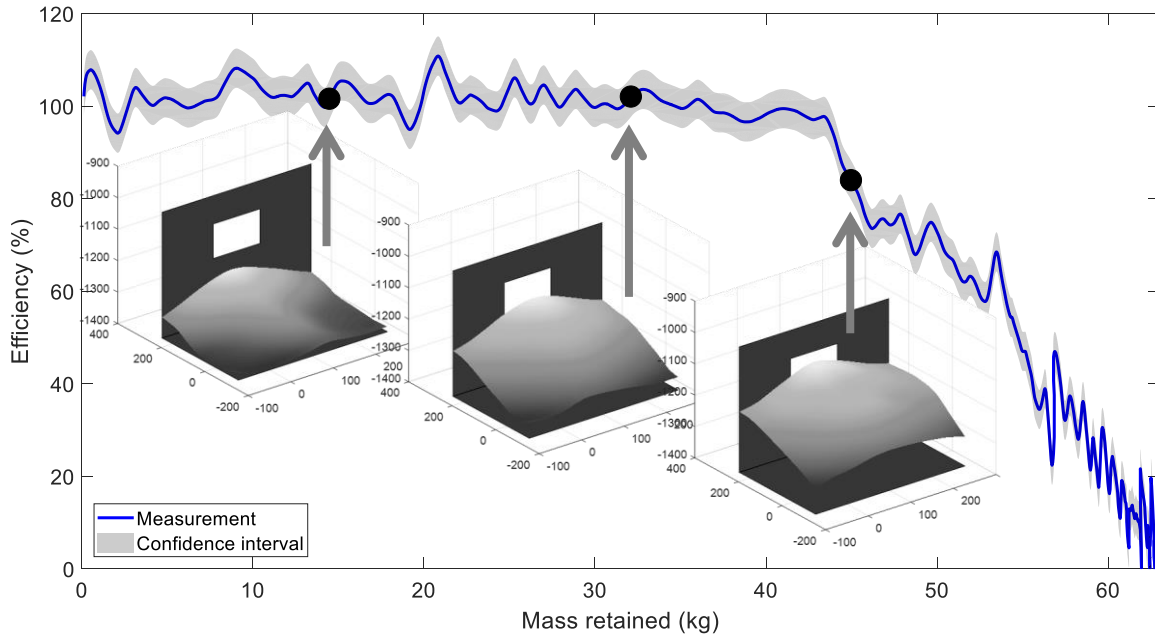


Figure 6.7. The retained mass and efficiency at which the stereo photos were obtained and the corresponding 3D representation of the sediment beds. The figures of the sediment bed also show the gully pot bottom and back wall including the outlet.

For each recording, the water inflow was carefully stopped, to prevent a collapse of the (loosely packed) sediment bed. The gully pot inlet was partially taken off (as can be seen in **Figure 6.5a**), small pebbles were added on top of the sediment bed to enhance the reference points and the 3D reconstruction of the bed (**Figure 6.6b**), and images were taken. The 3D reconstruction of the beds was performed with MATLAB and the beds were printed with a 3D printer using PLA. **Figure 6.5b** shows one of these beds, which was covered with a glued layer of sand (the same sand as originally used) for a realistic bed roughness.

6.3 Results and discussion

6.3.1 Preliminary observations in PIV and LDA measurements

Figure 6.8a shows the velocity field in plane 1 obtained with PIV for the test with sand trap depth of 0.39 m, outlet at the back, and discharge 1.0 L/s. The local flow velocity and direction are indicated with the small arrows, while the colours indicate the mean velocity. The waterjets from the inlet impinge on the water, causing air entrainment. The air bubbles distort the laser sheet strongly, causing a lack of data in that area.

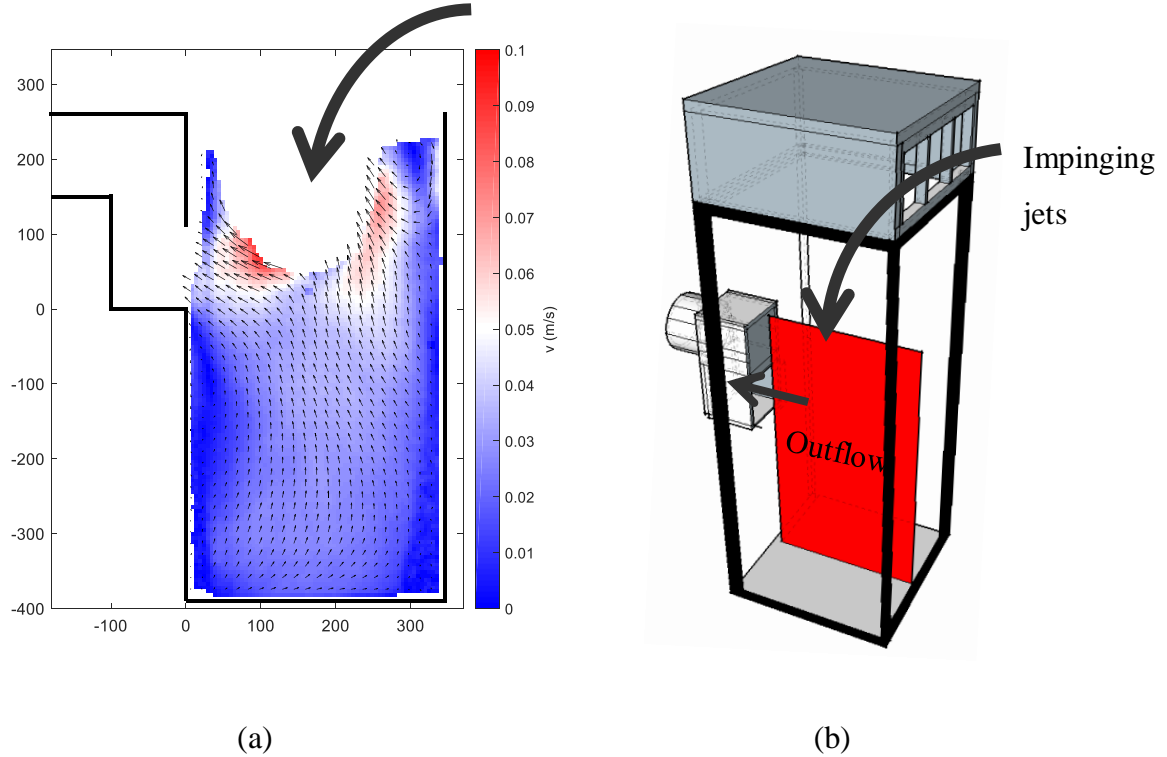


Figure 6.8. (a) Vector field and mean velocity for the test with a sand trap depth of 0.39 m, outlet at the back, and discharge 1.0 L/s. The white area in the upper part of the figure represents an area with a high fraction of air bubbles (entrained by the impinging waterjet) which disturbed the PIV measurements; (b) The POI and gully pot layout of the test.

The flow around the impinging jet is directed upwards. This is thought to be caused by the multiphase character of the flow. The entrained air bubbles rise and on their way to the water surface, the water is pulled upwards, which is not captured in the CFD simulations of Yang et al. (2018) and Faram and Harwood (2003). Avila et al. (2008) could not simulate water, air, and sediment in one CFD simulation, but did show that air entrainment significantly influences the flow field in a CFD simulation and their results are more comparable to **Figure 6.8a**. It is concluded that the flow directions in the monitored plane are determined by two low-pressure zones, namely at the outlet and at the right of the impinging jet, and one high-pressure zone, namely at the left of the impinging jet, where the water leaves the impinging jet.

The maximum velocities can be found close to the impinging jet. The colour bar represents a velocity range of 0 to 0.10 m/s. From the perspective of sedimentation, the latter corresponds with the settling velocity of a sand particle with a diameter of $\sim 630 \mu\text{m}$ (making use of the universal drag coefficient for spheres, Terfous et al. 2013).

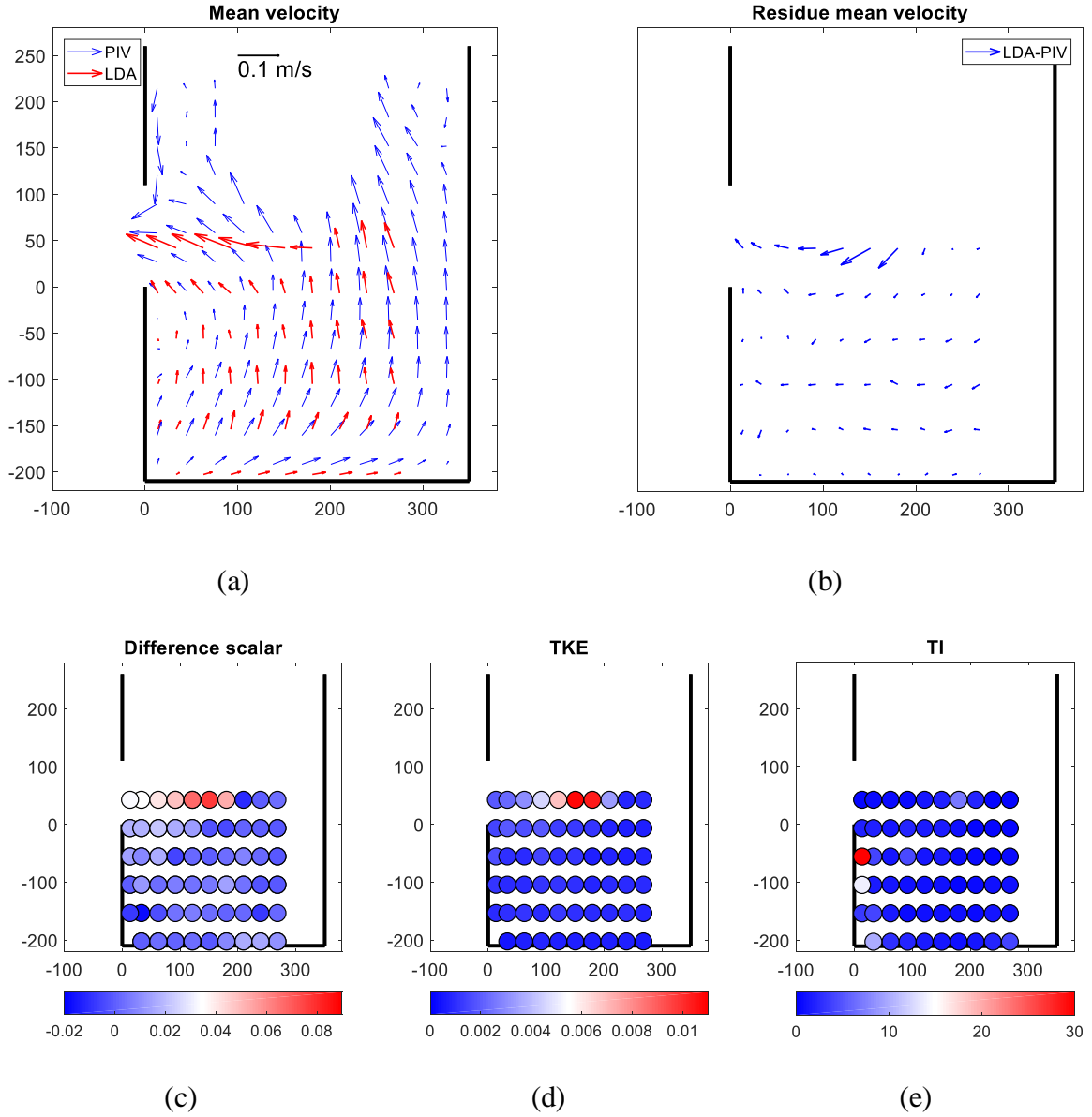


Figure 6.9. PIV and LDA results for the test with a sand trap depth of 0.21 m, outlet at the back, and discharge 1.0 L/s. **(a)-(b)** Comparisons of the mean flow velocity; **(c)** The difference scalar as defined by equation 18; **(d)-(e)** TKE and TI based upon the LDA measurements.

To be able to study the local turbulence in more detail, next to the PIV measurements, LDA measurements are performed. In **Figure 6.9a** the mean velocities obtained by both techniques are shown and **Figure 6.9b** shows the residue between the two vector fields for validation. The residue vector is defined as:

$$\Delta u_j = \overline{u_{j,LDA}} - \overline{u_{j,PIV}} \quad (19)$$

A scalar is defined to represent to what extent the magnitude and the direction of the flow of both measurements are comparable. This scalar is defined as the inner product of the difference

vector with the vector of the LDA measurement divided by the magnitude of the LDA measurement:

$$\sqrt{\sum_{j=1}^2 \Delta u_j^2} \cdot \cos(\theta) \quad (20)$$

In which θ is the angle between the residue vector and the LDA vector. This scalar is shown in **Figure 6.9c**. The difference between the two measurements is relatively large in the middle of the top row of the measurements, which is the position where air bubbles are entrained in the water. It is not known what measurement technique provides the best results in this situation. At other positions, the flow direction and velocity are more similar, indicating that the complete rebuilding of the setup in between the PIV and LDA measurement series did not significantly affect the flow field. In the remainder of this article, the LDA measurements are used to study local turbulence and the PIV measurements are used to study the overall flow field.

To assess whether the turbulence is isotropic, the fluctuations in all three directions are needed. To obtain the third velocity component (the measurements in **Figure 6.9** only contain two components), the LDA setup was rotated 90 degrees. These combined measurements were performed at 49 positions. Both measurements include the velocity in the z-direction, in which the turbulent fluctuations at all positions differ less than 30%. The standard deviations of the fluctuations relative to each other in the three directions are less than 40%. Therefore, the assumption of isotropy is made in further calculations. This provides the means to calculate the TKE and TI based upon two components, by slight changes of the definitions. For the TKE the factor $\frac{3}{4}$ replaces the factor $\frac{1}{2}$ to compensate for the third component, which effectively estimates the velocity fluctuations in the third direction by the two known directions:

$$TKE = \frac{3}{4}(\overline{u'^2} + \overline{v'^2}) \quad (21)$$

$$TI = \frac{\overline{u'^2 + v'^2}}{\overline{u^2 + v^2}} \quad (22)$$

The median (over all data points) of the turbulence intensity is 1.3, meaning that in most cases most energy is in the turbulence instead of in the mean flow, and therefore Taylor's hypothesis on frozen turbulence does not hold. The impinging jets induce a highly turbulent flow, in particular in their close proximity as can be seen by the TKE as displayed in **Figure 6.9b**.

In chapter 5 the removal efficiencies of this gully pot for sand particles with diameters of 125, 176, 389, and 1080 μm was evaluated. The turbulence strongly influences the flow path of the smaller particles, since the TKE (which obviously depends on the discharge) in **Figure 6.9d** is

at all evaluated locations larger than the square of the settling velocity of sand particles with a diameter of $<176\text{ }\mu\text{m}$, while it smaller at almost all locations for particles $>389\text{ }\mu\text{m}$. Therefore, an improved efficiency model (based on equation 1) needs to include turbulent effects. Additionally, the CFD model of Yang et al. (2018) overestimated the removal efficiency of small particles. This might be due to these turbulent effects, which keeps small particles in suspension and reduces settling.

In **Figure 6.10**, the power $-5/3$ dependency in the power spectrum is visible, indicating that there is turbulence indeed. The two velocity components show a similar power spectrum, and could also be displayed as one spectrum since isotropy was already assumed.

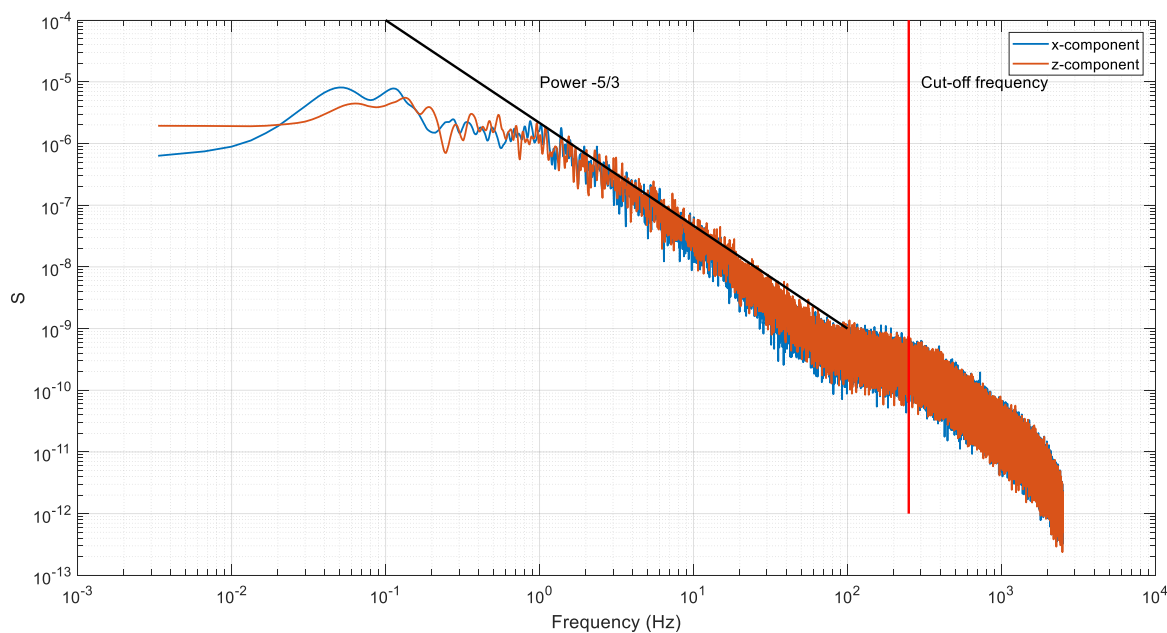


Figure 6.10. Power spectrum of the two velocity components of the top left measurement point in **Figure 6.9b**. The spectrum contains the expected power $-5/3$ dependency on the frequency. The cut-off frequency originates from the analog filter used in the measurement setup to cancel out high-frequency noise.

6.3.2 The effect of the sediment bed

In chapter 5 it was observed that the removal efficiency is initially relatively constant under a range of flow rates, resulting in a steady build-up of the sediment bed. The build-up rate changes once a substantial bed level is reached, resulting in additional through flow of sediment. The flow pattern is the driver of these processes.

Three artificial sediment beds were made, as described in section 6.2.6, to visualise the interaction between the flow pattern and the sediment bed. The bed shape depends on the

position of the impinging jets, the particle's characteristics, and the gully pot geometry. This section only focusses on one condition, namely a discharge of 1.0 L/s, a gully pot with the outlet at the back, a depth of 0.21 m, and sand with a D_{50} of 400 μm .

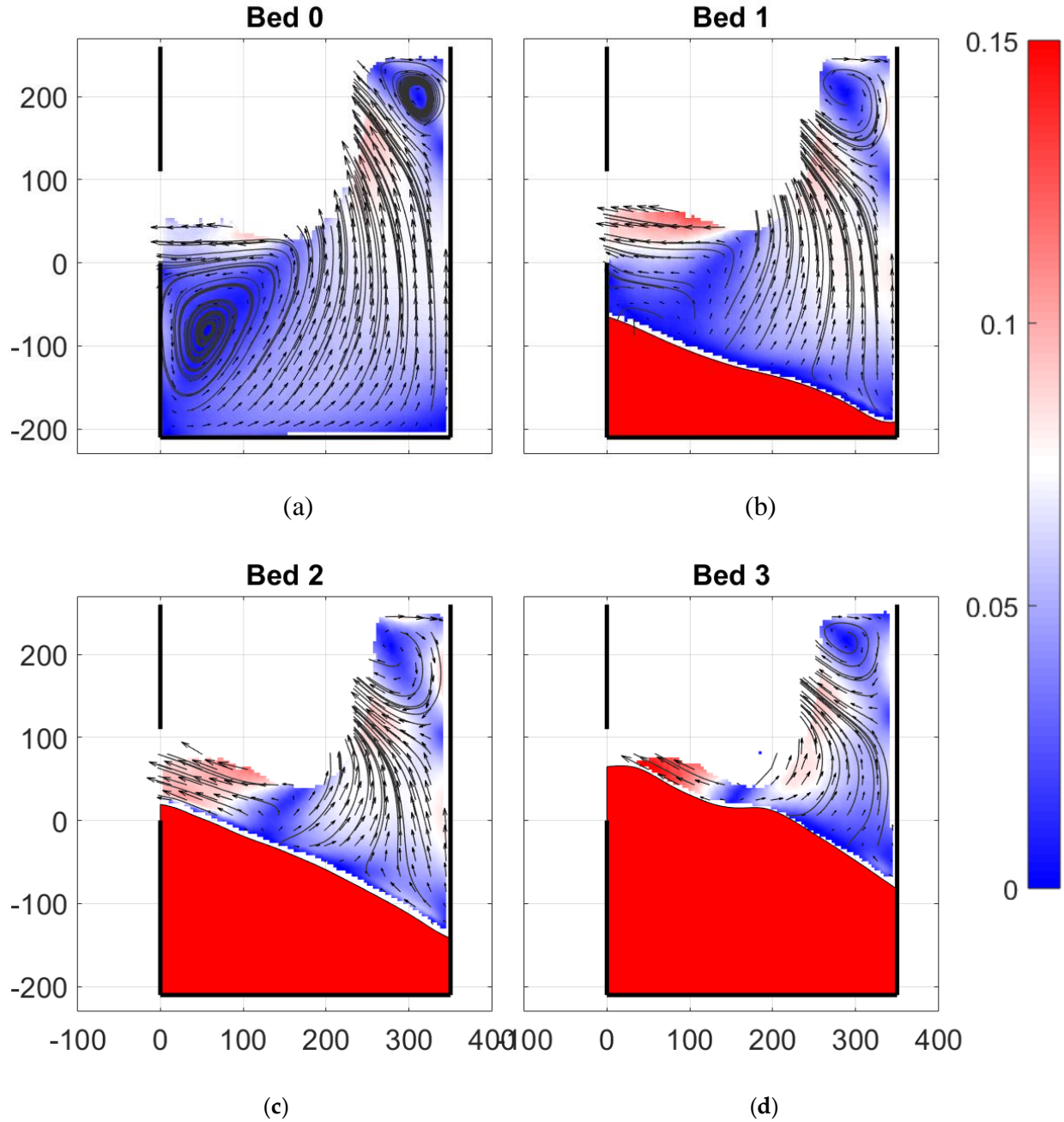


Figure 6.11. The effect of a growing sediment bed on the flow field. The sand traps in the figures are filled with sediment for approximately 0%, 24%, 62%, and 91%, respectively.

Figure 6.11 shows that, due to an increasing sediment bed level, the flow velocity close to the sediment bed increases, in particular close to the outlet. This is also the location where it was visually observed that the accumulation rate decreased and erosion took place, which started in between the situation of **Figure 6.11c** and **d**. In **Figure 6.11c** the flow velocity increases to

~ 0.10 m/s, which is already larger than the settling velocity of sand particles of $400\text{ }\mu\text{m}$. In **Figure 6.11d** flow velocities up to ~ 0.15 m/s are present. It is assumed that even higher flow velocities are present close to the outlet, but these are in this situation optically obscured by air bubbles and therefore could not be quantified using PIV.

While the flow velocity strongly increases due to an increasing sediment bed level, the flow directions stay relatively constant: the stagnant zone at the top right and a split between the area at the left and right of the impinging jet. While the flow at the left is mostly pointed towards the outlet, the flow at the right is mainly pointed towards the impinging jet. The only change is the sediment bed that replaces the stagnant zone at the bottom left of **Figure 6.11a**.

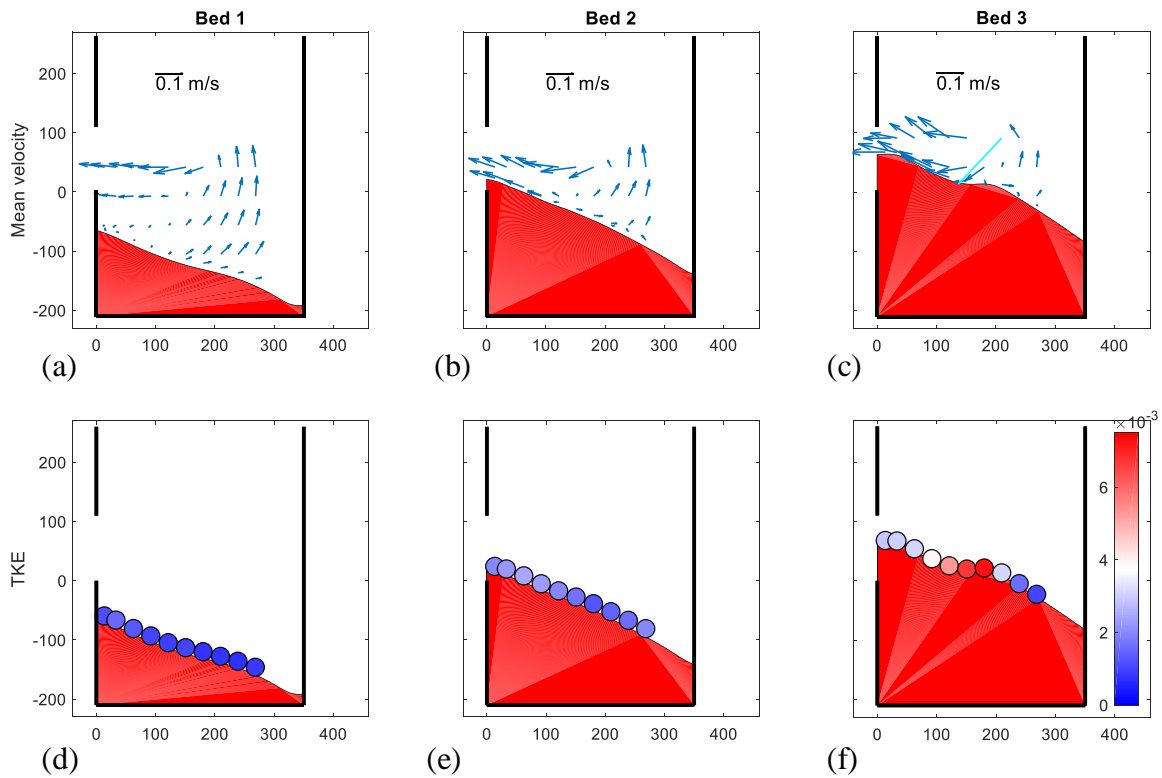


Figure 6.12. The effect of a growing sediment bed on the mean velocity, and the TKE (of which the latter is measured at 7 mm from to the sediment bed).

Figure 6.11 shows that the jets impinge on the water in the middle of the gully pot and the x-direction of the flow close to the jets is towards the left (i.e. towards the outlet). Therefore, the thickest sediment bed can be found on the left. In **Figure 6.11b** the flow velocity close to the bed is still relatively low and is therefore of relatively less importance for the shape of the bed than the position of the impinging jets and the high flow velocities close to the jet. In later stages, **Figure 6.11c** and **d**, the flow velocity close to the sediment bed is in the same order of magnitude as the settling velocity of the sediment; the sediment can therefore easily move over the bed as bed load. This causes the dip in the bed shape in **Figure 6.11d**.

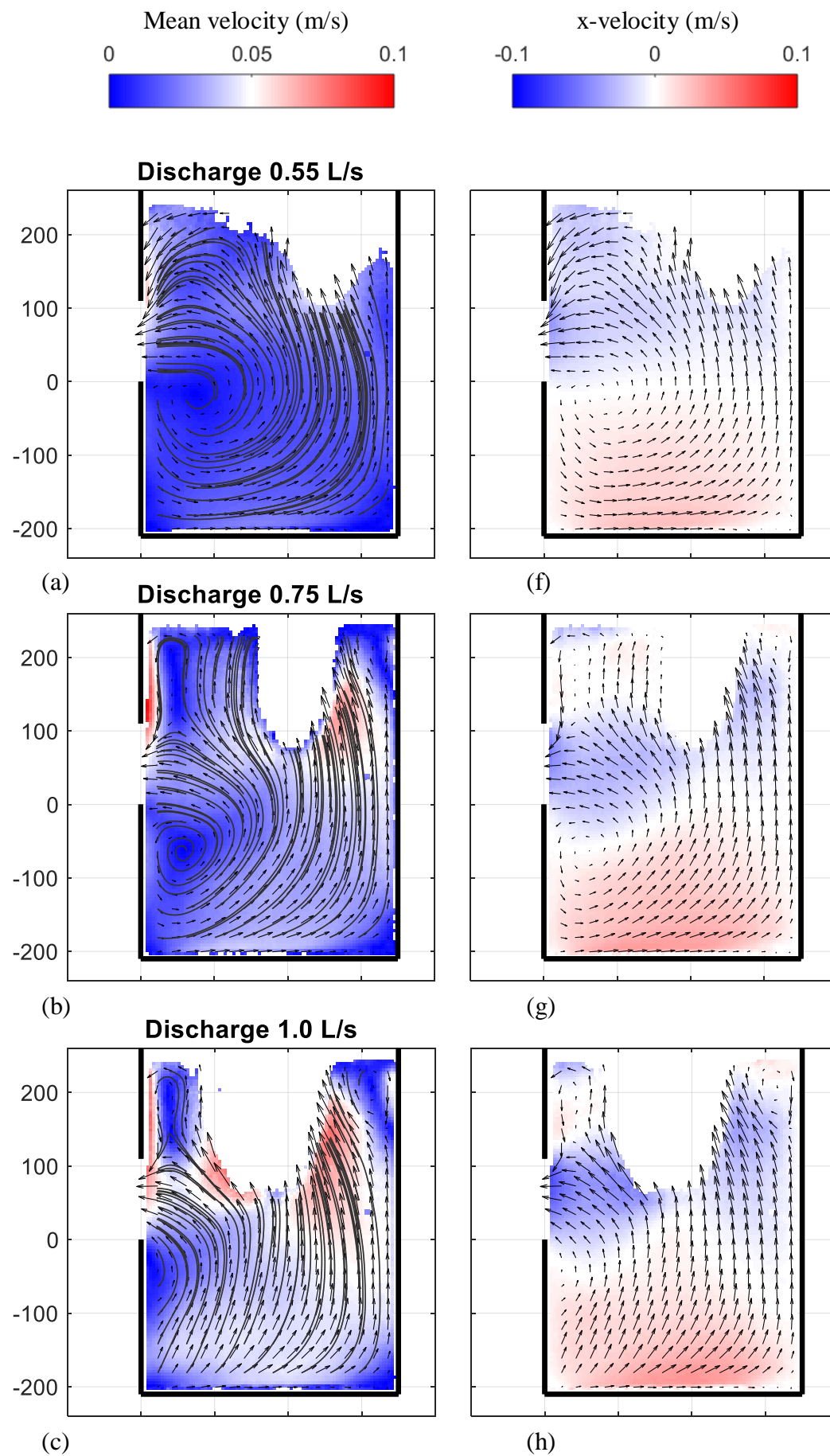
The velocities in **Figure 6.11** represent mean velocities (averaged over 1000 frames captured at 3 Hz). **Figure 6.12** shows the results of the LDA measurements, providing data on the mean velocity and turbulent fluctuations. The measurements for bed 3 contain an outlier in the mean velocity data, which is shown in another colour. This outlier is most likely due to air entrainment.

The TKE close to the bed reaches a maximum in the situation with the highest bed level, in particular in the region where the mean flow splits to the left and the right. The position of this splitting point might change over time and gives rise to a high TKE. The area close to the outlet is subjected to a lower TKE, but higher mean velocities. Since this is the area where resuspension was observed, it is a nice illustration that the combination of high mean flow and turbulence is required for local resuspension.

In the case of lower bed levels, both the mean flow and turbulent fluctuations close to the bed are damped. This result confirms the conclusion of Avila et al. (2011) that the overlaying water depth protects the sediment bed from the impact of the impinging jets as long as the sand trap is sufficiently deep.

6.3.3 The effect of the discharge

Section 5.3.2 shows that in the case of relatively high discharges (≥ 1.8 L/s) the measured efficiency (in a gully pot with the outlet at the back) is significantly smaller than the efficiency according to equation 1. Rainfall events causing these large discharges lasting at least 10 minutes occur ~2 times a year in The Netherlands (Beersma and Versteeg 2019). So, equation 1 can be used for most rainfall events if the sediment bed level is not too high. Nevertheless, the influence of the discharge on the flow pattern is assessed to clarify the effect of (high) discharges. **Figure 6.13** shows the mean velocity and x-velocity at several discharges in a gully pot with a depth of 0.21 m.



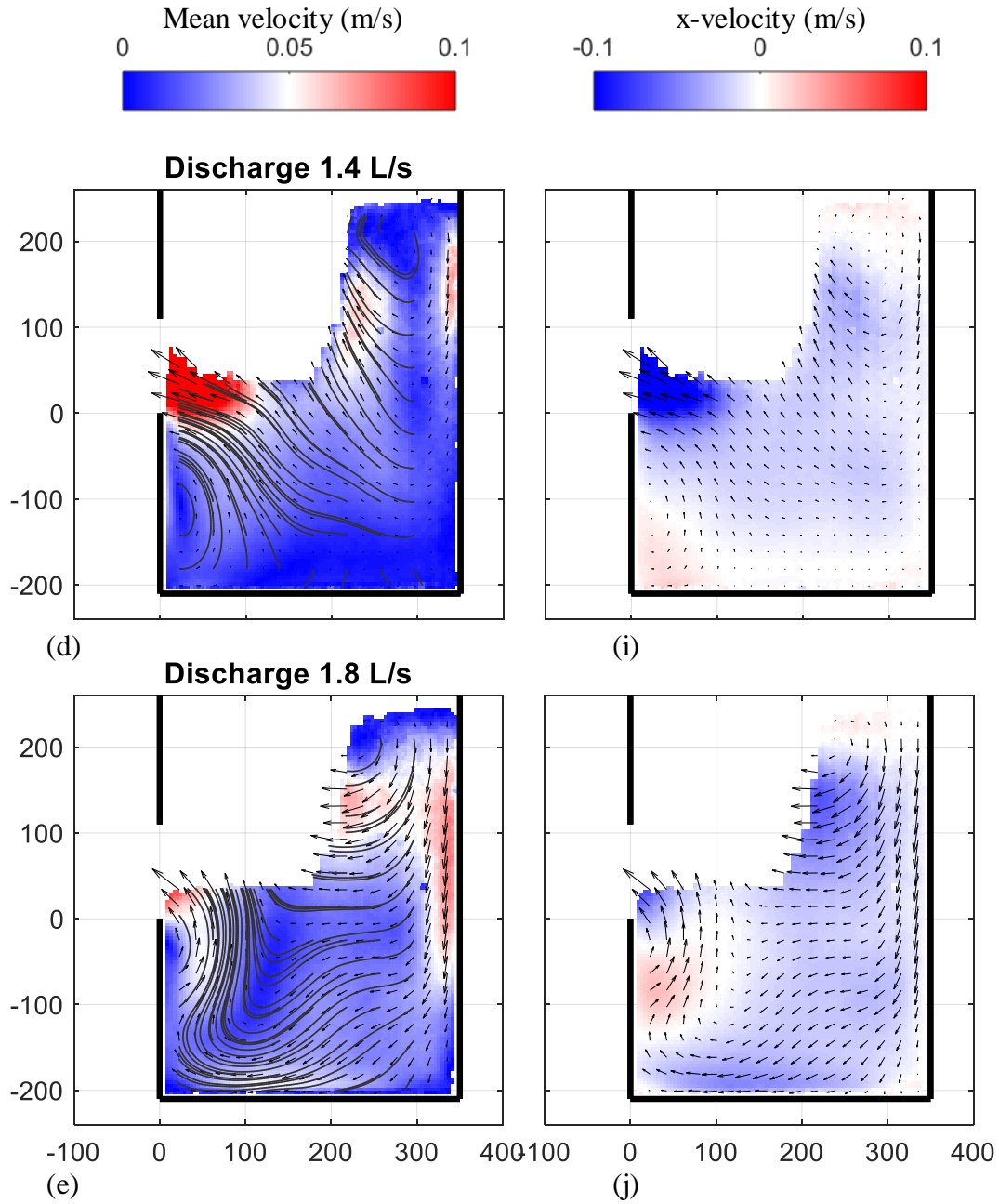


Figure 6.13. The effect of the discharge on the flow field. (a)-(e) Mean velocity; (f)-(j) x-velocity.

The water flows towards the outlet and the impinging jet, which together determine the flow pattern in the gully pot, in the POI. **Figure 6.13a-e** show that the impinging jets move to the left (i.e. the side of the outlet) at increased discharges. This moves the eddy, which is found below the outlet pipe, closer to the gully pot wall, until its influence on the surrounding flow becomes negligible in **Figure 6.13e**. This eddy affects the flow direction close to the gully pot bottom as can be seen in **Figures 14f-j**. At discharges < 1.4 L/s the flow is directed to the right, and at ~ 1.4 L/s the direction starts to change.

The monitored plane in **Figure 6.13** is the vertical plane of symmetry of the gully pot. **Figure 6.14** shows the horizontal flow field close to the gully pot bottom (plane 4 in **Figure 6.4**). The flow field at a discharge of 0.55 and 1.0 L/s is relatively symmetrical over a vertical line in the middle, while for a discharge of 1.8 L/s the flow field is asymmetrical. This asymmetry could be caused by an uneven spread of the discharge over the three impinging jets.

For the discharge of 0.55 and 1.0 L/s the in-plane velocity component is towards the bottom in **Figure 6.14**, which corresponds with towards the right in **Figure 6.13**, while at a discharge of 1.8 L/s, the flow directions change and an eddy is present.

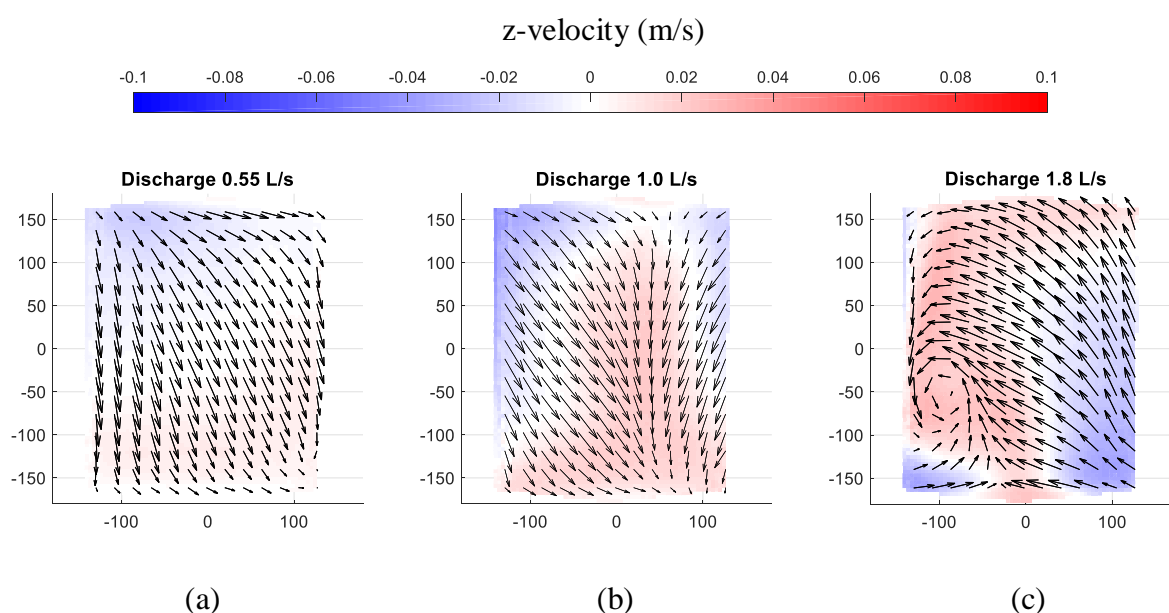


Figure 6.14. Flow field 3 cm above the gully pot bottom. The outlet is located at the top and the inlet at the bottom of the figures. The arrows indicate the in-plane flow direction and the colour scheme the out of plane component (blue towards the bottom and red towards the water surface).

Figure 6.13e-g show a smooth change in the flow pattern, while the flow velocities increase, the flow patterns are to a large extent similar. **Figure 6.13h** and **j** show a significant change in the flow pattern, which, at least, partially explains the observation in section 5.3.2 that the efficiency strongly decreases at discharges ≥ 1.8 L/s.

Another important effect is short-circuiting of the impinging jet to the outlet at these high discharges (**Figure 6.13d** and **e**), which causes direct transport of solids to the outlet. This implies that the gully pot can no longer be regarded as a completely mixed reactor, which was assumed in the derivation of equation 1.

6.3.4 The effect of the gully pot depth

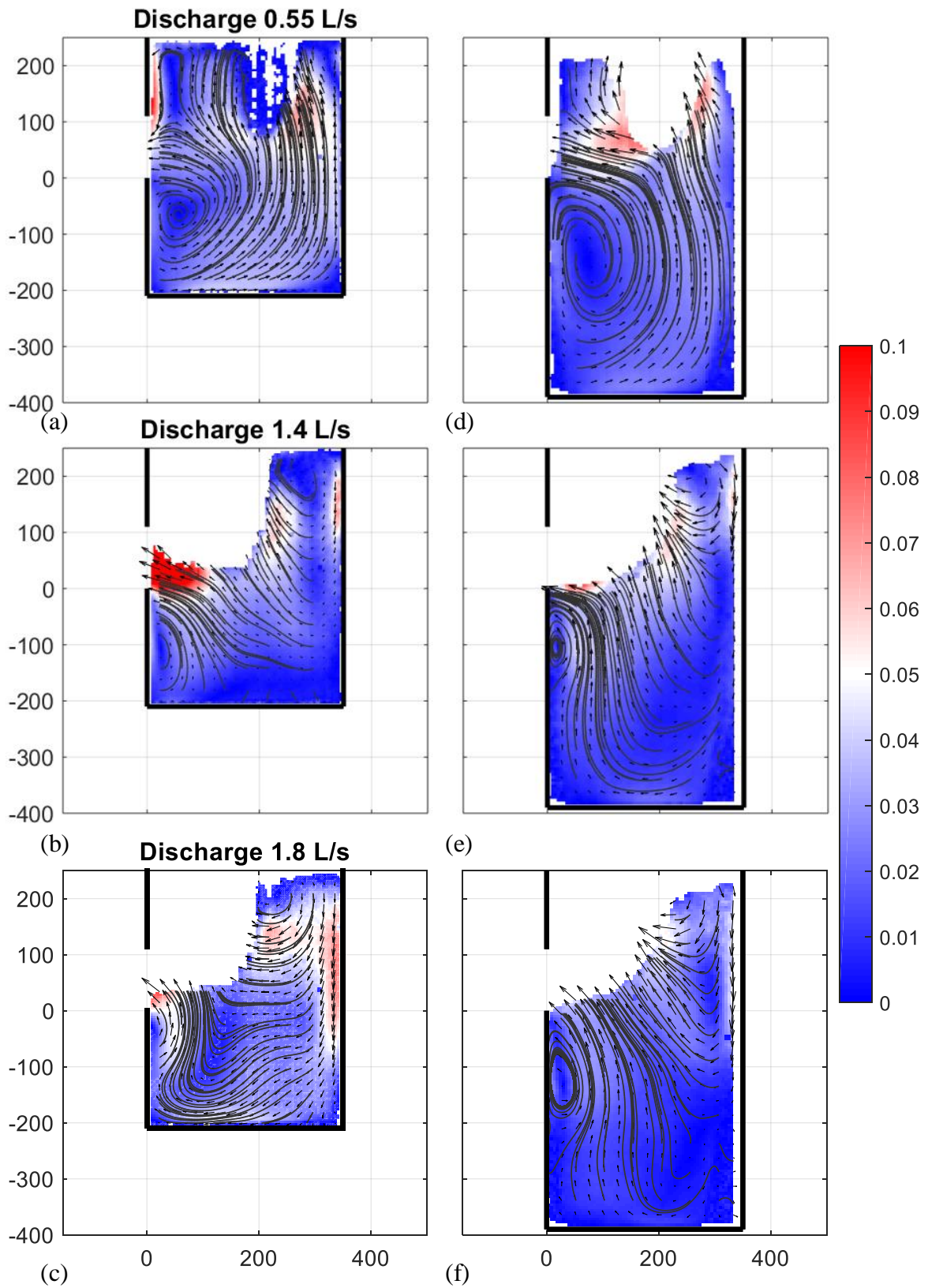
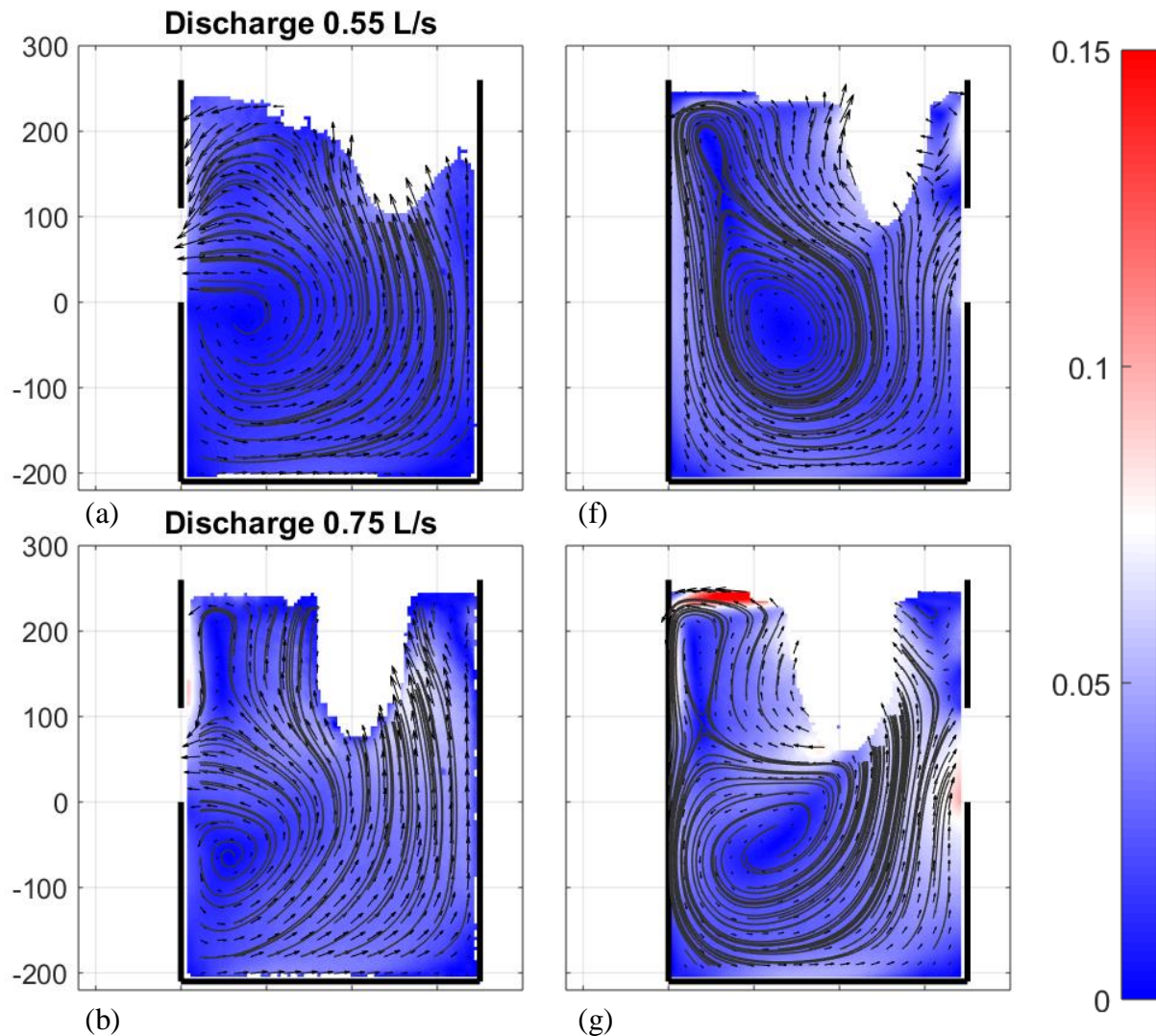


Figure 6.15. The effect of the gully pot depth on the flow field at several discharges. **(a)-(c)** Gully pot with depth 0.21 m; **(d)-(f)** Gully pot with depth 0.39 m.

In section 5.3.3 it is concluded that the depth of the gully pot determines at what bed level depth the accumulation rate starts to decrease, while the efficiency below or exceeding that depth is hardly influenced by the gully pot depth. Therefore, it is expected that the flow patterns are also relatively similar. **Figure 6.15** shows the comparison between the flow fields in gully pots with different depths.

The differences in the flow pattern shown in **Figure 6.15**, can mainly be found in the eddy below the outlet. This eddy is enlarged in the case of a deeper gully pot. In some areas, the flow velocities are higher in the shallower gully pot, which can be seen from the colour differences.

6.3.5 The effect of the outlet position



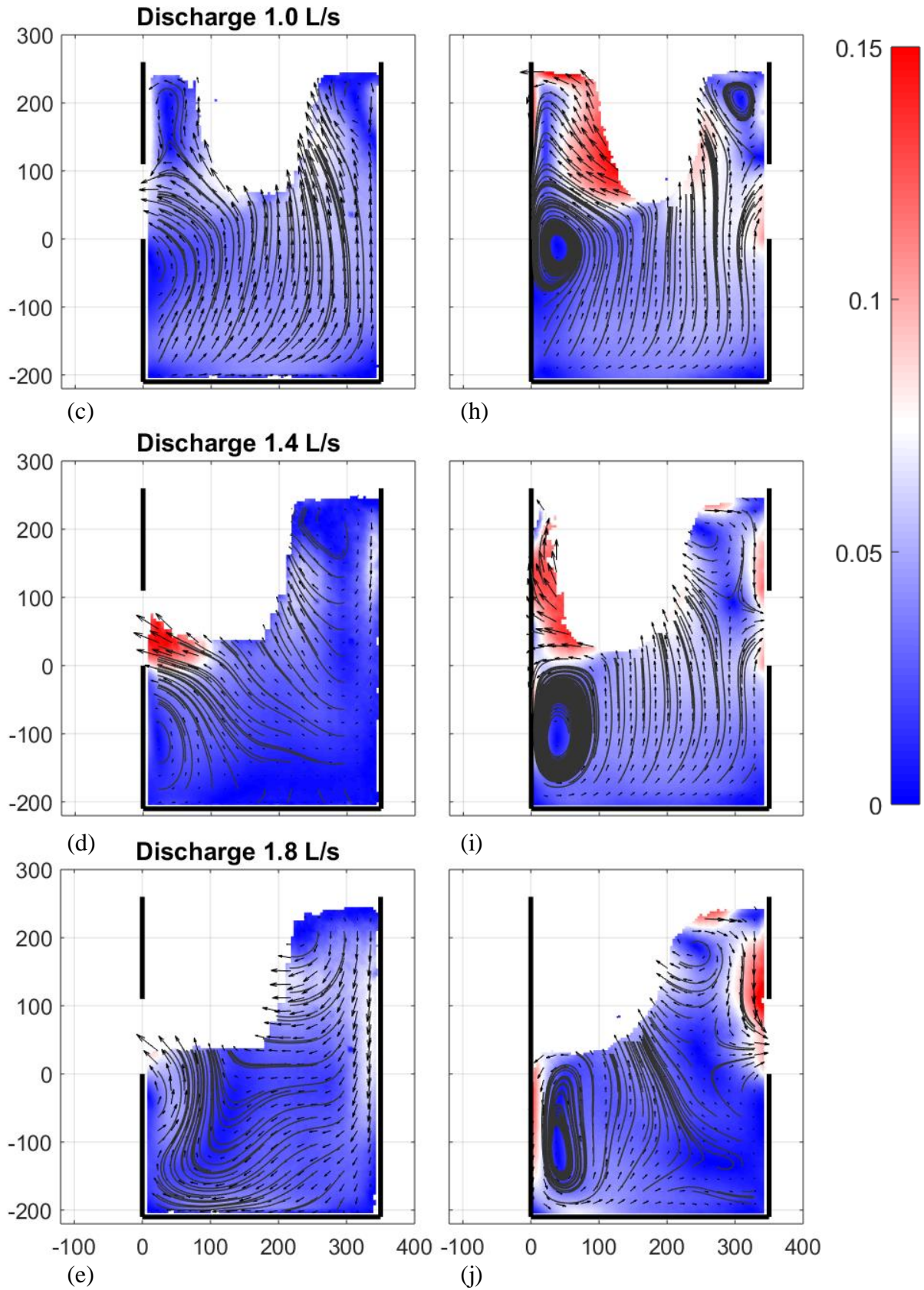


Figure 6.16. The effect of the outlet position on the flow field at several discharges. (a)-(e) Gully pot with outlet at the back; (f)-(j) Gully pot with outlet at the front.

The tests presented in section 5.3.5 with different outlet positions show that this parameter strongly influences the removal efficiency. The flow field of a gully pot with the outlet opposite to the inlet is compared with one with the outlet adjacent to the inlet in **Figure 6.16**.

For gully pots with an outlet at the front (**Figure 6.16f-j**) and discharge >0.55 L/s, the water which leaves the impinging jet is mainly directed upwards and to the back wall of the gully pot. This can effectively separate entrained solids and the outlet, which results in a larger removal efficiency than for gully pots with an outlet at the back (section 5.3.5). The assumption of a completely mixed reactor for equation 1 is violated, which explains why this equation cannot be used for this gully pot layout.

For a discharge of 0.55 L/s (**Figure 6.16f**), the flow is less strongly directed to the back wall of the gully pot. In this case, the impinging jet is close to the outlet at the front. This could cause immediate transport of entrained solids to the outlet pipe, which reduces the removal efficiency, compared with a gully pot with the outlet at the back.

6.4 Conclusions

Flow measurements have been performed with PIV and LDA on the flow field in a gully pot. The two measurement techniques provide similar mean flow velocities both in direction and magnitude in areas where no air bubbles are entrained in the water. The PIV measurements are used to study the overall flow field and the LDA measurements to study the turbulent fluctuations.

The multiphase character of the flow strongly influences the flow field in a gully pot. This affects the solids deposition and should, therefore, be incorporated in studies like e.g. Yang et al. (2018) and Faram and Harwood (2003) who simulated the removal efficiency in a gully pot by means of CFD.

The shape of the sediment bed depends on the solids' characteristics and the gully pot hydraulics. Regarding the hydraulics, the position of the impinging jets and the high flow velocities close to the impinging jets determine the distribution of sand in the gully pot in the initial stage. At higher bed levels, the flow velocity close to the bed increases and becomes important as well, since sediment can be transported over the bed as bed load. Finally, the accumulation rate decreases strongly in areas where both the mean flow velocity and turbulent kinetic energy (TKE) are high. In these areas, resuspension from the bed occurs. The sediment

bed level at which this situation is reached depends on the discharge, the gully pot layout, and the solids' characteristics.

Section 5.3.2 shows that the removal efficiency is significantly smaller at high discharges (≥ 1.8 L/s) than suggested by equation 1 for a gully pot with the outlet at the back. The PIV measurements show that the flow pattern strongly changes at discharges ≥ 1.4 L/s, which could partially explain the strongly decreased efficiency. Another import effect is short-circuiting of the impinging jet to the outlet at these high discharges, effectively reducing the retention time.

The discharge and outlet location strongly influence the flow pattern and removal efficiency. Therefore, reducing a gully pot to a completely mixed reactor, as proposed by Butler and Karunaratne (1995), is valid up to a point only. The assumption can be violated at high discharges due to effective separation of the inflow and the outflow in gully pots with the outlet at the front and due to short-circuiting in gully pots with the outlet at the back.

The removal efficiency depends on the solids' characteristics, the hydraulics, and the sediment bed level. In practice, only the latter two can be influenced. The hydraulics is mainly determined by the parameters discharge and outlet location. These parameters can be influenced in practice when a new urban area is designed by the choice of the number of gully pots and the type of connection of the outlet pipe. The sediment bed level can be controlled by the gully pot cleaning.

The results of this study may be used to calibrate the hydraulics of a CFD model of a gully pot. A validated model could be used to assess the effect of other gully pot geometries and hydraulic conditions on the flow pattern and the removal efficiency, eventually such a model can be applied to search for a geometry that optimises the removal efficiency. This could be achieved by manipulating the position of the impinging jets. The jets should preferably impinge on the water at maximum distance from the outlet regardless of the discharge.

The study presented in chapter 5 on the removal efficiency and this study on the flow field in the gully pot focussed on settling and erosion processes of relatively small solids (≤ 1 mm). The effect of gross solids on the flow field is likely to be stronger (two-way coupled) than in the case of small solids. The effect on the flow field and the removal efficiency needs to be addressed in an additional study.

7 SYNTHESIS AND DISCUSSION

7.1 Parameters correlated with wash-off

The accumulation of solids in gully pots is the result of three processes, namely the build-up of solids in a catchment, the wash-off of these solids from this catchment, and the removal of solids in the gully pot (see **Figure 7.1**). While in chapter 4 the accumulation rate of solids in gully pots is discussed (i.e. all three processes), chapter 2 deals with the transport of solids to gully pots (i.e. the first two processes).

It has been shown that the solids loading (chapter 2) is mainly correlated with the rain intensity, rain volume, and temperature. The street sweeping frequency, gully pot catchment area, discharge, and water volume are less strongly (although significantly) correlated to the solids loading. The accumulation of solids (chapter 4) has been evaluated by several models, which made use of all, or some of the previously mentioned parameters (except the temperature and water volume, since these were not evaluated). Some additional parameters related to the first two processes are also included in these models, namely the vegetation density, pavement type, antecedent dry period, and tree phase (of which the first two are not evaluated in the model for the solids loading).

The relation of the parameters gully pot catchment area, rain intensity, rain volume, water volume, discharge, antecedent dry period, temperature, street sweeping frequency, vegetation density, tree phase, and pavement type, with wash-off (models) is discussed in this section.

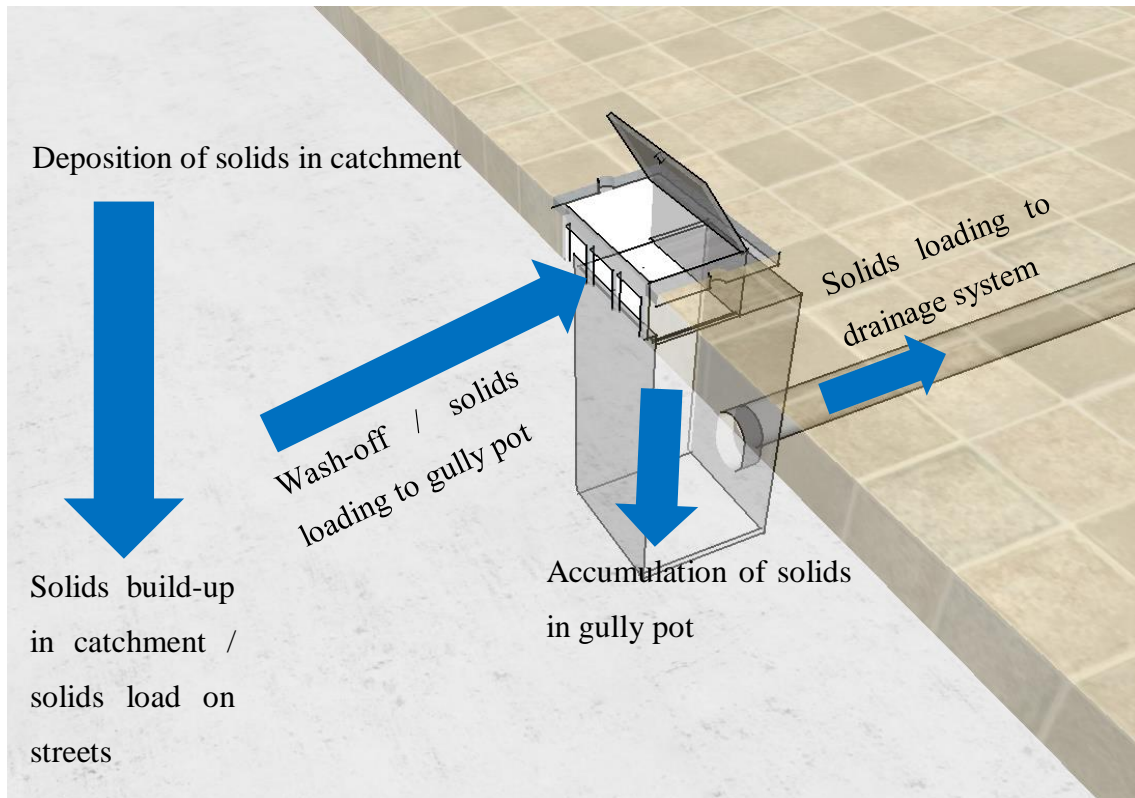


Figure 7.1. Overview of the processes (and their descriptions used in this thesis) related to the accumulation of solids in gully pots.

7.1.1 Gully pot catchment

The size of the gully pot catchment obviously contributes positively to the mass of solids washed-off to the gully pot, which was also found by Post et al. (2016).

7.1.2 Rain intensity, rain volume, water volume, discharge

Runoff is the main transport medium for street solids. Several parameters related to runoff contribute to wash-off. Firstly, the intensity of the rain contributes to the (drop impact driven) erosion of solids from the surface and subsequently transport capacity. The rain intensity multiplied with the catchment size is related to the discharge over the catchment and into the gully pot. A large discharge contributes positively to (flow driven) erosion of solids from the surface, while it can also erode solids from the sediment bed in a gully pot. The statistical models show indeed that the rain intensity and discharge (which are correlated) contribute positively to the solids loading to gully pots, while they can negatively contribute to the solids accumulation in gully pots. Shivalingaiah and James (1984) also found that rain intensity is most strongly correlated to solids wash-off.

While the parameters rain intensity and discharge represent the peak of the transport capacity, the parameters rain volume and water volume represent the mean transport capacity. Those parameters are positively related to wash-off.

7.1.3 Antecedent dry period

The relation of the antecedent dry period with wash-off is ambiguous in the statistical models. Moreover, in the cases this parameter was included in a model, it was one of the least significant parameters. Therefore, it is questionable whether this parameter could act as a proxy for the availability of solids for wash-off on the street surface, despite its common use.

7.1.4 Temperature

The temperature contributed positively to the wash-off of solids. This parameter might represent the erodibility of solids from the street surface (which was also suggested by Pratt et al. 1987), while the underlying processes can be many. It is worth considering whether a street could be seen as a pool of solids, such that the amount of solids is hardly correlated with the antecedent dry period, and the wash-off is actually driven by the erodibility of these solids, which might be influenced by the temperature.

7.1.5 Street sweeping

In chapters 2 and 3, the effect of street sweeping on the solids loading to gully pots is analysed. Chapter 2 describes an experiment lasting 5 months in which the solids loading to two clusters of gully pots was compared, which were subjected to substantially different sweeping frequencies. This showed that the sweeping frequency did not affect the solids loading. The time period of this experiment might have been an unfortunate choice, since it took place in a period with a limited solids loading. It might be that the effect of street sweeping is more effective in periods of relatively large solids loadings (for example during summer).

In chapter 3, data of other time periods are added in which the sweeping frequency mainly varies temporally and not spatially. For this dataset the sweeping frequency proved to contribute positively to the solids loading. The same relation holds for one of the models on the solids accumulation rate in chapter 4. Therefore, the general finding is, in accordance with Walker and Wong (1999), that an increased street sweeping frequency did not reduce the wash-off of solids.

7.1.6 Vegetation density, tree phase

The presence of vegetation contributes positively to the accumulation rate of solids in gully pots (evaluated in terms of volume), in particular during leaf abscission. The effect of leaf abscission on the mass of solids transported to a gully pot is not significant, but an effect of leaf abscission on the fraction of organic material in the solids loading can be distinguished. The data suggests that the relative fraction of organic material increases in case of limited runoff, which suggests that organic material can also be transported by other mechanisms (such as wind) to the gully pot. Wash-off models, in particular those that differentiate between different types of particles, need to address these different transport mechanisms, the vegetation density, and the tree phase.

7.1.7 Pavement type

The pavement type (asphalt compared to bricks) has been found to contribute significantly to the accumulation rate of solids in only one of the models, and was just below the significance level in this model, namely 0.01 while 0.05 is considered significant. Therefore, a wash-off model does not need to include this parameter.

It would make sense to include a parameter representing the structural condition of the road, in case the studied road is in a poor condition or constructed of loose material such as gravel, since more solids are available in those conditions. Moreover, those conditions would affect the flow and subsequently the solids transport. However, none of the monitored areas contained those type of roads.

7.2 Chaos in wash-off

The statistical models (regression trees and linear mixed models) developed in chapter 3 and 4 on the accumulation of solids in gully pots and the solids loading to gully pots show poor performance (i.e. low to modest R^2 values). This implies that these models cannot represent the processes for individual gully pots. Moreover, the two calibrated semi-physical Build-Up and Wash-Off (BUWO) models in chapter 3 explain the observations equally well as the mean value of the observations.

Literature on solids wash-off (e.g. Sartor and Boyd 1972; Pitt 1979; Pratt and Adams 1984; Ellis and Harrop 1984; Pitt et al. 2005) hardly offer generic conclusions on the quantifiability of wash-off and mainly site-specific relations with an unknown validity beyond the monitoring period and location have been identified. It is worth considering whether this lack of generality

is caused by inherent unpredictable behaviour (e.g. chaos) in the wash-off process, initiated by non-linear feedback loops in the subprocesses (such as deposition of solids, erosion by rain drop impact, sedimentation).

A first step could be to describe the individual processes in simple 1D mathematical models and search for non-linear feedbacks. If these are found, the impact of the individual processes on the overall wash-off can be evaluated. If the overall process proves to be inherently chaotic (under frequently occurring conditions), it would imply that a data-driven approach for a specific catchment is a better alternative than using a model from literature calibrated in another catchment.

7.3 Removal efficiency model

The Butler and Karunaratne (1995) model of the removal efficiency of a gully pot assumes that the gully pot is a completely mixed reactor. This assumption can be violated at high discharges, due to effective separation of the inflow and outflow in gully pots with the outlet at the front, and due to short-circuiting in gully pots with the outlet at the back. The model provides better results for large particles (1080 μm) than for small particles (125 μm), which might be due to the enhanced effect of turbulence on small particles.

A sediment bed is formed by the removed solids. The shape of this bed depends on the solids' characteristics and the gully pot hydraulics. Regarding the hydraulics, the position of the impinging jets and the high flow velocities close to the impinging jets determine the distribution of sand in the gully pot in the initial stage. At higher bed levels, the flow velocity close to the bed increases and becomes important as well, since sediment can be transported over the bed as bed load. Finally, the accumulation rate decreases strongly in areas where both the mean flow velocity and turbulent kinetic energy (TKE) are high. In these areas, bed erosion occurs. The sediment bed level at which this situation is reached depends on the discharge, the gully pot layout, and the solids' characteristics. The effect of the interaction of the (curved) sediment bed with the flow field and subsequently the removal efficiency, is not described by the current removal efficiency models.

Although curved sediment beds were formed in the lab experiments, during field measurements only flat beds were observed. This is most likely due to the intermittent character of storms, while in the lab experiments only constant discharges were evaluated. Nevertheless, flat beds will also interact with the flow field.

The Butler and Karunaratne (1995) model works sufficiently well in an empty gully pot in which no short-circuiting occurs. The model can be improved by including two additional processes, represented by at least two additional parameters, namely one representing the distance between the position the jets impinge on the water and the outlet, and one representing the free volume (volume of the sand trap not occupied by the sediment bed). A CFD model (see section 7.6), validated on the performed experiments, could assist in producing such a model.

7.4 Expected removal efficiency in practice

To determine whether gully pots are effective devices to remove solids from runoff, the expected discharge and characteristics of the solids have to be combined with the evaluated removal efficiencies of a common gully pot layout. Most monitored gully pots in chapter 2, 3, and 4 had a side inlet, an outlet at the back, and a cross-section similar to the gully pot evaluated in chapter 5. Gully pots with the outlet at the back require two bends in the lateral connection with the drainage pipe in the middle of the street. These bends provide flexibility, which makes the pipe less vulnerable to damage due to ground settlement.

A discharge of 1.8 L/s corresponds with a rain intensity of ~60 mm/hour, by dividing the discharge by a virtual drained area of 106 m² (which is the mean of catchments in the monitoring area of chapter 3). This rain intensity occurs approximately only once a year for 10 minutes in The Netherlands (Beersma and Versteeg 2019). So, this discharge can be seen as an upper limit for the evaluation of the removal efficiency.

Chapter 2 presents a settling velocity (v_{50}) range of particles <1800 μm between 0.01 and 0.06 m/s. This corresponds with the settling velocity of sand particles with a diameter between 110 and 400 μm (by applying the universal using the universal drag coefficient for spheres, e.g. Terfous et al. 2013). The removal efficiency of sand particles in this range has been evaluated in chapter 5. The efficiency at a discharge of 1.8 L/s for the particles with the lowest v_{50} is approximately 30% (before a substantial bed level is reached which reduces the efficiency).

Most rain events have considerably lower intensities; a rain event of 20.8 mm/hour lasting 30 minutes occurs twice a year, and corresponds to a discharge of 0.6 L/s. For the particles with the lowest v_{50} efficiencies of roughly 65% can be expected. Therefore, it can be concluded that gully pots remove a substantial fraction of suspended solids, provided they are cleaned before a substantial sediment bed is reached and the efficiency decreases.

7.5 Gully pot cleaning

As concluded in section 7.4, the removal efficiency of gully pots is relatively large in the phase before the sediment bed reaches a substantial height and affects the efficiency. Langeveld et al. (2016) found that the total mass removed by gully pot cleaning increased by a factor ~ 3 when the cleaning frequency was increased from once a year to six times a year, which means that the removal efficiency reduces within a few months. Similar conclusions have been drawn for the majority of the gully pots monitored by Post et al. (2016).

These numbers depend obviously on environmental factors, weather conditions, and the gully pot geometry as shown in chapter 4. Nevertheless, the timescale for reaching a substantial sediment bed is significantly shorter than the usual time interval of gully pot cleaning of one year.

7.6 Gully pot design

The removal efficiency and flow field measurements have shown that a gully pot cannot be schematised as a completely mixed reactor. The flow pattern influences the efficiency and consequently an improved gully pot design can increase the removal efficiency. CFD simulations could assist in the design process.

In order to optimise the geometry of a gully pot with respect to the removal efficiency using modelling tools, a (calibrated) model of the evaluated geometry should be developed. The turbulent intensities of such a CFD model can be validated using the LDA measurements, while the overall flow pattern could be validated with the PIV measurements. Then, assuming the validation is successful, the effect of a (slightly) changed geometry on the efficiency can be assessed.

Increased efficiencies are likely to be obtained by manipulating the position of the impinging jets. The jets should impinge on the water at maximum distance from the outlet (regardless of the discharge) to reduce short-circuiting. The cross-section of the gully pot is both expected to be positively related to the removal efficiency and the retention capacity. The depth of the gully pot proved to be mainly related to the retention capacity.

8 GENERAL CONCLUSIONS AND RECOMMENDATIONS

8.1 Conclusions

8.1.1 Solids accumulation in gully pots

Physical parameters linked to the build-up of solids in a catchment, the wash-off of these solids from this catchment, and the removal of solids in the gully pot contribute to the temporal and spatial variation of the accumulation rate in gully pots. Since none of these three processes seems to dominate the accumulation rate, all have to be taken into account for the formulation of an optimal gully pot design and cleaning strategy.

8.1.2 Transport of solids to gully pots

The solids loading to gully pots also strongly varies temporally and spatially (both in terms of mass and composition). The rain intensity, rain volume, and temperature have been identified as the most influential parameters. The rain intensity and rain volume are related to the erosion of solids from the street and the transport of solids over the street. The temperature might influence the erodibility of solids from the street.

The solids loading to gully pots is described with a Build-Up and Wash-Off (BUWO) model. However, the portability of the calibration parameters from one catchment to another was virtually absent. This proved that this BUWO model acts as a black-box model, implying that the calibration parameters don't represent physical quantities. Therefore, the calibration

parameters in urban hydrodynamic models should not be taken from literature; these models need to be calibrated with data from the studied area.

The D_{50} and the organic fraction of the solids loading are correlated, since the coarse sediment fraction consists mainly of organic material. The settling velocity of particles $<1800\text{ }\mu\text{m}$ ranges between 0.01 and 0.06 m/s and is strongly correlated with their organic fraction.

8.1.3 Gully pot hydraulics

The solids removal efficiency of a gully pot is initially relatively constant. The continuous removal of solids from runoff in gully pots creates a gradually increasing sediment bed. Over time, the evolution of the bed morphology starts to influence the flow field and hence the removal efficiency. The local mean flow velocity and turbulent kinetic energy increases, which reduces the settling of solids and/or resuspends solids from the sediment bed. Eventually, a global balance is obtained at which the deposition equals the resuspension. The sediment bed level at which this situation is reached depends on the discharge, the gully pot layout, and the solids' characteristics.

8.2 Recommendations

8.2.1 Research

The solids loading to gully pots and the accumulation of these solids in the gully pot is influenced by a large number of processes. Several of these subprocesses are likely to have chaotic characteristics. Therefore, it should be studied whether and under which conditions the loading and accumulation processes are chaotic processes. If these prove to be inherently chaotic, the common modelling approach needs to be re-evaluated.

Monitoring data on the solids loading and accumulation rate are scarce, in particular data covering all seasons and a number of sites/a large surface area. Therefore, new datasets have been created for this thesis. To avoid unnecessary labour-intensive fieldwork in future, a database should be created of all available literature, such as: e.g. Pratt and Adams (1984), Ellis and Harrop (1984), Sansalone et al. (1998), and Hong et al. (2016). Since each study had his own purpose and a generic measurement protocol was lacking, different parameters have been measured and different units have been used. Moreover, the confidence levels in the measured quantities are commonly missing. Nevertheless, a well-constructed database, could assist in the search for chaotic behaviour, and for model calibration and validation.

The accumulation of solids in the gully pot could eventually block its outlet (Post et al. 2016). This clogging process has not been observed in the performed lab experiments, and should be studied in future research. Clogging might be initiated by two phenomena which are not represented in the performed lab experiments, namely varying discharges, and obstruction by cohesive and/or large particles.

The lab experiments have been conducted at a constant discharge to determine the relation between the discharge and the removal efficiency. It has been observed that the sediment bed partially blocked the outlet, which increased the local flow velocity. The more the outlet is obstructed, the higher the local flow velocity until erosion and settling of solids reach a balance. In the case of intermittent discharges, this balance might not be reached.

The sediment bed shape depends on (amongst others) on the discharge. In the case of low discharges the maximum bed level is higher, than in the case of high discharges. If a low discharge is followed by a high discharge, a substantial part of the bed could be moved into the outlet and clog it. The same could happen due to the collapse of a curved sediment bed in a dry period (**Figure 8.1a and b**).

Large or cohesive particles could also initiate a blockage. These particles could partially block the outlet and other particles could further block the outlet (**Figure 8.1c and d**).

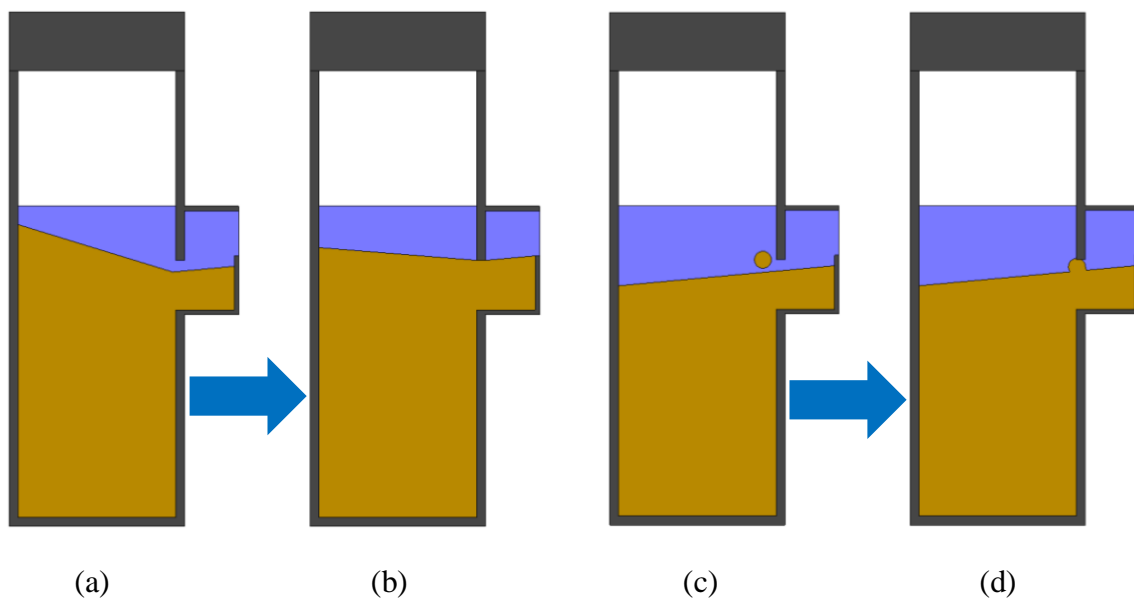


Figure 8.1. Clogging processes: (a) and (b) collapse of sediment bed achieved under low discharge conditions induced by high discharge or other forces/vibrations in a dry period; (c) and (d) large or cohesive particles suddenly block the outlet.

8.2.2 Applications

The removal efficiency of solids by gully pots depends on the solids' characteristics, the hydraulics, and the sediment bed level. In practice, only the latter two can be influenced.

The sediment bed level can be controlled by gully pot cleaning. A cleaning frequency of once every few months is required to substantially reduce the solids loading to drainage systems. Deeper gully pots could be selected when an urban area is (re)designed, to avoid the necessity of frequent cleanings and thus high cleaning costs, while keeping a high removal efficiency. Or the cross-sectional area of the gully pot could be increased to increase both the removal efficiency and the retention capacity.

The hydraulics are mainly determined by (next to the cross-sectional area) the discharge and the distance between the impinging jets and the outlet. The discharge can be influenced in practice when a new urban area is designed by the choice of the number of gully pots.

The distance between the impinging jets and the outlet could be influenced by the gully pot geometry. Regarding the monitored gully pots, most of them had a squared cross-section and an outlet at the back. The latter is chosen to include bends in the outlet pipe, providing extra flexibility in the outlet pipe to be able to cope with soil settling. To increase the distance between the impinging jets and the outlet pipe in these gully pots, a plate could be installed behind the inlet of the gully pot to keep the impinging jets at the front regardless of the discharge (as evaluated in chapter 5). The size of the gap between the grid and the plate should be chosen such that particles that can pass the grid won't get stuck between the plate and the inlet.

Street sweeping did not prove to reduce the solids loading and thus the accumulation rate of solids in gully pots. This may be partially due to the street sweeping method. It has been visually observed that most solids accumulate at the curb of the street. This is often also the place where cars are parked in residential areas, which was particularly apparent in the monitoring area of chapter 2 and 3. Street sweeping might become more effective when citizens are informed when the street will be swept and are requested to park their cars at one side of the road.

A similar approach could be used to inform citizens about gully pot cleaning. During the monitoring campaign presented in chapter 4, all gully pots should have been cleaned multiple times. However, several gully pots proved to be uncleaned, in many cases due to parked cars. Therefore, the sediment bed level stayed relatively high in these gully pots, resulting in an increased solids loading to the drainage pipes.

BIBLIOGRAPHY

- Amato, F., Querol, X., Johansson, C., Nagl, C., and Alastuey, A. (2010). "A Review on the Effectiveness of Street Sweeping, Washing and Dust Suppressants as Urban PM Control Methods." *Science of the Total Environment* 408 (16): 3070–3084. doi:10.1016/j.scitotenv.2010.04.025.
- Ashley, R.M., and Crabtree, R.W. (1992). "Sediment Origins, Deposition and Build-Up in Combined Sewer Systems." *Water Science & Technology* 25 (8): 1-12. doi:10.2166/wst.1992.0173.
- Ashley, R. M., Fraser, A., Burrows, R., and Blanksby, J. (2000). "The Management of Sediment in Combined Sewers." *Urban Water* 2 (4): 263–275. doi:10.1016/S1462-0758(01)00010-3.
- Ashley, R.M., and Hvitved-Jacobsen T. (2002). *Management of Sewer Sediments*. Boca Raton: CRC Press/Lewis Publishers. ISBN: 9780429134937.
- Ashley, R.M., Wotherspoon, D.J., Goodison, M.J., and McGregor, I. (1992). "The Deposition and Erosion of Sediments in Sewers." *Water Science & Technology* 26 (5-6): 1283-1293. doi:10.2166/wst.1992.0571.
- Avila, H., Pitt, R. and Clark, S.E. (2011). "Development of Effluent Concentration Models for Sediment Scoured from Catchbasin Sumps." *Journal of Irrigation and Drainage Engineering* 137 (3): 114–120. doi:10.1061/(ASCE)IR.1943-4774.0000183.
- Avila, H., Pitt, R. and Durrans, S.R. (2008). "Factors Affecting Scour of Previously Captured Sediment from Stormwater Catchbasin Sumps." *Journal of Water Management Modeling*. doi:10.14796/JWMM.R228-13.
- Baas, A.C. (2002). "Chaos, Fractals and Self-organization in Coastal Geomorphology: Simulating Dune Landscapes in Vegetated Environments." *Geomorphology* 48 (1-3): 309-328. doi:10.1016/S0169-555X(02)00187-3.

- Barbé, D.E., Cruise, J.F., and Mo, X. 1996. "Modeling the Buildup and Washoff of Pollutants on Urban Watersheds." *Journal of the American Water Resources Association* 32 (3): 511-519. doi:10.1111/j.1752-1688.1996.tb04049.x.
- Barrett, M.E., Irish, J.L.B., Malina, J. F., and Charbeneau, R.J. (1998). "Characterization of Highway Runoff in Austin, Texas, Area." *Journal of Environmental Engineering* 124 (2): 131–137. doi:10.1061/(ASCE) 0733-9372(1998)124:2(131).
- Beersma, J. and Versteeg, R. (2019). *Basisstatistiek voor Extreme Neerslag in Nederland* [Statistics of Extreme Rainfall in The Netherlands]. Amersfoort: STOWA.
- Bender, G.M. and Terstriep, M.L. (1984). "Effectiveness of Street Sweeping in Urban Runoff Pollution Control." *Science of the Total Environment* 33 (1-4): 185-192. doi:10.1016/0048-9697(84)90392-9.
- Bertrand-Krajewski, J.L., Briat, P. and Scrivener, O. (1993). "Sewer Sediment Production and Transport Modelling: A Literature Review." *Journal of Hydraulic Research* 31 (4): 435–460. doi:10.1080/00221689309498869.
- Bolognesi, A., A. Casadio, A. Ciccarello, M. Maglionico, and S. Arina 2008. "Experimental Study of Roadside Gully Pots Efficiency in Trapping Solids Washed off during Rainfall Events." In *Proceedings of the 11th International Conference on Urban Drainage*. Edinburgh, Scotland.
- Bonhomme, C. and Petrucci, G. (2017). "Should we Trust Build-up/Wash-off Water Quality Models at the Scale of Urban Catchments?" *Water Research* 108, 422-431. doi:10.1016/j.watres.2016.11.027.
- Breiman, L., Friedman, J.H., Olshen, R.A., and Stone, C.J. 1984. *Classification and Regression Trees*. New York: Chapman & Hall.
- Brinkmann, W.L.F. (1985). "Urban Stormwater Pollutants: Sources and Loadings." *GeoJournal* 11 (3): 277-283. doi:10.1007/BF00186341.
- Broeker, H.W. (1984). "Impact of Depositions on Sewer Operation." In *Proceedings of the 3rd International Conference on Urban Storm Drainage*. Göteborg, Sweden.
- Brunner, P.G. (1975). Die Verschmutzung des Regenwasserabflusses im Trennverfahren: Untersuchung unter besonderer Berücksichtigung der Niederschlagsverhältnisse im voralpinen Raum [The pollution of rainwater runoff in the separation process: Investigation with special consideration of the precipitation conditions in the pre-alpine area]. PhD thesis. TU München.

- Butler, D., and P. Clark. (1995). *Sediment Management in Urban Drainage Catchments*. London: Construction Industry Research & Information Association. ISBN: 9780860174097.
- Butler, D., and Karunaratne, S.H.P.G. (1995). "The Suspended Solids Trap Efficiency of the Roadside Gully Pot." *Water Research* 29 (2): 719–729. doi:10.1016/0043-1354(94)00149-2.
- Butler, D., and Memon, F.A. (1998). "Dynamic Modelling of Roadside Gully Pots during Wet Weather." *Water Research* 33 (15): 3364–3372. doi:10.1016/S0043-1354(99)00050-0.
- Butler, D., Thedchanamoorthy, S., and Payne, J.A. (1992). "Aspects of Surface Sediment Characteristics on an Urban Catchment in London." *Water Science & Technology* 25 (8): 13-19. doi:10.2166/wst.1992.0174.
- Camp, T.R. (1936). "A Study of the Rational Design of Settling tanks." *Sewage Works Journal* 8 (5): 742-758.
- Camp, T.R. (1946). "Sedimentation and the Design of Settling Tanks". *Transaction ASCE* 111: 895-958.
- Caradot, N., Granger, D., Chapgier, J., Cherqui, F., and Chocat, B. (2011). "Urban Flood Risk Assessment Using Sewer Flooding." *Water Science & Technology* 64 (4): 832-840. doi:10.2166/wst.2011.611.
- Charbeneau, R. J., and Barrett, M.E. (1998). "Evaluation of Methods for Estimating Stormwater Pollutant Loads." *Water Environment Research* 70 (7): 1295–1302. doi:10.2175/106143098X123679.
- Chen, Y., Cowling, P., Polack, F., Remde, S., and Mourdjis, P. (2017). "Dynamic Optimisation of Preventative and Corrective Maintenance Schedules for a Large Scale Urban Drainage System." *European Journal of Operational Research* 257 (2): 494–510. doi:10.1016/j.ejor.2016.07.027.
- Chow, M. F., Yusop, Z., and Abustan, I. (2015). "Relationship between Sediment Build-up Characteristics and Antecedent Dry Days on Different Urban Road Surfaces in Malaysia." *Urban Water Journal* 12 (3): 240–247. doi:10.1080/1573062X.2013.839718.
- Ciccarello, A., Bolognesi, A., Maglionico, M. and Artina, S. (2012). "The Role of Settling Velocity Formulation in the Determination of Gully Pot Trapping Efficiency: Comparison between Analytical and Experimental Data." *Water Science & Technology* 65 (1): 15–21. doi:10.2166/wst.2011.775.

Crabtree, R.W. (1989). "Sediment in Sewers." *Water and Environment Journal* 3 (6): 569-578. doi:10.1111/j.1747-6593.1989.tb01437.x.

Dankers, P.J.T. (2006). On the Hindered Settling of Suspensions of Mud and Mud-Sand Mixtures. PhD thesis. TU Delft.

Das, B. M. (2008). *Advanced Soil Mechanics*. London: Taylor & Francis. ISBN: 9781351215183.

De'ath, G., and Fabricius, K. E. (2000). "Classification and Regression Trees: A Powerful yet Simple Technique for Ecological Data Analysis." *Ecology* 81 (11): 3178–3192. doi:10.1890/0012-9658(2000)081[3178:CARTAP]2.0.CO;2.

De Man, H., Van den Berg, H.H.J.L., Leenen, E.J.T.M., Schijven, J.F., Schets, F.M., Van der Vliet, J.C., Van Knapen, F., and De Roda Husman, A.M. (2014). "Quantitative Assessment of Infection Risk from Exposure to Waterborne Pathogens in Urban Floodwater." *Water Research* 48: 90–99. doi:10.1016/j.watres.2013.09.022.

Deletic, A., Ashley, R.M. and Rest, D. (2000). "Modelling Input of Fine Granular Sediment into Drainage Systems via Gully Pots." *Water Research* 34 (15): 3836–3844. doi:10.1016/S0043-1354(00)00133-0.

Deletic, A., and Orr, D.W. (2005). "Pollution Buildup on Road Surfaces." *Journal of Environmental Engineering* 131 (1): 49–59. doi:org//10.1061/ (ASCE)0733-9372(2005)131:1(49).

Drain, L. E. (1980). *The Laser Doppler Techniques*. Chichester: Wiley-Interscience.

Droppo, I.G., Irvine, K.N.C.K.J., Carrigan, E., Mayo, S., Jaskot, C., and Trapp, B. (2006). "Understanding the Distribution, Structure and Behaviour of Urban Sediments and Associated Metals toward Improving Water Management Strategies." In *Soil Erosion and Sediment Redistribution in River Catchments: Measurement, Modelling and Management*.

Egodawatta, P., Thomas, E., and Goonetilleke, A. (2007). "Mathematical Interpretation of Pollutant Wash-off from Urban Road Surfaces using Simulated Rainfall." *Water Research* 41 (13): 3025-3031. doi:10.1016/j.watres.2007.03.037.

Ellis, J.B., Chocat, B., Fujita, J., Marsalek, J., and Rauch, W. (2004). *Urban Drainage*. London: IWA Publishing. ISBN: 9781900222068.

- Ellis, J. B. and Harrop, D.O. (1984). "Variations in Solids Loadings to Roadside Gully Pots." *Science of the Total Environment* 33 (1-4): 203-211. doi:10.1016/0048-9697(84)90394-2.
- Faram, M. and Harwood, R. (2003). "A Method for the Numerical Assessment of Sediment Interceptors." *Water Science & Technology* 47 (4): 167-174. doi:10.2166/wst.2003.0246.
- Fletcher, I.J., and Pratt, C.J. (1981). "Mathematical Simulation of Pollutant Contributions to Urban Runoff from Roadside Gully Ponds." In *Proceedings of the 2nd International Conference on Urban Storm Drainage*. Urbana, USA.
- Fletcher, T.D., Shuster, W., Hunt, W.F., Ashley, R., Butler, D., Arthur, S., Trowsdale, S., Barraud, S., Semadeni-Davies, A., Bertrand-Krajewski, J.L., Steen Mikkelsen, P., Rivard, G., Uhl, M., Dagenais, D. and Viklander, M. (2015). "SUDS, LID, BMPs, WSUD and more – The Evolution and Application of Terminology Surrounding Urban Drainage." *Urban Water Journal* 12 (7): 525-542. doi: 10.1080/1573062X.2014.916314.
- Fox, J. (2008). *Applied Regression Analysis and Generalized Linear Models*. Thousand Oaks: Sage Publications. ISBN: 9781452205663.
- Freni, G., Mannina, G., and Viviani, G. 2009. "Urban Runoff Modelling Uncertainty: Comparison among Bayesian and Pseudo-Bayesian Methods." *Environmental Modelling & Software* 24 (9): 1100-1111. doi: 10.1016/j.envsoft.2009.03.003.
- Fulcher, G.A. (1994). "Urban Stormwater Quality from a Residential Catchment." *Science of the Total Environment* 146-147: 535–542. doi:10.1016/0048-9697(94)90279-8.
- Galloway, J.N., Thornton, J.D., Norton, S.A., Volchok, H.L., and McLean, R.A. (1982). "Trace Metals in Atmospheric Deposition: A Review and Assessment." *Atmospheric Environment* 16 (7): 1677-1700. doi:10.1016/0004-6981(82)90262-1.
- Gaume, E., Villeneuve, J.P., and Desbordes, M. (1998). "Uncertainty Assessment and Analysis of the Calibrated Parameter Values of an Urban Storm Water Quality Model." *Journal of Hydrology* 210 (1-4): 38-50. doi:10.1016/S0022-1694(98)00171-1.
- Gelhardt, L., Huber, M., and Welker, A. (2017). "Development of a Laboratory Method for the Comparison of Settling Processes of Road-deposited Sediments with Artificial Test Material." *Water, Air, & Soil Pollution* 228 (12): 467. doi:10.1007/s11270-017-3650-8.
- Genesio, R., and Tesi, A. (1991). "Chaos Prediction in Nonlinear Feedback Systems." *IEEE Proceeding D-control Theory and Applications* 138 (4): 313–320. doi:10.1049/ip-d.1991.0042.

- Gromaire-Mertz, M.C., Garnaud, S., Gonzalez, A. and Chebbo, G. (1999). "Characterisation of Urban Runoff Pollution in Paris." *Water Science and Technology*, 39 (2): 1-8. doi:10.1016/S0273-1223(99)00002-5.
- Grottker, M. (1987). "Runoff Quality from a Street with Medium Traffic Loading." *Science of the Total Environment* 59: 457-466. doi:10.1016/0048-9697(87)90469-4.
- Grottker, M. (1990). "Pollutant Removal by Gully Pots in Different Catchment Areas." *Science of the Total Environment*, 93: 512-522. doi:10.1016/0048-9697(90)90142-H.
- Halverson, H.G., Gleason, S.B., and Heisler, G.M. (1985). "Leaf Duration and the Sequence of Leaf Development and Abscission in Northeastern Urban Hardwood Trees." *Urban Ecology* 9: 323-335. doi:10.1016/0304-4009(86)90007-0.
- Heikkila, J., Olli, S. (1997). "A Four-step Camera Calibration Procedure with Implicit Image Correction." In *Proceedings of IEEE Computer Society Conference on Computer Vision and Pattern Recognition*. San Juan, Puerto Rico.
- Herngren, L.F. (2005). Build-up and Wash-off Process Kinetics of PAHs and Heavy Metals on Paved Surfaces using Simulated Rainfall. PhD thesis. Queensland University of Technology.
- Het Samenwerkingsorgaan Holland Rijnland (2015). *Actualisatie En Harmonisatie Van Het Verkeersmodel Holland Rijnland* [Update and Harmonisation of the Holland Rijnland Traffic Model]. Leiden: Holland Rijnland. <https://www.odwh.nl/dsresource?objectid=caf8a300-7d43-4280-b6a9-a80e2cf0992b&type=org&&>.
- Hixon, L.F., and Dymond, R.L. (2018). "State of the Practice: Assessing Water Quality Benefits from Street Sweeping." *Journal of Sustainable Water in the Built Environment* 4 (3). doi:10.1061/JSWBAY.0000860.
- Hong, Y., Bonhomme, C., Minh-Hoang, L., and Chebbo, G. (2016). "A New Approach of Monitoring and Physically-based Modelling to Investigate Urban Wash-off Process on a Road Catchment Near Paris." *Water Research* 102: 96-108. doi:10.1016/j.watres.2016.06.027.
- Howard, A.K., Mohseni, O., Gulliver, J.S., and Stefan, H.G. (2012). "Hydraulic Analysis of Suspended Sediment Removal from Storm Water in a Standard Sump." *Journal of Hydraulic Engineering* 138 (6): 491-502. doi:10.1061/(ASCE)HY.1943-7900.0000544.
- Irish, L.B., Lesso, W.G., Barrett, M.E., Malina, J.F., Charbeneau, R.J., and Ward, G.H. (1995). *An Evaluation of the Factors Affecting the Quality of Highway Runoff in the Austin, Texas Area*. Austin: Center for Research in Water Resources, The University of Texas at Austin.

- James, W., and Shivalingaiah, B. (1985). "Storm Water Pollution Modelling: Buildup of Dust and Dirt on Surfaces Subject to Runoff." *Canadian Journal of Civil Engineering* 12 (4): 906–915. doi:10.1139/l85-103.
- Jartun, M., Ottessen, R.T., Steinnes, E., and Volden, T. (2008). "Runoff of Particle Bound Pollutants from Urban Impervious Surfaces Studied by Analysis of Sediments from Stormwater Traps." *Science of the Total Environment* 396 (2-3): 147-163. doi:10.1016/j.scitotenv.2008.02.00.
- Jenson, S.K. and Domingue, J.O. (1988). "Extracting Topographic Structure from Digital Elevation Data for Geographic Information System Analysis." *Photogrammetric Engineering and Remote Sensing* 54 (11): 1593-1600. doi:0099-1112/88/5411-1593\$02.25/0.
- Kerri, K. D., J. A. Racine, and R. B. Howell. (1985). "Forecasting Pollutant Loads from Highway Runoff." *Transportation Research Record* 1017: 39–46.
- Lager, J. A., W. G. Smith, W. G. Lynard, R. M. Finn, and E. J. Finnemore. (1977). *Urban Stormwater Management and Technology: Update and Users' Guide*. Cincinnati: U.S. EPA.
- Langeveld, J. G., E. Liefing, and R. Schilperoort. (2016). *Regenwaterproject Almere* [Storm Water Project Almere]. Amersfoort: Stichting RIONED en STOWA.
- Lau, S.L. and Stenstrom, M.K. (2005). "Metals and PAHs Adsorbed to Street Particles." *Water Research* 39 (17): 4083-4092. doi:10.1016/j.watres.2005.08.002.
- Lepot, M., Pouzol, T., Borruel, X.A., Suner, D., and Bertrand-Krajewski, J.L. (2017). "Measurement of Sewer Sediments with Acoustic Technology: From Laboratory to Field Experiments." *Urban Water Journal* 14 (4): 369–377. doi:10.1080/1573062X.2016.1148181.
- Liu, A., Goonetilleke, A., and Egodawatta, P. (2012). "Inherent Errors in Pollutant Build-up Estimation in considering Urban Land Use as a Lumped Parameter." *Journal of Environmental Quality* 41 (5): 1690–1694. doi:10.2134/jeq2011.0419.
- Melanen, M. (1981). *Quality of Runoff Water in Urban Areas*. Helsinki: National Board of Waters.
- Memon, F.A., and Butler, D. (2002). "Assessment of Gully Pot Management Strategies for Runoff Quality Control Using a Dynamic Model." *Science of the Total Environment* 295 (1–3): 115–129. doi:10.1016/S0048-9697(02) 00056-6.

- Moghadas, H., Mirzavand, R., and Mousavi, P. (2019). "Early Detection of Flood in Urban Catch Basins Using Radio Frequency Slot Line Array." *Measurement* 134: 515–518. doi:10.1016/j.measurement.2018.10.102.
- Montgomery, D.C., Peck, E.A. and Vining, G.G. (2012). *Introduction to Linear Regression Analysis*. New York: John Wiley & Sons. ISBN: 9780470542811.
- Morgan, D., Johnston, P., Osei, K. and Gill, L. (2017). "Sediment Build-up on Roads and Footpaths of a Residential Area." *Urban Water Journal* 14 (4): 378–385. doi:10.1080/1573062X.2016.1148182.
- Muthusamy, M., Tait, S., Schellart, A., Beg, M.N.A., Carvalho, R.F., and De Lima, J.L. (2018). "Improving Understanding of the Underlying Physical Process of Sediment Wash-off from Urban Road Surfaces." *Journal of Hydrology* 557: 426-433. doi:10.1016/j.jhydrol.2017.11.047.
- Naves, J., Anta, J., Suárez, J., and Puertas, J. (2019). "WASHTREET - Hydraulic, Wash-off and Sediment Transport Experimental Data Obtained in an Urban Drainage Physical Model." *Zenodo*. doi:10.5281/zenodo.3233918.
- Naves, J., Rieckermann, J., Cea, L., Puertas, J., and Anta, J. (2020). "Global and Local Sensitivity Analysis to Improve the Understanding of Physically-based Urban Wash-off Models from High-resolution Laboratory Experiments." *Science of the Total Environment* 709. doi:10.1016/j.scitotenv.2019.136152.
- Nieuwstadt, F.T.M., Westerweel, J., Boersma, B.J. (2016). *Turbulence: Introduction to Theory and Application of Turbulent Flows*. Cham: Springer. ISBN: 9783319315997.
- Novotny, V., Sung, H.M., Bannerman, R., and Baum, K. (1985). "Estimating Nonpoint Pollution from Small Urban Watersheds." *Journal of Water Pollution Control Federation* 57 (4): 339-348.
- Philippe, J. P. and Ranchet, J. (1987). *Pollution des Eaux de Ruissellement Pluvial en Zone Urbaine. Synthèse des Mesures sur Dix Bassins Versants en Région Parisienne* [Pollution of rainwater runoff in urban areas. Summary of measures on ten watersheds in the Paris Region]. Laboratoire Central des Ponts et Chaussées.
- Pitt, R. (1979). *Demonstration of NonPoint Pollution Abatement through Improved Street Cleaning Practices*. Washington DC: U.S. EPA.

Pitt, R., Williamson, D., Voorhees, J., and Clark, S. (2005). "Review of Historical Street Dust and Dirt Accumulation and Washoff Data." *Journal of Water Management Modeling*. doi:10.14796/JWMM.R223-12.

Post, J.A.B., Langeveld, J.G., and Clemens, F.H.L.R. (2017). "Quantifying the Effect of Proactive Management Strategies on the Serviceability of Gully pots and Lateral Sewer Connections." *Structure and Infrastructure Engineering* 13 (9): 1230-1238. doi:10.1080/15732479.2016.1260602.

Post, J.A.B., Pothof, I.W.M., Dirksen, J., Baars, E.J., Langeveld, J.G., and Clemens, F.H.L.R. (2016). "Monitoring and Statistical Modelling of Sedimentation in Gully Pots." *Water Research* 88: 245-256. doi:10.1016/j.watres.2015.10.021.

Pratt, C.J. and Adams, J.R.W. (1984). "Sediment Supply and Transmission via Roadside Gully Pots." *Science of the Total Environment* 33 (1-4): 213-224. doi:10.1016/0048-9697(84)90395-4.

Pratt, C.J., Elliot, G.E.P., and Fulcher, G.A. (1987). "Suspended Solids Discharge from Highway Gully Pots in a Residential Catchment." *Science of the Total Environment* 59: 355-364. doi:10.1016/0048-9697(87)90459-1.

Rodriguez-Iturbe, I., Febres De Power, B., Sharifi, M.B., and Georgakakos, K.P. (1989). "Chaos in Rainfall." *Water Resources Research* 25 (7): 1667-1675. doi:10.1029/WR025i007p01667.

Sabin, L.D., Lim, J.H., Venezia, M.T., Winer, A.M., Schiff, K.C., and Stolzenbach, K.D. (2006). "Dry Deposition and Resuspension of Particles-associated Metals near a Freeway in Los Angeles." *Atmospheric Environment* 40 (39): 7528-7538. doi:10.1016/j.atmosenv.2006.07.004.

Sansalone, J., Koran, J.J., Smithson, J.M., and Buchberger, S.G. (1998). "Physical Characteristics of Urban Roadway Solids Transported during Rain Events." *Journal of Environmental Engineering* 124 (5): 427-440. doi:10.1061/(ASCE)0733-9372(1998)124:5(427).

Sartor, J. D. and Boyd, G. B. (1972). *Water Pollution Aspects of Street Surface Contaminants*. Washington DC: U.S.EPA.

Shaheen, D.G. (1975). *Contributions of Urban Roadway Usage to Water Pollution*. Washington DC: U.S.EPA.

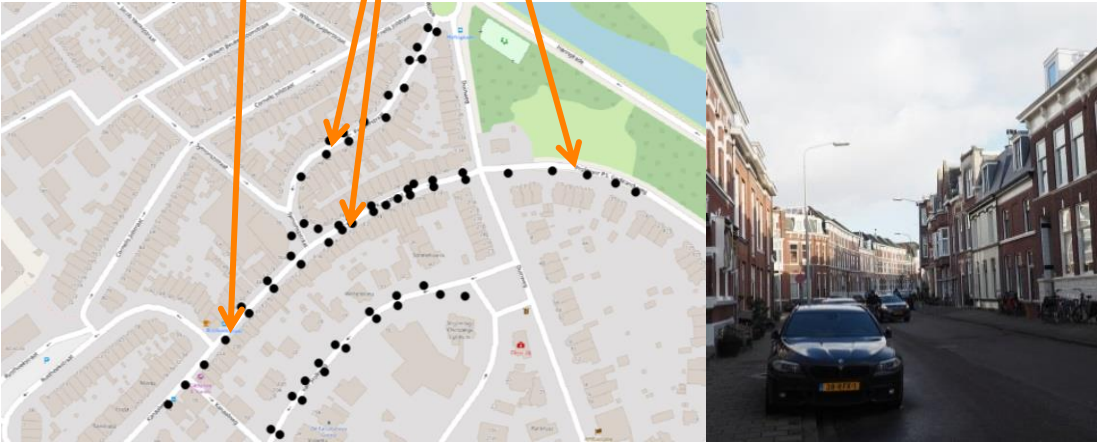

- Shaw, S.B., Stedinger, J.R., and Walter, M.T. (2010). "Evaluating Urban Pollutant Buildup/Wash-off Models Using a Madison, Wisconsin Catchment." *Journal of Environmental Engineering* 136 (2): 194–203. doi:10.1061/(ASCE)EE.1943-7870.0000142.
- Shivalingaiah, B., and James, W. (1984). "Algorithms for Buildup, Washoff, and Routing Pollutants in Urban Runoff." In *Proceedings of the Third International Conference on Urban Storm Drainage*. Göteborg, Sweden.
- Shorshani, M.F., Bonhomme, C., Petrucci, G., André, M., and Seigneur, C. (2014). "Road Traffic Impact on Urban Water Quality: a Step towards Integrated Traffic, Air and Stormwater Modelling." *Environmental Science and Pollution Research* 21: 5297-5310. doi: 10.1007/s11356-013-2370-x.
- Silvagni, G. and Volpi, F. (2002). "A Model able to Estimate the Phenomenon of Silting of Roadside Gully Pots." In *Proceedings of the Second International Conference New Trends in Water and Environmental Engineering for Safety and Life: Ecocompatible Solutions for Aquatic Environments*. Capri, Italy.
- Simperler, L., Keckeis, K. and Ertl, T. (2019). "Using a Solids Mass Balance Model for Impact Estimation of Stormwater Management Measures on Sewer Operation." In *Proceedings of the 9th International Conference on Sewer Processes & Networks*. Aalborg, Denmark.
- Sivakumar, B. (2000). "Chaos Theory in Hydrology: Important Issues and Interpretations." *Journal of Hydrology* 227 (1-4): 1-20. doi:10.1016/S0022-1694(99)00186-9.
- Sivakumar, B., Berndtsson, R., Olsson, J., and Jinno, K. (2001). "Evidence of Chaos in the Rainfall-runoff Process." *Hydrological Sciences Journal* 46 (1): 131-145. doi:10.1080/02626660109492805.
- Spekkers, M.H., Kok, M., Clemens, F.H.L.R., and Ten Veldhuis, J.A.E. (2013). "A Statistical Analysis of Insurance Damage Claims Related to Rainfall Extremes." *Hydrology & Earth System Sciences Discussions* 9 (10): 913–922. doi:10.5194/hess-17-913-2013.
- Sutherland, R.C. and Jelen, S.L. (1997). "Contrary to Conventional Wisdom, Street Sweeping can be an Effective BMP." *Advances in Modeling the Management of Stormwater Impacts* 5 (9): 179-190. doi:10.14796/JWMM.R195-09.
- Swanson, L. (2001). "Linking Maintenance Strategies to Performance." *International Journal of Production Economics* 70 (3): 237-244. doi:10.1016/S0925-5273(00)00067-0.

- Tang, Y., Zhu, D.Z., Rajaratnam, N., and Van Duin, B. (2016). “Experimental Study of Hydraulics and Sediment Capture Efficiency in Catchbasins.” *Water Science & Technology* 74 (11): 2717-2726. doi:10.2166/wst.2016.448.
- Ten Veldhuis, J.A.E., and Clemens, F.H.L.R. (2011). “The Efficiency of Asset Management Strategies to Reduce Urban Flood Risk.” *Water Science & Technology* 64 (6): 1317–1324. doi:10.2166/wst.2011.715.
- Ten Veldhuis, J.A.E., Clemens, F.H.L.R., and Gelder, P.V. (2009). “Fault Tree Analysis for Urban Flooding.” *Water Science & Technology* 59 (8): 1621-1629. doi:10.2166/wst.2009.171.
- Terfous, A., Hazzab, A., and Ghenaim, A. (2013). “Predicting the Drag Coefficient and Settling Velocity of Spherical Particles.” *Powder Technology* 239: 12-20. doi:10.1016/j.powtec.2013.01.052.
- Tscheikner-Gratl, F., Caradot, N., Cherqui, F., Leitão, J. P., Ahmadi, M., Langeveld, J.G., Le Gat, Y., Scholten, L., Roghani, B., Rodríguez, J.P., Lepot, M., Stegeman, B., Heinrichsen, A., Kropp, I., Kerres, K., do Céu Almeida, M., Bach, P.M., Moy de Vitry, M., Sá Marques, A., Simões, N.E., Roualt, P., Hernandez, N., Torres, A., Werey, C., Rulleau, B., and Clemens, F.H.L.R. (2019). “Sewer Asset Management – State of the Art and Research Needs.” *Urban Water Journal* 16 (9): 662–675. doi:10.1080/1573062X.2020.1713382.
- Van Bijnen, M., Korving, H., Langeveld, J.G., and Clemens, F.H.L.R. (2018). “Quantitative Impact Assessment of Sewer Condition on Health Risk.” *Water* 10 (3): 245. doi:10.3390/w10030245.
- Van der Zon, N. (2013). *Kwaliteitsdocument AHN2* [Quality Document AHN2]. Amersfoort: Rijkswaterstaat & Waterschappen.
- Vaze, J. and Chiew, S. (2002). “Experimental Study of Pollutant Accumulation on an Urban Road Surface.” *Urban Water* 4 (4): 379-389. doi:10.1016/S1462-0758(02)00027-4.
- Verjus, R., Guillou, S., Ezersky, A., and Angilella, J.R. (2016). “Chaotic Sedimentation of Particle Pairs in a Vertical Channel at Low Reynolds Number: Multiple States and Routes to Chaos.” *Physics of Fluids* 28 (12): 123303. doi:10.1063/1.4968559.
- Viswanath, D. S., and G. Natarajan. (1989). *Data Book on the Viscosity of Liquids*. New York: Hemisphere Publishing Corporation. ISBN: 9780891167785.

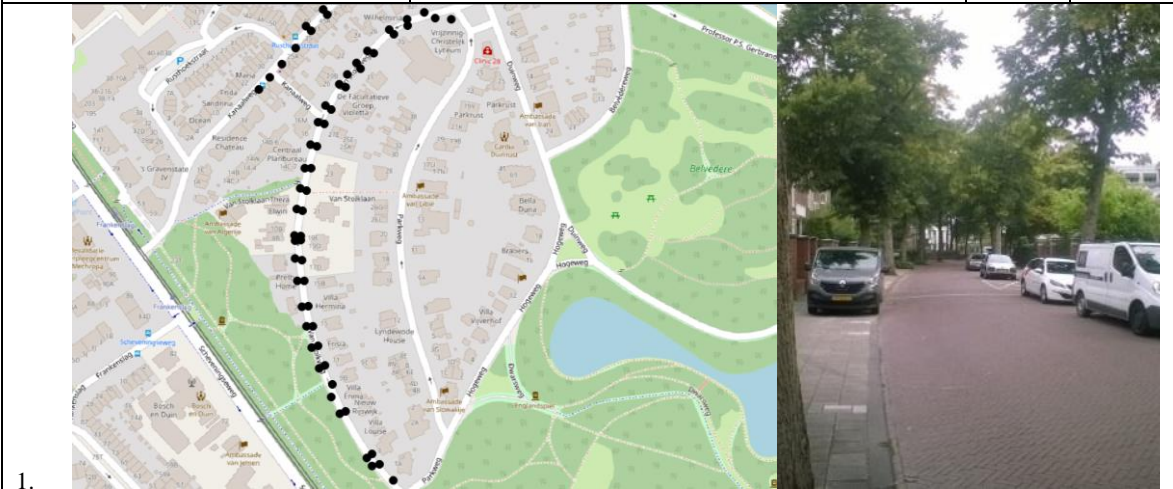
- Wada, Y., Miura, H., and Muraoka, O. (1996). "Influence of Discharge Pollutant from the Highway at Rainfall on Water Quality of the Public Water Body." In *Proceedings of the 7th International Conference on Urban Storm Drainage*. Hannover, Germany.
- Walker, T.A., and Wong, T.H.F. (1999). *Effectiveness of Street Sweeping for Stormwater Pollution Control*. Melbourne: Cooperative Research Centre for Catchment Hydrology.
- Welker, A., Gelhardt, L., and Dierschke, M. (2019). "Vegetation and Temporal Variability of Particle Size Distribution (PSD) and Organic Matter of Urban Road Deposited Sediments in Frankfurt am Main." In *Proceedings of Novatech 2019*. Lyon, France.
- Westerweel, J., Elsinga, G.E., and Adrian, R.J. (2013). "Particle Image Velocimetry for Complex and Turbulent Flows." *Annual Review of Fluid Mechanics*, 45: 409-436. doi:10.1146/annurev-fluid-120710-101204.
- Westerweel, J., and Scarano, F. (2005). "Universal Outlier Detection for PIV Data." *Experiments in Fluids* 39: 1096-1100. doi:0.1007/s00348-005-0016-6.
- Wicke, D., Cochrane, T.A., and O'Sullivan, A. (2012). "Build-up Dynamics of Heavy Metals Deposited on Impermeable Urban Surfaces." *Journal of Environmental Management* 113: 347-354. doi:10.1016/j.jenvman.2012.09.005.
- Wilczek, M., and Narita, Y. (2012). "Wave-Number-Frequency Spectrum for Turbulence from a Random Sweeping Hypothesis with Mean Flow." *Physical Review E* 86 (6). doi:10.1103/PhysRevE.86.066308
- Wijesiri, B., Egodawatta, P., McGree, J., and Goonetilleke, A. (2015). "Process Variability of Pollutant Build-up on Urban Road Surfaces." *Science of the Total Environment* 518-519: 434-440. doi:10.1016/j.scitotenv.2015.03.014.
- Xanthopoulos, C. and Augustin, A. (1992). "Input and Characterization of Sediments in Urban Sewer Systems." *Water Science & Technology* 25 (8): 21-28. doi:10.2166/wst.1992.0175.
- Yang, H., Zhu, D.Z., and Li, L. (2018). "Numerical Modeling on Sediment Capture in Catch Basins." *Water Science & Technology* 77 (5): 1346-1354. doi:10.2166/wst.2018.009.
- Zhang, Z. (2000). "A Flexible New Technique for Camera Calibration." *IEEE Transactions on Pattern Analysis and Machine Intelligence* 22 (11): 1330-1334.

Zafra, C.A., Temprano, J., and Tejero, I. (2008). "Particle Size Distribution of Accumulated Sediments on an Urban Road in Rainy Weather." *Environmental Technology* 29 (5): 571-582. doi:10.1080/09593330801983532.

APPENDIX A MONITORING AREAS CHAPTER 4

Street and city	Traffic intensity (#/day)	Vegetation factor	Sweeping (#/year)
Kanaalweg Den Haag	5000 2000 500	0	109
			
Keukenhoflaan Den Haag	30 300	3.8	5
			

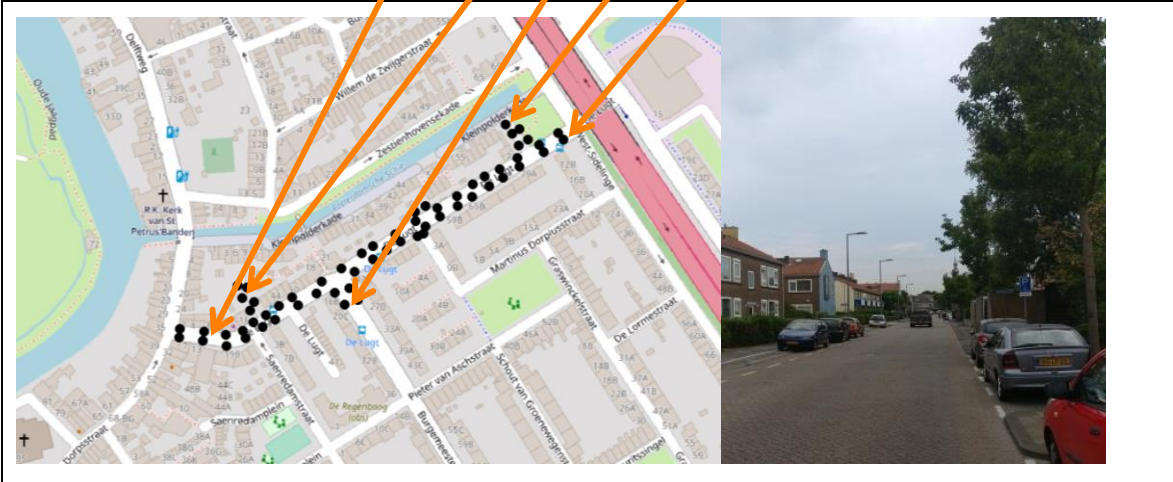
Van Stolkweg Den Haag	989	237	10
--------------------------	-----	-----	----

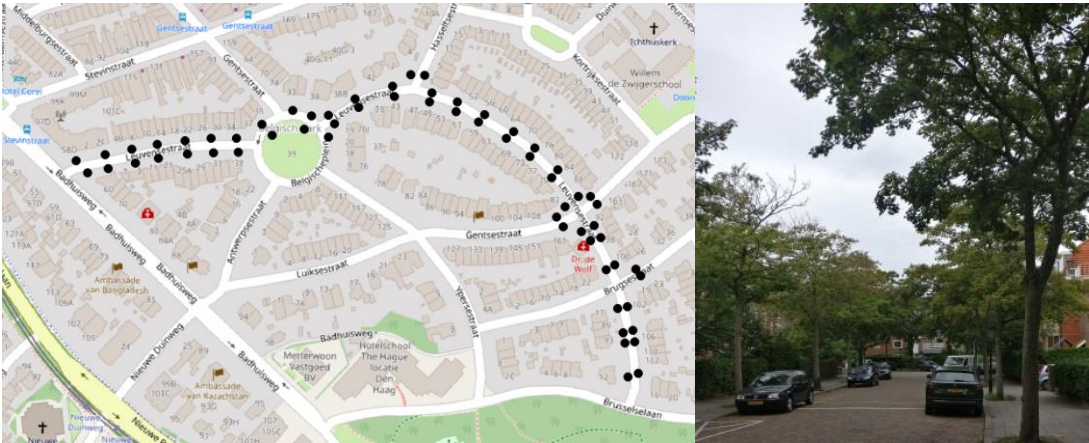
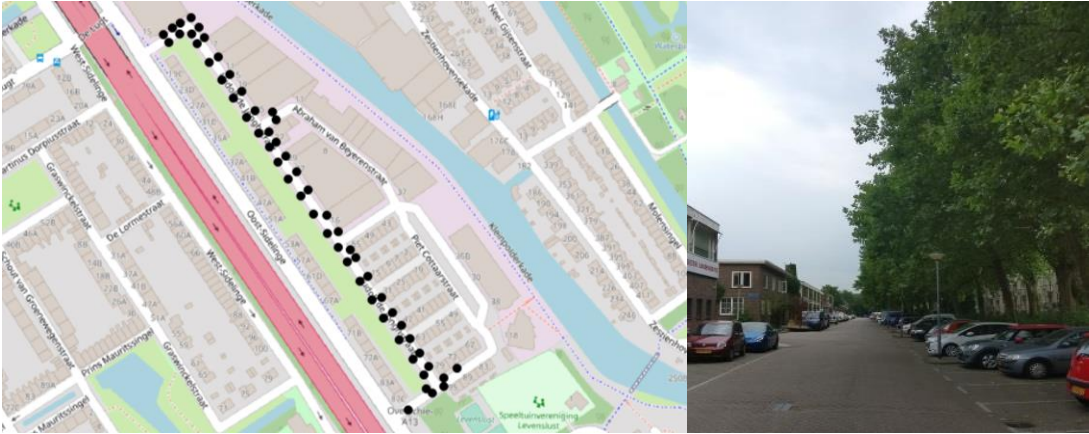


Paul Krugerlaan Den Haag	5020 4750 4500 4870 5580	24	133
-----------------------------	--------------------------	----	-----



De Lugt Rotterdam	1000 30 5000 30 6000	4.4	39
----------------------	----------------------	-----	----



<p>Leuvensestraat Den Haag</p>	<p>900</p>	<p>133</p>	<p>65</p>
			
<p>Ludolf de Jonghstraat Rotterdam</p>	<p>1000</p>	<p>770</p>	<p>39</p>
			

APPENDIX B VALIDATION STATISTICAL MODELS CHAPTER 4

In this appendix the validation of the LMM used in chapter 4 is described. Firstly, Cook's Distance was used to identify observations that are possibly influential outliers. Observations with a distance larger than 3 times the mean distance were removed to avoid wrong associations, which reduced the datasets by a few percent.

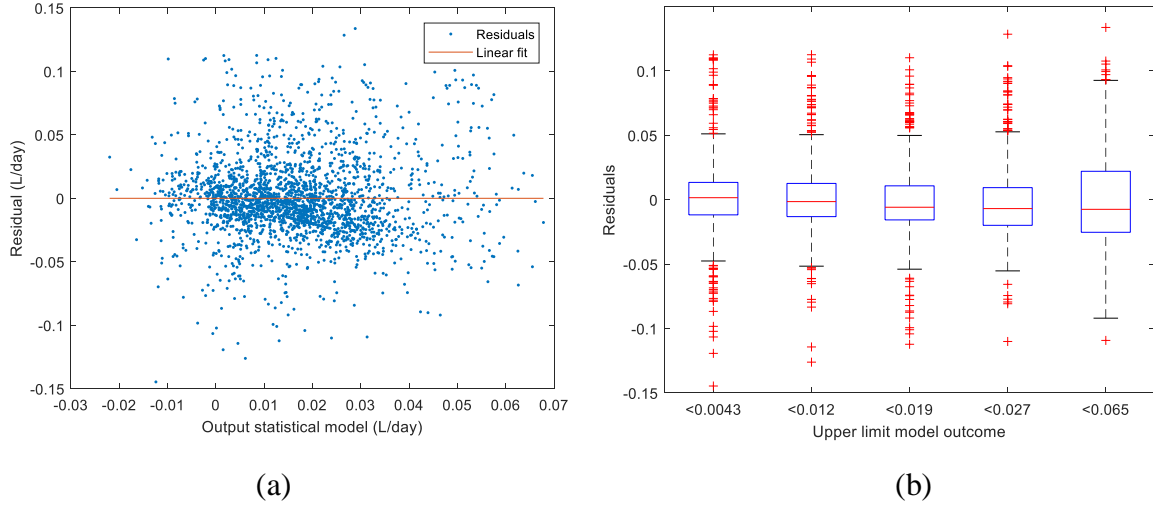


Figure B1. Residuals of the model based upon dataset 2. **(a)** Model residuals contain no trend with the model outcome; **(b)** The variance of the residuals is relatively similar over the range of the model outcome.

Secondly, the residuals should not have a trend with the model outcome (which can be observed in Figure B1). Moreover, the residuals should have homogeneity in their variance, meaning that the variance should be similar over the range of the model outcome. Fox (2008) showed that for a simple linear regression model heterogeneity degrades the least-square estimators substantially when the ratio between the largest and smallest variance is 4 or more, which is not the case for both datasets.

Thirdly, the independence of the observations was verified. The accumulation rate in gully pots located close to each other could be correlated, which is assessed with a Mantel correlogram per street. The Mantel statistic identifies whether a positive or negative relation exists at a certain distance (as an example the Mantel correlogram for Van Stolkweg is shown in Figure B2). No significant correlations ($p < 0.05$) were identified. Therefore, in line with the findings by Post et al. (2016), spatial correlation in solids accumulation in gully pots is neglected.

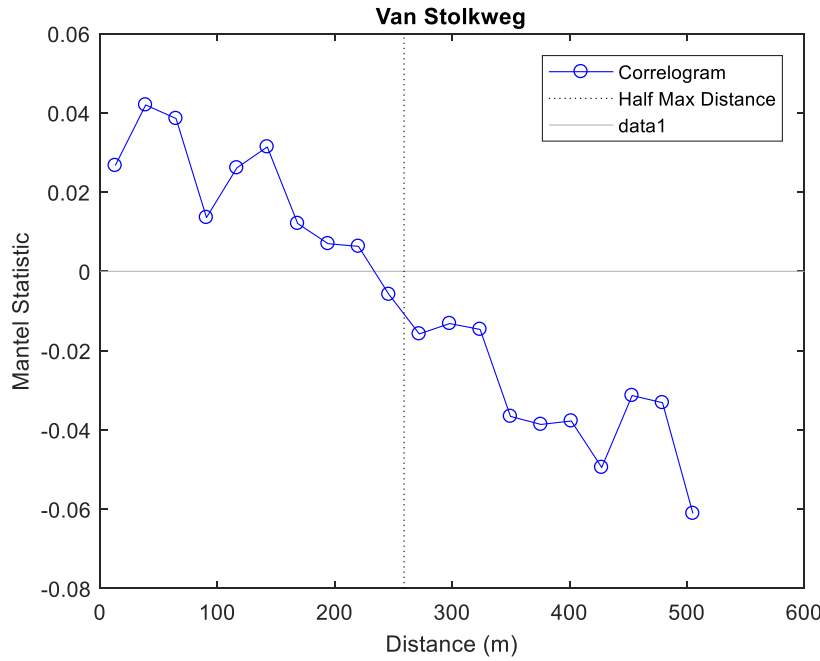


Figure B2. Mantel correlogram Van Stolkweg.

Autocorrelation in the accumulation rate in the same gully pot is expected due to the analysis method. The calculated accumulation rate (equation 1 in section 4.2.2) is the slope of the sediment depth based upon two sequential depth measurements. Therefore, an error in one depth measurement affects both the accumulation rate prior and after this measurement, causing a negative autocorrelation at lag 1. This type of correlation can be accounted for in a statistical model by an autoregressive error model.

The number of measurements in one series for one gully pot is very limited, namely 2 to 13. The autocorrelation of such a short time series has a negative autocorrelation at lag 1, due to its definition.

Figure B3 shows the strength of the autocorrelation of the residuals at lag 1 for the measurements, which contains a peak at -0.5 originating from measurement series of length 2. The figure also shows the autocorrelation of random numbers in series of the same length as the measurement series. A two-sample Kolmogorov-Smirnov test was performed to identify whether these two distributions differ significantly. This null hypothesis was rejected. Therefore, an autoregressive error model has not been added to avoid overfitting.

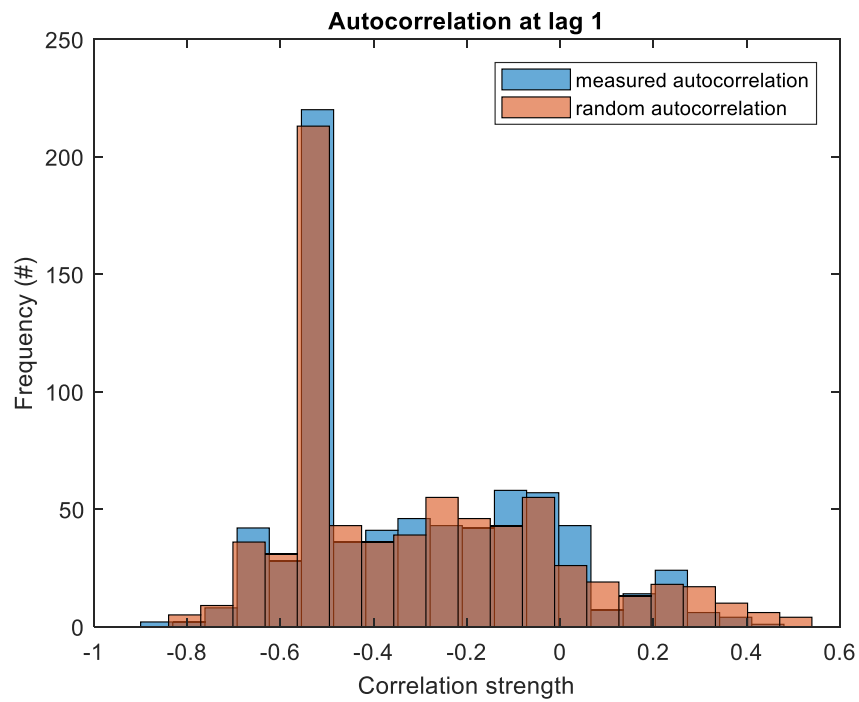


Figure B3. Correlation strength at lag 1 of the measured autocorrelation (dataset 1) and autocorrelation of random values with the same time series length.

Table B1. The β -values, standard errors, and p -values of the parameters used in the LMMs. Associations are considered significant if the p -value<0.05.

		Dataset 1			Dataset 2		
Variable		β	SE	p -value	β	SE	p -value
Connected area		$5.4 \cdot 10^{-5}$	$1.3 \cdot 10^{-5}$	$1.3 \cdot 10^{-4}$	$5.4 \cdot 10^{-5}$	$1.2 \cdot 10^{-5}$	$9.3 \cdot 10^{-6}$
Vegetation factor		$3.1 \cdot 10^{-5}$	$4.3 \cdot 10^{-6}$	$2.8 \cdot 10^{-13}$	$3.7 \cdot 10^{-5}$	$4.2 \cdot 10^{-6}$	$7.9 \cdot 10^{-18}$
Leafless phase		$-1.3 \cdot 10^{-2}$	$2.9 \cdot 10^{-3}$	$2.9 \cdot 10^{-6}$	$-7.6 \cdot 10^{-3}$	$2.1 \cdot 10^{-3}$	$3.4 \cdot 10^{-4}$
Leaf growth phase		$-1.4 \cdot 10^{-2}$	$3.8 \cdot 10^{-3}$	$2.5 \cdot 10^{-4}$	$-7.3 \cdot 10^{-3}$	$2.7 \cdot 10^{-3}$	$6.9 \cdot 10^{-3}$
Full capacity phase		$-1.3 \cdot 10^{-2}$	$2.8 \cdot 10^{-3}$	$6.7 \cdot 10^{-6}$	$-1.1 \cdot 10^{-2}$	$1.8 \cdot 10^{-3}$	$1.9 \cdot 10^{-9}$
Traffic intensity		No rel.	No rel.	No rel.	No rel.	No rel.	No rel.
Pavement type (asphalt)		No rel.	No rel.	No rel.	$6.0 \cdot 10^{-3}$	$2.4 \cdot 10^{-3}$	$1.2 \cdot 10^{-2}$
Commercial land use		No rel.	No rel.	No rel.	No rel.	No rel.	No rel.
Street sweeping		No rel.	No rel.	No rel.	No rel.	No rel.	No rel.
Rainfall volume		$4.6 \cdot 10^{-3}$	$7.8 \cdot 10^{-4}$	$3.2 \cdot 10^{-9}$	$3.7 \cdot 10^{-3}$	$6.6 \cdot 10^{-4}$	$2.1 \cdot 10^{-8}$
Rainfall intensity		No rel.	No rel.	No rel.	No rel.	No rel.	No rel.
Dry period		$-7.0 \cdot 10^{-4}$	$2.4 \cdot 10^{-4}$	$3.0 \cdot 10^{-3}$	$5.6 \cdot 10^{-4}$	$1.7 \cdot 10^{-4}$	$6.6 \cdot 10^{-4}$
Discharge		$-4.2 \cdot 10^{-3}$	$1.1 \cdot 10^{-3}$	$2.3 \cdot 10^{-4}$	$-4.7 \cdot 10^{-3}$	$7.0 \cdot 10^{-4}$	$3.8 \cdot 10^{-11}$
Cross section		No rel.	No rel.	No rel.	No rel.	No rel.	No rel.
Top inlet		$8.8 \cdot 10^{-3}$	$2.2 \cdot 10^{-3}$	$6.2 \cdot 10^{-5}$	$1.3 \cdot 10^{-2}$	$2.1 \cdot 10^{-3}$	$1.1 \cdot 10^{-9}$
Filling degree		$-1.7 \cdot 10^{-2}$	$4.6 \cdot 10^{-3}$	$1.5 \cdot 10^{-4}$	$-2.6 \cdot 10^{-2}$	$3.4 \cdot 10^{-3}$	$3.4 \cdot 10^{-14}$

APPENDIX C ASSESSED VARIABLES CHAPTER 4

Table C1. Variables used in the models in chapter 4.

Variable	Type	Range dataset 1	Range dataset 2	Units
Response variable				
Accumulation rate	Continuous	[-2.1 – 0.94]	[-0.78 – 0.40]	L/day
Solids build-up variables				
Connected area	Continuous	[6.25 – 794]	[6.25 – 794]	m ²
Vegetation factor	Continuous	[0 – 769]	[0 – 769]	#m ²
Tree phase	Categorical	Leaf growth/Full capacity/ Leaf abscission/Leafless	Leaf growth/Full capacity/ Leaf abscission/Leafless	-
Traffic intensity	Continuous	[30 – 6000]	[30 – 6000]	#/day
Pavement type	Categorical	[Asphalt/Bricks]	[Asphalt/Bricks]	-
Commercial land use	Categorical	[Yes/No]	[Yes/No]	-
Street sweeping	Continuous	[5 – 133]	[5 – 133]	#/year
Solids wash-off variables				
Rainfall volume	Continuous	[0.053 – 6.0]	[0.072 – 4.6]	mm/day
Rainfall intensity	Continuous	[1.1 – 85]	[3.4 – 85]	mm/hour

Antecedent dry period	Continuous	[0 – 21]	[0 – 21]	days
Solids retention variables				
Discharge	Continuous	[0.0029 – 16]	[0.0071 – 16]	L/s
Cross-sectional area	Continuous	[0.045 – 0.16]	[0.045 – 0.16]	m ²
Inlet	Categorical	[Top/Side]	[Top/Side]	-
Filling degree	Continuous	[0 – 3.4]	[0 – 3.4]	-

APPENDIX D TREE PHASES CHAPTER 3

4-25-2018		3-5-2018	
Leaf growth phase		End of leaf growth phase	
24-5-2018		4-6-2018	
Max. leaves phase		Max. leaves phase	
25-6-2018		2-8-2018	
Max. leaves phase		Max. leaves phase	

30-8-2018		11-9-2018	
Max. leaves phase		Max. leaves phase	
10-10-2018		6-11-2018	
End of max. leaves phase		Leaf abscission phase	
28-11-2018		14-12-2018	
End of leaf abscission phase		No leaves phase	

10-1-2019		5-2-2019	
No leaves phase		No leaves phase	
8-3-2019		28-3-2019	
End of no leaves phase		Leaf growth phase	
30-4-2019		22-5-2019	
End of leaf growth phase		Max. leaves phase	

7-6-2019		28-6-2019	
Max. leaves phase		Max. leaves phase	
29-7-2019		2-9-2019	
Max. leaves phase		Max. leaves phase	
30-9-2019		12-10-2019	
End of Max. leaves phase		Leaf abscission phase	

11-11-2019		2-12-2019	
End of leaf abscission phase		No leaves phase	
30-12-2019		24-1-2019	
No leaves phase		No leaves phase	
20-2-2020		12-3-2020	
No leaves phase		Leaf growth phase	

24-4-2020

Leaf
growth
phase



APPENDIX E ASSESSED VARIABLES CHAPTER 3

Table E1. Explanatory variables used in the regression tree in chapter 3.

Variable	Type	Range	Units
Response variable			
Solids loading	Continuous	[0-70.1]	$\text{g}\cdot\text{day}^{-1}$
Solids build-up variables			
Gully pot catchment area	Continuous	[12.25 – 217]	m^2
Tree phase	Categorical	Leaf growth/Full capacity/	
Leaf abscission/No leaves	-		
Temperature	Continuous	[3.3 – 21.2]	$^{\circ}\text{C}$
Street sweeping	Continuous	[0-0.125]	$\# \cdot \text{week}^{-1}$
Antecedent dry period	Continuous	[0 – 22]	days
Solids wash-off variables			
Rainfall volume	Continuous	[0.080 – 8.1]	$\text{mm}\cdot\text{day}^{-1}$
Rainfall intensity	Continuous	[1.2 – 53]	$\text{mm}\cdot\text{hour}^{-1}$
Discharge	Continuous	[0.0040 – 3.2]	L/s
Water volume	Continuous	[0.99 – 1800]	$\text{L}\cdot\text{day}^{-1}$

APPENDIX F TESTS OVERVIEW CHAPTER 5

Table F1. Overview of the conducted sedimentation tests as described in chapter 5.

Test name	Depth (m)	Discharge (L/s)	Sand supply (g/s)	Sand size (μm)	Outlet
D20F055S04Ba	0.21	0.55	1.28	389	Back
D20F055S04Ba	0.21	0.55	1.39	389	Back
D20F100S04Ba	0.21	1.0	3.02	389	Back
D20F140S04Ba	0.21	1.4	5.68	389	Back
D20F140S04Ba_1	0.21	1.4	5.84	389	Back
D20F180S04Ba	0.21	1.8	6.13	389	Back
D20F200S04Ba	0.21	2.0	7.12	389	back
D20F055S02Ba	0.21	0.55	1.29	176	Back
D20F100S02Ba	0.21	1.0	2.88	176	Back
D20F100S02Ba_1	0.21	1.0	2.00	176	Back
D20F140S02Ba	0.21	1.4	6.02	176	Back
D20F180S02Ba	0.21	1.8	6.78	176	Back
D20F035S01Ba	0.21	0.35	0.801	125	Back
D20F055S01Ba	0.21	0.55	1.29	125	Back
D20F100S01Ba	0.21	1.0	3.04	125	Back
D20F140S01Ba	0.21	1.4	5.51	125	Back
D20F180S01Ba	0.21	1.8	6.45	125	Back
D20F055S10Ba	0.21	0.55	1.50	1080	Back
D20F055S10Ba_1	0.21	0.55	1.52	1080	Back
D20F10S10Ba	0.21	1.0	4.16	1080	Back
D20F140S10Ba	0.21	1.4	5.35	1080	Back
D20F180S10Ba	0.21	1.8	6.39	1080	Back

D29F055S04Ba	0.30	0.55	1.26	389	Back
D29F100S04Ba	0.30	1.0	2.10	389	Back
D29F14S04Ba	0.30	1.4	5.49	389	Back
D29F180S04Ba	0.30	1.8	6.91	389	Back
D38F100S04Ba	0.39	1	3.03	389	Back
D38F140S04Ba	0.39	1.4	5.61	389	Back
D38F180S04Ba	0.39	1.8	6.25	389	Back
D20F055S04Si	0.21	0.55	1.04	389	Side
D20F100S04Si	0.21	1.0	2.92	389	Side
D20F100S04Si	0.21	1.0	3.09	389	Side
D20F140S04Si	0.21	1.4	5.43	389	Side
D20F180S04Si	0.21	1.8	6.33	389	Side
D20F055S04Fr	0.21	0.55	0.962	389	Front
D20F100S04Fr	0.21	1.0	2.92	389	Front
D20F140S04Fr	0.21	1.4	5.57	389	Front
D20F180S04Fr	0.21	1.8	6.15	389	Front
D20F200S04Fr	0.21	2.0	6.94	389	Front

SUMMARY

A substantial part of urban surfaces is to some extent impermeable. Rainfall on these areas turns into runoff, which mobilises solids present on these surfaces. This runoff is removed from urban built areas by different type of drainage systems via gully pots. The objective of a gully pot is twofold, namely 1) to convey runoff to the drainage system with minimal hydraulic losses, while 2) to remove entrained solids to protect the downstream system.

The continuous removal of suspended solids results in a growing sediment bed in the gully pot. This sediment bed can eventually reduce the hydraulic capacity of the gully pot and increase the probability of urban flooding due to rainfall. The increasing sediment bed also reduces the removal efficiency, which implies that more solids are transported to the downstream drainage system.

Therefore, the objective of this study is to quantify the related processes, which are the build-up of solids on the street, the transport of solids to gully pots, and the removal of solids in gully pots. Which would assist the decision of the optimal cleaning interval of the sand trap.

Four research questions have been formulated to meet the study objective:

1. What is the solids loading to gully pots in terms of mass and composition?
2. Does street sweeping reduce the solids loading to gully pots?
3. What is the removal efficiency of solids of a gully pot?
4. How do the in-gully-pot hydraulics influence the removal efficiency?

Part I: Transport of solids to gully pots

The solids loading, both in terms of mass and composition, to 104 gully pots was monitored over a period ~2 years at a sampling rate of once per 3-4 weeks to identify the main drivers of this process. A Regression Tree (RT) based on these data identifies the rain intensity, rain volume, and temperature as the most influential parameters on the mass of the solids loading.

The performance of this model is modest ($R^2 = 0.60$), therefore the solids loading to an individual gully pot should not be predicted with the model, but the performance for a set of gully pots (i.e. the dynamics of the loading to the drainage system) is relatively good ($R^2 = 0.92$).

An RT allows local relations within subgroups of the data, which results in a very flexible type of modelling, and produces a site-specific model. Moreover, these types of models describe the dynamics, but lack the fundamental understanding of the processes. Consequently, the solids loading is also modelled with (semi-physical) Build-Up and Wash-Off (BUWO) models. These models are used to represent the concentration of particles in runoff from catchments. However, similar to literature, the BUWO models calibrated on the newly acquired data are not portable to other catchments, since either each gully pot catchment has to be modelled separately with a large range of calibration parameters, or the application of one model results in poor performance. This might imply that the calibration parameters of the model only act as fitting parameters and don't represent physical processes. This implies that the BUWO model acts as a black-box model and cannot be used in another catchment without calibration data of the new catchment.

The D_{50} and the organic fraction are correlated, since the coarse sediment fraction consists mainly of organic material. Both parameters are strongly influenced by leaf abscission. Moreover, the relative fraction of large, organic material seem to increase during periods of limited rainfall, which suggests that these solids can also be transported via other mechanisms than rain. The settling velocity of the particles $<1800 \mu\text{m}$ is strongly correlated with their organic fraction.

Street sweeping does not decrease the solids loading to gully pots. In the occasions a significant relation was identified, it increased the solids loading.

Part II: Solids accumulation in gully pots

The evolution of the sediment bed level in 407 gully pots located in the cities of The Hague and Rotterdam was monitored over a period of ~ 14 months. These time series have been used to identify the main drivers of the accumulation process with two statistical models, namely a Linear Mixed Model (LMM) and a Regression Tree (RT). Three processes could contribute to the accumulation rate, namely the solids build-up in a catchment, the transport of solids from the catchment to the gully pot, and the removal of solids by the gully pot. The statistical analysis shows that none of these three processes is dominant, since the three most influential

parameters, namely the surrounding vegetation density, rainfall volume, and sediment bed level, are related to all three processes. These parameters influence the overall dynamics of the solids accumulation in gully pots, however the R^2 values of the evaluated models are poor, indicating that the solids accumulation rate in a single gully pot cannot be predicted by the models.

Both the solids accumulation in gully pots and the solids loading to gully pots show to some extent unpredictable behaviour. Literature on wash-off also hardly draws generic conclusions on the quantifiability of wash-off. Therefore, it is worth evaluating whether these processes are (under certain conditions) inherently chaotic.

Part III: Gully pot hydraulics

The removal efficiency of solids and the flow velocity field in a gully pot were studied by means of scale 1:1 lab experiments. The solids accumulation process is initially dominated by settling in the gully pot. Over time, the evolution of the bed morphology starts to influence the flow field, which was quantified by means of Particle Image Velocimetry (PIV) and Laser Doppler Anemometry (LDA) measurements. The local mean flow velocity and turbulent kinetic energy close to the bed increases due to an increasing bed level, which reduces the settling of solids and/or resuspends solids from the bed (in case of low bed levels, the overlaying water protects the sediment bed).

Eventually, a global balance is reached at which the deposition equals the resuspension and the removal efficiency becomes zero. The sediment bed level at which this situation is reached depends on the discharge, the gully pot layout, and the solids' characteristics. These parameters also influence the shape of the sediment bed.

The removal efficiency equations found in literature conceptualise the gully pot as a completely mixed reactor, which implies that the gully pot geometry would not affect the removal efficiency. However, the removal efficiency is strongly affected by the combination of the position the jets impinge on the water and the gully pot's outlet position. The assumption can be violated at high discharges due to effective separation of the inflow and the outflow in gully pots with the outlet at the front and due to short-circuiting in gully pots with the outlet at the back. This effect should be taken into account in the design of new gully pots.

The removal efficiency of clean gully pots in practice is expected to be relatively high. Even during intense rainstorms occurring once a year for 10 minutes a minimal efficiency of 30%

can be expected, but efficiencies $>65\%$ can easily be achieved in more regular conditions. In case of substantial sediment bed levels this efficiency can drop quickly. Therefore, cleaning gully pots once every few months protects the downstream drainage system effectively.

SAMENVATTING

Een substantieel deel van het oppervlak in steden is tot op zekere hoogte impermeabel. Neerslag op deze gebieden verandert in afstromend hemelwater dat de op deze oppervlakken aanwezige deeltjes mobiliseert. Via straatkolken wordt dit hemelwater uit stedelijke bebouwde gebieden verwijderd door verschillende soorten rioolssystemen. Het doel van een straatkolk is tweeledig, namelijk 1) de afvoer van hemelwater naar het riool met minimale hydraulische verliezen, terwijl 2) zwevende deeltjes worden verwijderd om het stroomafwaartse deel van het riool te beschermen.

De continue verwijdering van deeltjes resulteert in een groeiend sediment bed in de straatkolk. Dit sediment bed kan uiteindelijk de hydraulische capaciteit van de straatkolk verminderen en de kans op water op straat vergroten. Het toenemende sediment bed vermindert ook de afvangefficiëntie, wat inhoudt dat er meer deeltjes naar het stroomafwaartse deel van het riool worden getransporteerd.

Daarom is het doel van deze studie om de gerelateerde processen, namelijk de ophoping van deeltjes op straat, het transport van deeltjes naar kolken en de verwijdering van deeltjes in kolken, te kwantificeren. Zodat een onderbouwde keuze voor het reinigingsinterval van de zandvang kan worden gemaakt.

Hiertoe zijn vier onderzoeksvragen geformuleerd:

1. Wat is de aanvoer van deeltjes naar straatkolken in termen van massa en samenstelling?
2. Vermindert straatvegen de deeltjes aanvoer naar straatkolken?
3. Wat is de deeltjes afvangefficiëntie van een straatkolk?
4. Hoe beïnvloedt de hydraulica in de straatkolk de afvangefficiëntie?

Deel I: De aanvoer van deeltjes naar straatkolken

De aanvoer van deeltjes naar straatkolken, zowel in termen van massa als samenstelling, is met frequentie van eenmaal per 3-4 weken gemonitord in 104 straatkolken gedurende een periode van ~2 jaar om de belangrijkste aandrijfmechanismes van dit proces te identificeren. Op basis van deze data is een regressieboom gemaakt die de regenintensiteit, het regenvolume en de temperatuur als de invloedrijkste parameters, wat betreft de massa van de deeltjes, identificeert. De prestatie van dit model is echter matig ($R^2 = 0,60$), daarom moet de aanvoer van deeltjes naar een individuele straatkolk niet met dit model worden voorspeld. De prestatie voor een verzameling straatkolken (oftewel de dynamiek van de aanvoer naar het rioolsysteem) is relatief goed ($R^2 = 0,92$).

Een regressieboom maakt gebruik van lokale relaties binnen subgroepen van de data. Dit resulteert in een zeer flexibel en locatie specifiek model. Bovendien beschrijven dit soort modellen wel de dynamiek, maar missen ze het fundamentele begrip van de processen. Daarom is de aanvoer van deeltjes ook gemodelleerd met (semi-fysische) Build-Up en Wash-Off (BUWO)-modellen. Deze modellen worden gebruikt om de concentratie van deeltjes in afstromend hemelwater te schatten. Net als in de literatuur zijn de BUWO-modellen die zijn gekalibreerd op de nieuw verkregen data echter niet overdraagbaar naar andere gebieden. Of elk stroomgebied van de kolken moest afzonderlijk worden gemodelleerd met een groot aantal kalibratieparameters tot gevolg, of de modelprestatie was zeer laag bij het gebruik van één model. Dit zou kunnen betekenen dat de kalibratieparameters van het model alleen fungeren als fit parameters en geen fysieke processen representeren, wat impliceert dat het BUWO-model fungeert als een black-box model en niet in een ander stroomgebied kan worden gebruikt zonder ijk data van het nieuwe stroomgebied.

De D_{50} en de organische fractie zijn gecorreleerd doordat de grove deeltjes fractie voornamelijk uit organisch materiaal bestaat. Beide parameters worden sterk beïnvloed door bladval. Bovendien lijkt het relatieve aandeel van groot organisch materiaal toe te nemen tijdens periodes van beperkte regenval, wat suggereert dat deze deeltjes ook via andere mechanismen dan regen kunnen worden getransporteerd. De bezinksnelheid van de deeltjes $<1800 \mu\text{m}$ is sterk gecorreleerd met hun organische fractie.

Straatvegen vermindert niet de aanvoer van deeltjes naar straatkolken. In de gevallen waarin een significant verband werd vastgesteld, verhoogde straatvegen juist de aanvoer van deeltjes.

Deel II: De ophoping van deeltjes in straatkolken

De ontwikkeling van de sliblaag in 407 straatkolken in de steden Den Haag en Rotterdam is gedurende een periode van ~14 maanden gevolgd. Deze tijdreeksen zijn gebruikt om de belangrijkste aandrijfmechanismes van het ophopingsproces te identificeren met twee statistische modellen, namelijk een lineair gemengd model en een regressieboom. Drie processen zouden kunnen bijdragen aan de ophopingssnelheid, namelijk de opbouw van deeltjes op straat, het transport van deze deeltjes van de straat naar de kolk en het afvangen ervan door de kolk. De statistische analyse laat zien dat geen van deze drie processen dominant is, aangezien de drie meest invloedrijke parameters, namelijk de hoeveelheid vegetatie in de omgeving, het neerslagvolume en de slibdiepte, gerelateerd zijn aan alle drie deze processen. Deze parameters beïnvloeden de algehele dynamiek van de ophoping van deeltjes in straatkolken, maar de R^2 -waarden van de geëvalueerde modellen zijn laag, wat aangeeft dat de ophoping van deeltjes in een individuele straatkolk er niet mee kan worden voorspeld.

Zowel de ophoping van deeltjes in straatkolken als de aanvoer van deeltjes naar straatkolken vertonen tot op zekere hoogte onvoorspelbaar gedrag. In de literatuur over wash-off wordt ook nauwelijks generieke conclusies over de kwantificeerbaarheid van wash-off getrokken. Daarom is het de moeite waard om te onderzoeken of deze processen (onder bepaalde omstandigheden) inherent chaotisch zijn.

Deel III: De hydraulica van straatkolken

De afvang efficiëntie van deeltjes en het snelheidsveld in een straatkolk zijn bestudeerd door middel van schaal 1:1 laboratoriumexperimenten. Het ophopingsproces van deeltjes wordt aanvankelijk gedomineerd door bezinking in de straatkolk. Na verloop van tijd begint de morfologie van het sediment bed het stromingsveld te beïnvloeden. Dit stromingsveld is gekwantificeerd door middel van Particle Image Velocimetry (PIV) en Laser Doppler Anemometry (LDA) metingen. De lokale gemiddelde stroomsnelheid en turbulente kinetische energie dicht bij het bed neemt toe naar mate het sediment bed toeneemt, waardoor de bezinking van deeltjes verminderd en/of deeltjes uit het bed worden geresuspendeerd (bij lage bed niveaus beschermt de waterkolom het sediment bed).

Uiteindelijk wordt een globaal evenwicht bereikt waarbij de bezinking van deeltjes gelijk is aan de resuspensie, waarmee de afvang efficiëntie nul wordt. Het sediment bed niveau waarop deze situatie wordt bereikt, is afhankelijk van het debiet, de geometrie van de straatkolk en de

eigenschappen van de deeltjes. Deze parameters hebben ook invloed op de vorm van het sediment bed.

De modellen van de afvangefficiëntie in de literatuur conceptualiseren de straatkolk als een volledig gemengde reactor, wat impliceert dat de geometrie van de straatkolk de afvangefficiëntie niet beïnvloedt. De afvangefficiëntie wordt echter sterk beïnvloed door de combinatie van de positie waarop het instromende water in de straatkolk valt en de positie van de uitlaat. Bij hoge debieten wordt niet aan de aanname voldaan door een effectieve scheiding van de instroom en de uitstroom in straatkolken met de uitlaat aan de voorkant en door kortsluit stromen in straatkolken met de uitlaat aan de achterkant. Met dit effect moet rekening worden gehouden bij het ontwerp van nieuwe kolken.

De verwachting is dat de afvangefficiëntie van lege straatkolken in praktijk relatief hoog zal zijn. Zelfs tijdens intense regenbuien die eens per jaar gedurende 10 minuten voorkomen, kan een minimale efficiëntie van 30% worden verwacht, maar voor vaker voorkomende buien kan een efficiëntie >65% worden verwacht. Bij substantiële sediment bed niveaus kan deze efficiëntie echter snel dalen. Daarom kan het stroomafwaartse deel van het riool effectief worden beschermd door straatkolken eens in de paar maanden te reinigen.

LIST OF PUBLICATIONS

Peer-review publications:

Rietveld, M.W.J., Clemens, F.H.L.R., Langeveld, J.G. (2020). “Monitoring and Statistical Modelling of the Solids Accumulation Rate in Gully Pots.” *Urban Water Journal* 17 (6): 549-559. doi:10.1080/1573062X.2020.1800760.

Rietveld, M.W.J., Clemens, F.H.L.R., Langeveld, J.G. (2020). “Solids Dynamics in Gully Pots.” *Urban Water Journal* 17 (7): 669-690. doi:10.1080/1573062X.2020.1823430.

Rietveld, M.W.J., De Rijke, D., Langeveld, J.G., Clemens, F.H.L.R. (2020). “Sediment Morphology and the Flow Velocity Field in a Gully Pot: An Experimental Study.” *Water* 12 (10). doi:10.3390/w12102937.

Rietveld, M.W.J., Clemens, F.H.L.R., Langeveld, J.G. (in press). “Monitoring and Characterising the Solids Loading Dynamics to Drainage Systems.” *Urban Water Journal*.

Rietveld, M.W.J., Clemens, F.H.L.R., Langeveld, J.G. (submitted). “The Mismatch between Long Term Monitoring Data and Modelling of Solids Wash-off to Gully Pots.” Submitted to *Urban Water Journal*.

Congress publications:

Rietveld, M.W.J., Clemens, F.H.L.R., Langeveld, J.G. (2021). “Flow Pattern Visualisation in a Roadside Gully Pot.” In *Proceedings of the 6th IAHR Europe Congress*. Warsaw, Poland.

Rietveld, M.W.J., Clemens, F.H.L.R., Langeveld, J.G. (2019). “Measuring the Solids Loading of Urban Drainage System via Runoff.” In *Proceedings of Novatech 2019*. Lyon, France.

Rietveld, M.W.J., Langeveld, J.G., Mobron, N., Clemens, F.H.L.R. (2018). “From Unknown to Uncertain: a Statistical Model on Gully Pot Silting”. In *Proceedings of the conference on Urban Drainage Modelling*. Palermo, Italy.

ABOUT THE AUTHOR

Matthijs Willem Jan (Matthijs) Rietveld was born in Papendrecht, The Netherlands on November 27th 1991 and completed his grammar school education at the Wartburg College in Rotterdam in 2010. In 2013 he completed his BSc Applied Physics with a thesis entitled “Flow Characterisation of Newtonian and non-Newtonian Liquids in a Stirred Vessel. During his MSc Applied Physics, at the same university, he focussed mainly on fluid- and thermodynamics. He finished this study in 2015 with a thesis entitled “Dripping in Solar Stills”. After his graduation he worked at Deltares in the department of hydraulic structures. In November 2016, he started as a PhD candidate at Delft University of Technology, Faculty of Civil Engineering & GeoSciences, Department of Water management, section Sanitary Engineering under the supervision of Prof.dr.ir. Francois Clemens and Dr.ir. Jeroen Langeveld.

His research focusses on the transport of solids towards and in gully pots, which are inlets of the drainage system for runoff. His work has been published in international peer-reviewed journals and presented at international conferences. Next to his research, he supervised several BSc and MSc students and assisted in the course Urban Drainage and Water Management.

Matthijs is currently working as Asset Engineer Reliability at PWN.